Příloha 1

Sediva H, Dusatkova P, Kanderova V, Obermannova B, Kayserova J, Sramkova L, Zemkova D, Elblova L, **Svaton M**, Zachova R, Kolouskova S, Fronkova E, Sumnik Z, Sediva A, Lebl J, Pruhova S. Short Stature in a Boy with Multiple Early-Onset Autoimmune Conditions due to a *STAT3* Activating Mutation: Could Intracellular Growth Hormone Signalling Be Compromised? *Horm Res Paediatr.* 2017;88(2):160-166. doi: 10.1159/000456544.

Novel Insights from Clinical Practice

HORMONE RESEARCH IN PÆDIATRICS

Horm Res Paediatr 2017;88:160–166
DOI: 10.1159/000456544

Received: August 30, 2016
Accepted: January 16, 2017
Published online: March 2, 2017

Short Stature in a Boy with Multiple Early-Onset Autoimmune Conditions due to a *STAT3* Activating Mutation: Could Intracellular Growth Hormone Signalling Be Compromised?

Hana Sediva[a] Petra Dusatkova[a] Veronika Kanderova[c] Barbora Obermannova[a] Jana Kayserova[b] Lucie Sramkova[c] Dana Zemkova[a] Lenka Elblova[a] Michal Svaton[c] Radana Zachova[b] Stanislava Kolouskova[a] Eva Fronkova[c] Zdenek Sumnik[a] Anna Sediva[b] Jan Lebl[a] Stepanka Pruhova[a]

[a]Department of Paediatrics, 2nd Faculty of Medicine, Charles University in Prague and University Hospital Motol, Prague, Czech Republic; [b]Department of Immunology, 2nd Faculty of Medicine, Charles University in Prague and University Hospital Motol, Prague, Czech Republic; [c]Department of Paediatric Haematology and Oncology, 2nd Faculty of Medicine, Charles University in Prague and University Hospital Motol, Prague, Czech Republic

Established Facts

- Constitutive activation of STAT3 (signal transducer and activator of transcription 3) due to a germline gain-of-function *STAT3* mutation has recently been identified as a cause of multiple early-onset autoimmune conditions and growth impairment.

Novel Insights

- We revealed a previously unreported, heterozygous, de novo c.2144C>T (p.Pro715Leu) variant within the transactivation domain of *STAT3*, whose pathogenicity was functionally tested, in a boy born small for gestational age with progressive postnatal growth failure. He developed type 1 diabetes in late infancy and autoimmune thyroid disease, bicytopenia, and lymphoproliferative disease in the subsequent years.
- We thoroughly assessed the growth hormone-IGF-I axis and revealed partial growth hormone insensitivity. We proposed a potential role for STAT3 in intracellular post-receptor growth hormone signalling.

Keywords
STAT3 · Activating mutation · Short stature · Growth hormone · Growth hormone signal transduction · Growth hormone sensitivity · STAT5

Abstract
Background: Germline *STAT3* gain-of-function (GOF) mutations cause multiple endocrine and haematologic autoimmune disorders, lymphoproliferation, and growth impairment. As the JAK-STAT pathway is known to transduce the growth hormone (GH) signalling, and STAT3 interacts with STAT5 in growth regulation, we hypothesised that short stat-

E-Mail karger@karger.com
www.karger.com/hrp

Stepanka Pruhova
Department of Paediatrics, 2nd Faculty of Medicine
Charles University in Prague, University Hospital Motol, V Uvalu 84
CZ–150 06 Prague 5 (Czech Republic)
E-Mail Stepanka.Pruhova@fnmotol.cz

ure in *STAT3* GOF mutations results mostly from GH insensitivity via involving activation of STAT5. ***Case Report:*** A boy with a novel *STAT3* c.2144C>T (p.Pro715Leu) mutation presented with short stature (–2.60 SD at 5.5 years). He developed diabetes mellitus at 11 months, generalised lymphoproliferation, autoimmune thyroid disease, and immune bicytopenia in the subsequent years. At 5.5 years, his insulin-like growth factor-1 (IGF-I) was 37 µg/L (–2.22 SD) but stimulated GH was 27.7 µg/L. Both a standard IGF-I generation test (GH 0.033 mg/kg/day sc; 4 days) and a high-dose prolonged IGF-I generation test (GH 0.067 mg/kg/day sc; 14 days) failed to significantly increase IGF-I levels (37–46 and 72–87 µg/L, respectively). The boy underwent haematopoietic stem cell transplantation at 6 years due to severe neutropenia and massive lymphoproliferation, but unfortunately deceased 42 days after transplantation from reactivated generalised adenoviral infection. ***Conclusions:*** Our findings confirm the effect of *STAT3* GOF mutation on the downstream activation of STAT5 resulting in partial GH insensitivity.

Introduction

Recently, several groups reported on a new monogenic syndrome of multiple endocrine and haematologic autoimmune disorders, lymphoproliferation, susceptibility to infections and growth impairment [1–3] due to constitutive activation of signal transducer and activator of transcription 3 (STAT3), 1 of 7 members of the mammalian STAT family of transcription factors. Nineteen affected individuals with activating germline *STAT3* gene mutations have been identified within the first 3 studies published in 2014–2015 [1–3].

STAT proteins mediate cellular responses to cytokines, mostly as a part of the JAK-STAT signalling pathway. The receptor-associated JAK kinases activate STAT monomer proteins by phosphorylation. Phosphorylated STAT induces target gene expression that influences cell proliferation, differentiation, and apoptosis [4, 5]. Specifically, individual STAT family members respond to particular cytokine signals, which are expected to have effects on T-cell differentiation fates. Therefore, differentiation towards T helper 1 (Th1) cells is induced by the interferon gamma (IFNγ)-STAT1-interleukin 12 (IL-12)-STAT4 axis; Th2 cell differentiation is induced by the IL-4-STAT6 axis; and regulatory T-cell (Treg) fate is induced by the IL-2-STAT5 axis [3, 4]. STAT5b is a major signalling molecule in the growth hormone (GH) signalling pathway, and its activation is essential for the expression of genes encoding insulin-like growth factor-1 (IGF-I) and insulin-like growth factor binding protein (IGF-BP3) [6]. The activation of STATs is strictly regulated under normal conditions. Dysregulation of STAT signalling leads to a spectrum of clinical presentations, ranging from susceptibility to infection [7], autoimmunity [2], enhanced survival of tumour cells [8], and growth impairment.

STAT3 has been assigned an important role in promoting the expansion and activation of Th17 through the IL-6-STAT3 axis [4]. Additionally, STAT3 is suggested to inhibit the proliferation of Treg through interactions with STAT5 signalling [9]. Th17 and Tregs play a crucial role in the development of autoimmunity. Another suggested outcome of STAT3 and STAT5 interactions is growth regulation [1, 6].

STAT3 variants have been associated with 4 different clinical presentations: (a) common *STAT3* single nucleotide polymorphisms were shown to alter the susceptibility to Crohn disease [10], psoriasis [11], and multiple sclerosis [12]; (b) germline autosomal dominant loss-of-function *STAT3* mutations lead to hyperimmunoglobulin E syndrome, which is a primary immunodeficiency characterised by elevated serum IgE, Th17 deficiency and impaired bone and tooth development [7]; (c) somatic gain-of-function (GOF) mutations have been detected in multiple carcinomas, T-cell large granular lymphocytic leukaemia, myelodysplastic syndrome, and aplastic anaemia and are typically associated with poor prognosis [13], which has encouraged intensive research into specific STAT3 inhibitors [14, 15]; and (d) germline GOF *STAT3* mutations have recently been identified in patients with multiple early-onset organ-specific and haematologic autoimmune conditions, lymphoproliferation, predisposition to mycobacterial and other infections, and short stature [1–3]. We present an additional case that allowed us to investigate the immune system and the GH-IGF-I axis.

Case Presentation

The male proband was born from a twin pregnancy conceived by in vitro fertilisation. He was delivered prematurely in the 36th gestational week due to preeclampsia in the mother. The proband's birth weight was 2,190 g (–1.51 SD) and his birth length was 44 cm (–1.96 SD), indicating mild prenatal growth impairment [16]. The proband was shorter and weighed slightly less at birth than his twin sister (length 46 cm, –0.92 SD; weight 2,200 g, –1.26 SD). Except for transient neonatal hypoglycaemia and mild unconjugated hyperbilirubinaemia requiring 3 days of phototherapy, the proband's postnatal adaptation was normal.

Within the first year of life, the proband was apparently failing to thrive; at the age of 11 months, his weight was 6,585 g (–3.1 SD) [17]. At this age, he presented with diabetic ketoacidosis. His initial blood glucose, pH and HbA_{1c} were 24.2 mmol/L, 7.178, and 6% (42 mmol/mol), respectively. A diagnosis of type 1 diabetes (T1D) was confirmed by the detection of a high titre of antiglutamic acid decarboxylase autoantibody IgG (1,617 IU/mL; normal range 0–10) [18]. Anti-islet-cell antibodies were not present, although significant positivity of the tyrosine phosphatase protein related to the IA2 molecule (1,150 IU/L; normal range 0–600 [19]) was revealed at a subsequent investigation at 2.5 years of age. The proband's HLA haplotype was DQB1*0302, 05, i.e., a risk haplotype for T1D.

Since 1.5 years of age, the proband had gradually developed generalised lymphadenomegaly. A lymph node biopsy revealed aetiologically uncharacteristic chronic inflammation with florid activation of the germinal centres, not suggestive of an iconological condition. No infectious agent was found. Shortly thereafter, hepatosplenomegaly without focal lesions was detected, an additional sign of lymphoproliferation.

During screening for T1D-associated autoimmune disorders, the proband was diagnosed with autoimmune thyroid disease and hypothyroidism at 2.5 years and was initiated on thyroxin replacement. At 3.5 years, he developed immune thrombocytopenia (minimal platelet count 17×10^9/L) that resolved spontaneously over 2 weeks; however, the thrombocytopenia recurred at 5.5 years and was accompanied by neutropenia and a positive direct antiglobulin test (minimum platelet count 19×10^9/L, absolute neutrophil count 250). The proband underwent a 1-week course of oral corticosteroids at a dose of 2 mg/kg, with gradual reduction until discontinuation over 5 weeks. The corticosteroids attenuated the lymphoproliferation, normalised the platelet count and improved the neutropenia. However, in the subsequent weeks, the bicytopenia recurred, and the spleen and lymph nodes became further enlarged. Six weeks of mercaptopurine administration was not effective. Due to ongoing severe neutropenia and massive lymphoproliferation, a haematopoietic stem cell transplantation was provided at 6 years. The boy unfortunately deceased 42 days after transplantation due to reactivation of generalised adenoviral infection.

Immunological investigation showed an undetectable level of IgE with fluctuating levels of other immunoglobulins. The proportion of FOXP3+CD25+Tregs (out of CD4+ cells) was lowered to 2.8%, low relative and absolute number of CD16+CD56+ NK cells was also noticed (2%, $0.03 \times 10/9$/L), with otherwise normal values in number and function of T and B lymphocytes. A panel of autoantibodies was negative (ANA, ANCA, ASCA, anti-gliadin Ab), with the exception of T1D-associated antibodies.

Postnatal Growth and the GH-IGF-I Axis

The heights of the patient's parents are 180 cm (father) and 162 cm (mother). Following partial intrauterine growth restriction, he had no postnatal catch-up growth and continued growing close to –2.5 SD (Fig. 1). At 2.5 years of age, the patient's bone age corresponded with his calendar age, but his bone age became slightly retarded at 5.5 years, when he underwent endocrine assessment for short stature. His height was 103 cm (–2.60 SD); his peak GH concentration following insulin-induced hypoglycaemia was 27.7 μg/L, although his IGF-I level was low (37 μg/L; –2.22 SD) and his IGF-BP3 level was low normal (2.27 mg/L; –0.85 SD) [20, 21]. Because these results were suggestive of decreased sensitivity to GH,

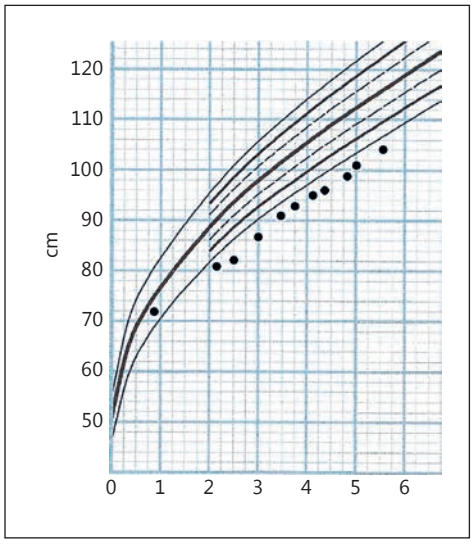

Fig. 1. Growth chart of our male proband with a *STAT3* GOF mutation.

we performed a standard IGF-I generation test (GH 0.033 mg/kg/day sc for 4 consecutive days) that led to an insufficient increase in IGF-I from 37 to 46 μg/L [20, 21]. We proceeded with a high-dose prolonged IGF-I generation test (GH 0.067 mg/kg/day sc for 14 consecutive days), which also led to an insufficient increase in IGF-I from 72 μg/L (–1.67 SD) to 87 μg/L (–1.43 SD) and only a partial rise in IGF-BP3 from 2.70 mg/L (–0.69 SD) to 3.29 mg/L (–0.15 SD) [20, 21].

An anthropometric evaluation at 5.5 years revealed a slightly disproportionate stature with limb shortening (sitting height 59.4 cm [–1.9 SD], subischial leg length 45.4 cm [–2.6 SD], and arm span 103.5 cm [98.8% of height, over the 25th percentile]) [17]. The patient had subtle craniofacial dysmorphism and brachycephaly (cephalic index 92), although his head circumference was normal (50.2 cm [–1.2 SD]). His shoulder width and thoracic circumference (55 cm, –0.8 SD) were consistent with his height, although the thorax was transversally narrow, with a relatively larger sagittal diameter (thoracic index 83.3 [2.3 SD]). These abnormalities were previously noted at 2.5 years and showed no tendency to progress over time. The boy apparently had delayed teeth eruption; his first tooth appeared at the age of 14 months, which was 7 months later than in his twin sister. His neuropsychological developmental milestones were normal.

Methods

Genetic Testing

Genomic DNAs were extracted from peripheral blood using QIAamp DNA Blood Mini Kit (Qiagen, Hilden, Germany). Genetic analysis was performed using direct sequencing as described previously [22]. Primers for coding exons and the exon/intron boundaries of the *STAT3* gene are available from the authors.

Functional Studies

A detailed description of the methods used to evaluate the functional impact of the detected mutation can be found in the supplementary material (see www.karger.com/doi/10.1159/000456544 for all online suppl. material). Briefly, we performed (1) the phosphoflow analysis by stimulating the patient's thawed peripheral blood mononuclear cells (PBMC) by IL-6, IL-2, INFγ, and IL-27, and then stained by anti-phospho-STAT3 (Tyr705) Alexa 488, anti-phospho-STAT1 (Tyr701) Alexa 647, anti-phospho-STAT5 (Tyr694) PE (all from BD Biosciences, San Jose, CA, USA), and anti-phospho-STAT1 (Tyr701) PE (Cell Signalling Technologies, Danvers, MA, USA); the LSR II flow cytometer (BD Biosciences) was used for data collection; (2) the patient's mRNA from PBMCs stimulated by IL-6 was extracted using RNeasy Plus Micro Kit (QIAGEN) and reverse transcribed with the iScript cDNA synthesis kit (Bio-Rad); suppressor of cytokine signalling 3 (*SOCS3*) transcript was measured by real-time quantitative reverse transcription-polymerase chain reaction using TaqMan® Gene Expression Assay (Life Technologies); results represent the fold-change compared with unstimulated healthy control after normalisation to endogenous *GAPDH* gene expression levels; and (3), the cDNA from patients and 1 healthy control (before stimulation) was used for the analysis of exons 22 and 23 splicing on a chip-based Agilent Bioanalyser (Agilent Technologies).

The study was approved by the institutional Ethics Committee, and the involved subjects or their parents consented in writing.

Results

Genetic Testing

The genetic analysis of the *STAT3* gene revealed a previously unreported, heterozygous, de novo c.2144C>T mutation. Substitution of thymine for cytosine in coding nucleotide 2144 is predicted to cause change of leucine for proline in position 715 of the STAT3 protein (p.Pro715Leu). The mutation is located within the transactivation domain of the protein that is responsible for transcriptional activation and recruitment of cotranscriptional factors, such as histone acetyltransferase [23]. Moreover, the mutated nucleotide corresponds to the last base on exon 22, which can affect the splicing process: the MaxEntScan score (predicting the splicing rate) of c.2144C>T decreased by 17% when compared with the wild-type sequence, and the mutation caused a disruption of exonic splicing enhancer according to the exonic splicing enhancer finder [24]. In addition, no polymorphism has been described in this position of the gene and the mutated amino acid is situated in an evolutionarily conserved area of the genome. A previously published pathogenic mutation, proven by functional analyses of cell lines [2], in a patient with a similar phenotype is situated to the same transactivation domain immediately next to this mutation (p.Thr716Met). Furthermore, predictions from in silico models (Sift, Polyphen2, Provean, Mutation Taster) assessed this variant as pathogenic. Both parents and the patient's sister tested negative for the entire mutation, suggesting de novo occurrence of the mutation.

Additional Case Report

Moreover, we subsequently identified another patient (patient 2) carrying the same mutation c.2144C>T. She is a 22-year-old woman born small for gestational age at the 36th week of gestation (birth weight 2,040 g, –1.85 SD; birth length 42 cm, –3.5 SD) with an extremely low final height of 125 cm (–6.7 SD) and body weight of 22.2 kg (–9.3 SD). She always had normal function of the anterior pituitary but her IGF-I level was low (83 μg/L; –2.69 SD at the age of 13 years). Sensitivity to GH had never been tested. She developed chronic lung impairment after several pulmonal infections leading to bronchiectasis, pulmonary hypertension, and restrictive lung disease requiring long-term oxygenotherapy. Since 1 year of age, she had hepatosplenomegaly and generalised lymphadenomegaly. She had several attacks of autoimmune cytopenia (thrombocytopenia, anaemia) and had been treated with corticosteroids and immunosuppressives for several years. Her IgE level was undetectable and the level of FOXP3+CD25+ Tregs was 0.7% (out of CD4+ T-cells). The genetic investigation using whole exome sequencing did not reveal another cause for her growth retardation and immune dysregulation.

Functional Studies

In accordance with previous observations in patients with *STAT3* GOF mutations [1] we detected normal to reduced phosphorylation of STAT3 in CD3+T-cells from both patients when compared to healthy controls. Moreover, STAT1 phosphorylation was reduced upon IFNγ stimulation, and STAT5 phosphorylation was slightly reduced upon IL-2 stimulation in both patients (online suppl. Fig. 1).

The suppression of STAT1 and STAT5 phosphorylation was attributed to enhanced activity of STAT3 in the study by Milner et al. [1]. In our experiments, where only frozen PBMCs instead of Epstein-Barr virus-transformed cell lines were available, we prestimulated the PBMCs with IL-6 for 30 min and for 24 h to activate more STAT3 signalling. After the prestimulation period, STAT5 phosphorylation upon IL-27 stimulation was substantially reduced (Fig. 2). The prestimulation tests were performed only in patient 2, as no more frozen cells were available from the deceased patient 1.

We also examined the gene expression levels of SOCS3, a major downstream target in patient 2. Both basal and

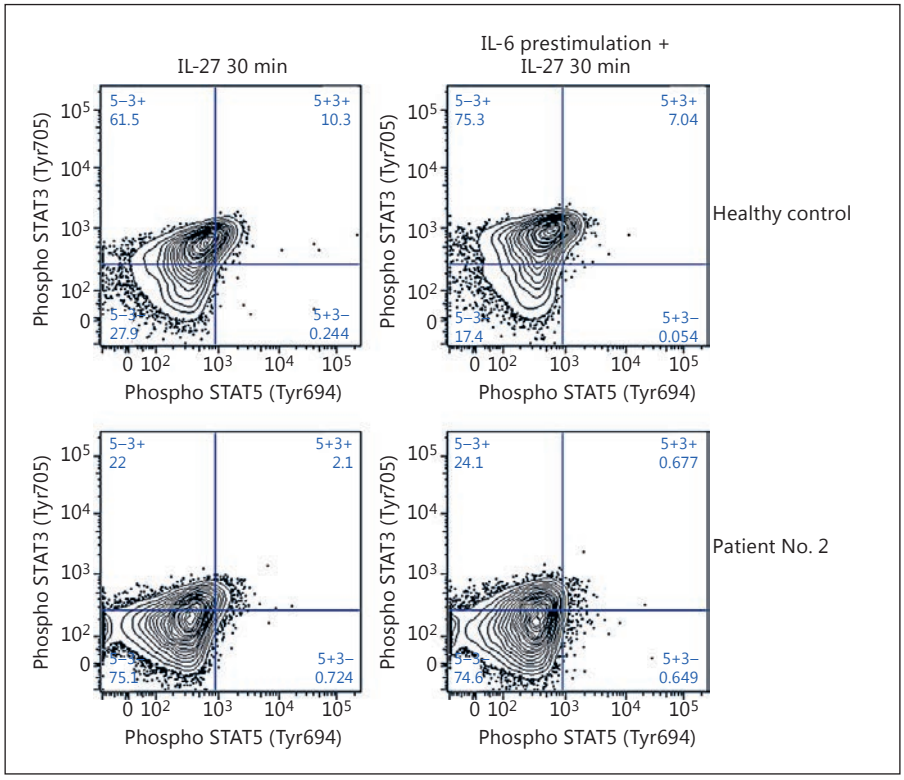

Fig. 2. STAT5 phosphorylation in primary T-cells in response to IL-27 without/with IL-6 prestimulation. Expression of pSTAT5 (Tyr694) in response to IL-27 (100 ng/mL, 30 min) in primary CD3+ T-cells from patient No. 2 (left bottom) was reduced compared to a healthy control (left top). Upon prestimulation with IL-6 (10 ng/mL, 30 min, right) a reduction of the expression of pSTAT5 (Tyr694) in response to IL-27 (100 ng/mL, 30 min) was more pronounced.

stimulated levels of gene expression did not differ from healthy controls (online suppl. Fig. 2). This difference could be caused by the variability of cellular composition and by the effects of immunosuppressive treatment in primary patient samples.

To elucidate the role of the mutation in splicing, we examined the splicing of exons 22 and 23 using primers located in those exons. We observed 2 peaks on the capillary electrophoresis in a healthy control, the shorter one apparently corresponding to the STAT3b variant, which used an alternative acceptor site within the *STAT3* exon 23 [25]. In both patients, there were 2 additional small peaks several base pairs longer than the physiological products, which could possibly show the retention of a small part of the intron in the vicinity of the mutation (online suppl. Fig. 3). However, none of the tools we used predicted any alternative splice site in this region.

Taken together, our results show that the loss-of-function effect of the mutation was highly unlikely and mostly supported the observed clinical phenotype of GOF mutation. In addition, the undetectable IgE levels and low levels of FOXP3+CD25+ Tregs are also completely consistent with published laboratory characteristics in patients carrying a *STAT3* GOF mutation [26].

Discussion

The functional consequences of *STAT3* GOF mutations at the molecular level likely differ according to the localisation of the mutation. Mutations within the DNA binding domain are proposed to enhance DNA binding, which results in prolonged nuclear retention [1]; mutations within the SH domain are proposed to delay dephosphorylation; and mutations within the transactivation domain are proposed to enhance transactivation, which also occurred in our patients. Some mutations were shown to cause constitutive activation of STAT3, whereas other mutations caused only hypersensitivity to interleukin stimulation. This difference does not appear to affect the phenotype, possibly because hypersensitivity to low levels of interleukins is sufficient for persistent activation of the STAT3 pathway [3]. The slightly different splicing of *STAT3* in the patients suggests the possibility of a combined effect of missense GOF mutation and of an altered STAT3 isoform with unknown function. However, deciphering the interplay would require a further extensive study.

At the cellular level, STAT3 activation leads to enhanced transcription of several genes with direct effects

on immune cell differentiation and genes that may affect GH signalling through interactions with other signalling pathways.

Clinically, the patients with *STAT3* GOF mutation described in preceding reports had some similarities to STAT5b-deficient patients. These patients share endocrine abnormalities, such as short stature and recurrent infections and immune disorders [27]. STAT5b is a STAT5 subtype and a crucial mediator of GH-stimulated *IGF1* gene transcription. The mutations of *STAT5b* are well described as causing changes in the GH signalling pathway [27]. Therefore, interactions between STAT3 transcriptional activity and other similar signalling pathways may be expected. Multiple pathophysiological mechanisms of this phenomenon have been suggested. (a) Negative regulation by a STAT3 target: (a1) SOCS3 could influence the activation of several STATs, including STAT5. However, the negative regulation by an increased level of SOCS3 was not detected in all studied samples including ours [28]. Nevertheless, our tested sample could be influenced by ongoing treatment. (a2) Milner et al. [1] demonstrated that cytokine-induced phosphorylation of STAT5 in patients with a *STAT3* GOF mutation was lower than in healthy controls. We also detected slightly impaired cytokine signalling expressed as reduced STAT1 and STAT5 activation upon IFNγ, IL-2, and IL-27 stimulation in patient T-cells. Moreover, when we prestimulated patient cells with IL-6 to overactivate the STAT3 axis, the phosphorylation of STAT5 was almost undetectable. (b) STAT3 and STAT5 are also thought to have direct opposite effects on certain genes. (c) Some authors state that the balance between activated STAT5 and STAT3 and the resulting competition for binding to target gene loci rather than the absolute intensity of their signal has an effect on gene transcription [29]. This process has been shown in the development of autoimmunity and cancer [29]. The above-described interactions between STAT5 and STAT3 signalling would explain the growth impairment in our patient and other patients with *STAT3* GOF mutations.

Previous articles on *STAT3* GOF mutations did not analyse the proband's growth in detail. From the available fragmentary data, probands generally appear to be short at birth, and some of them have overt intrauterine growth restriction. Some authors speculated about the causative impact of foetal insulinopaenia in those who developed diabetes soon after birth; however, that would presume foetal onset of the β-cell autoimmune destruction that had not been proven yet [1–3]. The majority of patients did not experience postnatal catch-up growth, and their growth impairment progressed gradually over time. Other common features include delayed tooth eruption and retarded bone age. Therefore, we considered that dysregulation of the GH-IGF-I axis may be involved.

We aimed to investigate the GH-IGF-I axis using a GH stimulation test and 2 versions of the IGF-I stimulation test. Previously published cases, when tested, had stimulated GH and baseline IGF-I concentrations ranging from normal to low [1]. In our proband and in patient 2, the baseline IGF-I level was repeatedly low, whereas the stimulated GH level in the proband was high. The GH stimulation test had previously been performed in only 2 reported patients [1] and showed low or normal GH levels after stimulation and partial growth response to GH therapy. In our case, we initially documented both the standard IGF-I generation test and a long-term high-dose IGF-I generation test, which demonstrated insufficient responses of IGF-I to GH administration, thus revealing partial GH insensitivity.

To date, 3 patients with *STAT3* GOF mutations have been empirically treated with GH [1]. Two of these patients demonstrated a good response, and 1 patient demonstrated a minimal response to GH therapy. Similar to the immunological findings, the results of GH-IGF-I axis testing and the empiric response to GH therapy differ from case to case. Neither of the 2 patients with *STAT3* GOF mutation, including the 2 patients bearing the exact same mutation, had the same clinical features [1]. Testing for GH treatment responses in patients with *STAT3* GOF mutation may be useful in individual cases.

Conclusion

We presented a case of a patient with a wide range of symptoms, including growth impairment, lymphoproliferation, frequent respiratory tract infections, and multiple early-onset autoimmune disorders, due to a heterozygous germline *STAT3* GOF mutation. Our findings are in agreement with previous reports on the critical role of STAT3 in the development of autoimmune diseases, although we emphasise the effect of STAT3 on the GH axis, leading to partial GH insensitivity. Monogenic causes of autoimmunity provide insight into the pathophysiology of dysregulation of the immune system and may help to develop novel treatments.

Acknowledgment

This paper was supported by a research project of the Agency for Health Care Research, Ministry of Health of the Czech Republic, No. 16-31211A, and by the project for conceptual development of research organisation 00064203/6001 (Ministry of Health of the Czech Republic). E.F. was supported by GBP302/12/G101 from the Grant Agency of the Czech Republic. Instruments and infrastructure were supported by the Ministry of Education, Youth and Sports NPU I No. LO1604.

Disclosure Statement

The authors have not declared any conflicts of interest.

References

1 Milner JD, Vogel TP, Forbes L, Ma CA, Stray-Pedersen A, Niemela JE, et al: Early-onset lymphoproliferation and autoimmunity caused by germline STAT3 gain-of-function mutations. Blood 2015;125:591–600.
2 Flanagan SE, Haapaniemi E, Russell MA, Caswell R, Allen HL, De Franco E, et al: Activating germline mutations in STAT3 cause early-onset multi-organ autoimmune disease. Nat Genet 2014;46:812–814.
3 Haapaniemi EM, Kaustio M, Rajala HLM, van Adrichem AJ, Kainulainen L, Glumoff V, et al: Autoimmunity, hypogammaglobulinemia, lymphoproliferation and mycobacterial disease in patients with activating mutations in STAT3. Blood 2015;125:639–649.
4 Knosp CA, Johnston JA: Regulation of CD4+ T-cell polarization by suppressor of cytokine signalling proteins. Immunology 2012;135:101–111.
5 Levy DE, Darnell JE: Stats: transcriptional control and biological impact. Nat Rev Mol Cell Biol 2002;3:651–662.
6 Nadeau K, Hwa V, Rosenfeld RG: STAT5b deficiency: an unsuspected cause of growth failure, immunodeficiency, and severe pulmonary disease. J Pediatr 2011;158:701–708.
7 Minegishi Y, Saito M, Tsuchiya S, Tsuge I, Takada H, Hara T, et al: Dominant-negative mutations in the DNA-binding domain of STAT3 cause hyper-IgE syndrome. Nature 2007;448:1058–1062.
8 O'Shea JJ, Holland SM, Staudt LM: JAKs and STATs in immunity, immunodeficiency, and cancer. N Engl J Med 2013;368:161–170.
9 Wei L, Laurence A, O'Shea JJ: New insights into the roles of Stat5a/b and Stat3 in T cell development and differentiation. Semin Cell Dev Biol 2008;19:394–400.
10 Barrett JC, Hansoul S, Nicolae DL, Cho JH, Duerr RH, Rioux JD, et al: Genome-wide association defines more than 30 distinct susceptibility loci for Crohn's disease. Nat Genet 2008;40:955–962.
11 Tsoi LC, Spain SL, Knight J, Ellinghaus E, Stuart PE, Capon F, et al: Identification of 15 new psoriasis susceptibility loci highlights the role of innate immunity. Nat Genet 2012;44:1341–1348.
12 Jakkula E, Leppä V, Sulonen AM, Varilo T, Kallio S, Kemppinen A, et al: Genome-wide association study in a high-risk isolate for multiple sclerosis reveals associated variants in STAT3 gene. Am J Hum Genet 2010;86:285–291.
13 Koskela HLM, Eldfors S, Ellonen P, van Adrichem AJ, Kuusanmäki H, Andersson EI, et al: Somatic STAT3 mutations in large granular lymphocytic leukemia. N Engl J Med 2012;366:1905–1913.
14 Furqan M, Akinleye A, Mukhi N, Mittal V, Chen Y, Liu D: STAT inhibitors for cancer therapy. J Hematol Oncol 2013;6:90.
15 Lavecchia A, Di Giovanni C, Novellino E: STAT-3 inhibitors: state of the art and new horizons for cancer treatment. Curr Med Chem 2011;18:2359–2375.
16 Voigt M, Fusch C, Olbertz D, Hartmann K, Rochow N, Renken C, et al: Analyse des Neugeborenenkollektivs der Bundesrepublik Deutschland: 12. Mitteilung: Vorstellung engmaschiger Perzentilwerte (-kurven) für die Körpermasse Neugeborener. Geburtshilfe Frauenheilkd 2006;66:956–970.
17 Kobzova J, Vignerova J, Blaha P, Krejcovsky L, Riedlova J: The 6th nationwide anthropological survey of children and adolescents in the Czech Republic in 2001. Cent Eur J Public Health 2004;12:126–130.
18 Anti-Glutamic Acid Decarboxylase (GAD) ELISA (IgG). Lübeck, Euroimmun, 2007.
19 IA-2 and GAD Autoantibody RIA Kit. Cardiff, RSR Limited, 2011.
20 Elmlinger MW, Kühnel W, Weber MM, Ranke MB: Reference ranges for two automated chemiluminescent assays for serum insulin-like growth factor I (IGF-I) and IGF-binding protein 3 (IGFBP-3). Clin Chem Lab Med 2004;42:654–664.
21 Coutant R, Dorr H-G, Gleeson H, Argente J: Diagnosis of endocrine disease: limitations of the IGF1 generation test in children with short stature. Eur J Endocrinol 2012;166:351–357.
22 Pruhova S, Dusatkova P, Sumnik Z, Kolouskova S, Pedersen O, Hansen T, Cinek O, Lebl J: Glucokinase diabetes in 103 families from a country-based study in the Czech Republic: geographically restricted distribution of two prevalent GCK mutations. Pediatr Diabetes 2010;11:529–535.
23 Wang R, Cherukuri P, Luo J: Activation of Stat3 sequence-specific DNA binding and transcription by p300/CREB-binding protein-mediated acetylation. J Biol Chem 2005;280:11528–11534.
24 Cartegni L, Wang J, Zhu Z, Zhang MQ, Krainer AR: ESEfinder: a web resource to identify exonic splicing enhancers. Nucleic Acids Res 2003;31:3568–3571.
25 Schaefer TS, Sanders LK, Park OK, Nathans D: Functional differences between Stat3alpha and Stat3beta. Mol Cell Biol 1997;17:5307–5316.
26 Johnson MB, Flanagan SE, Martins TB, Hill HR, Hattersley AT, McDonald TJ: Low IgE is a useful tool to identify STAT3 gain-of-function mutations. Clin Chem 2016;62:1536–1538.
27 Kofoed EM, Hwa V, Little B, Woods KA, Buckway CK, Tsubaki J, Pratt KL, Bezrodnik L, Jasper H, Tepper A, Heinrich JJ, Rosenfeld RG: Growth hormone insensitivity associated with a STAT5b mutation. N Engl J Med 2003;349:1139–1147.
28 Palmer DC, Restifo NP: Suppressors of cytokine signaling (SOCS) in T cell differentiation, maturation, and function. Trends Immunol 2009;30:592–602.
29 Yang X-P, Ghoreschi K, Steward-Tharp SM, Rodriguez-Canales J, Zhu J, Grainger JR, et al: Opposing regulation of the locus encoding IL-17 through direct, reciprocal actions of STAT3 and STAT5. Nat Immunol 2011;12:247–254.

Supplementary Material

Short stature in a boy with multiple early-onset autoimmune conditions due to a STAT3 activating mutation: Could intracellular growth hormone signalling be compromised?

Methods:

Phosphoflow

Thawed peripheral blood mononuclear cells (PBMCs) were re-suspended in RPMI 1640 with L-glutamine, 25 mM HEPES, 100 U/mL penicillin, and 100 mg/mL streptomycin (Lonza, Basel, Switzerland) supplemented with 10% heat-inactivated foetal bovine serum (Thermo Fisher Scientific, Rockford, IL, USA). They rested in a 37°C, 5% CO2, fully humidified incubator for 1 hour; afterwards, they were washed with serum-free RMPI 1640 with L-glutamine, 25 mM HEPES, 100 U/mL penicillin, and 100 mg/mL streptomycin (Lonza) and stimulated with IL-6 (10 ng/mL), IL-2 (100 ng/mL), INFγ (500 ng/mL), and IL-27 (100 ng/mL) (all from Sigma Aldrich, St. Louis, MO, USA) for the indicated time points at 37°C. After stimulation, the cells were fixed with 4% methanol-free formaldehyde (Sigma-Aldrich) for 10 minutes at room temperature, washed in PBS, re-suspended in 90% ice-cold methanol and incubated overnight in -20°C. Cells were then stained with fluorochrome-conjugated antibodies: anti-phospho-STAT3 (Tyr705) Alexa 488, anti-phospho-STAT1 (Tyr701) Alexa 647, and anti-phospho-STAT5 (Tyr694) PE (all from BD Biosciences, San Jose, CA, USA), anti-phospho-STAT1 (Tyr701) PE (Cell Signalling Technologies, Danvers, MA, USA), together with anti-CD45 Pacific Blue and anti-CD3 APC (Exbio Praha, Vestec, Czech Republic) or anti-CD3 PE-Cy7 (Beckman Coulter, Miami, FL, USA). The data were collected with an LSR II flow cytometer (BD Biosciences) and analysed with FlowJo software (Treestar, Ashland, OR, USA).

Real-time quantitative RT-PCR

Thawed PBMCs were re-suspended in RPMI 1640 with L-glutamine, 25 mM HEPES, 100 U/mL penicillin, and 100 mg/mL streptomycin (Lonza) supplemented with 10% heat-inactivated foetal bovine serum (Thermo Fisher Scientific). They rested in a 37°C, 5% CO2, fully humidified incubator for 1 hour; afterwards, they were stimulated with IL-6 (50 ng/mL) (Sigma Aldrich) for 40 hours at 37°C and 5% CO2. After stimulation, the cells were washed in PBS and mRNA was extracted using RNeasy Plus Micro Kit (QIAGEN) and reverse transcribed with iScript *cDNA synthesis kit* (Bio-Rad). Suppressor of cytokine signalling 3 (*SOCS3*) transcript was measured by real-time quantitative reverse transcription-polymerase chain reaction using TaqMan® Gene Expression Assay (Life Technologies). Results represent the fold-change compared with unstimulated healthy control after normalisation to endogenous *GAPDH* gene expression levels.

STAT3 mRNA splicing

The cDNA from patients and one healthy control (before stimulation) was used for the analysis of exons 22 and 23 splicing with the primers located in the 5' region of exon 22 (5': GCGCTGCCCCATACCTGAA) and in the 3' region of exon 23: (5':TCAGCAGGAGGGCAGTTTG). PCR products were analysed with a chip-based Agilent Bioanalyser (Agilent Technologies).

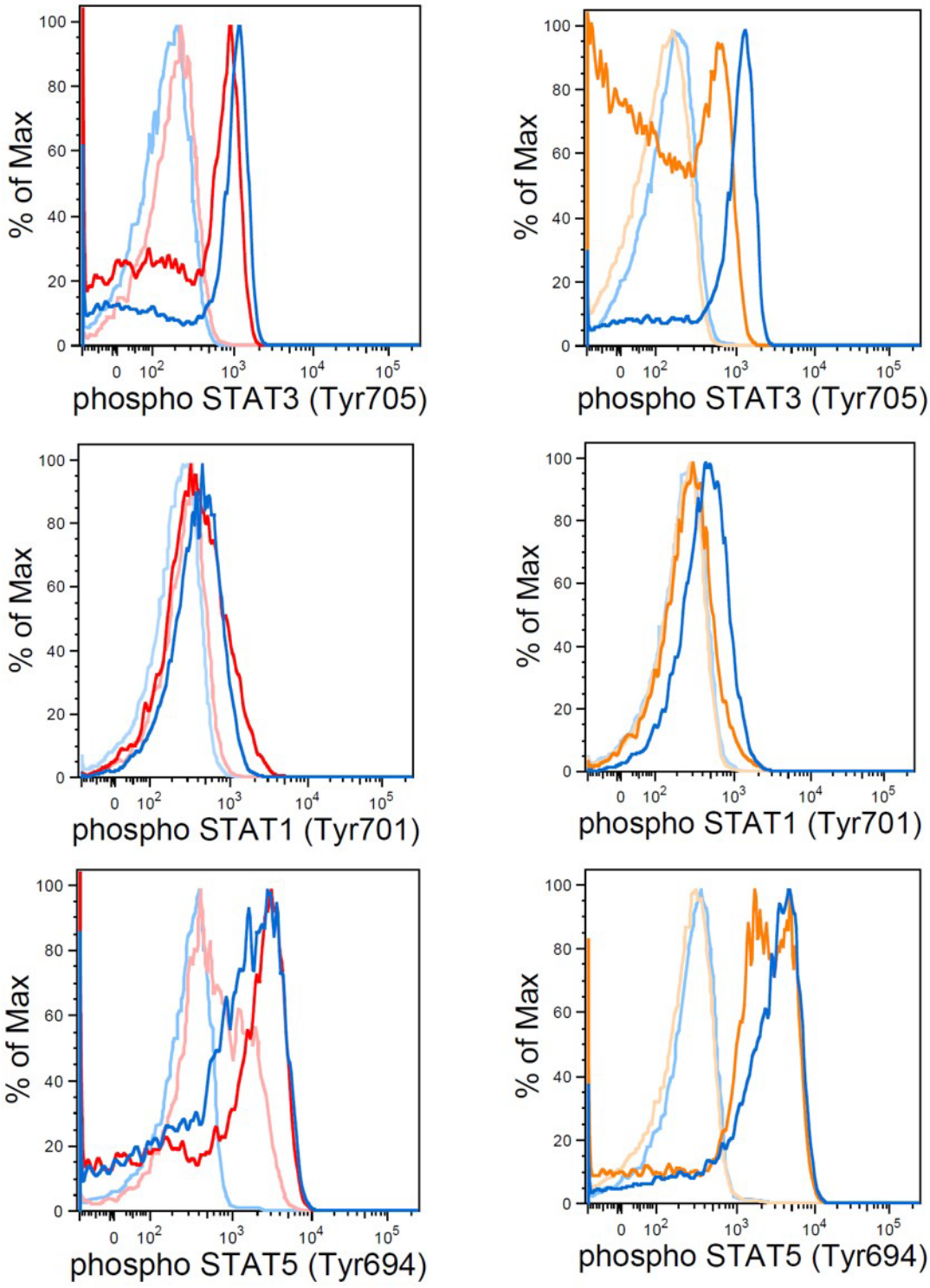

Supplementary Figure 1: STAT3, STAT1 and STAT5 phosphorylation in primary T-cells in response to IL-6, IFNγ, and IL-2. Expression of pSTAT3 (Tyr705), pSTAT1 (Tyr701), and pSTAT5 (Tyr694) measured by flow cytometry in primary CD3+ T-cells from Patient #1 (red) and Patient #2 (orange) was slightly reduced compared to healthy controls (blue). Numbers represent the change in mean intensity fluorescence (MFI) between non-

stimulated (light) and stimulated (dark) cells after 15 min stimulation with IL-6 (10 ng/mL), IFNγg (500 ng/mL), and IL-2 (100 ng/mL). In patient #2, data are representative of two independent experiments.

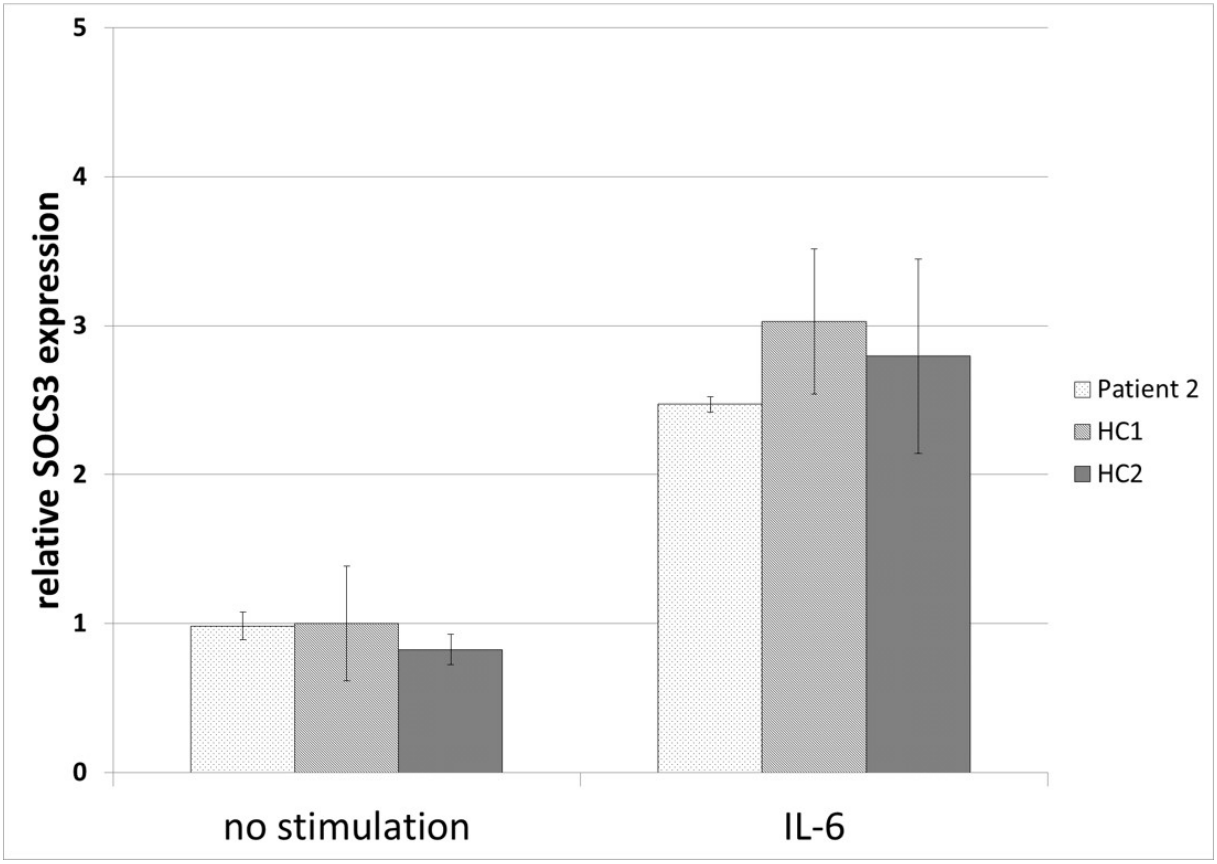

Supplementary Figure 2: SOCS3 gene expression in PBMCs. Expression of SOCS3 was measured by quantitative RT-PCR in thawed primary PBMCs of one patient and two healthy controls without stimulation and after IL-6 stimulation (50 ng/ml, 40 hours). Results represent mean relative expression of SOCS3 compared to one healthy control after normalisation to the expression of GAPDH. Error bars represent 1 SD.

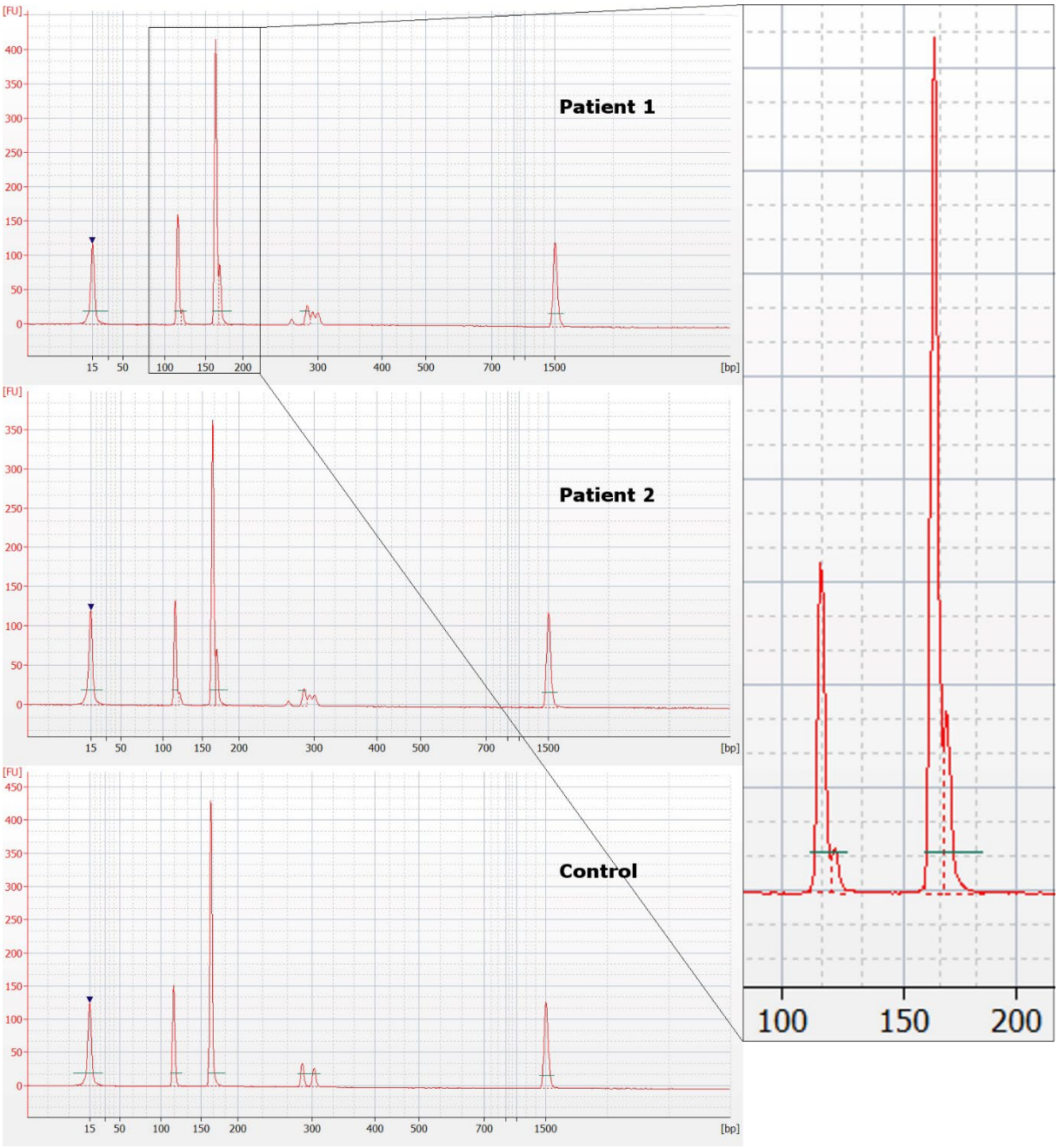

Supplementary Figure 3: The effect of STAT3 c.2144C>T mutation on the splicing of exons 22 and 23. The 15 and 1500 bp peaks are size markers, the shorter PCR product likely corresponds to STAT3β variant, which uses an alternative acceptor site within STAT3 exon 23. In both patients, there were two additional small peaks several bp longer than physiological products, which can possibly show the retention of a small part of the intron in the vicinity of the mutation.

Příloha 2

Svaton M*, Skvarova Kramarzova K*, Kanderova V, Mancikova A, Smisek P, Jesina P, Krijt J, Stiburkova B, Dobrovolny R, Sokolova J, Bakardjieva-Mihaylova V, Vodickova E, Rackova M, Stuchly J, Kalina T, Stary J, Trka J, Fronkova E*, Kozich V*. A homozygous deletion in the SLC19A1 gene as a cause of folate-dependent recurrent megaloblastic anemia. *Blood.* 2020 Jun 25;135(26):2427-2431. doi: 10.1182/blood.2019003178.

Authorship

Contribution: W.Z. collected and analyzed the data and wrote the manuscript; Y.Z. designed and supervised the study, analyzed the data, and revised the manuscript; B.H., L.J., J.Y., J.D., S.W., and Y.L. collected the data and critically discussed the manuscript; C.Z. and Z.G. performed IHC and analyzed data; B.D. headed the CAR-T generation team; and A.H.C. provided CAR-T technique and support.

Conflict-of-interest disclosure: A.H.C. is a founding member of Shanghai YaKe Biotechnology Ltd., a biotechnology company focusing on research and development of tumor cellular immunotherapy. The remaining authors declare no competing financial interests.

Correspondence: Yonghong Zhang, Department of Pediatric Lymphoma, Beijing Boren Hospital; Department of Hematology Oncology, National Center for Children's Health, Beijing Children's Hospital, Capital Medical University, Beijing 100070, China; e-mail: zhangyongh@borenhospital.com.

Footnotes

For original data, please contact the corresponding author.

The online version of this article contains a data supplement.

REFERENCES

1. Molyneux EM, Rochford R, Griffin B, et al. Burkitt's lymphoma. *Lancet*. 2012;379(9822):1234-1244.
2. Pagano L, Caira M, Valentini CG, Fianchi L. Clinical aspects and therapy of sporadic burkitt lymphoma. *Mediterr J Hematol Infect Dis*. 2009;1(2): e2009030.
3. Egan G, Goldman S, Alexander S. Mature B-NHL in children, adolescents and young adults: current therapeutic approach and emerging treatment strategies. *Br J Haematol*. 2019;185(6):1071-1085.
4. Minard-Colin V, Auperin A, Pillon M, et al. Results of the randomized Intergroup trial Inter-B-NHL Ritux 2010 for children and adolescents with high-risk B-cell non-Hodgkin lymphoma (B-NHL) and mature acute leukemia (B-AL): Evaluation of rituximab (R) efficacy in addition to standard LMB chemotherapy (CT) regimen [abstract]. *J Clin Oncol*. 2016;34(15). Abstract 10507.
5. Cairo M, Auperin A, Perkins SL, et al. Overall survival of children and adolescents with mature B cell non-Hodgkin lymphoma who had refractory or relapsed disease during or after treatment with FAB/LMB 96: a report from the FAB/LMB 96 study group. *Br J Haematol*. 2018;182(6):859-869.
6. Porter DL, Levine BL, Kalos M, Bagg A, June CH. Chimeric antigen receptor-modified T cells in chronic lymphoid leukemia. *N Engl J Med*. 2011;365(8):725-733.
7. Maude SL, Frey N, Shaw PA, et al. Chimeric antigen receptor T cells for sustained remissions in leukemia. *N Engl J Med*. 2014;371(16):1507-1517.
8. Neelapu SS, Locke FL, Bartlett NL, et al. Axicabtagene ciloleucel CAR T-cell therapy in refractory large B-cell lymphoma. *N Engl J Med*. 2017; 377(26):2531-2544.
9. Schuster SJ, Svoboda J, Chong EA, et al. Chimeric antigen receptor T cells in refractory B-cell lymphomas. *N Engl J Med*. 2017;377(26):2545-2554.
10. Avigdor A, Shouval R, Jacoby E, et al. CAR T cells induce a complete response in refractory Burkitt lymphoma. *Bone Marrow Transplant*. 2018; 53(12):1583-1585.
11. Rivers J, Annesley C, Summers C, et al. Early response data for pediatric patients with non-Hodgkin lymphoma treated with CD19 chimeric antigen receptor (CAR) T-cells [abstract]. *Blood*. 2018;132(suppl 1). Abstract 2957.
12. Cheson BD, Pfistner B, Juweid ME, et al; International Harmonization Project on Lymphoma. Revised response criteria for malignant lymphoma. *J Clin Oncol*. 2007;25(5):579-586.
13. Pan J, Yang JF, Deng BP, et al. High efficacy and safety of low-dose CD19-directed CAR-T cell therapy in 51 refractory or relapsed B acute lymphoblastic leukemia patients. *Leukemia*. 2017;31(12):2587-2593.
14. Pan J, Niu Q, Deng B, et al. CD22 CAR T-cell therapy in refractory or relapsed B acute lymphoblastic leukemia. *Leukemia*. 2019;33(12): 2854-2866.
15. Lee DW, Gardner R, Porter DL, et al. Current concepts in the diagnosis and management of cytokine release syndrome [published correction appears in *Blood*. 2015;126(8):1048]. *Blood*. 2014;124(2):188-195.
16. Neelapu SS, Tummala S, Kebriaei P, et al. Chimeric antigen receptor T-cell therapy - assessment and management of toxicities. *Nat Rev Clin Oncol*. 2018;15(1):47-62.
17. Yang ZZ, Grote DM, Ziesmer SC, et al. Soluble IL-2Rα facilitates IL-2-mediated immune responses and predicts reduced survival in follicular B-cell non-Hodgkin lymphoma. *Blood*. 2011;118(10):2809-2820.
18. Shah NN, Maatman T, Hari P, Johnson B. Multi targeted CAR-T cell therapies for B-cell malignancies. *Front Oncol*. 2019;9:146.

DOI 10.1182/blood.2019002008

TO THE EDITOR:

A homozygous deletion in the *SLC19A1* gene as a cause of folate-dependent recurrent megaloblastic anemia

Michael Svaton,[1,*] Karolina Skvarova Kramarzova,[1,*] Veronika Kanderova,[1] Andrea Mancikova,[2] Petr Smisek,[3] Pavel Jesina,[4] Jakub Krijt,[4] Blanka Stiburkova,[4,5] Robert Dobrovolny,[4] Jitka Sokolova,[4] Violeta Bakardjieva-Mihaylova,[1] Elena Vodickova,[6] Marketa Rackova,[1] Jan Stuchly,[1] Tomas Kalina,[1] Jan Stary,[3] Jan Trka,[1] Eva Fronkova,[1,†] and Viktor Kozich[4,†]

[1]Childhood Leukemia Investigation Prague, Department of Pediatric Hematology and Oncology, Second Faculty of Medicine, Charles University and University Hospital Motol, Prague, Czech Republic; [2]Department of Cell Biology, Faculty of Science, Charles University, Prague, Czech Republic; [3]Department of Pediatric Hematology and Oncology, Second Faculty of Medicine, Charles University and University Hospital Motol, Prague, Czech Republic; [4]Department of Pediatrics and Adolescent Medicine, First Faculty of Medicine, Charles University and General University Hospital, Prague, Czech Republic; [5]Institute of Rheumatology, Prague, Czech Republic; and [6]Department of Clinical Hematology, University Hospital Motol, Prague, Czech Republic

Megaloblastic anemia resulting from ineffective hematopoiesis in the bone marrow (BM) is one of the main hematologic signs of folate or vitamin B_{12} deficiency. Functional deficiencies of these 2 vitamins originate from nutritional, gastrointestinal, or genetic factors, and their clinical symptoms result from the impaired synthesis of nucleotides in hematopoietic cells and S-adenosylmethionine in the nervous system.[1] Folates are pteroyl(poly)glutamate derivatives with various 1-carbon moieties at the pterine ring, with

Table 1. Laboratory markers during the second episode of anemia

Markers	Biological material	Reference range	Before treatment with folic acid*	With folic acid treatment†
Blood count				
Hemoglobin, g/L		135-175	**61-99**	131
Red blood cells $\times 10^{12}$/L		4-5.8	**2.02-3.21**	4.34
Hematocrit, %		40-50	**17.1-30.4**	41
Mean cell volume, fL		82-98	82.1-97.3	94.5
Reticulocytes, %		0.5-2.5	0.62-**3.71**	0.52
Routine biochemistry				
Bilirubin, μmol/L	Serum	2-17	**42.2-60.6**	17.4
Lactate dehydrogenase, μkat/L	Serum	1.67-3.17	**13.38-115.66**	2.6
Ferritin, μg/L	Serum	17-304	**413.2-954.8**	**1036.3**
Iron, μmol/L	Serum	7.2-29	**49.4-50.5**	**6.7**
B vitamins and related metabolites				
Folate, nmol/L	Serum	4.53-21.5	7.3-14.3	***>45***
Folate, nmol/L	Erythrocytes	1185-2841	**1155.2**	2175.4
Vitamin B_{12}, ng/L	Serum	197-771	**138-*2000***	***866***
Holotranscobalamin II, pmol/L	Serum	19-119	44	**151**
Total homocysteine, μmol/L	Plasma	5.2-11.3	**31.5 to ≥50**	9.49
Cystathionine, nmol/L	Plasma, serum	80-1000	187-217	99
Methionine, μmol/L	Plasma, serum	12-40	26-27	17
Sarcosine, μmol/L	Plasma, serum	0.7-3	**5.2**	1.85
Methylmalonic acid, nmol/L	Plasma	<270	136.8	204.5
Methylmalonic acid, mmol/mol creatinine	Urine	<15	<15	<15
AICAr, mmol/mol creatinine	Urine	0.04-1.01	**1.87**	0.18

Levels out of reference range are shown in bold; supraphysiological concentrations resulting from administration of respective vitamins are shown in italics.

*Ranges with the minimal and maximal observed levels during the period in which therapy with cyanocobalamin only was administered (days 1155-1414; single values are from day 1261).

†The levels at follow-up of 1 month of combined cyanocobalamin and folic acid therapy (day 1444, 3 days after the last cyanocobalamin injection).

the major circulating form being 5-methyltetrahydrofolate. Folates are delivered to tissues by at least 5 transporters with different kinetic properties and variable expression.[2,3] Two inherited disorders in folate transport, hereditary folate malabsorption and cerebral folate deficiency resulting from mutations in the *SLC46A1*[4] and *FOLR1*[5] genes, have been reported in humans.

Reduced folate carrier (RFC; FOLT1) is encoded by the *SLC19A1* gene and facilitates the cellular uptake of anionic folates,[6] of folate analogs such as methotrexate (MTX), and 2′3′-cyclic-GMP-AMP, a second messenger that activates the antiviral stimulator of interferon genes pathways.[7] Loss of its function leads to MTX resistance in cancer cells.[8,9] A murine model of RFC deficiency showed embryonic lethality before E9.5. These mice could be partially rescued by supplementing the pregnant dams with folic acid; however, all liveborn mice died within 12 days because of the absence of hematopoiesis in BM, spleen, and liver.[10] To our knowledge, no inherited disease caused by loss-of-function mutations in the *SLC19A1* gene has been described in humans.

In our study, we presented the first case of recurrent severe megaloblastic anemia in a patient with a homozygous *SLC19A1* mutation. The patient's history was unremarkable with normal growth and development until age 15 years, when he presented with the first episode of severe anemia (hemoglobin [Hb], 5 g/dL), mild hemolysis, hyperhomocysteinemia of 34.7 μmol/L, low total vitamin B_{12} levels of 138 ng/L, and normal serum folates of 10.7 nmol/L. He denied having any bleeding, limb numbness, any other neurologic symptoms, or symptoms of glossitis. He reported poor eating habits with decreased intake of food for 6 months preceding his presentation, avoidance of vegetables, and avoidance of morning meals. He responded well to treatment with cyanocobalamin and folate, but he returned at age 17 years with a second episode of severe anemia (Hb, 7.8 g/dL) and signs of hemolysis with elevated bilirubin (46 μmol/L), hyperhomocysteinemia, and low total vitamin B_{12} levels (for laboratory and clinical details, see Table 1 and supplemental Data, available on the *Blood* Web site). BM aspiration showed 48% megaloblastic erythroid precursors with dysplastic signs, and the peripheral blood smear revealed sporadic macro-ovalocytes, frequent schistocytes, and hypersegmented neutrophils (supplemental Figure 1). Flow cytometry of the BM showed abundant erythropoietic precursors. Despite parenteral cyanocobalamin therapy, anemia and hyperhomocysteinemia persisted. The laboratory abnormalities and clinical signs normalized within a month but only after adding folic acid (10 mg/day) to the patient's therapy. In contrast, carefully monitored withdrawal of folic acid resulted in an immediate increase in homocysteine to levels of 17 to 31 μmol/L, despite persisting normal folate levels in serum (Figure 1A).

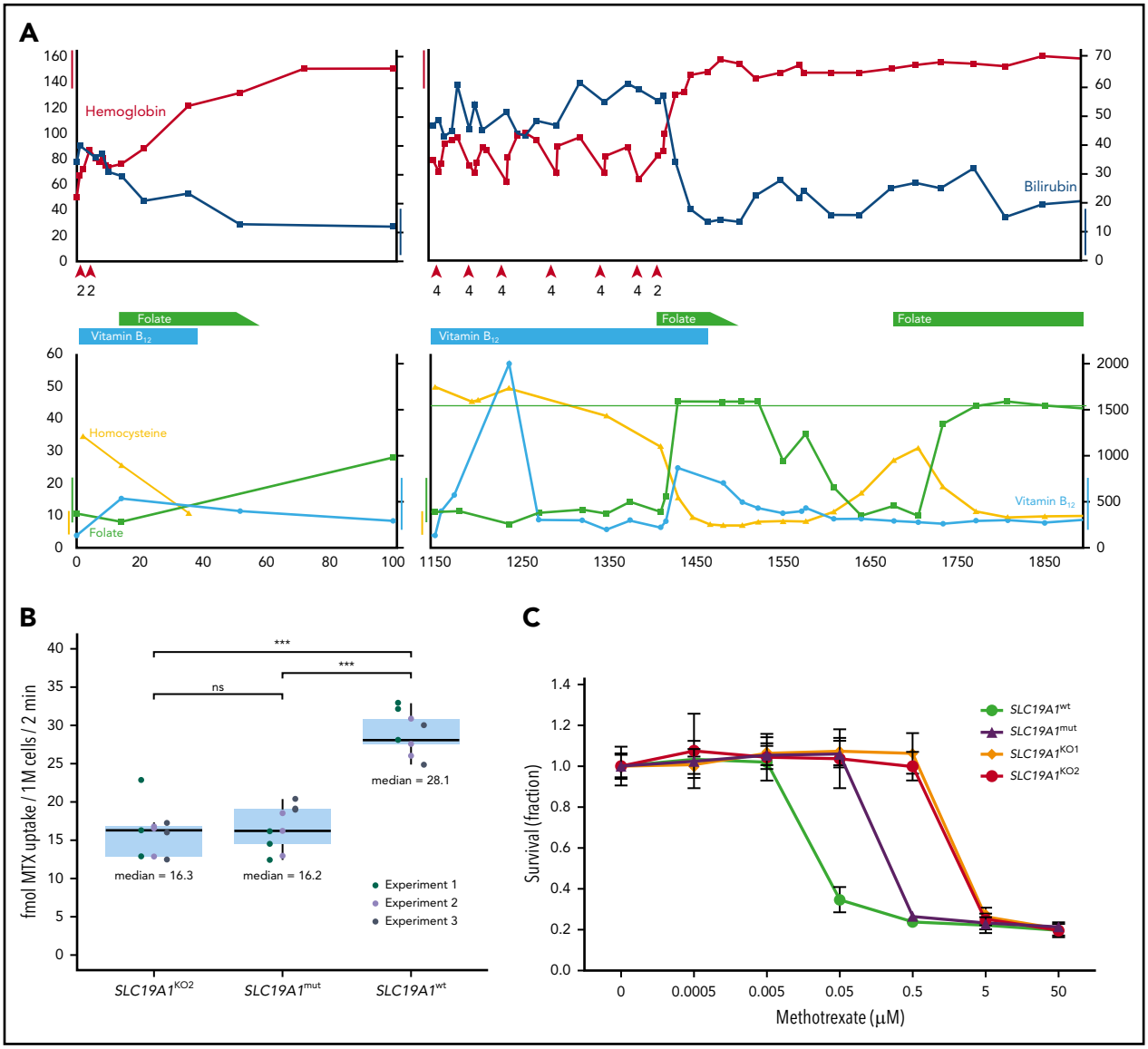

Figure 1. Course of patient's disease and functional evaluation of the *SLC19A1* mutation. (A) The graphs show the results of laboratory tests obtained after the patient's first and second disease attacks and the course of treatment. The x-axis represents days from his first hospital admission (interrupted for a period between day 100 and 1150, when he was monitored in the outpatient department, and laboratory results were normal). The hemoglobin levels (g/L; red) are plotted on the left y-axis, and total bilirubin (μmol/L; blue) is plotted on the right y-axis. The serum folate levels (nmol/L; green) are plotted in the lower part of the graph, with homocysteine (μmol/L; orange) on the left y-axis and vitamin B_{12} levels (ng/L; blue) on the right y-axis. Reference ranges are marked by bars in the corresponding colors on both axes. Treatment is indicated between both graphs, with erythrocyte transfusions marked by red arrows and the number of units given. (B) MTX uptake assay into wild-type and monoclonal gene-edited K562 model cell lines. The graph shows the amount of [3H]MTX per 1 million cells after 2-minute incubation with 0.5 μmol/L [3H]MTX. MTX uptake into the *SLC19A1*^{KO} and *SLC19A1*^{mut} cells was significantly decreased in comparison with the *SLC19A1*^{wt}. The data points were obtained from 3 independent experiments (each with 3 technical replicates) and tested by two-way analysis of variance with Bonferroni corrections; horizontal lines in the boxplots indicate medians and the 25th and 75th percentiles. (C) Sensitivity of wild-type and monoclonal gene-edited K562 model cell lines to MTX. Cell proliferation assays of the K562 cell lines with CRISPR/Cas9 introduced homozygous (*SLC19A1*^{mut}) mutation found in the patient compared with a wild-type control and to a complete *SLC19A1* KO (2 representative clones carrying different frameshift mutations). The assay was performed in 3 separate experiments, each of which was performed in 6 replicates. The results are shown as the mean and standard deviation of all values, which were normalized to the appropriate controls in each experiment. ns, not significant. ***$P < .001$.

Whole exome sequencing revealed a homozygous 3bp deletion, c.634_636delTTC (rs757838708), in the *SLC19A1* gene inherited from heterozygous parents. This variant leads to a deletion of phenylalanine residue 212 (p.Phe212del) located in a highly conserved Lys204-Arg214 peptide sequence that is crucial for the function of RFC[11] (supplemental Figure 2).

To test the pathogenicity of the p.Phe212del mutation, we generated a model system using genome-editing techniques to produce a monoclonal homozygous *SLC19A1*^{mut} K562 cell line and 2 clones with full *SLC19A1* gene knockouts (KOs) as a result of frameshift mutations (supplemental Figure 4C-D). First, we tested the capacity of the mutated RFC protein to transport radioactively labeled MTX into cells. The ability of the *SLC19A1*^{mut} clone to transport MTX into K562 cells was significantly decreased by ~42% compared with the *SLC19A1*^{wt} clone ($P < .001$), and it was similar to that of the *SLC19A1*^{KO} clone (Figure 1B). The residual MTX transport into *SLC19A1*^{mut} and *SLC19A1*^{KO} cells

represents the capacity of all other endogenously expressed folate transporters[12] with the exception of RFC. Confocal microscopy using a monoclonal anti-RFC antibody showed the presence of antigen in the *SLC19A1*^{mut} clone, which indicated sufficient (although slightly decreased) expression of the p.Phe212del mutant (supplemental Figure 5). Next, we examined the resistance of these cell lines to the cytotoxic effects of MTX. As expected, the homozygous *SLC19A1*^{mut} clone showed an increased resistance to MTX compared with the *SLC19A1*^{wt} cells (50% inhibitory concentration [IC_{50}], 0.287 vs 0.036 μM). However, the IC_{50} of the *SLC19A1*^{mut} clone was still about an order of magnitude lower compared with that of the 2 clones with a complete *SLC19A1* KO (IC_{50}, 3.078 and 1.681 μM; Figure 1C). In summary, these experiments clearly and congruently showed that homozygous deletion of the Phe212 residue impairs transport of MTX and increases the resistance of genetically modified cells to this cytotoxic anti-folate drug, which uses RFC to enter the cells.

This patient presented a diagnostic conundrum that was resolved owing to next-generation sequencing analysis. The biochemical findings at the beginning of both episodes of anemia were dominated by low concentrations of serum vitamin B_{12}, probably caused by poor nutrition and/or increased demand for cobalamin in the remethylation pathway. The absence of serum folate deficiency obscured the role of folates in the patient's anemia; however, folates were decreased in erythrocytes in the single analysis performed when the patient was not treated with folic acid. The classical metabolic consequences of folate deficiency such as decreased serum methionine and increased cystathionine were not present, but there was markedly increased total homocysteine and sarcosine in blood and the purine de novo synthesis intermediate 5-amino-4-imidazolecarboxamide riboside (AICAr) in urine,[13-15] as well as their normalization only after introducing folic acid treatment, which strongly indicates a functional folate deficiency in tissues.[13,16]

The episodic clinical course in the patient was milder than that observed in the KO mouse model.[10] Because of the existence of multiple folate transporters and their complex biology,[2] it is conceivable that under conditions of normal dietary folate intake, the other folate transporters may compensate for the impaired RFC transport activity.[17] Indeed, an increased expression of the *SLC46A1* and *FOLR2* genes (7- to 14-fold messenger RNA increase in the patient compared with healthy controls) was observed in the patient's bone marrow as well as in the gene-edited mutant and KO K562 cells (supplemental Figure 6). These data indicate a grossly increased total capacity of alternative (albeit less kinetically favorable) folate transporters that may compensate for the impaired function of the p.Phe212del RFC under conditions of sufficient folate intake and moderate cellular needs (see supplemental Results). However, inadequate folate intake combined with increased demand for folates reported in adolescent males[18,19] may have contributed to episodes of anemia in our patient.

Our study describes the first human patient with recurrent megaloblastic folate–dependent anemia resulting from a homozygous p.Phe212del mutation in the *SLC19A1* gene. Several lines of evidence support the causal role of this mutation in the pathogenesis of anemia in this patient. First, the role of RFC in hematopoietic cells was clearly demonstrated in a KO mouse model.[10] Second, the low frequency of this mutation in available population databases (see supplemental Results) and its location in the conserved cytosolic loop of RFC supports the hypothesis of its pathogenicity. Third, detailed functional testing in CRISPR/Cas9-edited K562 cells clearly showed the decreased ability of the mutant protein to transport 5-methyltetrahydrofolate analog MTX; because of the intrinsic limitations of the cellular transport studies, the degree of functional impairment could not be exactly quantitated and some residual activity of p.Phe212del RFC cannot be ruled out. Fourth, the clinical observation of severe anemia with megaloblastic changes in the patient's BM suggestive of impaired maturation and ineffective hematopoiesis as well as the signs of demyelination on electromyography are indeed compatible with clinically significant tissue folate deficiency. Finally, the reversal of anemia and rapid drop of total homocysteine and AICAr concentration only after the addition of folic acid to cyanocobalamin therapy during the second episode is typical for folate deficiency.[20]

In summary the above data support the key role of defective folate transport to hematopoietic cells in the development of anemia in this patient. We propose that there may be additional individuals with germline mutations in *SLC19A1*; however, their phenotypes could be masked either by mandatory folate fortification or by the commonly used combined treatment with vitamin B_{12} and folic acid in those with unresolved megaloblastic anemia without properly elucidated primary cause.

Acknowledgments

This work was supported in part by grant no. 17-04941Y from the Czech Science Foundation (K.S.K. and M.S.), grants no. PRIMUS/19/MED/004 (K.S.K. and M.R.) and no. GAUK 502119 (M.R.) from Charles University, and grants no. NV18-07-00430 (E.F. and J. Stary) and no. NV19-01-00307 (V. Kozich) from the Czech Health Research Council. Institutional support was provided by programs 00064203 (University Hospital Motol, Prague, Czech Republic), RVO-VFN 64165 (General University Hospital in Prague), RVO 00023728 (Institute of Rheumatology), Progress Q26 (Charles University), ERDF OPPK CZ.2.16/3.1.00/28007, and CZ.2.16/3.1.00/24505. The research infrastructure was supported by program LO1604 (Ministry of Education, Youth and Sports, Czech Republic).

Authorship

Contribution: M.S., K.S.K., and B.S. performed and planned the research, analyzed and interpreted the data, and wrote the manuscript; V. Kanderova, V.B.-M., E.V., A.M., J.K., M.R., R.D., J. Sokolova, J. Stuchly, and T.K. performed the research and analyzed the data; P.S. and P.J. collected and interpreted the data and clinically evaluated the patient; E.F., V. Kozich, J.T. and J. Stary designed the study and wrote the paper; and all authors revised the paper and approved the final version.

Conflict-of-interest disclosure: The authors declare no competing financial interests.

ORCID profiles: M.S., 0000-0003-2966-3687; K.S.K., 0000-0003-4860-7453; A.M., 0000-0003-4487-1943; J.K., 0000-0002-1738-654X; B.S., 0000-0003-2465-1476; R.D., 0000-0003-0081-156X; J. Sokolova, 0000-0002-0453-3336; T.K., 0000-0003-4475-2872; E.F., 0000-0002-6900-8145; V. Kozich, 0000-0001-5820-5277.

Correspondence: Viktor Kozich, Department of Pediatrics and Adolescent Medicine, First Faculty of Medicine, Charles University and General University Hospital, Ke Karlovu 455/2, 128 08 Prague 2, Czech Republic; e-mail: viktor.kozich@vfn.cz; and Eva Fronkova, Childhood Leukemia Investigation Prague, Department of Pediatric Hematology and Oncology, Second Faculty of Medicine, Charles University and University

Hospital Motol, V Uvalu 84, 150 06 Prague 5, Czech Republic; e-mail: eva.fronkova@lfmotol.cuni.cz.

Footnotes

*M.S. and K.S.K. contributed equally to this article as joint first authors.

†E.F. and V. Kozich contributed equally to this article as joint senior authors.

For original data, please contact michael.svaton@lfmotol.cuni.cz.

The online version of this article contains a data supplement.

REFERENCES

1. Newman AC, Maddocks ODK. One-carbon metabolism in cancer. *Br J Cancer*. 2017;116(12):1499-1504.
2. Alpers DH. Absorption and blood/cellular transport of folate and cobalamin: Pharmacokinetic and physiological considerations. *Biochimie*. 2016;126:52-56.
3. Whetstine JR, Flatley RM, Matherly LH. The human reduced folate carrier gene is ubiquitously and differentially expressed in normal human tissues: identification of seven non-coding exons and characterization of a novel promoter. *Biochem J*. 2002;367(pt 3):629-640.
4. Qiu A, Jansen M, Sakaris A, et al. Identification of an intestinal folate transporter and the molecular basis for hereditary folate malabsorption. *Cell*. 2006;127(5):917-928.
5. Steinfeld R, Grapp M, Kraetzner R, et al. Folate receptor alpha defect causes cerebral folate transport deficiency: a treatable neurodegenerative disorder associated with disturbed myelin metabolism. *Am J Hum Genet*. 2009;85(3):354-363.
6. Matherly LH, Hou Z, Deng Y. Human reduced folate carrier: translation of basic biology to cancer etiology and therapy. *Cancer Metastasis Rev*. 2007;26(1):111-128.
7. Ritchie C, Cordova AF, Hess GT, Bassik MC, Li L. SLC19A1 Is an Importer of the Immunotransmitter cGAMP. *Mol Cell*. 2019;75(2):372-381.e5.
8. Zhao R, Sharina IG, Goldman ID. Pattern of mutations that results in loss of reduced folate carrier function under antifolate selective pressure augmented by chemical mutagenesis. *Mol Pharmacol*. 1999;56(1):68-76.
9. Zhao R, Goldman ID. Resistance to antifolates. *Oncogene*. 2003;22(47):7431-7457.
10. Zhao R, Russell RG, Wang Y, et al. Rescue of embryonic lethality in reduced folate carrier-deficient mice by maternal folic acid supplementation reveals early neonatal failure of hematopoietic organs. *J Biol Chem*. 2001;276(13):10224-10228.
11. Liu XY, Witt TL, Matherly LH. Restoration of high-level transport activity by human reduced folate carrier/ThTr1 thiamine transporter chimaeras: role of the transmembrane domain 6/7 linker region in reduced folate carrier function. *Biochem J*. 2003;369(pt 1):31-37.
12. Biswal BK, Verma RS. Differential usage of the transport systems for folic acid and methotrexate in normal human T-lymphocytes and leukemic cells. *J Biochem*. 2009;146(5):693-703.
13. Herbert V, Streiff RR, Sullivan LW, McGeer PL. Deranged purine metabolism manifested by aninoimidazolecarboxamide excretion in megaloblastic anaemias, haemolytic anaemia, and liver disease. *Lancet*. 1964;2(7349):45-46.
14. Deodhar SD, Pittman G. A study of the metabolism of 4-amino-5-imidazolecarboxamide (AIC) in folic acid deficiency in rats. *Cleve Clin Q*. 1966;33(4):191-194.
15. Baggott JE, Morgan SL, Sams WM, Linden J. Urinary adenosine and aminoimidazolecarboxamide excretion in methotrexate-treated patients with psoriasis. *Arch Dermatol*. 1999;135(7):813-817.
16. Allen RH, Stabler SP, Lindenbaum J. Serum betaine, N,N-dimethylglycine and N-methylglycine levels in patients with cobalamin and folate deficiency and related inborn errors of metabolism. *Metabolism*. 1993;42(11):1448-1460.
17. Qiu A, Min SH, Jansen M, et al. Rodent intestinal folate transporters (SLC46A1): secondary structure, functional properties, and response to dietary folate restriction. *Am J Physiol Cell Physiol*. 2007;293(5):C1669-C1678.
18. Monsen AL, Refsum H, Markestad T, Ueland PM. Cobalamin status and its biochemical markers methylmalonic acid and homocysteine in different age groups from 4 days to 19 years. *Clin Chem*. 2003;49(12):2067-2075.
19. Pfeiffer CM, Johnson CL, Jain RB, et al. Trends in blood folate and vitamin B-12 concentrations in the United States, 1988-2004. *Am J Clin Nutr*. 2007;86(3):718-727.
20. Antony AC. Evidence for potential underestimation of clinical folate deficiency in resource-limited countries using blood tests. *Nutr Rev*. 2017;75(8):600-615.

DOI 10.1182/blood.2019003178

SUPPLEMENTARY MATERIALS FOR

A homozygous deletion in the *SLC19A1* gene as a cause of folate-dependent recurrent megaloblastic anemia

Michael Svaton[#], Karolina Skvarova Kramarzova[#], Veronika Kanderova, Andrea Mancikova, Petr Smisek, Pavel Jesina, Jakub Krijt, Blanka Stiburkova, Robert Dobrovolny, Jitka Sokolova, Violeta Bakardjieva-Mihaylova, Elena Vodickova, Marketa Rackova, Jan Stuchly, Tomas Kalina, Jan Stary, Jan Trka, Eva Fronkova[#], and Viktor Kozich[#]

[#] These authors contributed equally.

SUPPLEMENTARY METHODS

Patient and samples

The patient was referred to the specialized childhood hematological department for severe anemia. Informed consents for the genetic study and further functional testing were obtained from the patient and his parents. Residual bone marrow (BM) samples with negative minimal residual disease of patients treated for acute lymphoblastic leukemia after hematopoietic stem cell transplant and peripheral blood (PB) of healthy donors were used as controls (informed consents for research purposes were obtained from patients/donors or their guardians). All studies including sample use and collection have been approved by the IRB of Second Faculty of Medicine of Charles University and University Hospital Motol.

Whole exome and *SLC19A1* gene sequencing

DNA was isolated from a BM aspirate and from PB from the patient and his parents using a QIAamp DNA Blood Mini Kit (QIAGEN, Hilden, Germany). Sequencing libraries were prepared using a SureSelect XT Human All Exon V5+UTRs kit for whole exome sequencing using a NextSeq 500 instrument (Illumina, San Diego, USA). Sequenced reads were aligned against the human reference genome hg19 using BWA software[1], and genomic variants were called using samtools[2] and VarScan 2[3]. Variant annotation was performed using SnpEff[4]. All exons and flanking intronic regions in the patient and the region containing the c.634_636TTC variant in both parents were analyzed by Sanger sequencing using conditions described elsewhere[5]. Reference sequence NM_194255.3 was used to describe the variant.

Expression of folate transporters in bone marrow leukocytes and gene-edited K562 cell lines

Leukocytes from BM samples of the patient at the time of diagnosis during his first presentation and at day 1421 (266 days after the beginning of his second presentation and start of vitamin B_{12} treatment) and two healthy controls (patients 3 years after HSCT for acute lymphoblastic leukemia with no residual disease) were isolated using a Ficoll-Paque gradient (GE Healthcare). Two biological replicates of each model cell line were harvested, washed in PBS and further

processed as the BM samples. Total RNA from the BM as well as cell line samples was isolated using RNeasy Mini Kit (Qiagen) and transcribed to cDNA by iScript kit (Bio-Rad, Hercules, CA, USA). Gene expression levels of folate transporters were determined by the following TaqMan Gene Expression Assays (Thermo Fisher Scientific) *SLC19A1* (Hs00953344_m1), *SLC46A1* (Hs00611081_m1), *FOLR1* (Hs06631528_s1), *FOLR2* (Hs01044732_g1), *FOLR3* (Hs00357145_g1) and *GAPDH* (Hs99999905_m1) gene that was used for normalization. The qPCR reactions were performed on the Applied Biosystems 7500 Fast Real-Time PCR System (Applied Biosystems, Foster City, USA) and the expression normalized to *GAPDH* control gene expression in two healthy donors using the delta-delta Ct method[6].

Determination of metabolites

Serum folate and vitamin B_{12} levels were measured using the Elecsys Folate III and Vitamin B_{12} II assays on Cobas e411 and Cobas 6000 analyzers (all Roche Diagnostics, Basel, Switzerland) in two laboratories, respectively. Plasma total homocysteine (tHcy) was determined using a commercial Liquid Stable (LS) 2-Part Homocysteine Reagent enzymatic kit (Axis-Shield, Scotland) and a Hitachi 902 automatic analyzer from Roche Diagnostics, respectively. Serum methionine was determined by ion exchange chromatography with ninhydrine detection on an automatic amino acids analyzer AAA 400 (Ingos, Czech Republic) according to a modification of a previously published method[7]. Urinary organic acids including methylmalonic acid (MMA) were assayed by gas chromatography-mass spectrometry (Trace 1310 -TSQ Quantum XLS, Thermo Fisher Scientific, Waltham, USA) according to a previously published method[8]. Plasma MMA was determined using a commercial ClinMass® LC-MS/MS Complete Kit (Recipe, München, Germany). Cystathionine and sarcosine (N-methylglycine) in serum or plasma, and 5-amino-4-imidazolecarboxamide riboside (AICAr) in urine were determined by modified LC-MS/MS methods[9,10] as described below.

LC-MS/MS methods

All LC-MS/MS methods were performed on a system consisting of the Agilent 1290 Infinity LC System (Agilent Technologies, Palo Alto, USA) coupled with an API 4000 triple quadrupole mass spectrometer with an electrospray ion source. The system was operated using Analyst software,

version 1.4 (Applied Biosystems, Foster City, USA). Detection of analytes was carried out using positive electrospray ionization technique and selected multiple reaction monitoring.

Determination of AICAr

Urinary concentration of AICAr was determined using a modified method reported previously[10]. Urine was diluted to a creatine concentration of 1 mmol/L and injected onto a reversed-phase column (Prontosil, C18-AQ column; 200x4 mm; 3-µm particle size; Bischoff, Leonberg, Germany), and the analytes were separated using a gradient elution of a 0.1% formic acid solution in water (A) and a 0.1% formic acid solution in acetonitrile (B). The gradient profile began with 100% A, followed by a linear increase to 20% B over 12 min and an increase to 60% B at 13 min. The column was then regenerated with 100% A for another 9 min. The flow rate was 0.4 ml/min. The precursor→product mass transition for AICAr was 259.2→110. The retention time of AICAr was 8.4 min.

Determination of cystathionine and sarcosine

Cystathionine and sarcosine were determined using commercially available kit for amino acid analysis (EZ:faast, Phenomenex, Torrance, USA). Fifty µL of a sample (plasma or serum) was processed according to the manufacturer's instructions. The internal standard solution, which is a component of the kit, was supplemented by 1 µM cystathionine-d_4 (CDN Isotopes, Quebec, Canada) and 5 µM sarcosine-d_3 (CDN Isotopes). The precursor→product mass transitions for the derivatization products of cystathionine and sarcosine, and of the internal standards cystathionine-d4 and sarcosine-d_3 were 479.3→230.3 and 218.3→116.0, and 483.3→234.3 and 221.3→119.0, respectively. The retention times of cystathionine and sarcosine were 11.5 and 5.8 min, respectively.

Cell culture

The hypotriploid K562 cell line purchased from the German Collection of Microorganisms and Cell Cultures (DSMZ, Braunschweig, Germany) was cultured in RPMI 1640 medium, containing 1mg/L of folic acid and supplemented with 10% FBS and antibiotics (all Thermo Fisher Scientific). No

difference in proliferation or survival among different engineered K562 populations was observed in this media probably due to the upregulated non-RFC dependent transport of folic acid into the cells. HEK293T cells (ATCC - American Type Culture Collection, Manassas, VA, USA) used for testing of CRISPR/Cas9 nuclease activity were cultured in Dulbecco's Modified Eagle Medium supplemented with 10% FBS and antibiotics (all Thermo Fisher Scientific).

***SLC19A1*^{mut} gene-edited K562 model cell lines**

CRISPR/Cas9 and exogenous donor design

A guide RNA (gRNA) for the CRISPR/Cas9 nuclease directed to the close proximity of c.634_636TTC in the *SLC19A1* gene was designed using the MIT CRISPR Design Tool (Supplementary Figure 3A) and was synthesized in the form of a ssDNA oligonucleotide (Integrated DNA Technologies, Coralville, USA). The oligo was PCR amplified and cloned into pSpCas9(BB)-2A-GFP (PX458) (a gift from Feng Zhang; Addgene plasmid # 48138) using an In-Fusion HD cloning kit (Takara Bio, Kyoto, Japan). The CRISPR/Cas9 plasmid was transfected into HEK293T cells using Lipofectamine 3000 (Thermo Fisher Scientific). Three days later, DNA from HEK293T cells was PCR amplified with primers covering the CRISPR/Cas9 cut site (F: 5`-CTTCTCTCTCGTGCGGCCC-3´ and R: 5`-GGCCGAGTTGAAGACCCAC-3´; PCR was performed at 95°C for 5 min, followed by 40 cycles of 95°C for 30 s, 60°C for 30 s and 68°C for 45 s). Amplicons were analyzed by surveyor nuclease assays (Integrated DNA Technologies) according to the manufacturer´s instructions. The respective fragmentation products were observed, and CRISPR/Cas9 performance was confirmed (Supplementary Figure 3B). The MIT CRISPR Design Tool was also used to determine *in silico* off-target cleavage sites of the CRISPR/Cas9 nuclease. DNA from HEK293T cells transfected with the CRISPR/Cas9 plasmid was PCR amplified using primers covering the predicted exonic off-target sites (OT-1, F: 5`-ATGCACGATTCACTCCTGGG-3´ and R: 5`-ATGACCTGCACGTTGACCTT-3´; OT-2, F: 5`-TGTTCATGGCCGCTGTTTTG-3´ and R: 5`-AACAGCCATACTGCAGGTCC-3´; PCR was performed at 95°C for 5 min, followed by 40 cycles of 95°C for 30 s, 60°C for 30 s and 68°C for 45 s). The amplicons were then analyzed by Surveyor nuclease assays as described above, and no

promiscuous activity of the SLC19A1-targeted CRISPR/Cas9 nuclease was observed at the predicted sites (Supplementary Figure 3C).

Exogenous donor DNA containing the c.634_636delTTC mutation of the *SLC19A1* gene was designed and synthesized in the form of a ssDNA oligonucleotide (Integrated DNA Technologies) with homology arms spanning approx. 60 bp on each side of the trinucleotide c.634_636TTC. The donor also contained three silent single nucleotide polymorphisms (SNPs), allowing for the design of homology directed repair (HDR)-specific PCR (Supplementary Figure 3D).

CRISPR/Cas9 gene editing

A plasmid with a CRISPR/Cas9 nuclease directed to the close proximity of c.634_636TTC in the *SLC19A1* gene and exogenous donor DNA containing the c.634_636delTTC mutation were transfected into the K562 cell line using the Amaxa Nucleofector System (Lonza, Basel, Switzerland). Using a FACS Aria (BD Biosciences, San Jose, USA), the single-cell sorting of GFP-expressing cells into 96-well plates was performed, and monoclonal colonies were harvested three weeks later and analyzed by homology-directed repair (HDR) analysis, as described below. Through this analysis, we identified a monoclonal population that was homozygous for c.634_636delTTC (Supplementary Figures 4B and 4C).

To further study the impact of the patient's mutation on RFC function, K562 cell lines with full knockout of the *SLC19A1* gene were generated. The CRISPR/Cas9 plasmid alone was electroporated into the K562 cell line, and the transfected cells were then cultured in media supplemented with 0.5 µM MTX (Medac GmbH, Wedel, Germany) for five days. Single-cell colonies from the bulk population that was enriched for *SLC19A1* knockout cells (as verified by amplicon sequencing of the edited locus in bulk cells; data not shown) were prepared as described above. Their genotype was confirmed by Sanger sequencing, and two representative clones (each harboring deleterious variants at each of the three copies of the *SLC19A1* gene) were chosen for further functional testing (Supplementary Figure 4D).

HDR analysis

DNA isolated from bulk or monoclonal populations of cells edited with the CRISPR/Cas9 nuclease and the exogenous donor was PCR amplified using the HDR-specific forward primer and a general reverse primer (F: 5`-AAGCGCAGCCTCTTCAAC-3´ and R: 5`-CAGCACTGAGTCCCCACAG-3´, Supplementary Figure 4A). Candidate monoclonal populations showing HDR screening positivity were then PCR amplified using primers located outside of the edited area (F: 5`-CTTCTCTCTCGTGCGGCCC-3´ and R: 5`-GGCCGAGTTGAAGACCCAC-3´) and Sanger sequenced (Supplementary Figure 4B). Sequencing traces of *SLC19A1*^{mut} cell line homozygous for c.634_636delTTC are shown in Supplementary Figure 4C.

Functional testing of the *SLC19A1* mutation

Methotrexate uptake assay in K562 cells

Wild-type and gene-edited K562 cells were harvested from 75 cm2 flasks, transferred into 15 ml tubes and centrifuged at 150 x g for 5 min. The size of different cell lines did not differ upon microscopic examination or flow-cytometric evaluation. Medium was removed and cells were resuspended in 5 ml of ice-cold Krebs-Ringer-Phosphate Buffer (KPB), pH 7.4. After a subsequent centrifugation step with supernatant removal, the assay was initiated by the addition of 300 µl of 0,5 µM $^{[3H]}$MTX (disodium salt; Hartmann Analytic, Braunschweig, Germany) in KPB, and the tubes were shaken at 120 rpm at 37°C for 2 minutes. Cell suspension was divided into 3 aliquots (140 µl) and transport flux was stopped by dilution with 5 ml ice cold KPB. The cell fraction was separated by centrifugation (150 x g, 5 min) and washed twice in ice cold KPB. Before the last centrifugation, cells were counted. After transferring the cell pellets with 80 µl KPB to scintillation vials, cells were lysed by incubation with 100 µl of 1 M NaOH overnight at room temperature and neutralized by 50 µl of 2 M HCl. Radioactivity was measured by liquid scintillation counting after 4 ml of the Ultima Gold scintillation cocktail (Sigma-Aldrich) was added.

Cell proliferation assay in K562 model cell lines

The activity of the folate transporter in wild-type cells and gene-edited K562 cells was assessed via CellTiter 96® AQueous One Solution Cell Proliferation Assays (Promega, Fitchburg, USA; performed according to the manufacturer's instructions) after being cocultured with MTX for three days (concentration range: 0.0005 µM – 50 µM MTX).

Statistical analysis

Data from the MTX uptake assay in K562 cell lines were collected in three independent experiments performed on different days, and each experiment was done in triplicate. The differences in MTX accumulation in cell lines were tested by two-way ANOVA (the factors were the genetic variant and the experiment number), p-values<0.001 after Bonferroni correction were considered statistically significant. Data from the proliferation assays performed with the K562 cell lines were collected from three independent experiments (each with six replicates). Analysis of the data was performed using Prism 7 (GraphPad Software, La Jolla, USA) and respective IC_{50} values were calculated in the R-project[11] using the drc package[12].

Analysis of RFC protein expression

Confocal microscopy

The K562 cells grown on 170 µm cover slides coated with gelatin were fixed with 4% formaldehyde in PBS for 10 min at 4°C, followed by permeabilization with 0.05% TWEEN, and blocking with 10% goat serum/PBS overnight at 4°C. The monoclonal primary anti-RFC antibody (mouse, sc-390948, Santa Cruz) was diluted 1:50 and incubated overnight at 4°C. The secondary antibody (goat anti mouse IgG conjugated to AlexaFluor 488 A-11001, Thermo Fischer Scientific) was diluted to 1mg/ml and incubated for 1 hour at 37°C. All antibodies were diluted with blocking buffer. The nuclei were counterstained by DAPI.

The stained cells were scanned with Laser Scanning Confocal Microscope Leica SP8X (Leica Microsystems GmbH, Wetzlar, Germany). All confocal images were acquired with HC PL APO 63x/1.40 OIL CS2 objective. DAPI and Alexa Fluor 488 were excited with 405nm and 499nm,

respectively. The detector emission wavelengths were set to 410–489nm and 505–582nm, respectively. Alexa Fluor 488 was detected with HybridDetector using counting mode in 12 bits per channel and gated detection (0.3–6 ns). The Nyquist resolution used for image acquisitions was 41nm/px. The individual channels were deconvolved by Maximum likelihood estimation algorithm using HuygensPro software (Scientific Volume Imaging b.v., Hilversum, The Netherlands). Cropping, final resolution adjustments and conversion to 8 bits per channel was done in LAS X (Leica Microsystems) and Adobe Photoshop CS6 (Adobe Systems, Inc., San Jose, CA). The signal levels were adjusted to correspond to original fluorescence intensity.

For original data, please contact michael.svaton@lfmotol.cuni.cz.

SUPPLEMENTARY RESULTS

Detailed clinical and biochemical findings during second episode, and response to therapy

After his second hospital admission, the patient underwent extensive medical evaluation. His grossly elevated serum homocysteine (above the measurable range of 50 µmol/l) (Figure 1) was consistent with vitamin B_{12} or folate deficiency; however, his plasma methionine (27 µmol/l) and cystathionine levels (217 nmol/l) were normal. The patient's vitamin B_{12} level was decreased (138 ng/L), unfortunately serum holotranscobalamin II and MMA were not determined before vitamin B_{12} treatment. The serum folate concentrations were in the normal to low normal range (7.3 – 14.3 nmol/l), erythrocyte folates were determined once showing decreased concentration of 509.9 µg/l. To explore the putative folate deficiency, we analyzed the concentrations of sarcosine and the purine *de novo* synthesis intermediate 5-amino-4-imidazolecarboxamide riboside (AICAr) as markers of abnormal folate metabolism[13–16]. The patient's plasma sarcosine concentration was moderately elevated (5.2 µmol/l) and the urinary concentration of AICAr was markedly increased (1.97 mmol/mol creat.) prior to folic acid administration. These data together with low folate concentration in erythrocyes are consistent with a functional folate deficiency in haematopoietic cells. All reference ranges are available in Table 1.

The patient´s anemia was unresponsive to regular supplementation with cyanocobalamin (at a dose of 1000 µg intramuscularly twice a week for the first 5 administrations and then continuously once per month), he required repeated transfusions in approximately 6-week periods during which his total serum vitamin B_{12} concentrations were within the therapeutic range. Furthermore, he experienced a new onset of neurological symptoms: weakness of the lower limbs with decreased peripheral nerve conduction speed on the lower extremities of both motor and sensory nerves (n. tibialis sin. 41.5, n.peroneus dx. 43.7, and n.suralis sin. 41.4 m/s), indicating demyelination despite continuous vitamin B_{12} therapy for 10 months between days 1155 and 1467. Levels of MMA in plasma were retrospectively measured in frozen stored samples taken at day 1261 (3 weeks after vitamin B_{12} application, without folic acid therapy) and at day 1926 (459 days after the last cyanocobalamin injection, during this period patient was treated only with folic acid) – both were within normal range, urinary levels were below the reference range at several

occasions. These data during the second episode indicate vitamin B_{12} sufficiency at all timepoints since day 1162 regardless of cyanocobalamin therapy. Despite no biochemical signs of vitamin B12 deficiency hyperhomocysteinemia persisted between days 1155 and 1434 (above 31.5 µmol/) suggesting tissue folate deficiency as a culprit. Indeed, patient's anemia resolved only after addition of 10 mg of folic acid per day to therapy with cyanocobalamin, and homocysteine, sarcosine and AICAr normalized rapidly when folic acid treatment was started. Moreover, hemoglobin and all other laboratory markers remained within reference range on only folic acid therapy without cyanocobalamin injections. In summary these clinical and biochemical findings are fully compatible with folate deficiency in tissues[13–17].

Detailed genetic analysis

To exclude the presence of additional variants, the entire coding sequence and flanking intronic and 5´ and 3´-regions of the *SLC19A1* gene were sequenced using patient's genomic DNA. Homozygosity for the c.634_636delTTC deletion was confirmed in the patient and heterozygosity was demonstrated in both of his parents (Supplementary Figure 2B); in addition, homozygosity for a common variant c.80A>G (p.His27Arg) rs1051266 was observed. The pathogenicity of the c.634_636delTTC deletion could not be determined with the widely used *in silico* prediction tools such as PolyPhen-2[18] or SIFT[19] as it does not lead to an amino acid change but to an in-frame deletion; moreover, with a CADD[20] score of 15.8, the mutation is likely to be classified as benign with hard filtering. However, the mutation was classified as having high damaging impact with a 99% CI using the MSC method[21]. The c.634_636delTTC variant was observed in the gnomAD database[22] with an allele frequency of 0.014% with zero homozygous count, but the Exome Variant Server NHLBI GO Exome Sequencing Project (ESP) reported 6 homozygotes for this mutation among 6258 individuals without details on their phenotypes.

Analysis of RFC protein expression and its cellular localization

We examined the expression of the RFC protein in the patient's PB and BM leukocytes as well as in both cell line models. Although Baslund et al.[23] described RFC protein expression on the surface of PB lymphocytes, we tested two commercially available anti-RFC antibodies for flow cytometry

and were not able to specifically detect the wild-type or mutant RFC antigen (data not shown). Immunostaining and confocal microscopy of the wild-type and gene-edited K562 cells using conditions described in the Supplementary Methods showed that the RFC transporter localized partially to the plasma membrane with lower signal of the mutant protein detected at the plasma membrane (Supplementary Figure 5).

Analysis of folate transporter gene expression

The existence of 5 folate transporters with different kinetic properties, pH optima, substrate specificity, and tissue expression makes inferences on compensatory mechanisms for delivering folates from circulation to tissues challenging. RFC is an important transporter of 5-MTHF into the cells, however, the transport activity of both the PCFT (even at pH 7.4) and folate receptors 1-3 has been clearly shown in a number of studies.[24,25]

We observed an increase in the expression of *SLC46A1* and *FOLR2* genes in patient's bone marrow cells isolated from samples obtained at diagnosis (7-fold higher and 9-fold higher, respectively) and at day 1421 during his second presentation while he was treated with vitamin B_{12} (13-fold and 14-fold higher, respectively) compared to samples from two healthy controls. We observed a similar hyperexpression pattern in the K562 model cell lines (Supplementary Figure 6). These results are consistent with previously published data on *FOLR2* hyperexpression in an RFC-deficient cell line[26].

Although the other transporters have in general less favorable kinetic properties or pH optimum, it is plausible to hypothesize that their overexpression and consequently increased total folate transport activity may compensate for the decreased activity of the mutant RFC.

SUPPLEMENTARY FIGURES

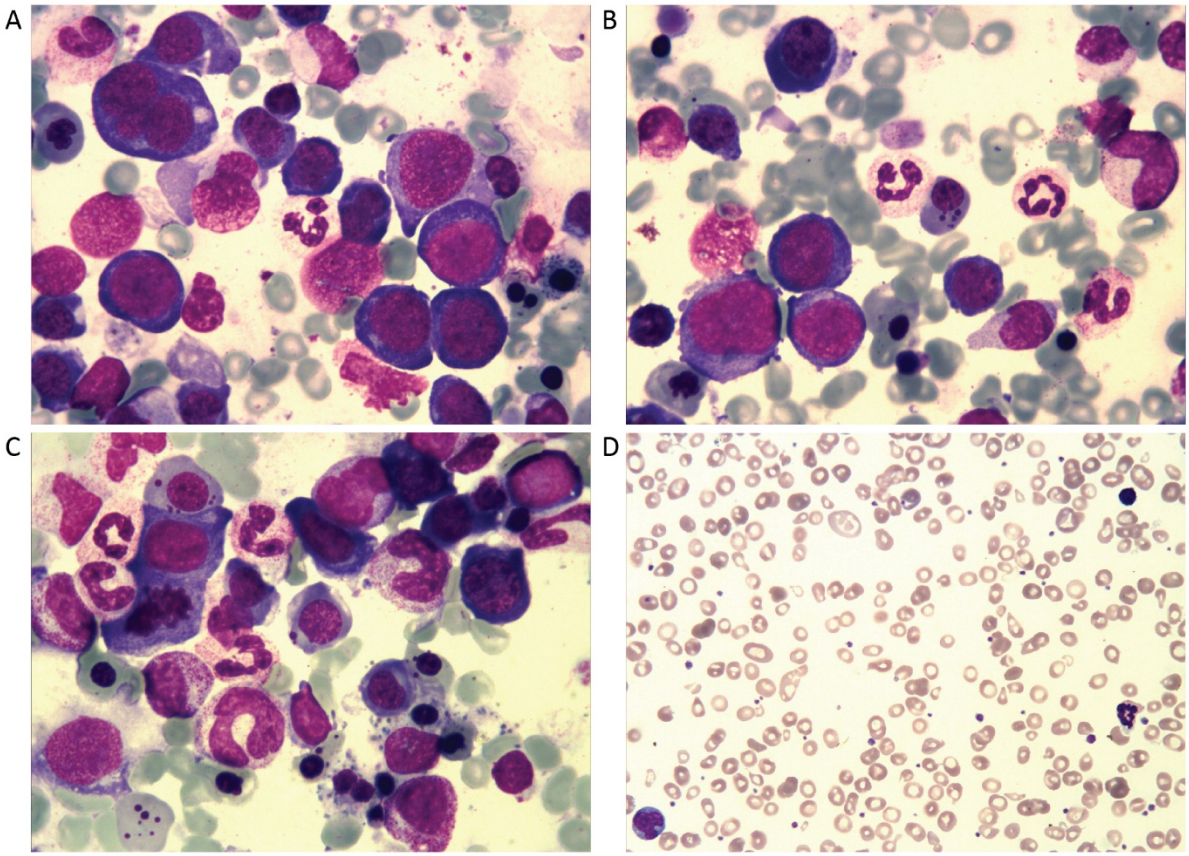

Supplementary Figure 1. Bone marrow (A-C) and peripheral blood (D) morphology evaluation in the patient. **(A)** Megaloblastic changes in the bone marrow. Erythroid hyperplasia: erythroblasts mostly show asynchrony of nuclear/cytoplasmic development, and the nuclei have open, loose chromatin structures. Multinucleation: irregular shape of nuclei, chromatin mass extrusion, irregular outline of the cytoplasm and nuclear fragments (Howell – Jolly body, basophilic stippling) in the cytoplasm of erythroblasts are present. Frequent cellular shadows. **(B)** Erythroid and myeloid abnormalities. Megaloblasts: upper left megaloblast shows irregular nucleus shape, lower left late megaloblast shows irregular nuclear mass with chromatin mass extrusion and irregular outline of the cytoplasm, and middle polychromatophilic erythroblast shows an eccentrically located nucleus and nuclear fragments (Howell - Jolly bodies). On the right, a giant metamyelocyte, a hypersegmented mature neutrophil and, lower, a large band form, are present. **(C)** Erythroid and myeloid abnormalities. Megaloblasts: the nuclei have open (lacy) chromatin patterns. Binuclear polychromatophilic megaloblasts with asynchronous maturation

and one nucleus in mitosis. Late erythroblasts with irregularly shaped nuclei and outline of cytoplasm. Frequent nuclear fragments (Howell-Jolly bodies and basophilic stippling) are visible in their cytoplasms. Two giant metamyelocytes are present, one of them with a bizarrely shaped nucleus (lower left). Cellular shadows. **(D)** Peripheral blood smear showing sporadic macro-ovalocytes and frequent schistocytes. A hypersegmented neutrophil is also present. (Original magnification ×1000 for panels A-C and ×500 for panel D; May-Grünwald Giemsa stain, LEICA DM2500 optical microscope with LEICA DFC295 camera and N PLAN 50x/0.90 oil and HI PLAN 100x/1.25 oil objectives were used for imaging and LAS V4.4 software for acquisition; Leica Microsystems)

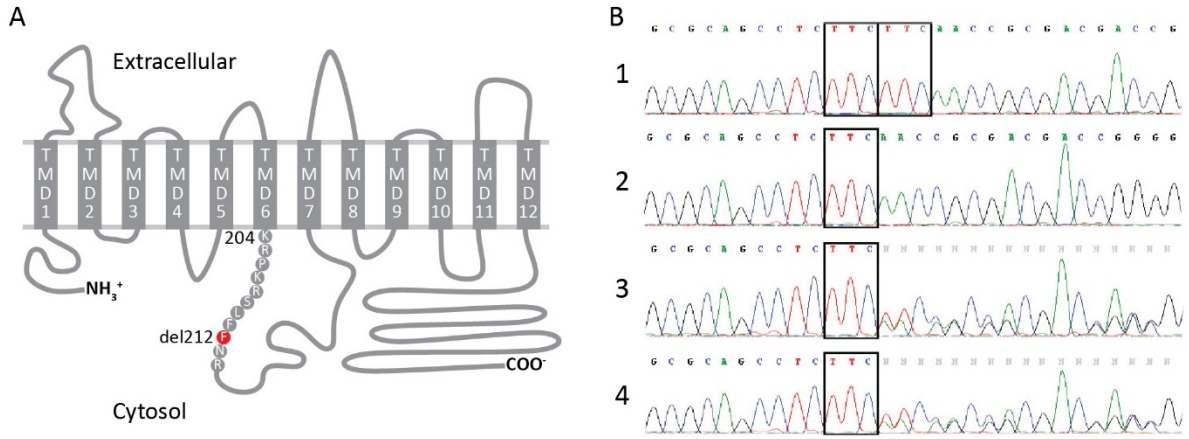

Supplementary Figure 2. Molecular genetic findings. (A) Localization of the phenylalanine deletion found in the patient (marked in red) within the conserved Lys204–Arg214 peptide sequence in the central loop of RFC connecting trans-membrane domains 6 and 7. The protein structure scheme was adapted from Hou & Matherly. [27] **(B)** Sequence trace of part of the *SLC19A1* gene. Compared to the wild-type sequence of a control subject (trace 1), the patient exhibits a homozygous deletion of one of the TTC trinucleotides (trace 2). The mother (trace 3) and father (trace 4) of the patient exhibit sequence doubling starting at nucleotide 634, indicating heterozygosity for the c.634_636TTC mutation.

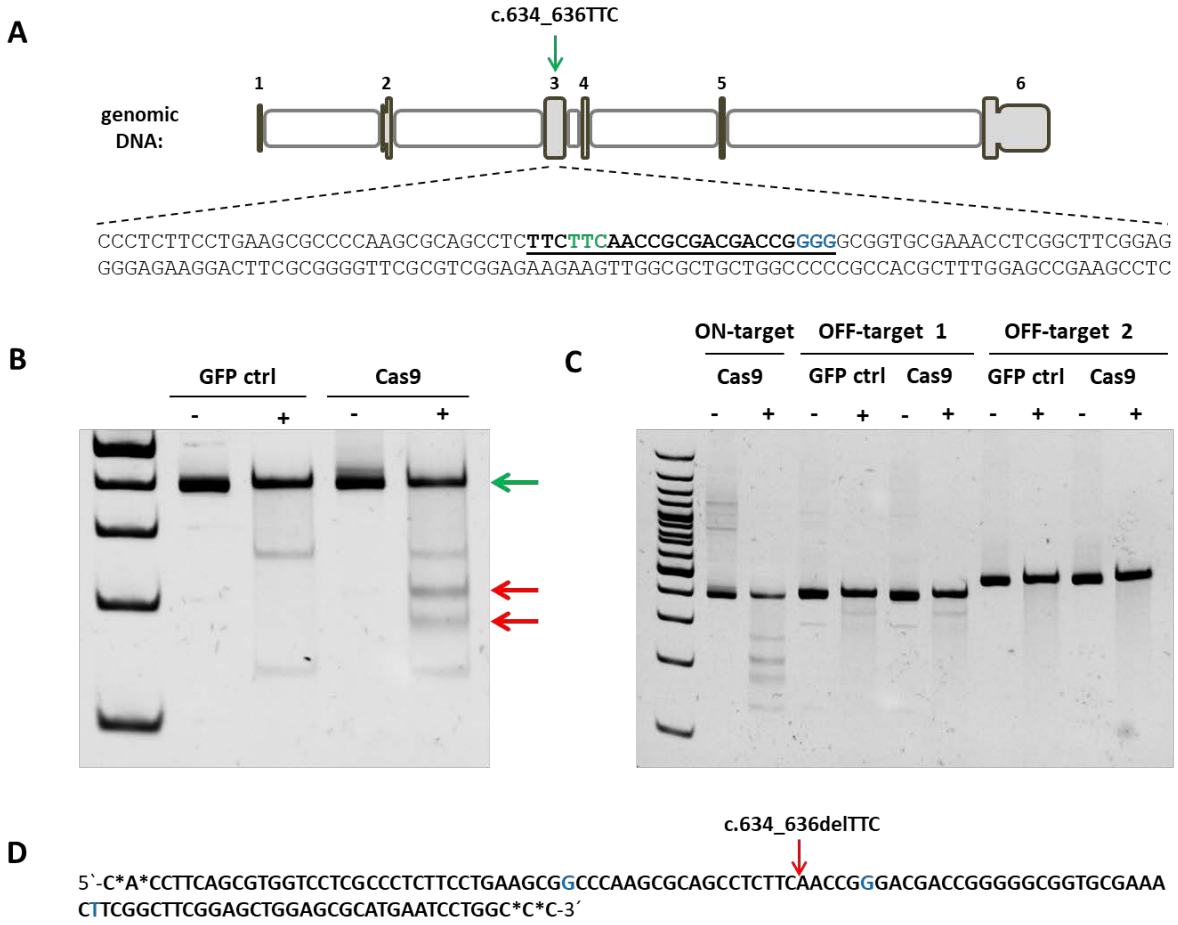

Supplementary Figure 3. Design and performance of the *SLC19A1*-targeting gene-editing tools. **(A)** gRNA design of the CRISPR/Cas9 nuclease targeting the *SLC19A1* gene in close proximity to c.634_636TTC. Exons are labeled by numbers; the green arrow indicates trinucleotide c.634_636TTC. The sequence of the gRNA is underlined in the detailed genomic dsDNA; the PAM sequence is labeled in blue, and the trinucleotide c.634_636TTC is shown in green. **(B)** Surveyor nuclease assay of the CRISPR/Cas9 nuclease. GFP ctrl: HEK293T cells transfected with the control GFP plasmid. Cas9: HEK293T cells transfected with the CRISPR/Cas9 plasmid. (+): Surveyor nuclease added. (-): Untreated control. The green arrow indicates uncut amplicon, and the red arrows show cleavage products. **(C)** Off-target analysis. Surveyor nuclease assay of the ON-target site and two in-silico predicted OFF-target sites. **(D)** Design of an exogenous ssDNA donor carrying the c.634_636delTTC mutation of the *SLC19A1* gene. The red arrow indicates c.634_636delTTC, and the introduced silent single nucleotide polymorphisms are labeled in blue. Asterisks indicate phosphorothioate bonds added at the 5′ and 3′ termini.

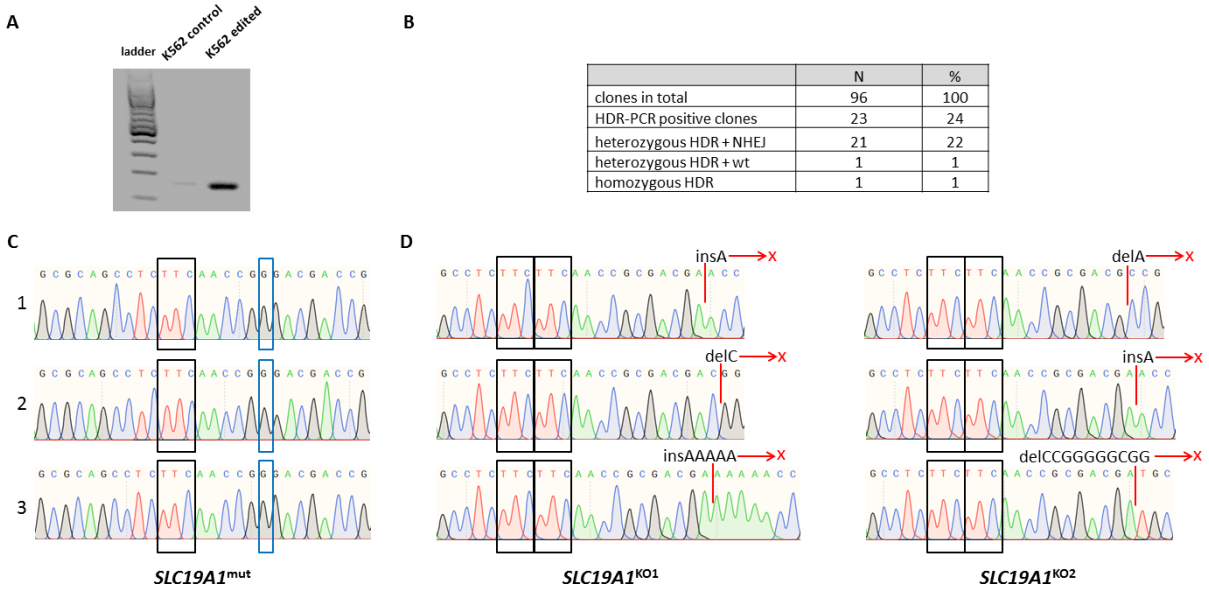

	N	%
clones in total	96	100
HDR-PCR positive clones	23	24
heterozygous HDR + NHEJ	21	22
heterozygous HDR + wt	1	1
homozygous HDR	1	1

Supplementary Figure 4. Introduction of the c.634_636delTTC mutation into the *SLC19A1* gene in the hypotriploid K562 cell line. (A) PCR analysis of homology-directed repair in bulk gene-edited cells. **(B)** Clonal selection of gene-edited cells. The number of positive clones via HDR-PCR screening with subsequent identification of gene-editing events on particular alleles by Sanger sequencing. HDR: homology directed repair, NHEJ: non-homologous end joining. **(C)** Genotype of the monoclonal K562 cell lines with homozygous *SLC19A1* c.634_636delTTC and **(D)** two clones with full knock-out of the *SLC19A1* gene. The black box shows the trinucleotide TTC. The blue boxes show the introduced silent single nucleotide polymorphisms. The red crosses indicate a frameshift that results in a subsequent stop codon.

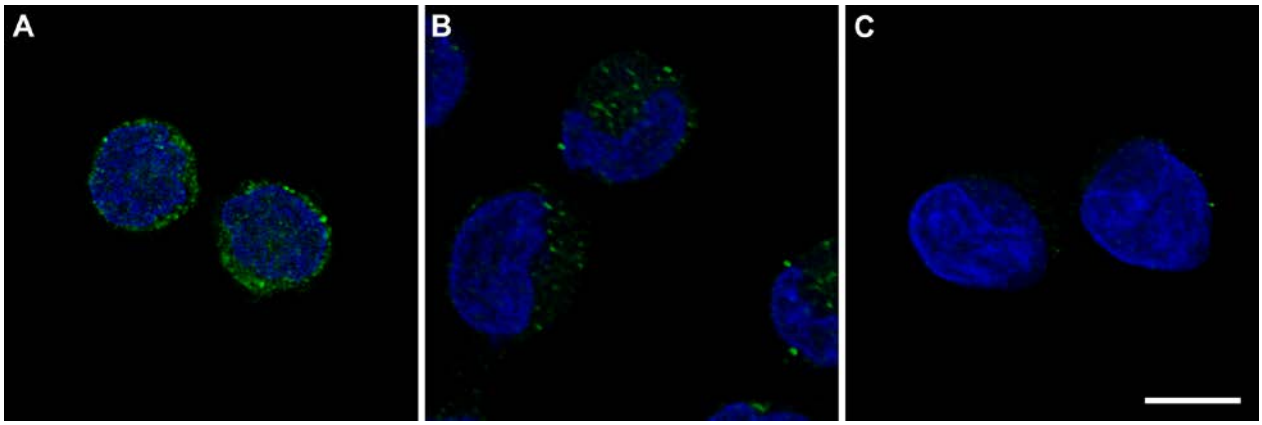

Supplementary Figure 5. Detection of RFC antigen in wild-type and gene-edited K562 cells by immunostaining and confocal microscopy. (A) RFC in the wild-type K562 cells was preferentially localized in the plasma membrane, forming fine granules. However, the signal was also apparent inside the cells. **(B)** *SLC19A1*^{mut} cells exhibited lower signal of RFC in the plasma membrane with higher proportion of intracellular signal. **(C)** In the cells with a complete *SLC19A1* knockout, only a very weak signal was detectable and can be attributed to the detection background. (Scalebar 10µm)

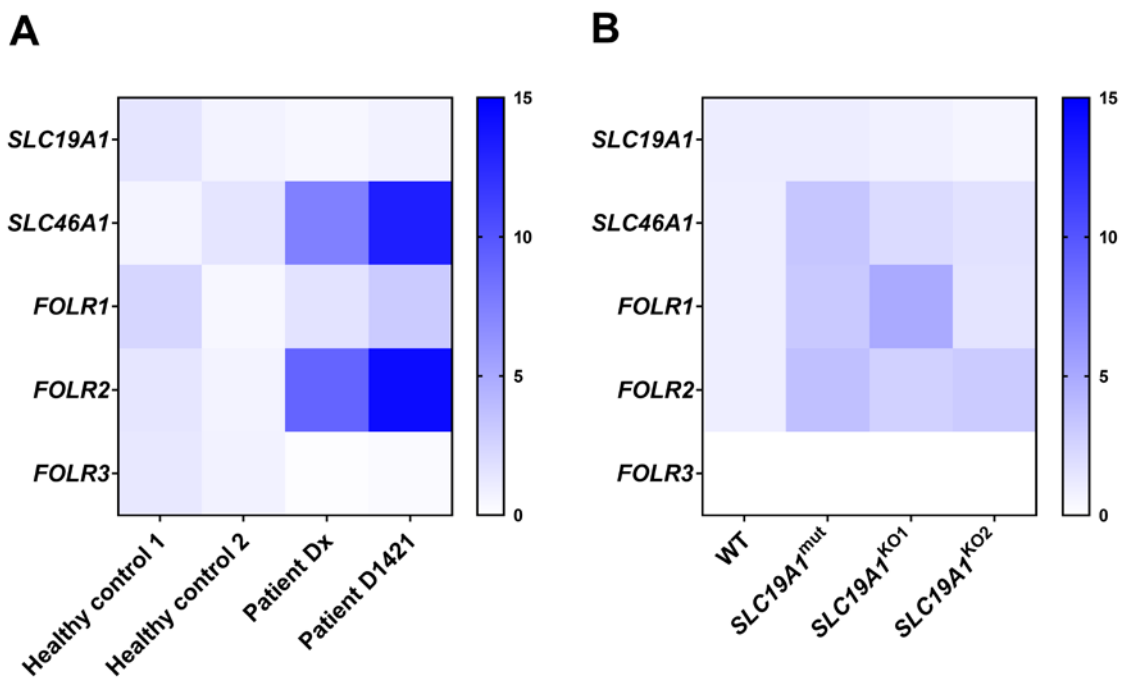

Supplementary Figure 6. Expression of folate transporters in bone marrow leukocytes and K562 model cell lines. Visualization of relative expression of genes encoding main folate transporters in the patient at diagnosis and during vitamin B_{12} treatment during his second episode compared to two healthy controls **(A)** and the model cell lines with patient's mutation or complete *SLC19A1* knockout compared to wild-type K562 cell line **(B).**

REFERENCES

1. Li H, Durbin R. Fast and accurate short read alignment with Burrows-Wheeler transform. *Bioinformatics*. 2009;25(14):1754–1760.

2. Li H, Handsaker B, Wysoker A, et al. The Sequence Alignment/Map format and SAMtools. *Bioinformatics*. 2009;25(16):2078–2079.

3. Koboldt DC, Zhang Q, Larson DE, et al. VarScan 2: Somatic mutation and copy number alteration discovery in cancer by exome sequencing. *Genome Res.* 2012;22(3):568–576.

4. Cingolani P, Platts A, Wang LL, et al. A program for annotating and predicting the effects of single nucleotide polymorphisms, SnpEff. *Fly (Austin).* 2012;6(2):80–92.

5. Pavlíková M, Sokolová J, Janošíková B, et al. Rare Allelic Variants Determine Folate Status in an Unsupplemented European Population. *J. Nutr.* 2012;142(8):1403–1409.

6. Livak KJ, Schmittgen TD. Analysis of Relative Gene Expression Data Using Real-Time Quantitative PCR and the 2−ΔΔCT Method. *Methods*. 2001;25(4):402–408.

7. Hommes FA. Techniques in Diagnostic Human Biochemical Genetics : A Laboratory Manual. New York: Wiley—Liss; 1991.

8. Chalmers RA. Organic Acids in Man. London: Chapman and Hall Ltd.; 1982.

9. Kožich V, Krijt J, Sokolová J, et al. Thioethers as markers of hydrogen sulfide production in homocystinurias. *Biochimie*. 2016;126:14–20.

10. Zikanova M, Krijt J, Skopova V, et al. Screening for adenylosuccinate lyase deficiency using tandem mass spectrometry analysis of succinylpurines in neonatal dried blood spots. *Clin. Biochem.* 2015;48(1–2):2–7.

11. R Core Development Team. A language and environment for statistical computing. *www.R-project.org*. 2013;

12. Ritz C, Baty F, Streibig JC, Gerhard D. Dose-Response Analysis Using R. *PLoS One*. 2015;10(12):e0146021.

13. Allen RH, Stabler SP, Lindenbaum J. Serum betaine, N,N-dimethylglycine and N-methylglycine levels

in patients with cobalamin and folate deficiency and related inborn errors of metabolism. *Metabolism.* 1993;42(11):1448–60.

14. Herbert V, Streiff RR, Sullivan LW, Mcgeer PL. Deranged purine metabolism manifested by aninoimidazolecarboxamide excretion in megaloblastic anaemias, haemolytic anaemia, and liver disease. *Lancet*. 1964;284(7349):45–46.

15. Deodhar SD, Pittman G. A study of the metabolism of 4-amino-5-imidazolecarboxamide (AIC) in folic acid deficiency in rats. *Cleve. Clin. Q.* 1966;33(4):191–4.

16. Baggott JE, Morgan SL, Sams WM, Linden J. Urinary adenosine and aminoimidazolecarboxamide excretion in methotrexate-treated patients with psoriasis. *Arch. Dermatol.* 1999;135(7):813–817.

17. Antony AC. Evidence for potential underestimation of clinical folate deficiency in resource-limited countries using blood tests. *Nutr. Rev.* 2017;75(8):600–615.

18. Adzhubei I, Jordan DM, Sunyaev SR. Predicting functional effect of human missense mutations using PolyPhen-2. 2013.

19. Kumar P, Henikoff S, Ng PC. Predicting the effects of coding non-synonymous variants on protein function using the SIFT algorithm. *Nat. Protoc.* 2009;4(7):1073–1081.

20. Kircher M, Witten DM, Jain P, et al. A general framework for estimating the relative pathogenicity of human genetic variants. *Nat. Genet.* 2014;46(3):310–315.

21. Itan Y, Shang L, Boisson B, et al. The mutation significance cutoff: gene-level thresholds for variant predictions. *Nat. Methods*. 2016;13(2):109–110.

22. Karczewski KJ, Francioli LC, Tiao G, et al. Variation across 141,456 human exomes and genomes reveals the spectrum of loss-of-function intolerance across human protein-coding genes. *bioRxiv*. 2019;531210.

23. Baslund B, Gregers J, Nielsen CH. Reduced folate carrier polymorphism determines methotrexate uptake by B cells and CD4+ T cells. *Rheumatology*. 2008;47(4):451–453.

24. Qiu A, Jansen M, Sakaris A, et al. Identification of an Intestinal Folate Transporter and the Molecular Basis for Hereditary Folate Malabsorption. *Cell*. 2006;127(5):917–928.

25. Sierra EE, Goldman ID. Characterization of Folate Transport Mediated by a Low pH Route in Mouse L1210 Leukemia Cells with Defective Reduced Folate Carrier Function. *Biochem. Pharmacol.* 1998;55(9):1505–1512.

26. Sierra EE, Brigle KE, Spinella MJ, Goldman ID. Comparison of transport properties of the reduced folate carrier and folate receptor in murine L1210 leukemia cells. *Biochem. Pharmacol.* 1995;50(8):1287–1294.

27. Hou Z, Matherly LH. Biology of the major facilitative folate transporters SLC19A1 and SLC46A1. *Curr. Top. Membr.* 2014;73(1–2):175–204.

Příloha 3

Svaton M, Sukova M, Sedlacek P, Skotnicova A, Vodickova E, van Wijk R, Divoka M, Mojzikova R, Kalina T, Trka J, Fronkova E, Stary J. Hydrops fetalis and failure of hematopoietic stem cell transplantation - A long route to the diagnosis of *SPTA1*-associated hereditary spherocytosis. *Blood Cells Mol Dis.* 2022 Jul;95:102664. doi: 10.1016/j.bcmd.2022.102664.

Blood Cells, Molecules and Diseases 95 (2022) 102664

Contents lists available at ScienceDirect

Blood Cells, Molecules and Diseases

journal homepage: www.elsevier.com/locate/bcmd

Hydrops fetalis and failure of hematopoietic stem cell transplantation – A long route to the diagnosis of *SPTA1*-associated hereditary spherocytosis

To the editor

We report the case of a female newborn with severe congenital anemia presenting as hydrops fetalis, followed by a clinical picture of transfusion-dependent hypoproliferative anemia. The most common causes of hydrops fetalis due to a severe non-immune hemolytic anemia are homozygous alpha-thalassemia, pyruvate kinase deficiency and other non-spherocytic anemias, autosomal recessive (AR) hereditary spherocytosis (HS), hereditary xerocytosis and congenital dyserythropoietic anemia (CDA) [1]. Congenital hemolytic anemia with reticulocytopenia and dysplasia of erythroid precursors is rare and CDA should be included in the differential diagnosis [2]. The diagnostic process in our patient was complicated by inconclusive laboratory testing due to her transfusion dependency and her final diagnosis was only established after the introduction of whole exome sequencing (WES).

The second child of healthy, nonconsanguineous parents who was delivered by caesarean section at the 36th week of gestation with signs of intrauterine distress presented at birth with a clear picture of fetal erythroblastosis. The patient was hypotrophic (birth weight 1630 g), hydropic and pale, with circulatory failure, respiratory distress, skin bleeding, hepatosplenomegaly and blueberry muffin spots. The patient's complete blood count (CBC) analysis revealed severe anemia with Hb 37 g/L, MCV 117 fL, reticulocytopenia 0.06% (0.023×10^9/L), erythroblastosis 597/100 WBC and thrombocytopenia 78×10^9/L. The total bilirubin level was 95 μmol/L, the direct bilirubin level was 68 μmol/L, the Coombs test was negative and congenital infections were excluded.

After successful management during the critical neonatal period, the patient became stable. She had symptoms of hemolytic anemia and remained dependent on transfusions at intervals of 2–3 weeks. The CBC at 4 months of age showed normocytic anemia with reticulocytopenia 0.0011×10^9/L. Bone marrow aspiration performed at week 1 and month 4 showed 18.8%/42.4% erythroid precursors with significant dysplastic changes – megaloblasts (1.2%), binuclearity (4.4%), lobulated nuclei (7.6%), plasmatic bridges (2%) and eccentric nuclei (6.4%) were present at the latter time point (Fig. 1). Hemoglobin electrophoresis excluded hemoglobin variant and alpha- and beta-thalassemia were excluded by multiplex ligation-dependent probe amplification assay and Sanger sequencing, respectively. Repeated analysis of complete panel of erythrocyte enzymes excluded erythrocyte enzyme defect. EMA test did not show any abnormalities specific for an erythrocyte membrane defect and SDS-PAGE of red cell membrane band 3 did not show any abnormalities compatible with diagnosis of HS or CDA type II.

Chelation with deferoxamine (DFO) following erythrocyte transfusions and continuous oral deferiprone (DFP) was initiated at the age of 18 months due to signs of iron overload (serum ferritin above 1000 μg/L). At the age of 2.5 years, hematopoietic stem cell transplantation (HSCT) from a matched 9/10 (HLA-A allelic mismatch) unrelated donor was performed after myeloablative conditioning regimen composed of busulfan 19 mg/kg (according to AUC) + cyclophosphamide 200 mg/kg with ATG-Fresenius 40 mg/kg, ciclosporin A and methotrexate for graft-versus-host disease (GVHD) prophylaxis. She achieved engraftment of all three lineages with mixed chimerism of 19% without any toxicity or GVHD at day +28. Unfortunately, late graft failure developed at day +90, followed by full reconstitution via autologous hematopoiesis (Fig. 2A). Progressive splenomegaly with hypersplenism was an indication for splenectomy performed at day +118.

After the splenectomy, the transfusion intervals were prolonged to 6–8 weeks, hepatomegaly progressed, and the patient's reticulocyte levels increased to 2% (60×10^9/L) on average and above 10% (240×10^9/L) before transfusions (Hb <70 g/L; Fig. 2A) and her white blood count and thrombocyte levels normalized. Total bilirubin levels fluctuated between 40 and 70 μmol/L, with adequate icteric symptoms. Severe cardiac and moderate liver iron overload (MRI T2* myocardium 9.8 ms, liver 2.4 ms) was revealed at the age of 12 years. Chelation therapy was intensified with DFP and DFO (5 days per week). At the age of 18 years, the patient remains transfusion-dependent with asymptomatic cholecystolithiasis, mild cognitive dysfunction and craniofacial dysmorphia resembling thalassemia major.

Targeted genetic testing was performed to exclude known causes of CDA and did not reveal any mutations in *CDAN1* and *SEC23B* genes in the year 2004 or *KLF1* later in 2010 [3]. WES was performed, when it became available after 14 years, and finally identified two novel synonymous mutations in the *SPTA1* gene: c.1677G>A (p.G559G) and c.2805G>A (p.G935G) affecting pre-mRNA splicing. None of her parents had any clinical symptoms of anemia and the patient was compound heterozygous. In order to confirm the pathogenicity of both variants and confirm their effect on pre-mRNA splicing, we have sorted the patient's reticulocytes from peripheral blood and performed amplicon sequencing of the cDNA (Supplementary data).

The analysis of the splicing junctions has confirmed a complete loss of the splice donor site due to the paternal c.2805G>A mutation and insertion of 5 bases on the 3′ side of the exon-intron boundary, leading to a frameshift and premature stop codon p.Ala936Valfs*5. The maternal c.1677G>A mutation decreases splicing efficiency by over 90%, leading to two alternative splicing events, an insertion of 59 nucleotides due to the creation of a new splice donor 3′ from the exon-intron boundary leading to a frameshift and premature stop codon p.Leu560Valfs*6, together with an in-frame skipping of exon 13 (Fig. 2B). We have detected only 3% of correctly spliced transcripts with the maternal mutant variant. Severely affected alpha-spectrin production would explain the premature damage of erythroblasts already in the bone marrow and the decreased life-span of reticulocytes captured in the

https://doi.org/10.1016/j.bcmd.2022.102664
Received 4 January 2022; Received in revised form 29 March 2022; Accepted 11 April 2022
Available online 16 April 2022

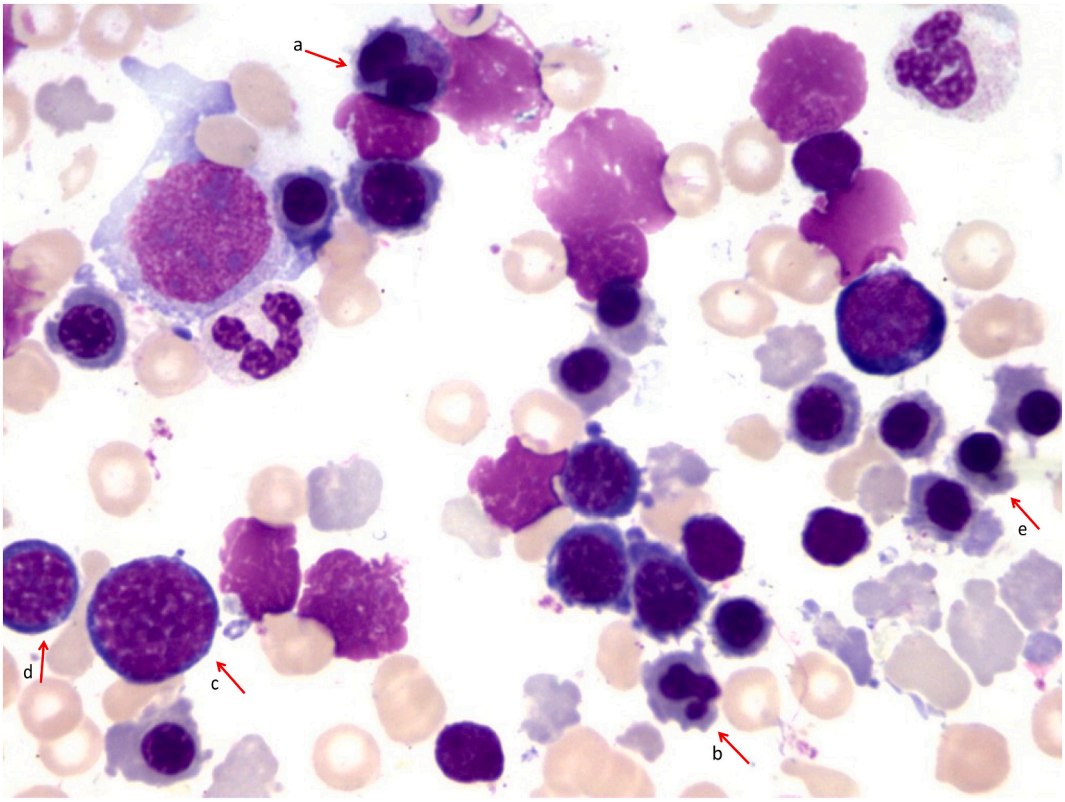

Fig. 1. Bone marrow morphology at 4 months of age, showing erythroid hyperplasia with significant abnormalities of erythroid precursors: binucleated forms (a), irregular nuclear mass and outline of cytoplasm (b), megaloblasts (c), nuclei with open (lacy) chromatin patterns (d), late erythroblasts with irregular outline of cytoplasm and Howell-Jolly bodies (e); (May-Grünwald-Giemsa staining, original magnification ×500).

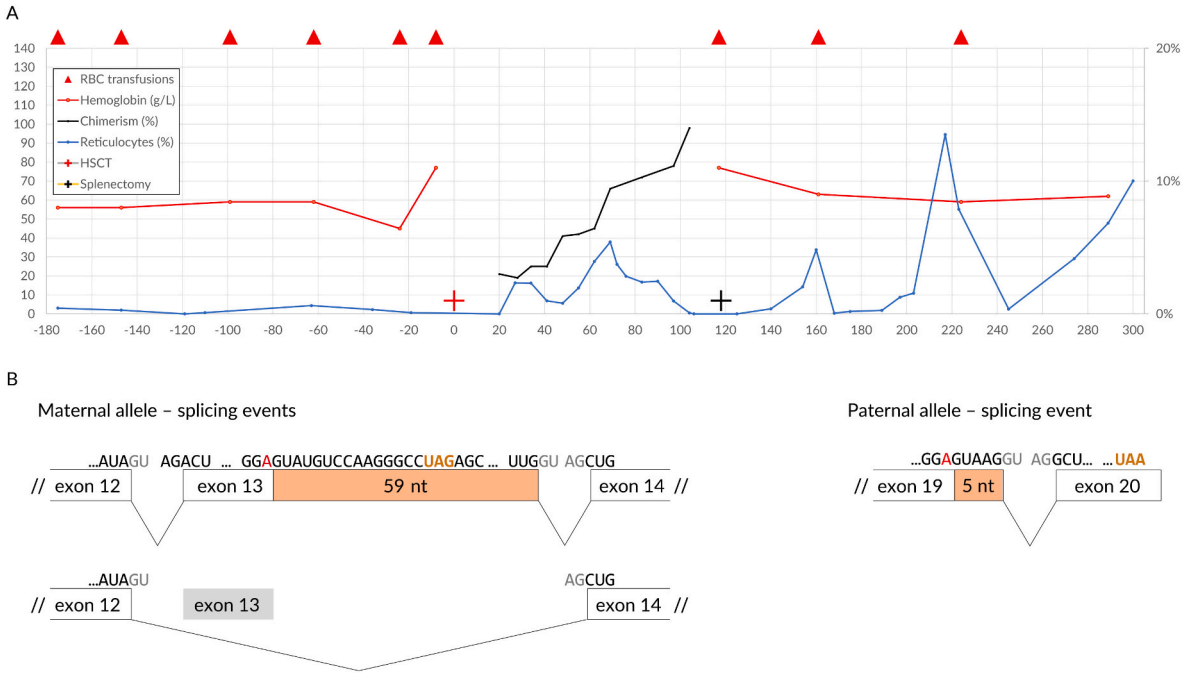

Fig. 2. Laboratory markers of patient's anemia and splicing of mutant *SPTA1*. (A) Course of the anemia 6 months before HSCT (day 0, red cross) and 6 months after splenectomy (day +118, gray cross). Patient's hemoglobin measured before erythrocyte transfusions (red triangles, top) is shown in red (g/L, left axis) and the relative reticulocyte count in blue (%, right axis). Hemoglobin levels and erythrocyte transfusions in the period after HSCT are not shown, as they are influenced by the HSCT. Chimerism of autologous hematopoietic stem cells is shown in black (%, right axis). (B) Scheme of the alternative splicing events of *SPTA1* pre-mRNA due to the mutations in *SPTA1* on both alleles. The mutations are marked in red and the premature stop codons introduced by the splicing changes are marked in orange.

spleen, resulting in the phenotype of ineffective erythropoiesis rather than the hemolytic anemia that is typical of HS.

Patient's reticulocytopenia with hyperplasia and dysplasia of erythroid precursors in the bone marrow, moderate hyperbilirubinemia and hepatosplenomegaly supported the diagnosis of unclassified CDA [3], which was the indication for HSCT. The morphological picture was not compatible with CDA types I and III and genetic testing excluded known causes for CDA types I, II and IV during the follow-up after HSCT. Despite a full myeloablative conditioning regimen, the patient developed secondary graft failure with autologous reconstitution, which is a possible complication in hemolytic anemia with hypercellular bone marrow [4,5]. Splenectomy resulted in only a slight and temporary prolongation of intervals between transfusions and an improvement of the patient's extensive reticulocytopenia. Since the early neonatal period, the patient's transfusion dependency complicated all diagnostic investigations, as the intervals between transfusions were never longer than 8 weeks. Membrane deformability measured by osmotic gradient ektacytometry performed 6 weeks after transfusion was aberrant but not typical for HS (Fig. 3).

Unlike the majority of patients with HS successfully managed by splenectomy in early childhood [2,6], rare cases of complete alpha-spectrin deficiency due to biallelic null *SPTA1* mutations have more severe phenotype and remain transfusion dependent if they are not cured by HSCT [7]. Molecular genetics play an essential role in the differential diagnosis of hereditary anemias. Only 18% of patients clinically suspected of having CDA showed matching phenotypes and genotypes in a recent gene panel study by Russo et al. and the majority received a final diagnosis of congenital hemolytic anemia. Almost all of the patients were transfusion-dependent with reduced reliability of enzyme assays or tests for erythrocyte membrane defects [8]. The correct diagnosis of AR-HS caused by alpha-spectrin deficiency in our patient was only resolved by implementing WES in the diagnostic process.

Data availability statement

For original data, please contact michael.svaton@lfmotol.cuni.cz.

Funding

This work was supported by the Ministry of Health of the Czech Republic, grant No. 18-07-00430.

Ethics approval and patient consent statement

This study was performed with an informed consent of the patient and patient's parents, according to the Declaration of Helsinki and approved by the Institutional Review Board of University Hospital Motol.

Author contributions

Michael Svaton: Conceptualization, Methodology, Formal analysis, Visualization, Writing- Original draft preparation; **Martina Sukova**: Investigation, Resources, Writing - Original Draft; **Petr Sedlacek**: Investigation; **Aneta Skotnicova**: Methodology; Investigation; **Elena Vodickova**: Investigation, Visualization; **Richard (H.A.) van Wijk**: Methodology, Investigation; **Martina Divoka**: Investigation; **Renata Mojzikova**: Investigation; **Tomas Kalina**: Methodology, Formal analysis, Resources; **Jan Trka**: Conceptualization, Resources, Supervision; **Eva Fronkova**: Conceptualization, Methodology, Supervision, Project administration, Funding acquisition, Writing - Review & Editing; **Jan Stary**: Conceptualization, Investigation, Writing - Original Draft, Writing - Review & Editing, Supervision, Project administration, Funding acquisition.

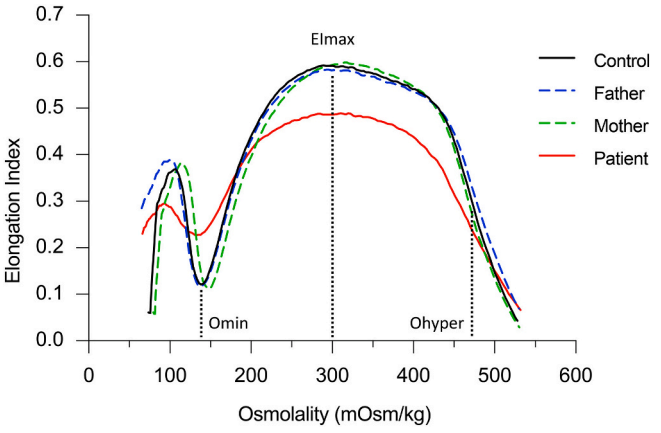

Fig. 3. Osmotic gradient ektacytometry of patients' erythrocytes. Deformability, expressed as elongation index, as a function of an osmotic gradient showed decreased maximal deformability (EImax), normal Omin, and slightly decreased Ohyper of the patient, compared to her parents and a normal control. The pattern is aberrant but not typical for hereditary spherocytosis.

Declaration of competing interest

The authors declare no relevant conflict of interest.

Acknowledgements

The authors would like to thank Dr. Vladimir Divoky from the Palacky University Olomouc for his kind help with laboratory testing and his valuable advice. All authors revised the manuscript and approved the final version.

Appendix A. Supplementary data

Supplementary data to this article can be found online at https://doi.org/10.1016/j.bcmd.2022.102664.

References

[1] A.M. Quinn, B.N. Valcarcel, M.M. Makhamreh, H.B. Al-Kouatly, S.I. Berger, A systematic review of monogenic etiologies of nonimmune hydrops fetalis, Genet Med. 23 (1) (2021) 3–12, https://doi.org/10.1038/s41436-020-00967-0.
[2] J.A. Rothman, J.L. Stevens, F.L. Gray, T.A. Kalfa, How I approach hereditary hemolytic anemia and splenectomy, Pediatr. Blood Cancer 67 (11) (2020) 1–8, https://doi.org/10.1002/pbc.28337.
[3] A. Iolascon, I. Andolfo, R. Russo, Congenital dyserythropoietic anemias, Blood 136 (11) (2020) 1274–1283, https://doi.org/10.1182/blood.2019000948.
[4] M. Miano, D.-J. Eikema, M. Aljurf, et al., Stem cell transplantation for congenital dyserythropoietic anemia: an analysis from the European Society for Blood and Marrow Transplantation, Haematologica 104 (8) (2019) e335–e339, https://doi.org/10.3324/haematol.2018.206623.
[5] S. van Straaten, M. Bierings, P. Bianchi, et al., Worldwide study of hematopoietic allogeneic stem cell transplantation in pyruvate kinase deficiency, Haematologica 103 (2) (2018) e82–e86, https://doi.org/10.3324/haematol.2017.177857.
[6] S. Tole, P. Dhir, J. Pugi, et al., Genotype–phenotype correlation in children with hereditary spherocytosis, Br. J. Haematol. 191 (3) (2020) 486–496, https://doi.org/10.1111/bjh.16750.
[7] S. Chonat, M. Risinger, H. Sakthivel, et al., The Spectrum of SPTA1-associated hereditary spherocytosis, Front. Physiol. 10 (July) (2019) 1–7, https://doi.org/10.3389/fphys.2019.00815.
[8] R. Russo, I. Andolfo, F. Manna, et al., Multi-gene panel testing improves diagnosis and management of patients with hereditary anemias, Am. J. Hematol. 93 (5) (2018) 672–682, https://doi.org/10.1002/ajh.25058.

M. Svaton[a], M. Sukova[b], P. Sedlacek[b], A. Skotnicova[a], E. Vodickova[c], R. van Wijk[d], M. Divoka[e], R. Mojzikova[f], T. Kalina[a], J. Trka[a], E. Fronkova[a], J. Stary[b,*]

[a] *CLIP – Childhood Leukaemia Investigation Prague, Department of Paediatric Haematology and Oncology, Second Faculty of Medicine, Charles University and University Hospital Motol, Prague, Czech Republic*

[b] *Department of Paediatric Haematology and Oncology, Second Faculty of Medicine, Charles University and University Hospital Motol, Prague, Czech Republic*
[c] *Department of Clinical Haematology, University Hospital Motol, Prague, Czech Republic*
[d] *Central Diagnostic Laboratory, University Medical Center Utrecht, Utrecht University, Utrecht, the Netherlands*
[e] *Department of Hemato-Oncology, Faculty of Medicine and Dentistry, Palacky University Olomouc and University Hospital Olomouc, Olomouc, Czech Republic*
[f] *Department of Biology, Faculty of Medicine and Dentistry, Palacky University Olomouc, Olomouc, Czech Republic*

[*] Corresponding author at: Department of Paediatric Haematology and Oncology, Second Faculty of Medicine, Charles University and University Hospital Motol, V Uvalu 84, 150 06 Prague 5, Czech Republic.
E-mail address: jan.stary@fnmotol.cz (J. Stary).
Editor: Mohandas Narla

Hydrops fetalis and failure of hematopoietic stem cell transplantation – A long route to the diagnosis of *SPTA1*-associated hereditary spherocytosis

Supplementary Methods

WES was performed using the SureSelectXT Human All Exon V5+UTRs kit (Agilent Technologies, Santa Clara, CA, USA) and the NextSeq 500 instrument (Illumina, San Diego, CA, USA). Variant calling was performed using VarScan2[1] and samtools[2] on reads aligned to the hg19 human reference genome with BWA.[3] The effect of the identified *SPTA1* mutations on pre-mRNA splicing was evaluated with MaxEntScan.[4] To elucidate the impact of both mutations, patient reticulocytes were sorted using FACS Aria III (BD Biosciences, Franklin Lakes, NJ, USA) as $FSC^{low}SYTO16^{+}CD45^{-}$ cells, and total RNA was isolated using the RNeasy Plus Micro Kit (QIAGEN, Hilden, Germany) and reverse-transcribed with the iScript cDNA Synthesis Kit (Bio-Rad Berkeley, CA, USA). The cDNA spanning exon 13 was amplified using DNA oligos with Illumina TruSight adapter overhangs (Merc, Darmstadt, Germany) with specific 3' sequences complementary to the exon 11-12 junction: 5'-GAGTAGACAAGAGGCCTTCCTGG-3' and exon 14-15 junction: 5'-CTTCAAGTTCTGTATGTCCTTGTAATCTTC-3' and similarly with exon 17-18 junction-spanning primer: 5'-CCACCTACCTTGGAAAGGACC-3' and exon 20-21 junction primer: 5'-CTGTTGTTGCTGGCAGGC-3' for exon 19 amplification. Standard PCR conditions with 35 cycles of 1 min at 94°C, 1 min at 63°C and 30 s at 72°C were used. The amplicons were sequenced on the MiSeq instrument using the v2 500-cycle Reagent Kit (Illumina, San Diego, CA, USA). Single reads were aligned to the same reference with STAR[5] and the splicing junctions were analyzed and plotted with ggsashimi[6] and the frequency of specific sequences for the major splicing events was manually confirmed in the raw FASTQ files.

Supplementary Results

The MaxEntScan analysis of both *SPTA1* mutations predicted a decrease of splicing efficiency and a potential loss of the splice donor sites with the strongest nearby alternative splice sites 59 and 5 bases from the exon-intron boundary on the 3' side of the c.1677G>A and c.2805G>A mutation, respectively. Because analysis of patient's red blood cells was complicated by frequent transfusions, $SYTO16^{+}$ cells were sorted for the analysis of *SPTA1* mRNA by amplicon sequencing to confirm the true biological effect of the mutations. In both cases, we have confirmed the predicted effect of the mutation on the mRNA level. However, we have also observed a second alternative splicing junction in the case of the c.1677G>A mutation. The predicted insertion of 59 nucleotides on the 3' side of the exon-intron boundary was identified in 22 % of reads. We have also detected a complete skipping of exon 13 in 16 % of the analyzed reads and the correct splicing junction was identified in 50 % of the analyzed reads (**Supplementary Figure 1A**). The presence of the mutated sequence together with correct splicing was identified only in 3 % of the analyzed reads. In case of the c.2805G>A mutation, we have only detected the correctly spliced sequence carrying the mutant nucleotide in 0.03 % of reads, confirming the loss of the splice donor site due to this mutation. The mutation led to the predicted insertion of 5 nucleotides and introduction of a premature stop codon. The ratio between the wild-type and mutant nucleotide was 1:0.6 suggesting a nonsense-mediated decay of the mutant mRNA (**Supplementary Figure 1B**).

Supplementary Figures

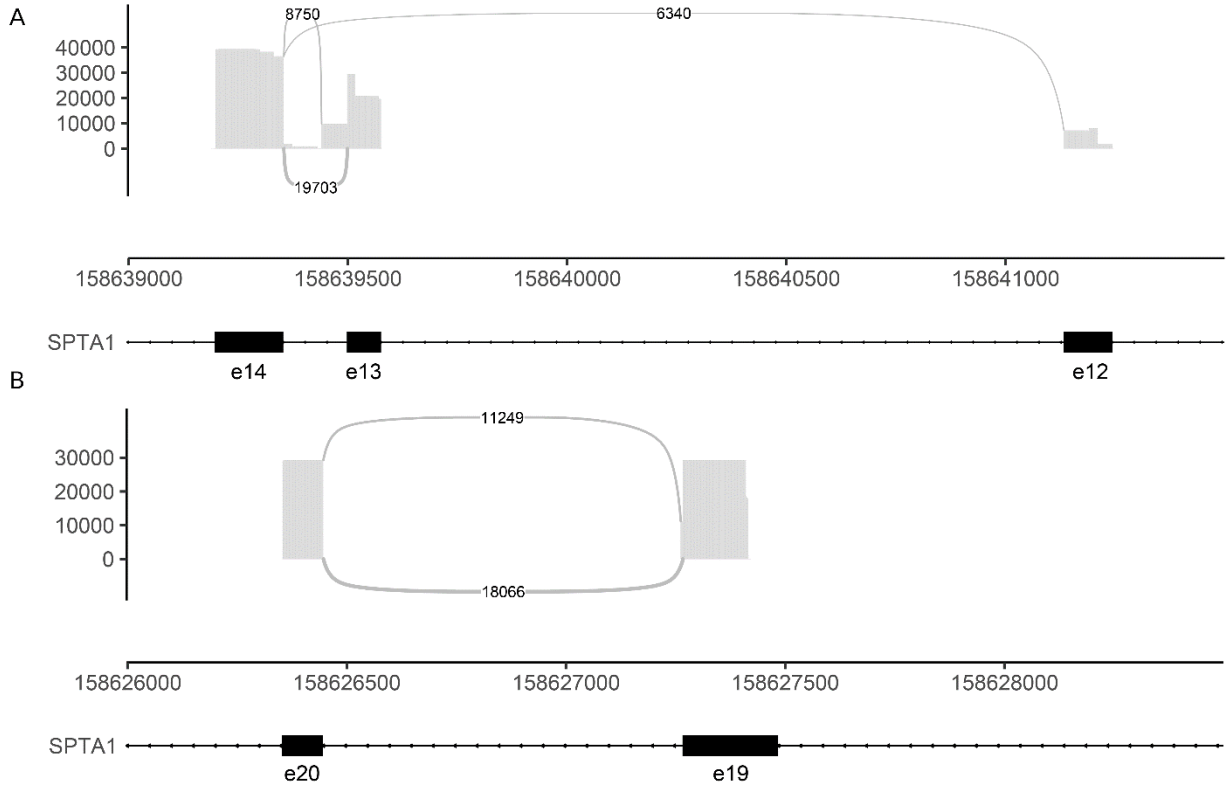

Supplementary Figure 1. Analysis of splicing junctions. Sashimi plots of aligned amplicon single-end reads to the hg19 human reference genome and results of the splicing junction analysis by ggsashimi. Numbers of reads corresponding to the identified splicing junctions are shown in the plot and the coverage is plotted as a histogram with the genomic position on the x-axis and the coverage of positions on the y-axis.

References

1. Koboldt DC, Zhang Q, Larson DE, et al. VarScan 2: Somatic mutation and copy number alteration discovery in cancer by exome sequencing. Genome Res 2012;22(3):568–576.
2. Li H, Handsaker B, Wysoker A, et al. The Sequence Alignment/Map format and SAMtools. Bioinformatics 2009;25(16):2078–2079.
3. Li H, Durbin R. Fast and accurate short read alignment with Burrows-Wheeler transform. Bioinformatics 2009;25(14):1754–1760.
4. Yeo G, Burge CB. Maximum Entropy Modeling of Short Sequence Motifs with Applications to RNA Splicing Signals. J Comput Biol 2004;11(2–3):377–394.
5. Dobin A, Davis CA, Schlesinger F, et al. STAR: ultrafast universal RNA-seq aligner. Bioinformatics 2013;29(1):15–21.
6. Garrido-Martín D, Palumbo E, Guigó R, Breschi A. ggsashimi: Sashimi plot revised for browser- and annotation-independent splicing visualization. PLOS Comput Biol 2018;14(8):e1006360.

Příloha 4

Fejtkova M, Sukova M, Hlozkova K, Skvarova Kramarzova K, Rackova M, Jakubec D, Bakardjieva M, Bloomfield M, Klocperk A, Parackova Z, Sediva A, Aluri J, Novakova M, Kalina T, Fronkova E, Hrusak O, Malcova H, Sedlacek P, Liba Z, Kudr M, Stary J, Cooper MA, **Svaton M***, Kanderova V*. TLR8/TLR7 dysregulation due to a novel TLR8 mutation causes severe autoimmune hemolytic anemia and autoinflammation in identical twins. *Am J Hematol.* 2022 Mar 1;97(3):338-351. doi: 10.1002/ajh.26452.

Received: 23 December 2021 | Accepted: 24 December 2021

DOI: 10.1002/ajh.26452

RESEARCH ARTICLE

TLR8/TLR7 dysregulation due to a novel *TLR8* mutation causes severe autoimmune hemolytic anemia and autoinflammation in identical twins

Martina Fejtkova[1] | Martina Sukova[2] | Katerina Hlozkova[1] | Karolina Skvarova Kramarzova[1] | Marketa Rackova[1] | David Jakubec[3,4] | Marina Bakardjieva[1] | Marketa Bloomfield[5,6] | Adam Klocperk[6] | Zuzana Parackova[6] | Anna Sediva[6] | Jahnavi Aluri[7] | Michaela Novakova[1] | Tomas Kalina[1] | Eva Fronkova[1] | Ondrej Hrusak[1] | Hana Malcova[8] | Petr Sedlacek[2] | Zuzana Liba[9] | Martin Kudr[9] | Jan Stary[2] | Megan A. Cooper[7] | Michael Svaton[1] | Veronika Kanderova[1]

[1]CLIP - Childhood Leukaemia Investigation Prague, Department of Paediatric Haematology and Oncology, Second Faculty of Medicine, Charles University and University Hospital Motol, Prague, Czech Republic

[2]Department of Paediatric Haematology and Oncology, Second Faculty of Medicine, Charles University and University Hospital Motol, Prague, Czech Republic

[3]Bioinformatics Group, Institute of Organic Chemistry and Biochemistry, Czech Academy of Sciences, Prague, Czech Republic

[4]Department of Software Engineering, Faculty of Mathematics and Physics, Charles University, Prague, Czech Republic

[5]Department of Paediatrics, First Faculty of Medicine, Charles University and Thomayer University Hospital, Prague, Czech Republic

[6]Department of Immunology, Second Faculty of Medicine, Charles University and University Hospital Motol, Prague, Czech Republic

[7]Division of Rheumatology/Immunology, Department of Pediatrics, Washington University School of Medicine, St. Louis, Missouri, USA

[8]Department of Paediatric and Adult Rheumatology, University Hospital Motol, Prague, Czech Republic

[9]Department of Paediatric Neurology, Second Faculty of Medicine, Charles University and University Hospital Motol, Prague, Czech Republic

Correspondence
Veronika Kanderova and Michael Svaton, CLIP - Childhood Leukemia Investigation Prague, Department of Pediatric Hematology and Oncology, Second Faculty of Medicine, Charles University and University Hospital Motol, V Uvalu 84, 15006, Prague 5, Czech Republic.
Email: veronika.kanderova@lfmotol.cuni.cz (V. K.) and michael.svaton@lfmotol.cuni.cz (M. S.)

Funding information
This work was supported by grants obtained from the Ministry of Health of the Czech Republic no. NV18-05-00162, NV18-07-00430 and NV19-05-00332, Charles University projects PRIMUS/19/MED/04 and GA UK 362119, European Regional Development Fund projects CZ.2.16/3.1.00/

Abstract

Our study presents a novel germline c.1715G>T (p.G572V) mutation in the gene encoding Toll-like receptor 8 (*TLR8*) causing an autoimmune and autoinflammatory disorder in a family with monozygotic male twins, who suffer from severe autoimmune hemolytic anemia worsening with infections, and autoinflammation presenting as fevers, enteritis, arthritis, and CNS vasculitis. The pathogenicity of the mutation was confirmed by in vitro assays on transfected cell lines and primary cells. The p.G572V mutation causes impaired stability of the TLR8 protein, cross-reactivity to TLR7 ligands and reduced ability of TLR8 to attenuate TLR7 signaling. This imbalance toward TLR7-dependent signaling leads to increased pro-inflammatory responses, such as nuclear factor-κB (NF-κB) activation and production of pro-inflammatory cytokines IL-1β, IL-6, and TNFα. This unique *TLR8* mutation with partial TLR8 protein loss and hyperinflammatory phenotype mediated by TLR7 ligands represents a novel

Michael Svaton and Veronika Kanderova contributed equally to this work.

24505 and CZ.02.1.01/0.0/0.0/16_019/0000729, the Jeffrey Modell Foundation and the St. Louis Children's Hospital Foundation. Institutional support was provided from the Ministry of Education, Youth and Sports of the Czech Republic project for the conceptual development of research organization - University Hospital Motol 00064203

inborn error of immunity with childhood-onset and a good response to TLR7 inhibition.

1 | INTRODUCTION

The innate immune system serves as the first line of defense against infection. It employs pattern recognition receptors (PRRs) that recognize evolutionarily conserved molecular structures of microorganisms. Toll-like receptors (TLRs), a family of PRRs, are a group of single-spanning membrane proteins found on the surface or in endosomes of immune cells. Defects in TLR signaling pathways described in IRAK4 or MyD88 deficiencies are associated with bacterial susceptibility and impaired inflammatory responses to infection.[1] Conversely, gain-of-function in TLR8 leads to hyperresponsiveness to TLR8 ligands, hyperproduction of inflammatory cytokines, neutropenia and bone marrow failure.[2] The phylogenetically related endosomal TLR8 and TLR7 both detect viral and bacterial single-stranded (ss)RNA.[3,4] TLR8 is predominantly expressed in monocytes/macrophages, myeloid dendritic cells (mDCs), and granulocytes, whereas TLR7 in plasmacytoid dendritic cells (pDCs), B-cells, and monocytes/macrophages.[5,6] The stimulation of TLRs generally activates NF-κB, mitogen-activated protein-kinases (MAPK), and interferon (IFN) response factors, which subsequently trigger the transcription of inflammatory cytokines, chemokines and costimulatory molecules.[3] The signaling pathways downstream of TLR8 and TLR7 vary in different cell types. In monocytes, TLR8 activation promotes a strong NF-κB activation, type I IFN response and the production of Th1 polarizing cytokines, whereas TLR7 preferentially activates MAPK signaling and the production of Th17 polarizing cytokines. Interestingly, TLR7 inhibits TLR8-mediated type I IFN response.[7] Consistently, during the maturation of DCs, TLR8 and TLR7 negatively regulate each other.[8] A direct or indirect intraendosomal physical interaction of TLR8 and TLR7 is suggested to play a role in balancing these inflammatory outcomes.[9] Interestingly, because of their high homology, mutations near the ligand-binding site 1 of TLR8 can increase selectivity to TLR7-specific ligands.[10]

In addition to external pathogens, TLRs respond to endogenous ligands, such as the self-RNA within anti-ribonucleoprotein autoantibodies that drive systemic lupus erythematosus (SLE)[11] or rheumatoid arthritis[12] in mice. Interestingly, overexpression of human TLR8[13] or murine TLR7[14,15] is sufficient to drive autoimmune inflammation in mice; and murine TLR8 deficiency also leads to autoimmunity and autoinflammation by increasing TLR7-dependent responses.[16,17] Here, we present the first report of human partial TLR8 protein deficiency combined with TLR8/TLR7 dysregulation underlying severe autoimmune and inflammatory phenotypes.

2 | METHODS

2.1 | Whole exome sequencing

Sequencing libraries were prepared from DNA isolated from peripheral blood mononuclear cells (PBMCs) of one of the patients using the SureSelect Human All Exon V6+UTRs kit (Agilent Technologies, Santa Clara, CA) and sequenced on the NextSeq 500 Instrument (Illumina, San Diego, CA) according to the manufacturer's instructions. Resulting reads were aligned to the hg19 human reference genome with BWA.[18] Variant calling was performed with VarScan2[19] and samtools,[20] and variant annotation and filtering was done in Ingenuity® Variant Analysis (QIAGEN, Hilden, Germany) with a custom panel of potential candidate genes. No other potentially pathogenic mutations were identified from the Whole Exome Sequencing data in neither *TLR8*, *TLR7* nor any other known primary immunodeficiency (PID)-related genes.[21] No pathogenic variants in the *TLR8* gene have been reported in the ClinVar database at the time of this study. Other patients with *TLR8* gene mutations were identified via the GeneMatcher database,[22] and a collaboration that led to the publication of the gain-of-function cases by Aluri et al.[2] was established. The gnomAD database reports eight individuals who are hemizygous for a putative loss-of-function variant without confirmation of these variant calls or information on their phenotypes.

2.2 | Sanger sequencing

DNA was isolated from PBMCs of both siblings and their parents and used for PCR amplification of the p.G572 surrounding area of the *TLR8* gene using the forward 5′-GCAATGCTCAAGTGTTAAGTGGA and the reverse 5′-TACCAGGGACTTGCTTTCCAG primers. The expression of both alleles in mother's cells was confirmed using the cDNA obtained from sorted monocytes as described below with the forward 5′-GCTC TTACTGAATTGTCCGACTTG and the reverse 5′-GCAACTCGAGACGA GGAAACT primers. The amplicons were sequenced using BigDye Terminator 3.1 Cycle Sequencing Kit (Thermo Fischer Scientific, Waltham, CA) on 3730 DNA Analyzer (Thermo Fischer Scientific) according to manufacturer's instructions.

2.3 | Cell sorting

Monocytes were isolated on an FACS Aria III sorter (BD Biosciences [BD], San Jose, CA) based on Forward Scatter (FSC), Side Scatter

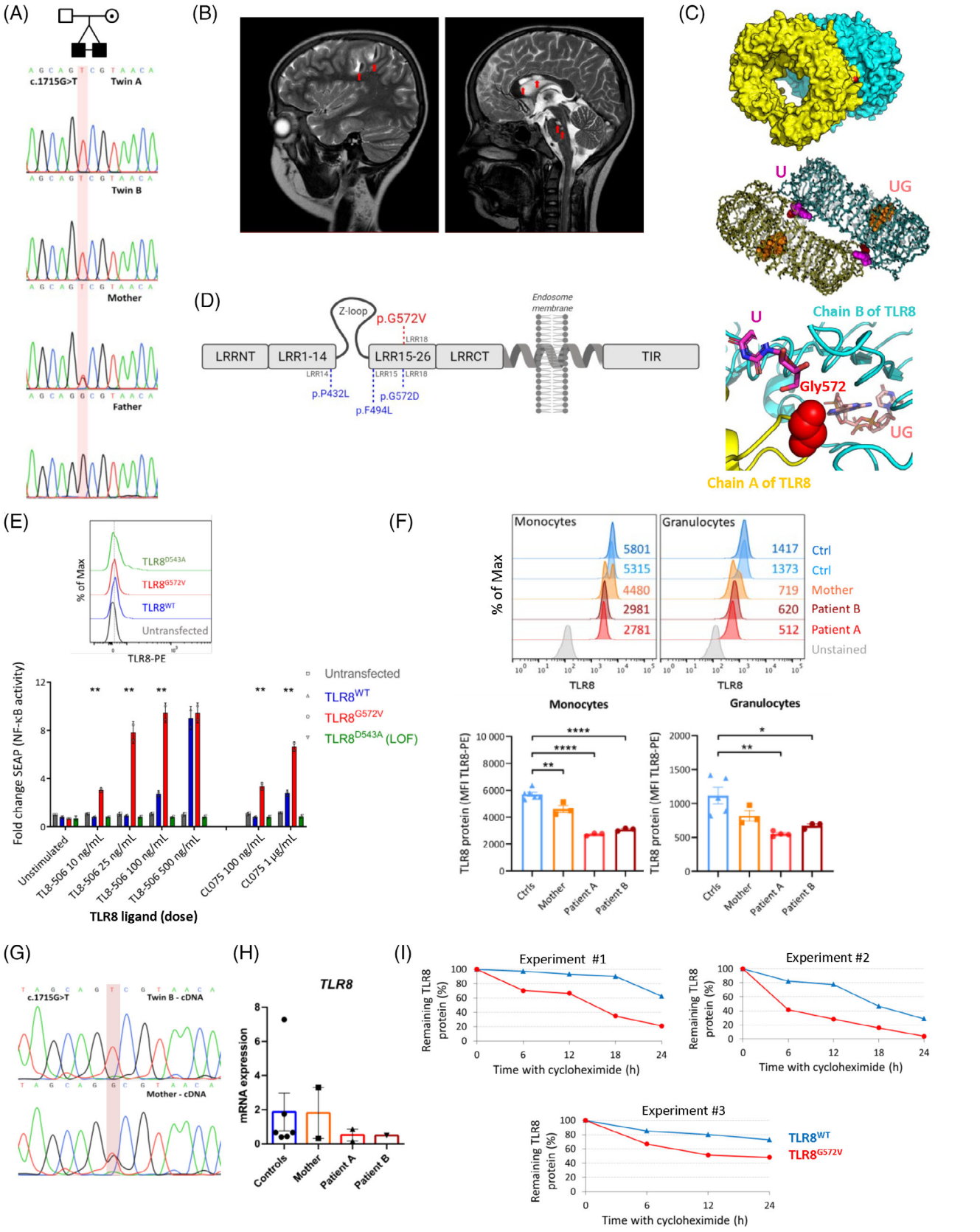

FIGURE 1 Legend on next page.

(SSC), CD45-Pacific Blue, and CD14-APC (Exbio, Vestec, Czech Republic) from the peripheral blood of both patients, their mother and healthy controls. T-cell subpopulations were sorted according to FSC, SSC and TCRαβ+CD4+CD127+CD25-(non-Treg) (or CD8+) CCR7+CD45RO− (naive T-cells), TCRαβ+CD4+CD127+CD25-(non-Treg) (or CD8+) CCR7+CD45RO+ (central memory T-cells), TCRαβ+CD4+CD127+-CD25-(non-Treg) (or CD8+) CCR7-CD45RO+ (effector memory T-cells), TCRαβ+CD4+CD127+CD25-(non-Treg) (or CD8+) CCR7-CD45RO− (terminally differentiated T-cells), TCRαβ+CD4+CD127dim/-CD25+ (Treg), TCRαβ+CD8+CD45RO-CCR7+CD127+CD95+ (stem cell memory T-cells), and TCRαβ+CD4+CD127+CD25-(non-Treg)CD45RO+CXCR5+ (follicular helper T-cells) using TCRαβ-APC, CCR7-PE-Cy7, and CD8-APC-Alexa Fluor 750 (Beckman Coulter [BC], Miami, FL), CD4-Alexa Fluor 700 and CD45RO-FITC (Exbio), CD127-PE-CF594, CD25-PE, and CXCR5-Brilliant Violet (BV) 421 (BD), and PD-1-BV605, CD95-BV510, and HLA-DR-PerCP-Cy5.5 (Biolegend, San Diego, CA).

2.4 | T-cell receptor β repertoire sequencing

DNA was isolated from the above listed T-cell subpopulations with the QIAamp DNA Micro Kit (Qiagen) and used for the preparation of sequencing libraries according to the EuroClonality-NGS working group protocol for the complete TRB-VJ gene rearrangements.[23] Final libraries were sequenced on the MiSeq instrument (Illumina) according to the manufacturer's instructions, and the data were analyzed using the ARResT/Interrogate application.[24] Only clonotypes with productive TRB-VJ rearrangements were selected and filtered based on their frequency in all reads obtained from each sample.

2.5 | *TLR8* and *TLR7* mRNA quantification

Total RNA was isolated from specific cell populations sorted from PBMCs using the FACS Aria III (BD) using the RNeasy Mini Kit (Qiagen) and transcribed to cDNA by an iScript kit (Bio-Rad, Hercules, CA). Gene expression levels of *TLR7* and *TLR8* were determined using TaqMan Gene Expression Assays for *TLR7* (Hs00152971_m1), *TLR8* (Hs00152972_m1), and the *GAPDH* (Hs99999905_m1) gene that was used for normalization; the qPCR reactions were performed on the Applied Biosystems 7500 Fast Real-Time PCR System (all Thermo Fisher Scientific). The gene expression was normalized to *GAPDH* control gene expression in three healthy donors using the delta–delta Ct method.

2.6 | Cell lines

HEK293 and HEK293T cell lines were purchased from American Type Culture Collection (Manassas, VA) and cultured in Dulbecco's Modified Eagle Medium (DMEM) supplemented with 10% fetal bovine serum (FBS) and antibiotics/antimycotics (all from Thermo Fisher Scientific).

2.7 | Plasmids

Plasmids encoding the mutant TRL8 (TLR8^{G572V} or TLR8^{D543A}) were prepared from the TLR8^{WT} construct (pUNO1-hTLR08b, NM_138636, InvivoGen, San Diego, CA) by site-directed mutagenesis (QuikChange™II XL Site-Directed Mutagenesis kit, Agilent Technologies, Santa Clara, CA) using the primer pairs 5′-TAAATTCTAGATGATGTGTTACGACTG CTATTCTGAAATAGTGTGAA-3′ and 5′-TTCACACTATTTCAGAATA GCAGTCGTAACACATCATCTAGAATTTA-3′ (for TLR8^{G572V}) or 5′-CAC TAGCATTATCAAAGGCTAGTCTATTGTTTGTCAAATCC-3′ and 5′-GG ATTTGACAAACAATAGACTAGCCTTTGATAATGCTAGTGCTCTTA-3′ (for TLR8^{D543A}). Successful mutagenesis was confirmed by Sanger sequencing. TLR8^{D543A} served as a negative control.[2]

2.8 | Cycloheximide chase assay

HEK293 and HEK293T cells were seeded in 6-well plates and transfected 24 h later with 4 μg of TLR8^{WT} or TLR8^{G572V} plasmid using Lipofectamine 3000 (Thermo Fisher Scientific) according to the manufacturer's protocol. After 48 h, proteosynthesis was inhibited using 50 μg/mL cycloheximide (Sigma Aldrich, Merck). TLR8 protein level

FIGURE 1 *TLR8* c.1715G>T mutation and partial TLR8 protein deficiency. A pedigree of the family and Sanger sequencing of the DNA (A). Large frontoparietal hemorrhagic lesions (red arrows) with smaller postischemic lesions in the brain stem and corpus callosum (smaller arrows) (B). TLR8 dimer from side view (PDB 3W3G16, G572 in red, top), structure of the liganded TLR8 dimer (middle) and detail of the interaction between G572 (in red) and the ssRNA40 degradation products (bottom)—uridine in ligand binding site 1 and UG dinucleotide in ligand binding site 2, PDB 4R08317 (C).[26] Linear diagram of TLR8 containing an N-terminal domain (LRRNT), a leucine-rich repeat (LRR) ligand recognition domain connected with the Z-loop between LRR 14 and 15, a C-terminal domain (LRRCT), a transmembrane domain anchoring TLR8 to the endosomal membrane and a Toll/interleukin-1 receptor (TIR) domain for signal transduction. Published mutations in LRR14, LRR15 and LRR18 are depicted in blue,[2] and the novel G572V mutation in LRR18 is in red (D). NF-κB transcriptional activity of TLR8^{WT}- and TLR8^{G572V}-containing HEK cells upon TL8-506/CL075 stimulation (E). Basal TLR8 protein levels (F). Sanger sequencing of the monocyte cDNA (G). The relative expression of *TLR8* mRNA (H). Enhanced degradation of mutant TLR8^{G572V} protein compared to TLR8^{WT} (I). Data acquired in two (H) and three (E, F, I) independent experiments, the results are expressed as the mean ± SEM. Histograms show representative data, MFI in numbers. $^{*}p < .05$, $^{**}p < .005$, $^{****}p < .0001$ (unpaired *t*-test). Protein structures visualized using PyMOL 2.3.0 [Color figure can be viewed at wileyonlinelibrary.com]

TABLE 1 Genetics and clinical characteristics

Patient	Patient A	Patient B
Sex	Male	Male
Current age (years)	11	11
Genetic variant		
Chromosome	X	X
Position (hg19)	12938874	12938874
Gene symbol	*TLR8*	*TLR8*
Transcript change	c.1715G>T	c.1715G>T
Transcript	NM_138636	NM_138636
Protein Change	p.G572V	p.G572V
Inheritance	Inherited from mother	Inherited from mother
CADD	25	25
PolyPhen2	0.999	0.999
SIFT	0	0
PhyloP	6.07	6.07
gnomAD AF	Not present	Not present
Clinical manifestation		
Age of onset	1.5 years	7 months
Primary manifestation	Noninfectious cervical lymphadenopathy with xathogranuloma, acute AIHA (6 years)	Transient red cell aplasia acute AIHA (2.5 years)
Chronic AIHA	Yes (positive for anti-red blood cell antibodies, C3d fragments and cold agglutinins)	Yes (positive for anti-red blood cell antibodies, C3d fragments and cold agglutinins)
Coombs testing	Positive (high)	Positive (high)
Thrombocytopenia	Transient during a flare of AIHA	No
Platelet antibody	No	No
Neutropenia	No	No
Episodes of pancytopenia	No	No
Lymphadenopathy	Yes	Yes
Hepatosplenomegaly	Yes	Yes
GI disease	Recurrent noninfectious enteritis	IBD-like disease, biliary obstruction during hemolysis
Lung disease	No	No
Mouth sores	Mild episodes	Mild episodes
Tracheal/larynx sxs	URTIs	URTIs
Hypogammaglobulinemia	Often lower IgG (correlating with CRP—infections)	Often lower IgG (correlating with CRP, SAA—infections)
Infections	*HHV6*, varicella and recurrent shingles, URTIs, *Salmonella enteritis*, *Clostridium enterocolitis*	URTIs, *Salmonella enteritis*, shingles
Skin and joints	Erythema nodosum	Erythema nodosum, polyarthritis
CNS	No symptoms or MRI findings	Multifocal ischemia characterized as SV-cPACNS with hemorrhagic transformation of ischemic stroke (11 years)
Therapy (duration)		
Corticosteroids	Since 6 years continuous PRD 0.2–2.5 mg/kg/day + methylprednisolone	Since 6 years continuous PRD 0.3–2.5 mg/kg/day + methylprednisolone
Other immunosuppression	Azathioprine (3–5 years)	
IVIG	HD-IVIG 2× (7 years) + post rituximab substitution	

TABLE 1 (Continued)

Patient	Patient A	Patient B
Rituximab	5 × 375 mg/m^2 (8 years)	
mTOR inhibition	Sirolimus—target levels of 10 μg/L (from 8 years)	
NSAIDs	–	Ibuprofen 1–2× daily (from 10 years)
anti-IL-1	–	Anakinra 100 mg daily (from 9 years)
Methotrexate	–	15 mg s.c. weekly (from 10 years)
Hydroxychloroquine	200 mg daily (from 12 years)	–
Supportive therapy	PPI, vit. D, anti-hypertensive therapy, antihistamines	PPI, TMP/SMX, zolendronate, vit. D, calcium, anti-hypertensive therapy
HSCT	–	MUD-HSCT (11 years)
T-cell clonality (highly abundant clones)		
Effector memory CD4+		CSVDTGTVYNEQFF (32.71%)
Effector memory CD8+	CASRDGKEVELFF (6.25%)	CASSGLNTEAFF (31.85%); CSARDRDTEAFF (6.07%)

Note: Characterization of the newly identified variant with selected annotation by VEP and an overview of the clinical course of the disease in both twins, including the therapies, with their respective start and duration. Expanded T-cell clones exceeding 5% of all sequenced reads in the selected T-cell subpopulations displayed with their AA CDR3 sequence and their relative abundance.

was detected upon 6, 12, 18, and 24 h inhibition w/wo cycloheximide using flow cytometry.

2.9 | Activity of the TLR8^{G572V} variant

Human HEK-Blue Null1 cells (InvivoGen) were cultured in DMEM supplemented with 10% FBS, normocin (50 μg/mL), and zeocin (100 μg/mL) (all from InvivoGen). NF-κB transcriptional activity was tested by the QUANTI-BLUE assay (InvivoGen). The HEK-Blue Null1 cell line was transfected with either TLR8^{WT} or TLR8^{G572V} (or TLR8^{D543A}) plasmids by transient transfection (Lipofectamine; Life Technologies, Thermo Fisher Scientific). Forty-eight hours post-transfection, the cells were seeded in a 96-well plate at a density of 30 000 cells/well and stimulated with 500 ng/mL or 1 μg/mL CL307, 100 ng/mL or 1 μg/mL CL075; 10, 25, 50, 100, or 500 ng/mL TL8-506; 5, 10, or 25 μg/mL imiquimod, 0.1 or 0.5 μg/mL gardiquimod (all from InvivoGen), and 100, 200, or 500 nM GS-9620 (Vesatolimod, MedChemExpress, Suite Q, Monmouth Junction, NJ) for 24 h. Then, 50 μL of the supernatant from each well was transferred to a 96-well plate with 150 μL of QUANTI-Blue solution (InvivoGen). The plate was incubated at 37°C for 1 h, and the secreted embryonic alkaline phosphatase (SEAP) levels were determined by reading the plate with a spectrophotometer at 650 nm. Untransfected HEK-Blue Null1 cells served as a negative control for TLR8 activation, as these cells are nonresponsive to TLR8 ligands. Fold-change was calculated by normalizing individual data to the unstimulated O.D. of the untransfected well. Similarly, Human HEK-Blue TLR7 cells (InvivoGen) were cultured in DMEM supplemented with 10% FBS, normocin (50 μg/mL), blasticidin (10 μg/mL), and zeocin (100 μg/mL) (all from InvivoGen). NF-κB transcriptional activity was tested using the QUANTI-BLUE assay (InvivoGen). The HEK-Blue TLR7 cell line was transfected by either TLR8^{WT} or TLR8^{G572V} plasmids, seeded in a 96-well plate 48 h post-transfection and stimulated with the same ligands and doses as HEK-Blue Null1. The plate was incubated at 37°C for 1 h, and SEAP levels were determined by reading the plate with a spectrophotometer at 650 nm.

2.10 | Western blotting

Cells were lysed for 30 min on ice in lysis buffer (1% lauryl maltoside (Calbiochem, Merck), 20 mM Tris (pH 7.5), 100 mM NaCl, 5 mM iodoacetamide, 50 mM NaF, 1 mM Na_3VO_4, and 2 mM EDTA (all from Sigma-Aldrich, Merck) containing 100× diluted Protease Inhibitor Cocktail Set III (Calbiochem, Merck). The protein concentration was adjusted to a final concentration of 1 mg/mL using a bicinchoninic acid assay kit according to the manufacturer's instructions (Thermo Fisher Scientific). Proteins were separated on SDS-PAGE gels and transferred to nitrocellulose membranes (Bio-Rad, Hercules, CA). Membranes were blocked at 8°C overnight in phosphate buffered saline (PBS) containing 7.5% low fat bovine milk and 0.05% Tween 20. Primary antibodies against TLR8 (clone D3Z6J, Cell Signaling Technologies) and β-actin (clone AC-74, Sigma-Aldrich, Merck) were used with peroxidase-conjugated secondary antibodies (Jackson Immunoresearch, West Grove, PA) and SuperSignal West Pico/Femto Chemiluminescent Substrates (Thermo Fisher Scientific). Signals were detected using a MINI HD6 scanner (UVITEC, Cambridge, UK) and analyzed with ImageJ software. TLR8 expression levels were normalized to those of β-actin.

2.11 | Immunophenotyping

Immunophenotyping of lymphocyte subpopulations was performed using the following antibody-fluorochrome conjugates: CD4-BV510, IgM-BV510, CD45RA-BV510, CD27-BV421, CD62L-BV421, CD8-FITC,

TABLE 2 Immunological findings

Cell population	Patient A	Patient B	Age-matched reference values
Leukocytes (cells/μL)	14 500	20 400	4500–14 500
Lymphocytes (cells/μL)	3720	*6793*	1300–7500
Neutrophils (cells/μL)	9490	*11 444*	1900–9700
Monocytes (cells/μL)	980	*1958*	0–1300
Eosinophils (cells/μL)	10	102	0–1000
Erythrocytes (cells/μL)	**2 660 000**	**3 600 000**	4 000 000–5 200 000
CD3+ T-cells (% lymphocytes; cells/μL)	*84; 3125*	*86; 5842*	60–76; 1200–2600
CD3+ CD4+ T-cells (% lymphocytes; cells/μL)	37; 1376	32; 2174	31–47; 650–1500
CD3+ CD8+ T-cells (% lymphocytes; cells/μL)	*41; 1525*	*46; 3125*	18–35; 370–1100
NK cells (% lymphocytes; cells/μL) (CD3-CD16+56+)	**0.8; 29**	**1.2; 82**	4–17; 100–480
Regulatory T-cells (% CD3+ T-cells) (CD4+CD25+CD127dim to −)	2.29	2.35	2.29–6.49
Naïve CD4+ (% CD4+ T-cells) (CD3+CD4+CD45RA+CD27+)	67	66	46–99
Central memory CD4+ (% CD4+ T-cells) (CD3+CD4+CD45RA−CD27+)	31	31	0.35–100
Effector memory CD4+ (% CD4+ T-cells) (CD3+CD4+CD45RA−CD27−)	1.8	1.6	0.27–18
Terminally diff. CD4 (% CD4+ T-cells) CD3+CD4+CD45RA+CD27−	0.2	0.1	0.0031–1.8
Th1 (% CD3+4+ T-cells) (CXCR3+CCR6-)	**10.7**	16.4	13.4–25.5
Th2 (% CD3+4+ T-cells) (CXCR3-CCR6-CCR4+CRTH2+)	0.23	0.37	0.19–1.33
Th17 (% CD3+4+ T-cells) (CXCR3-CCR6+)	5.82	5.83	3.53–12
Naïve CD8+ (% CD8+ T-cells) (CD3+CD8+CD45RA+CD27+)	80	83	16–100
Central memory CD8+ (% CD8+ T-cells) (CD3+CD8+CD45RA−CD27+)	4.1	3.7	1–6
Effector memory CD8+ (% CD8+ T-cells) (CD3+CD8+CD45RA−CD27−)	**3.4**	**2**	5–100
Terminally diff. CD8+ (% CD8+ T-cells) (CD3+CD8+CD45RA+CD27−)	**10**	**9.5**	15–41
% HLA-DR/CD3+CD4+ T-cells	3.4	3	N/A
% HLA-DR/CD3+CD8+ T-cells	8	6	N/A
Double negative CD4-CD8-T-cells (% TCRα cells)	*3.9*	*4.3*	<3.5
CD19+ B-cells (% lymphocytes; cells/μL)	9.6; 357	8.1; 550	13–27; 270–860
Naïve (% B-cells) (CD19+CD27-IgD+)	75	61	47.3–77
Transitionals (% B-cells) (CD19+CD27-CD24++CD38++)	*19*	6.4	4.6–8.3
Switched memory (% B-cells) (CD19+CD27+IgD−)	**8.8**	15	10.9–30.4
Marginal zone-like (% B-cells) (CD19+CD27+IgD+)	11	*19*	5.2–20.4
Plasmablasts (% B-cells) (CD19+CD27++CD38++)	**0.1**	1.1	0.6–5.3
CD21low (% B-cells) (CD19+CD21lowCD38low)	3.6	3.6	2.3–10
pDC (% leukocytes)	**0.019**	**0.012**	0.028–0.61
pDC (% DC)	**8.18**	**6.63**	9.59–58.8
mDC (% leukocytes)	0.16	0.11	0.057–0.34
mDC (% DC)	*69*	*61.6*	8.26–60

TABLE 2 (Continued)

Cell population	Patient A	Patient B	Age-matched reference values
Immunoglobulins			
IgG (g/l)	7.68	8.27	7.05–11.9
IgA (g/l)	*2.6*	*2.84*	0.79–1.37
IgM (g/l)	*5.3*	*3.75*	0.47–1.73
Autoantibodies			
ANA (IgG, IgM, IgA)	Mildly positive in IgG	Negative	
ENA	Negative	Negative	
ANCA	Negative	Negative	
ds-DNA	Negative	Negative	
RF (IgG) (IU/mL)	*31.1*	*33.6*	0–22
RF (IgA) (IU/mL)	6.8	4	0–22
RF (IgM) (IU/mL)	*>100*	*>100*	0–22
Anti-tropomyosin	Positive in titer 1:320	Positive in titer 1:160	
Anti-endomysium (IgG, IgA)	Negative	Negative	
ASCA IgG (U/mL)	*15.13*	*17.93*	0–10
ASCA IgA (U/mL)	5.21	5.91	0–10
CIC (arb.units)	*187*	*118*	10–46
CRP (mg/L)	*15.6*	1.8	0–8

Note: Peripheral blood analyses from the time of first admission to the hemato-oncologic department (8 years of age). Bold numbers—values below the reference limit; Italics numbers—values above the reference limit.

IgD-FITC, CD5-PE, CD28-PerCP-Cy5.5, IgM-PerCP-Cy5.5, IgD-PerCP-Cy5.5, and HLA-DR-PerCP-Cy5.5 (Biolegend), CD38-FITC, CD16-PE, CD56-PE, CD4-PerCP-Cy5.5, TCRγδ-PE-Cy7, CD3-APC, CD21-APC, and CD45-APC-H7 (BD), CD19-PE-Cy7, CD24-APC Alexa750, and CD8-APC-Alexa750 (BC), CD45RO-FITC and CD31-PE (Exbio), and CCR7-PE (Miltenyi Biotech, Bergisch Gladbach, Germany). Th1, Th2 and Th17 cells were determined using CD3-Alexa Fluor 700 (Exbio), CD8-V500 and CD45RA-APC-H7 (BD), CD4-BV650, CCR7-APC, CXCR3-PE, CCR6-BV605, CRTH2-FITC, and CCR4-BV421 (BioLegend), and Tregs using CD3-APC-H7, CD25-PE, and CD127-PE-CF594 (BD), CD4-Alexa Fluor 700 and CD19-APC (Exbio), and CD14-PE-Cy7 (BC). The immunophenotype of the DCs was detected using CD45-Pacific Blue (Dako, Glostrup, Denmark), CD3-FITC, CD16-FITC, CD19-FITC, CD20-FITC, CD56-FITC, CD14-PE-Dy594, and CD11c-APC (Exbio), HLA-DR-PE-Cy7 (BD), CD123-PE (Thermo Fisher Scientific), and subpopulations of monocytes with CD66c-FITC, CD13-PE, and CD33-PE-Cy7 (BC), HLA-DR-PerCP-Cy5.5 and CD11b-BV786 (Biolegend), CD45-APC-H7, IREM-2 (CD300e)-APC, CD15-V500 (BD), and CD16-Alexa Fluor 700 and CD14-Pacific Blue (Exbio). Data were collected with Canto II, Lyric, Aria II, or Aria III flow cytometers and analyzed with FlowJo software (BD).

2.12 | Intracellular staining

Whole blood samples or HEK293/T cells were fixed in 4% formaldehyde at room temperature for 10 min, permeabilized in 0.1% Triton X-100 in a water bath (37°C) for 15 min and frozen to −20°C in 10% glycerol in FBS (all from Thermo Fisher Scientific). After thawing, the samples were washed in PBS. TLR8 expression was detected using TLR8-PE (clone S16018A, Biolegend) and TLR7 expression was detected using TLR7-PE antibody (clone 533 707, R&D Systems, Minneapolis, MN) in lymphocytes, monocytes, or granulocytes (identified by FSC, SSC, CD14-APC-H7 (BD), and CD4-BV421 (Biolegend)) or in HEK293/T cells. PBMC from patients and HCs were isolated using a Ficoll-Paque gradient (GE Healthcare, Chicago, IL), resuspended in RPMI 1640 (Lonza, Basel, Switzerland) complemented with 10% FBS and antibiotics (Thermo Fisher Scientific) and stimulated using gardiquimod (0.5 μg/mL), imiquimod (10 μg/mL), TL8-506 (25 ng/mL), or ssRNA40/LyoVec™ (5 μg/mL, all from InvivoGen). After 5, 15, or 30 min in a water bath (37°C), the cells were fixed in 4% formaldehyde and permeabilized in 0.1% Triton X-100, and intracellular signaling was detected using anti-phospho-NF-κB p65 (Ser536)-Alexa Fluor 647 or PE (93H1, Cell Signaling Technology, Danvers, MA, USA) in CD45+CD14+monocytes (CD45-APC-H7 from BD and CD14-PB or PE from Exbio). The data were collected with an LSR II or Celesta flow cytometer and analyzed with FlowJo software (BD).

2.13 | Extracellular cytokine production

The Human Inflammatory Cytokine Kit (BD) was used for the detection of IL-1β, IL-8, IL-6, IL-10, and IL-12p70 in supernatants and patients' and healthy controls' plasma samples according to the manufacturer's instructions. The samples were acquired using a

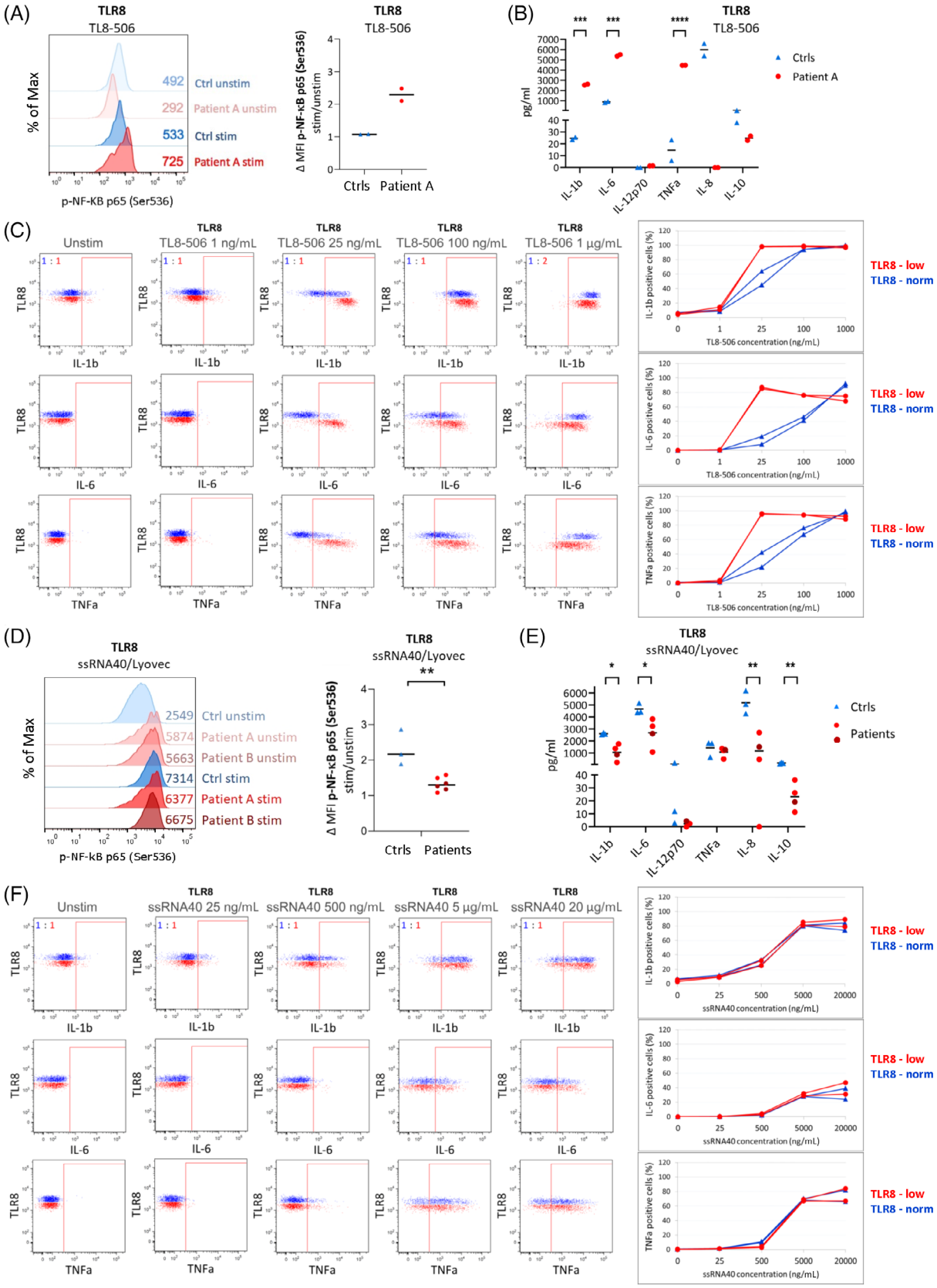

FIGURE 2 Legend on next page.

Celesta flow cytometer and analyzed with FlowJo software (BD). The Human Total IL-18/IL-1F4 Quantikine ELISA Kit (cat. DL180, R&D Systems), Human IFNγ Quantikine ELISA Kit (cat. DIF50, R&D Systems), and IFN Alpha ELISA Kit (cat. 41110-1, PBL Assay Science, Piscataway, NJ) were used for the detection of IL-18, IFNγ and IFNα respectively. The absorbance was measured at 450 nm and analyzed with a VERSAmax Tunable Microplate Reader with the appropriate SoftMaxPro software (Molecular Devices, Sunnyvale, CA).

2.14 | Intracellular cytokine production

Whole blood was withdrawn into ammonium heparin collection tubes and diluted 1:1 with RPMI 1640 (Lonza) complemented with 10% FBS and antibiotics (Thermo Fisher Scientific). To test for cytokine expression in TLR8-positive and TLR8-low monocytes, 100 μL samples were stimulated using gardiquimod (0.025–0.5 μg/mL), imiquimod (0.025–10 μg/mL), GS-9620 (50–1000 nM), ssRNA40/LyoVec™ (0.025–20 μg/mL), or TL8-506 (1–1000 ng/mL) for 6–8 h in 37°C along with brefeldin A (50 μg/mL, Sigma Aldrich, Merck). The surface markers were stained with HLA-DR-BV570 (Biolegend) and CD16-FITC (BC), the samples were fixed in 4% formaldehyde, permeabilized in 0.1% Triton X-100 and intracellular markers were detected using CD14-Pacific Blue or CD11c-Pacific Blue, and Lineage (CD3,19,20,56, CCR3)-FITC (Exbio), CD14-BV711, HLA-DR-BV605, TLR8-PE, IL-6-PE-Cy7, and IL-1β-Alexa Fluor 647 (Biolegend), and TNFα-Alexa Fluor 700, CD123-PE-Cy5.5, and CD45-APC-H7 (BD). Data were collected with an LSR II flow cytometer and Aurora spectral cytometer (Cytek Biosciences, Fremont, CA) and analyzed with FlowJo software (BD).

2.15 | Statistical analysis

Unpaired *t*-test for single comparison was used; *p*-value less than .05 was considered significant.

3 | RESULTS

We report a family with two male monozygotic twins who inherited a novel missense mutation c.1715G>T in the *TLR8* gene located on the X chromosome from their mother (Figure 1A); both siblings developed severe chronic AIHA with lymphoproliferative and progressive autoinflammatory disease. Their disease manifested as corticodependent AIHA at the age of 6 and 2.5 years (in twin A and B, respectively), refractory to second (Intravenous Immunoglobulins, IVIG) and third (azathioprine) line of therapeutics. The bouts of AIHA were induced by frequent respiratory and gastrointestinal infections (e.g., salmonellosis) and, eventually, also by fevers of unknown origin with elevated laboratory markers of inflammation. Both twins were referred to hemato-oncologic department at the age of 8 years, presenting with marked hepatosplenomegaly and cervical lymphadenopathy. The AIHA activity was characterized by high titers of anti-erythrocyte antibodies (IgG in twin A; IgM and IgG in twin B), C3d complement fragments and cold agglutinins (genetic characterization, extended clinical features and results of T-cell repertoire sequencing are summarized in Table 1, blood analyses in Table 2). In attempts to control the AIHA, rituximab (4×375 mg/m^2), followed by sirolimus were used in both patients, which enabled partial steroid detraction. Twin B, however, continued to suffer attacks of fever and developed autoinflammatory organ symptoms (polyarthritis, IBD-like enteropathy, and erythema nodosum). Anti-IL-1 (Anakinra), and eventually, methotrexate were added to his therapy. Despite the combined anti-inflammatory treatment, multifocal CNS vasculitis suddenly manifested with acute hemiparesis and aphasia due to the CNS hemorrhage at the age of 11 years (Figure 1B). This life-threatening event prompted the indication of hematopoietic stem cell transplantation (HSCT) from a matched unrelated donor after a myeloablative conditioning regimen. The post-transplant course was complicated by slow immunological reconstitution, reactivation of cytomegalovirus, adenovirus and EBV requiring prolonged antiviral therapy and thrombocytopenia corrected by eltrombopag. One year after HSCT, complete donor chimerism was achieved and no signs of graft-versus-host disease were present on tapering doses of steroids and cyclosporine A. Twin A continued to experience attacks of fever with panniculitis despite combined corticosteroid and sirolimus treatment. Therefore, hydroxychloroquine was added to the therapeutic regimen, resulting in marked clinical improvement after 1 month, enabling gradual cessation of corticosteroid therapy. Interestingly, the patients' mother has a history of polyarthritis and steroid-sensitive antiphospholipid syndrome.

TLR8 forms a homodimer that undergoes a conformation change upon ligand binding activating its downstream signaling. The c.1715G>T mutation leads to a substitution of glycine with valine at position 572 (p.G572V) in leucine-rich repeat (LRR) 18 in proximity to the first ligand-binding site[25–27] (Figure 1C,D) and could, therefore, affect the TLR8 activity.

FIGURE 2 The response of patients' cells to diverse TLR8 ligands. Phosphorylation (p-) of NF-κB p65 (Ser536) in monocytes (A) and production of pro-inflammatory cytokines from PBMCs upon stimulation with chemical TLR8 ligand TL8-506 (25 ng/mL) (B). Production of proinflammatory cytokines from mother's TLR8-low and TLR8-norm (healthy) cells upon stimulation with chemical TLR8 ligand TL8-506 (C). Phosphorylation of NF-κB p65 (Ser536) in monocytes (D) and production of pro-inflammatory cytokines from PBMC upon stimulation with TLR8 ligand ssRNA40/Lyovec (5 μg/mL) (E). Production of proinflammatory cytokines from mother's TLR8-low and TLR8-nom (healthy) cells upon stimulation with TLR8 ligand ssRNA40/Lyovec (F). Data acquired in two (A, B, C, F) and three (D, E) independent experiments, mean ± SEM. Histograms and dot plots show representative data, the gates indicate positivity for respective cytokine according to unstimulated state, MFI in numbers. $^*p < .05$, $^{**}p < .005$ (unpaired *t*-test) [Color figure can be viewed at wileyonlinelibrary.com]

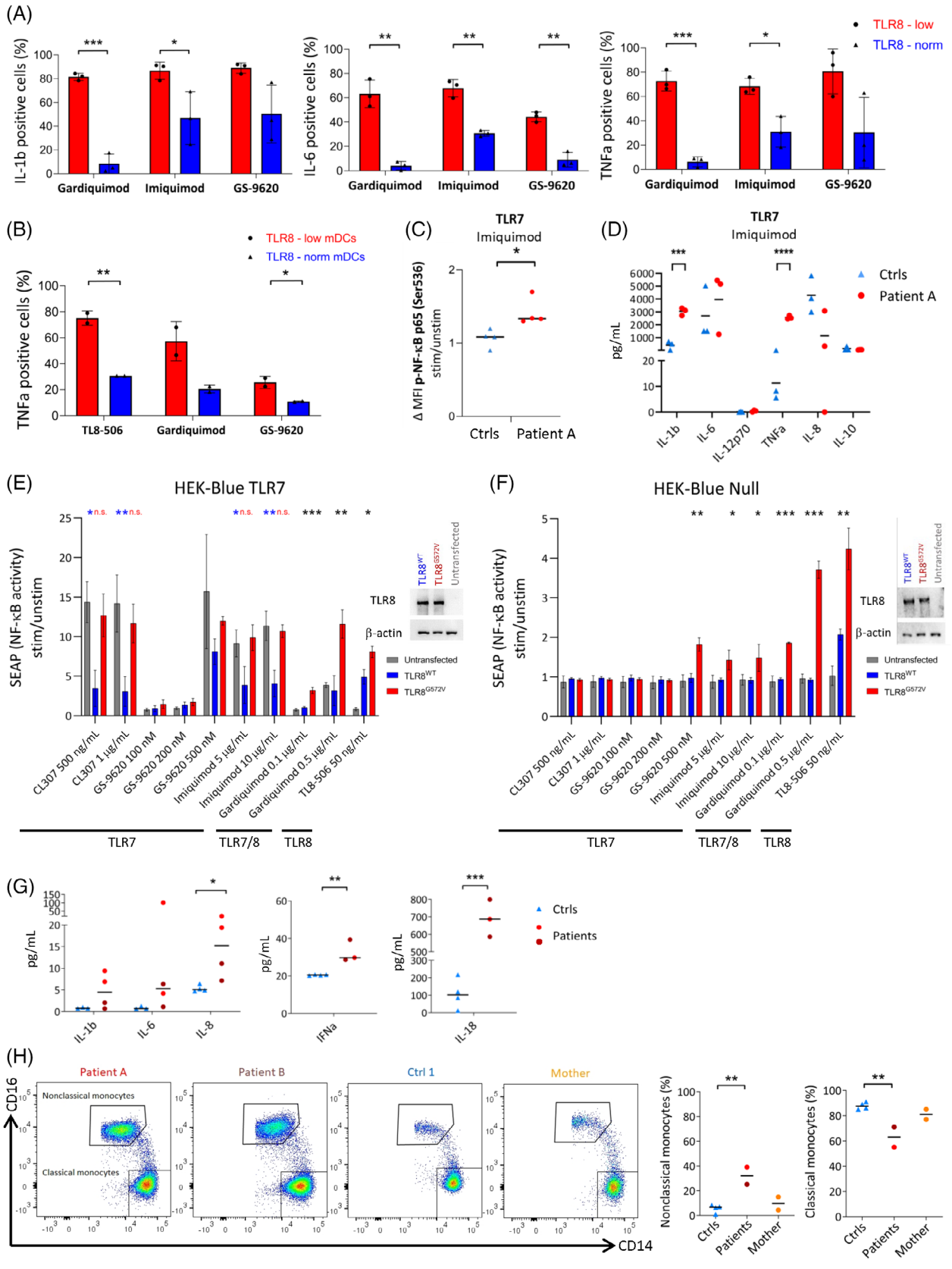

FIGURE 3 Legend on next page.

Once the wild-type TLR8 ($TLR8^{WT}$) and mutant TLR8 ($TLR8^{G572V}$) were transiently expressed in HEK-Blue TLR7/8-Null cells and stimulated with base analogs TL8-506 and CL075, $TLR8^{G572V}$ showed increased NF-κB transcriptional activity compared to $TLR8^{WT}$ (Figure 1E). However, TLR8 protein levels were half that of the healthy controls in the patients' cells (Figure 1F). An unexpected observation was made in the mother, whose cells could be separated into two populations based on TLR8 protein levels; a higher one (as controls) and a lower one (as the patients), due to random inactivation of the X chromosome bearing the c.1715G>T mutation (Figure 1F,G). We speculated that mRNA level or protein stability could be affected by the mutation. The *TLR8* mRNA levels were not significantly different in sorted monocytes of both twins compared to healthy controls (Figure 1H). However, upon transient transfection of $TLR8^{WT}$ and $TLR8^{G572V}$ into HEK293/T cells and stopping the proteosynthesis with cycloheximide, the mutant $TLR8^{G572V}$ protein was degraded more rapidly compared to $TLR8^{WT}$ (Figure 1I). Intriguingly, various TLR8 ligands elicited different responses. Chemical compounds, such as TL8-506 or CL075, bind only at site 1, enabling strong non-physiological TLR8 activation.[27] Stimulation with TL8-506 increased phospho- (p-)NF-κB and proinflammatory cytokine production in the patients' peripheral blood mononuclear cells (PBMCs, Figure 2A,B) and, consistently, in the mother's TLR8-low monocytes compared to her TLR8-norm monocytes (Figure 2C). However, ssRNA40 (which better mimics viral/bacterial RNA and requires two binding sites to physiologically activate TLR8[26]) did not trigger this hyperactivation (Figure 2D–F). Moreover, both the patients' and the mother's TLR8-low cells responded more to TLR7 ligands. We observed increased production of the proinflammatory cytokines IL-1β, IL-6, and TNFα by the mother's TLR8-low monocytes (Figure 3A) (similarly by her TLR8-low mDCs, Figure 3B) as well as enhanced p-NF-κB in the patients' monocytes (Figure 3C) and cytokine production in the patients' PBMCs (Figure 3D). Of note, *TLR7* gene, and basal TLR7 mRNA/protein levels were not affected. This suggests that mutant $TLR8^{G572V}$ could impair the interaction with TLR7[9,28] and skew the $TLR8^{G572V}$/TLR7 balance towards TLR7,[9] manifesting as a TLR7-dependent autoinflammatory phenotype. As expected, transient co-expression of $TLR8^{G572V}$ or $TLR8^{WT}$ with TLR7 in HEK-Blue TLR8-TLR7+ cells led to attenuation of TLR7 signaling in $TLR8^{WT}$-transfected cells,[7,9] but not in $TLR8^{G572V}$-transfected cells (Figure 3E). Moreover, $TLR8^{G572V}$ cross-reacted to diverse TLR7 ligands in comparison to $TLR8^{WT}$ in HEK-Blue TLR8-TLR7- cells (Figure 3F).

The dysregulation of TLR7 and TLR8 is well described in murine models where TLR8 deficiency causes TLR7-driven autoantibody production and glomerulonephritis[16]; structural studies also showed that TLR8 mutations near ligand binding site 1 skewed the affinity to TLR7 ligands[10]; however, little is known about these phenomena in humans. In this study, the patients presented with a partial TLR8 protein deficiency, with mutant $TLR8^{G572V}$ that did not impair TLR7 signaling and cross-responded to diverse TLR7 ligands. This imbalance between mutant $TLR8^{G572V}$ and TLR7 introduced a bias towards TLR7-dependent pro-inflammatory signaling. The successful use of hydroxychloroquine in twin A indirectly supports our findings.

Since TLR8 and TLR7 act in a balance to recognize ssRNA of external pathogens as well as endogenous ssRNA within immune complexes,[11,12] their imbalance may lead to pathological responses to microbes and drive autoinflammation. Indeed, both twins suffered from frequent enteritis and fevers and their AIHA worsened with infections. We found increased levels of multiple pro-inflammatory cytokines, type I interferons (Figure *3*G), and increased counts of pro-inflammatory nonclassical monocytes[29] in their peripheral blood (Figure 3H).

4 | DISCUSSION

The disparity in the disease severity between twin A and B is intriguing. It may be explained by different spectrum of pathogens encountered by the siblings, which may have revealed diverse autoantigens driving the severity of autoinflammatory phenomena. Interestingly, the disturbed recognition of autoantigens (self-nucleic acids) by endosomal TLRs contributes to the pathogenesis of SLE,[11] which may present with corresponding clinical features to those of our patients (AIHA, fevers, arthritis, and CNS vasculitis).[30] Both twins also had high plasma levels of autoantibodies, and increased double-negative TCRαβ+CD4-CD8-T-cells (Table 2), which are associated with autoimmunity. The development of autoimmunity can be intrinsic and/or extrinsic. Regulatory T-cells could be affected directly by TLR8 mutation[31] or indirectly by an inflammatory environment.[32] Moreover, dysregulated TLRs can affect the activity of antigen-presenting cells similar to a murine model of SLE with TLR8 deficiency and thus drive T-cell proliferation.[33] Hypothetically, the activated T-cells might also include autoreactive clones, which would subsequently activate autoreactive B-cells. Interestingly, both patients presented with

FIGURE 3 Imbalance in activation induced by TLR7 agonists in patients' cells and cellular models, and inflammatory phenotypes in patients' peripheral blood. Production of proinflammatory cytokines from mother's TLR8-low and TLR8-norm (healthy) monocytes (A) and mDCs (B) upon stimulation with TLR7 ligands Imiquimod (10 μg/mL) and GS-9620 (Vesatolimod, 500 nM), or TLR7/8 ligand Gardiquimod (0.5 μg/mL). Phosphorylation of NF-κB p65 (Ser536) in monocytes (C) and production of pro-inflammatory cytokines from PBMC upon stimulation with TLR7 ligand Imiquimod (10 μg/mL) (D). Impaired inhibitory effect of mutant $TLR8^{G572V}$ on TLR7 signaling compared to $TLR8^{WT}$. Black asterisks indicate significance between $TLR8^{WT}$ and mutant $TLR8^{G572V}$; blue asterisks indicate significance between untransfected cells and $TLR8^{WT}$-transfected cells; comparison between untransfected cells and $TLR8^{G572V}$-transfected cells is in red (E). $TLR8^{G572V}$ gain-of-function upon TLR8 stimulation (TL8-506) and upon TLR7 stimulation (GS-9620, Imiquimod) (F). Cytokine levels in patients' and controls' peripheral blood plasmas (G). Enriched nonclassical monocytes (CD45+CD66c-CD13+HLA-DR+IREM-2+CD14dimCD16+) in patients' monocytes pool (H). Data acquired in three (A, C, D, E, F, G) and two (B, H) independent experiments, mean ± SEM. Histograms, dot plots and WB show representative data. $^{*}p < .05$, $^{**}p < .005$, $^{***}p < .0005$, $^{****}p < .0001$ (unpaired *t*-test) [Color figure can be viewed at wileyonlinelibrary.com]

oligoclonality and expanded clonotypes within their effector T-cells subsets (Table 1). In summary, we show the first human partial TLR8 protein deficiency, which manifests as complex autoimmune and autoinflammatory phenotypes. The mutation causes TLR8 cross-reactivity to TLR7 ligands and leads to dysregulation of TLR8 and TLR7 responses. Finally, we propose the inclusion of partial TLR8 protein deficiency with TLR8/TLR7 dysregulation in the classification of Inborn Errors of Immunity.

ACKNOWLEDGMENTS

This study was performed in accordance with the recommendations of the Second Faculty of Medicine Ethics Committee Guidelines and the Declaration of Helsinki. We are especially grateful to the patients and their parents for giving us consent to perform all research activities associated with the disease and to publish the results. We also kindly acknowledge Nermina Saucier, Katerina Rejlova, and Pavel Semerak for their technical assistance.

CONFLICT OF INTEREST

Authors declare that they have no competing interests.

AUTHOR CONTRIBUTIONS

Martina Fejtkova and Veronika Kanderova designed, performed, and analyzed the ex vivo and in vitro experiments and immunophenotyping. Martina Sukova cared for the patients and provided clinical data. Michael Svaton and Eva Fronkova designed, performed, and analyzed the genetic tests. David Jakubec performed structural analyses. Jahnavi Aluri, Katerina Hlozkova, and Karolina Skvarova Kramarzova designed the in vitro cellular model and performed and analyzed the in vitro experiments. Michaela Novakova, Adam Klocperk, Zuzana Parackova, and Anna Sediva contributed to the immunological characterization of the patients and analyzed the ex vivo experiments. Marketa Rackova and Marina Bakardjieva performed in vitro and ex vivo experiments. Tomas Kalina, Marketa Bloomfield, and Ondrej Hrusak supervised the study, reviewed the manuscript and provided comments. Martina Sukova, Petr Sedlacek, Hana Malcova, Zuzana Liba, Martin Kudr, and Jan Stary provided medical care, critically reviewed the manuscript and provided comments. Veronika Kanderova, Michael Svaton, and Megan A. Cooper designed the project and supervised the research. Martina Fejtkova, Veronika Kanderova, and Michael Svaton wrote the manuscript. All of the authors provided critical input and agreed to this publication.

DATA AVAILABILITY STATEMENT

The data that support the findings of this study are available from the corresponding authors upon reasonable request.

ORCID

Martina Fejtkova https://orcid.org/0000-0002-6417-4486
Karolina Skvarova Kramarzova https://orcid.org/0000-0003-4860-7453
Marketa Rackova https://orcid.org/0000-0002-2991-8873
Marina Bakardjieva https://orcid.org/0000-0002-5919-6306
Marketa Bloomfield https://orcid.org/0000-0001-5330-9341
Adam Klocperk https://orcid.org/0000-0002-1526-4557
Zuzana Parackova https://orcid.org/0000-0002-2398-532X
Anna Sediva https://orcid.org/0000-0001-7730-2304
Michaela Novakova https://orcid.org/0000-0003-2964-5956
Tomas Kalina https://orcid.org/0000-0003-4475-2872
Michael Svaton https://orcid.org/0000-0003-2966-3687
Veronika Kanderova https://orcid.org/0000-0001-8513-1066

REFERENCES

1. Picard C, von Bernuth H, Ghandil P, et al. Clinical features and outcome of patients with Irak-4 and MyD88 deficiency. *Medicine*. 2010; 89(6):403-425. doi:10.1097/MD.0b013e3181fd8ec3
2. Aluri J, Bach A, Kaviany S, et al. Immunodeficiency and bone marrow failure with mosaic and germline TLR8 gain of function. *Blood*. 2021; 137(18):2450-2462. doi:10.1182/blood.2020009620
3. Farrugia M, Baron B. The role of toll-like receptors in autoimmune diseases through failure of the self-recognition mechanism. *Int J Inflam*. 2017;2017:1-12. doi:10.1155/2017/8391230
4. Eigenbrod T, Pelka K, Latz E, Kreikemeyer B, Dalpke AH. TLR8 senses bacterial RNA in human monocytes and plays a nonredundant role for recognition of streptococcus pyogenes. *J Immunol*. 2015;195(3): 1092-1099. doi:10.4049/jimmunol.1403173
5. Bender AT, Tzvetkov E, Pereira A, et al. TLR7 and TLR8 differentially activate the IRF and NF-κB pathways in specific cell types to promote inflammation. *ImmunoHorizons*. 2020;4(2):93-107. doi:10.4049/immunohorizons.2000002
6. Asano T, Boisson B, Onodi F, et al. X-linked recessive TLR7 deficiency in ~1% of men under 60 years old with life-threatening COVID-19. *Sci Immunol*. 2021;6(62). doi:10.1126/sciimmunol.abl4348
7. de Marcken M, Dhaliwal K, Danielsen AC, Gautron AS, Dominguez-Villar M. TLR7 and TLR8 activate distinct pathways in monocytes during RNA virus infection. *Sci Signal*. 2019;12(605):eaaw1347. doi: 10.1126/scisignal.aaw1347
8. Larange A, Antonios D, Pallardy M, Kerdine-Romer S. TLR7 and TLR8 agonists trigger different signaling pathways for human dendritic cell maturation. *J Leukoc Biol*. 2009;85(4):673-683. doi:10.1189/jlb.0808504
9. Wang J, Shao Y, Bennett TA, Shankar RA, Wightman PD, Reddy LG. The functional effects of physical interactions among toll-like receptors 7, 8, and 9. *J Biol Chem*. 2006;281(49):37427-37434. doi: 10.1074/jbc.M605311200
10. Zhang Z, Ohto U, Shibata T, et al. Structural analyses of toll-like receptor 7 reveal detailed RNA sequence specificity and recognition mechanism of agonistic ligands. *Cell Rep*. 2018;25(12):3371-3381.e5. doi:10.1016/j.celrep.2018.11.081
11. Lee PY, Kumagai Y, Li Y, et al. TLR7-dependent and FcγR-independent production of type I interferon in experimental mouse lupus. *J Exp med*. 2008;205(13):2995-3006. doi:10.1084/jem.20080462
12. Hoffmann MH, Skriner K, Herman S, et al. Nucleic acid-stimulated antigen-presenting cells trigger T cells to induce disease in a rat transfer model of inflammatory arthritis. *J Autoimmun*. 2011;36(3–4):288-300. doi:10.1016/j.jaut.2011.02.007
13. Guiducci C, Gong M, Cepika A-M, et al. RNA recognition by human TLR8 can lead to autoimmune inflammation. *J Exp med*. 2013; 210(13):2903-2919. doi:10.1084/jem.20131044
14. Deane JA, Pisitkun P, Barrett RS, et al. Control of toll-like receptor 7 expression is essential to restrict autoimmunity and dendritic cell proliferation. *Immunity*. 2007;27(5):801-810. doi:10.1016/j.immuni.2007.09.009
15. Fairhurst A, Hwang S, Wang A, et al. Yaa autoimmune phenotypes are conferred by overexpression of TLR7. *Eur J Immunol*. 2008;38(7): 1971-1978. doi:10.1002/eji.200838138

16. Demaria O, Pagni PP, Traub S, et al. TLR8 deficiency leads to autoimmunity in mice. *J Clin Invest*. 2010;120(10):3651-3662. doi:10.1172/JCI42081
17. Desnues B, Macedo AB, Roussel-Queval A, et al. TLR8 on dendritic cells and TLR9 on B cells restrain TLR7-mediated spontaneous autoimmunity in C57BL/6 mice. *Proc Natl Acad Sci*. 2014;111(4):1497-1502. doi:10.1073/pnas.1314121111
18. Li H, Durbin R. Fast and accurate short read alignment with Burrows-Wheeler transform. *Bioinformatics*. 2009;25(14):1754-1760. doi:10.1093/bioinformatics/btp324
19. Koboldt DC, Zhang Q, Larson DE, et al. VarScan 2: somatic mutation and copy number alteration discovery in cancer by exome sequencing. *Genome Res*. 2012;22(3):568-576. doi:10.1101/gr.129684.111
20. Li H, Handsaker B, Wysoker A, et al. The sequence alignment/map format and SAMtools. *Bioinformatics*. 2009;25(16):2078-2079. doi:10.1093/bioinformatics/btp352
21. Tangye SG, Al-Herz W, Bousfiha A, et al. Human inborn errors of immunity: 2019 update on the classification from the International Union of Immunological Societies Expert Committee. *J Clin Immunol*. 2020;40(1):24-64. doi:10.1007/s10875-019-00737-x
22. Sobreira N, Schiettecatte F, Valle D, Hamosh A. GeneMatcher: A Matching Tool for Connecting Investigators with an Interest in the Same Gene. *Human Mutation*. 2015;36(10):928-930. doi:10.1002/humu.22844
23. Brüggemann M, Kotrová M, Knecht H, et al. Standardized next-generation sequencing of immunoglobulin and T-cell receptor gene recombinations for MRD marker identification in acute lymphoblastic leukaemia; a EuroClonality-NGS validation study. *Leukemia*. 2019;33(9):2241-2253. doi:10.1038/s41375-019-0496-7
24. Bystry V, Reigl T, Krejci A, et al. ARResT/interrogate: an interactive immunoprofiler for IG/TR NGS data. *Bioinformatics*. 2016;33(3):435-437. doi:10.1093/bioinformatics/btw634
25. Tanji H, Ohto U, Motoi Y, Shibata T, Miyake K, Shimizu T. Autoinhibition and relief mechanism by the proteolytic processing of toll-like receptor 8. *Proc Natl Acad Sci U S A*. 2016;113(11):3012-3017. doi:10.1073/pnas.1516000113
26. Tanji H, Ohto U, Shibata T, et al. Toll-like receptor 8 senses degradation products of single-stranded RNA. *Nat Struct Mol Biol*. 2015;22(2):109-115. doi:10.1038/nsmb.2943
27. Tanji H, Ohto U, Shibata T, Miyake K, Shimizu T. Structural reorganization of the toll-like receptor 8 dimer induced by agonistic ligands. *Science*. 2013;339(6126):1426-1429. doi:10.1126/science.1229159
28. Itoh H, Tatematsu M, Watanabe A, et al. UNC93B1 physically associates with human TLR8 and regulates TLR8-mediated signaling. *PLoS One*. 2011;6(12):e28500. doi:10.1371/journal.pone.0028500
29. Mukherjee R, Kanti Barman P, Kumar Thatoi P, Tripathy R, Kumar Das B, Ravindran B. Non-classical monocytes display inflammatory features: validation in sepsis and systemic lupus erythematous. *Sci Rep*. 2015;5(July):1-14. doi:10.1038/srep13886
30. Bundhun PK, Kumari A, Huang F. Differences in clinical features observed between childhood-onset versus adult-onset systemic lupus erythematosus. *Medicine*. 2017;96(37):e8086. doi:10.1097/MD.0000000000008086
31. Peng G, Guo Z, Kiniwa Y, et al. Toll-like receptor 8-mediated reversal of CD4+ regulatory T cell function. *Science*. 2005;309(5739):1380-1384. doi:10.1126/science.1113401
32. La Cava A. Tregs are regulated by cytokines: implications for autoimmunity. *Autoimmun Rev*. 2008;8(1):83-87. doi:10.1016/j.autrev.2008.08.002
33. Tran NL, Manzin-Lorenzi C, Santiago-Raber ML. Toll-like receptor 8 deletion accelerates autoimmunity in a mouse model of lupus through a toll-like receptor 7-dependent mechanism. *Immunology*. 2015;145(1):60-70. doi:10.1111/imm.12426

How to cite this article: Fejtkova M, Sukova M, Hlozkova K, et al. TLR8/TLR7 dysregulation due to a novel *TLR8* mutation causes severe autoimmune hemolytic anemia and autoinflammation in identical twins. *Am J Hematol*. 2022;97(3):338-351. doi:10.1002/ajh.26452

Příloha 5

Formankova R, Kanderova V, Rackova M, **Svaton M**, Brdicka T, Riha P, Keslova P, Mejstrikova E, Zaliova M, Freiberger T, Grombirikova H, Zemanova Z, Vlkova M, Fencl F, Copova I, Bronsky J, Jabandziev P, Sedlacek P, Soukalova J, Zapletal O, Stary J, Trka J, Kalina T, Skvarova Kramarzova K, Hlavackova E, Litzman J, Fronkova E. Novel SAMD9 Mutation in a Patient With Immunodeficiency, Neutropenia, Impaired Anti-CMV Response, and Severe Gastrointestinal Involvement. *Front Immunol.* 2019 Sep 18;10:2194. doi: 10.3389/fimmu.2019.02194.

frontiers in Immunology

CASE REPORT
published: 18 September 2019
doi: 10.3389/fimmu.2019.02194

Novel SAMD9 Mutation in a Patient With Immunodeficiency, Neutropenia, Impaired Anti-CMV Response, and Severe Gastrointestinal Involvement

Renata Formankova[1†], Veronika Kanderova[1†], Marketa Rackova[1], Michael Svaton[1], Tomas Brdicka[2], Petr Riha[1], Petra Keslova[1], Ester Mejstrikova[1], Marketa Zaliova[1], Tomas Freiberger[3,4,5], Hana Grombirikova[3,5], Zuzana Zemanova[6], Marcela Vlkova[5,7], Filip Fencl[8], Ivana Copova[8], Jiri Bronsky[8], Petr Jabandziev[4,5,9], Petr Sedlacek[1], Jana Soukalova[5,10], Ondrej Zapletal[11], Jan Stary[1], Jan Trka[1], Tomas Kalina[1], Karolina Skvarova Kramarzova[1], Eva Hlavackova[5,7], Jiri Litzman[5,7] and Eva Fronkova[1†]*

[1] Department of Paediatric Haematology and Oncology, 2nd Faculty of Medicine, Charles University and University Hospital Motol, Prague, Czechia, [2] Institute of Molecular Genetics of the Czech Academy of Sciences, Prague, Czechia, [3] Molecular Genetics Laboratory, Center of Cardiovascular Surgery and Transplantation, Brno, Czechia, [4] CEITEC, Masaryk University, Brno, Czechia, [5] Faculty of Medicine, Masaryk University, Brno, Czechia, [6] Center of Oncocytogenetics, Institute of Clinical Biochemistry and Laboratory Diagnostics, 1st Faculty of Medicine, Charles University and General University Hospital, Prague, Czechia, [7] Department of Clinical Immunology and Allergology, St. Anne's University Hospital Brno, Brno, Czechia, [8] Department of Paediatrics, 2nd Faculty of Medicine, Charles University and University Hospital Motol, Prague, Czechia, [9] Department of Paediatrics, University Hospital Brno, Brno, Czechia, [10] Department of Medical Genetics, University Hospital Brno, Brno, Czechia, [11] Department of Pediatric Hematology, University Hospital Brno, Brno, Czechia

OPEN ACCESS

Edited by:
Yenan Bryceson,
Karolinska Institute (KI), Sweden

Reviewed by:
Kimberly Gilmour,
Great Ormond Street Hospital, United Kingdom
Silvia Clara Giliani,
University of Brescia, Italy

***Correspondence:**
Eva Fronkova
eva.fronkova@lfmotol.cuni.cz

[†]These authors have contributed equally to this work

Specialty section:
This article was submitted to Primary Immunodeficiencies, a section of the journal Frontiers in Immunology

Received: 23 January 2019
Accepted: 30 August 2019
Published: 18 September 2019

Citation:
Formankova R, Kanderova V, Rackova M, Svaton M, Brdicka T, Riha P, Keslova P, Mejstrikova E, Zaliova M, Freiberger T, Grombirikova H, Zemanova Z, Vlkova M, Fencl F, Copova I, Bronsky J, Jabandziev P, Sedlacek P, Soukalova J, Zapletal O, Stary J, Trka J, Kalina T, Skvarova Kramarzova K, Hlavackova E, Litzman J and Fronkova E (2019) Novel SAMD9 Mutation in a Patient With Immunodeficiency, Neutropenia, Impaired Anti-CMV Response, and Severe Gastrointestinal Involvement. Front. Immunol. 10:2194. doi: 10.3389/fimmu.2019.02194

Mutations in the Sterile alpha motif domain containing 9 (*SAMD9*) gene have been described in patients with severe multisystem disorder, MIRAGE syndrome, but also in patients with bone marrow (BM) failure in the absence of other systemic symptoms. The role of hematopoietic stem cell transplantation (HSCT) in the management of the disease is still unclear. Here, we present a patient with a novel mutation in *SAMD9* (c.2471 G>A, p.R824Q), manifesting with prominent gastrointestinal tract involvement and immunodeficiency, but without any sign of adrenal insufficiency typical for MIRAGE syndrome. He suffered from severe CMV (cytomegalovirus) infection at 3 months of age, with a delayed development of T lymphocyte functional response against CMV, profound T cell activation, significantly reduced B lymphocyte counts and impaired lymphocyte proliferative response. Cultured T cells displayed slightly lower calcium flux and decreased survival. At the age of 6 months, he developed severe neutropenia requiring G-CSF administration, and despite only mild morphological and immunophenotypical disturbances in the BM, 78% of the BM cells showed monosomy 7 at the age of 18 months. Surprisingly, T cell proliferation after CD3 stimulation and apoptosis of the cells normalized during the follow-up, possibly reflecting the gradual development of monosomy 7. Among other prominent symptoms, he had difficulty swallowing, requiring percutaneous endoscopic gastrostomy (PEG), frequent gastrointestinal infections, and perianal erosions. He suffered from repeated infections and periodic recurring fevers with the elevation of inflammatory markers. At 26 months

of age, he underwent HSCT that significantly improved hematological and immunological laboratory parameters. Nevertheless, he continued to suffer from other conditions, and subsequently, he died at day 440 post-transplant due to sepsis. Pathogenicity of this novel *SAMD9* mutation was confirmed experimentally. Expression of mutant *SAMD9* caused a significant decrease in proliferation and increase in cell death of the transfected cells.

Conclusion: We describe a novel *SAMD9* mutation in a patient with prominent gastrointestinal and immunological symptoms but without adrenal hypoplasia. Thus, SAMD9 mutations should be considered as cause of enteropathy in pediatric patients. The insufficient therapeutic outcome of transplantation further questions the role of HSCT in the management of patients with *SAMD9* mutations and multisystem involvement.

Keywords: SAMD9, MIRAGE, immunodeficiency, neutropenia, cytomegalovirus infection, dysphagia, hematopoietic stem cell transplantation, gastrointestinal disorder

BACKGROUND

In 2016, Narumi et al. (1) reported mutations in Sterile alpha motif domain-containing protein 9 (SAMD9) in 11 patients examined primarily for adrenal hypoplasia. Most of the patients shared strikingly similar phenotypes, and thus, a novel multisystem disorder, MIRAGE (myelodysplasia, infection, restriction of growth, adrenal hypoplasia, genital phenotypes, and enteropathy) syndrome, was defined. Two patients from the cohort developed myelodysplastic syndrome (MDS) accompanied by loss of the chromosome 7 carrying the SAMD9 mutation. In 2017, Buonocore et al. (2) found similar *de-novo*, heterozygous *SAMD9* mutations in 8 children with a complex multisystem growth restriction phenotype. Adrenal insufficiency was frequently but not constantly present.

The appropriate treatment of the patients with SAMD9 mutations is not currently known. Fourteen of 19 patients from the first two studies died, mostly due to severe infections, in first 2 years of age. Two patients from the surviving group developed MDS with monosomy 7 and received hematopoietic stem cell transplantation (HSCT). Monosomy 7, deletions of 7q or secondary somatic loss of function mutation in SAMD9 frequently developed as a compensatory mechanism for the mutated allele, which rescued the growth-restricting effect of the *SAMD9* mutation, but it could lead to MDS in some of the patients. Schwarz reported a germline *SAMD9* mutation in three siblings with MDS and monosomy 7. Interestingly, the patients had an otherwise mild phenotype with no signs of MIRAGE syndrome except for hypospadia and bifid scrotum in one boy, and even had an asymptomatic mother carrying the same mutation (3). Bluteau et al. found 6 patients with mutated *SAMD9* and 10 patients with a mutation in SAMD9 counterpart *SAMD9L* (4) in a cohort of 86 patients with BM failure of suspected inherited origin (5). The patients presented with mild BM failure and monosomy 7, and only one presented typical signs of MIRAGE syndrome.

CASE PRESENTATION

We describe the case of a Caucasian boy from the 4th gravidity of healthy, non-consanguineous parents. In the first month after a preterm birth (32 weeks and 3 days of pregnancy, weight 1,450 g), he manifested with bilateral bronchopneumonia and hepatopathy that progressed to septicemia with bradycardia and respiratory failure requiring ventilation support. Generalized primary cytomegalus virus (CMV) infection was confirmed at the age of 3 months. His health status was complicated by bilateral pneumonia followed by respiratory distress that demanded ventilation support complicated by disseminated intravascular coagulation and septic shock. A 6-week treatment with ganciclovir was introduced. Antimycotic treatment was introduced for suspected aspergillus infection. A huge persisting cutaneous defect in the gluteal region with uretroscrotal fistula was present from the second month of age complicated by scrotal abscess at the age of 5 months.

He suffered from recurrent upper respiratory tract infections but also sepsis of unknown origin with high fever, and high C-reactive protein (CRP) responding to antibiotic treatment. From the age of 14 months, he had recurring pneumonia with respiratory distress and septicemia at the age of 18 months. Recurrent oral, nasal and urethral candidiasis were confirmed.

Gastrointestinal Involvement

Because of hypoproteinic malnutrition, failure to thrive and inability to swallow presumably caused by frequent vomiting, percutaneous endoscopic gastrostomy (PEG) was introduced at the age of 5 months. PEG tube management was complicated by extensive leakage. He suffered from sublingual erosions, diarrhea, recurrent proctocolitis with intestinal bleeding, and chronic perianal erosions. Hemorrhagic proctocolitis caused by *Pseudomonas aeuruginosa* with septicemia manifested at the age of 13 months. Severe *Clostridium difficile* gastroenteritis demanding intensive care manifested at the age of 23 months. Gastroscopy and colonoscopy at 18 months of age did not reveal any significant disturbances. Histologic evaluation of the

duodenal mucosa showed a mild deficit of disaccharides and other enzymes of the brush-border and mild chronic non-active enteritis.

Hematopoietic System Involvement

Immediately after birth, the patient presented with transient thrombocytopenia and anemia (**Figure 1A**). From 6 months of age, he had significant neutropenia with absolute neutrophil count (ANC) $< 0.5 \times 10^9$/l. Granulocyte colony stimulating factor G-CSF was introduced at the age of 19 months. BM evaluation at 18 months of age revealed normocellularity with reduced myeloid lineage (31%) with gradual maturation and increased erythroid lineage (48%); megakaryocytes were in the normal range, and atypical cells were not documented.

Other Symptoms

Hypospadia, micropenis, central hypotonic syndrome, pseudobulbar syndrome, psychomotor retardation, and mild orofacial stigmatization with macroglossia and hypomimia were documented.

HSCT

The patient was indicated for HSCT for unspecified primary immunodeficiency with severe infections, neutropenia and lack of B-cells at the age of 26 months. Conditioning regimen included busulfan targeted to plasma concentrations of 500–700 ng/mL from days−5 to−2, fludarabine 40 mg/m^2/day from days−6 to−3 and alemtuzumab in total dose 1 mg/kg from days−8 to−6. Graft-vs.-host (GVHD) prophylaxis administered from day−1 consisted of cyclosporine A (CsA) and mycophenolate mofetil (MMF). Plasmapheresis was performed for high titers of anti-A antibodies in the situation of ABO incompatibility on days −10, −9, −8, and on day 0. He received a BM graft from his HLA identical older brother (2.6×10^8 nucleated cells/kg, 5.6×10^6 of CD34pos cells). Neutrophil engraftment defined as the first of 3 days with ANC above 0.5×10^9/l was achieved on day +18, thrombocyte engraftment (the thrombocytes count above 20×10^6/l without transfusion in previous 7 days) on day +33, respectively. Complete donor chimerism (>98% donor cells) in non-separated peripheral blood (PB) evaluated by PCR amplification of the microsatellite markers was documented from day +21. The early post-transplant period was complicated by mucositis grade III, febrile neutropenia and CMV reactivation on day +20 with good response to ganciclovir therapy. He was discharged on day +42, without signs of acute GVHD, with diarrhea, vomiting and inability to swallow, persisting from the pre-transplant period.

MMF was stopped on day +60, CsA on day +164. Recurrent febrile states with elevation of inflammatory markers, vomiting and abdominal pain started again from day +270. Gastroduodenoscopy and colonoscopy performed for suspicion of pseudo obstruction showed no pathology. In contrast with an unsatisfactory clinical condition, absolute numbers of CD3+ T cells, CD19+ B cells and CD3+CD16+56+ NK cells and proliferative response to phytohemagglutinin were comparable to controls 1 year after SCT. Serum concentrations of IgG, IgA, IgM were in the normal ranges on continuous treatment with IVIG, and BM evaluation showed normocellular trilineage hematopoiesis. On day +440, he developed sepsis with hemoculture positive for *Streptococcus salivarius* and rapid progression to septic shock and despite antibacterial treatment and intensive care he died from multiple organ failure.

CLINICAL AND LABORATORY INVESTIGATIONS

Genetic Analysis

The cytogenetic evaluation performed from PB at 5 months of age did not reveal any structural or numerical abnormality, and retrospective FISH evaluation using CEP7 probe did not reveal monosomy 7. Whole-genome SNP array and FISH analysis from BM sample taken at 18 months of age found monosomy 7 in 78.5% of interphase nuclei.

Whole-exome sequencing analysis was performed at 18 months of age. Mutations in the genes causing congenital neutropenia were excluded, as well as variants in genes causing dyskeratosis congenita, because Hoyeraal Hreidarsson syndrome was considered. No other potentially causative variants were found using the virtual panel of genes associated with bone marrow failure or immunodeficiency. After publication of the SAMD9 patient cohort in 2016, the data were reanalyzed, and a novel, previously unreported *de-novo* heterozygous mutation in the *SAMD9* gene (c.2471 G>A, p.R824Q) was reported. Although this change is predicted as tolerated by SIFT (6) and benign by PolyPhen2 (7), with a CADD (8) score of 15.2, the residue is located near previously reported mutations p.K821M (9) and p.N834Y (1), and the mutation was not found in the ExAC or gnomAD population databases (10).

Immunological Evaluation and Functional Testing

The results of immunological testing during the course of the disease are summarized in **Figure 1B**. Flow cytometry (FC) determination (first performed at the age of 5 months) of major lymphocyte subsets did not provide conclusive results. CD3 cells were overrepresented; their percentages fluctuated from 87 to 96% (ref. range 39–77%), absolute CD3 cell numbers from 2.99 to 9.88 10^9/l (ref. range 2.4–6.9 10^9/l). CD4 cell numbers were normal: 21–42% (ref. range 25–50%), absolute number 1.34–2.28 10^9/l (ref. range 1.04–5.10 10^9/l). CD8+ cells were abundant: 47–69% (ref. range 13–26%), absolute number 1.62–7.49 10^9/l (ref. range 0.6–2.2 10^9/l). CD19+ cells were markedly decreased with repeatedly estimated representation of 2% (ref. range 13–35%), absolute number 0.07–0.22 10^9/l (ref. range 0.7–2.5 10^9/l). CD4/C8 ratio varied between 0.30 to 0.83 (ref 0.7–3.08) NK cell (CD16/56+CD3-) numbers were normal: from 7 to 11% (ref. range 2–13%), abs number 0.76–0.38 (ref range 0.7–1.0 10^9/l).

Levels of immunoglobulins were elevated (IgG 10.6 g/l, IgM 7.1 g/l, IgA level was within ref. range: 0.204 g/l). Thereafter, IgG and IgA levels remained within normal levels, IgM decreased to 3.25 g/l. IgE: was repeatedly <17 UI/ml. Total hemolytic

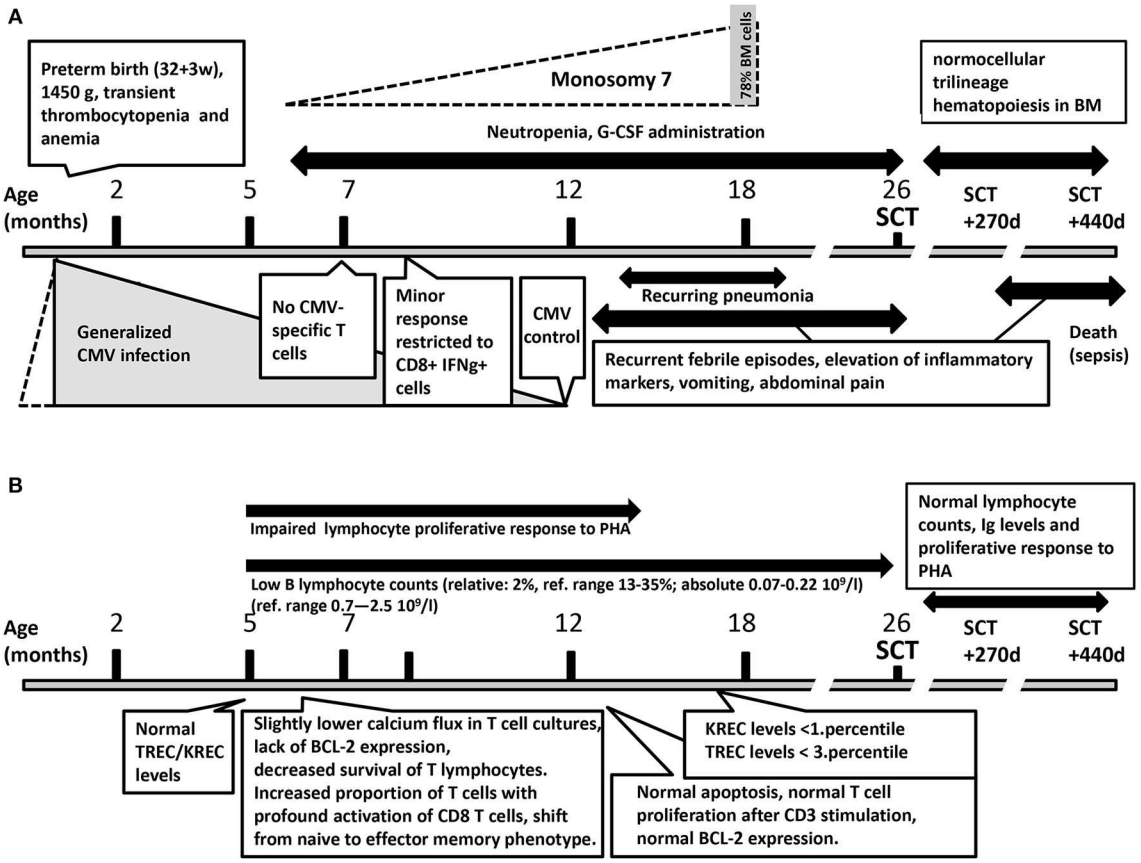

FIGURE 1 | (A) The results of hematological testing and infectious diseases during the course of the disease. **(B)** The results of immunological testing during the course of the disease. BM, bone marrow; CMV, cytomegalovirus; IFNg, interferon gamma; SCT, hematopoietic stem cell transplantation.

complement (CH 50) and granulocyte function test ("burst test) results were normal.

Detailed FC evaluation at 7 months of age revealed increased proportion of T cells, with profound activation of CD8 T cells (HLA-DR+ 72%) and shift from naive (6%) to effector memory phenotype (77%). This was presumably in response to persistently present CMV viremia. However, no functionally responding CMV specific T cells were detected. Minor response restricted to CD8+ IFNg+ producing cell was detected at 8.5 months of age that did not lead to CMV control. CMV reactivation control was restored only at one year of age (PCR CMV negativity). Retrospective analysis of neonatal dry blood spot did not reveal any presence of CMV.

Lymphocyte proliferation in response to phytohemagglutinin (PHA) using 3H-Thymidine incorporation was repeatedly found reduced between 5 and 14 months of age. At 7 months of age, activated T-cell cultures were established by stimulating PBMCs with immobilized anti-CD3ε antibody followed by propagation in the presence of IL-2. These cultures displayed reduced viability, accompanied by the lack of anti-apoptotic Bcl-2 protein expression (**Figures 2A,B**). Upon CD3 re-stimulation, they showed slightly decreased calcium flux (**Figure 2C**), while no difference in overall tyrosine phosphorylation after TCR stimulation was observed (data not shown). However, examination of activated T-cell cultures newly established 6 months later (coincident with CMV control) revealed normal level of apoptosis, normal cell proliferation and Bcl-2 expression comparable to controls (data not shown).

Neither T-cell receptor excision (TREC) nor kappa-deleting element excision (KREC) circle levels were decreased at 5 months of age in PB, but at 17 months of age, the KREC numbers were decreased to the levels observed in SCID patients, and TREC levels were reduced below the 3rd percentile of age-matched controls.

FUNCTIONAL EVALUATION OF *SAMD9* MUTATION

Transient ectopic expression of wt SAMD9 resulted in a significant decrease in proliferation of the transfected cells. The impact of mutant SAMD9 was even more profound resulting in a dramatic drop in the number of proliferating cells (**Figure 3A**). Expression of SAMD9 (both wt and mutant) also caused an increase in apoptosis. Interestingly, mutant SAMD9 induced primary necrosis of the cultured cells further demonstrating the gain-of-function impact of p.R824Q on SAMD9 (**Figure 3B**).

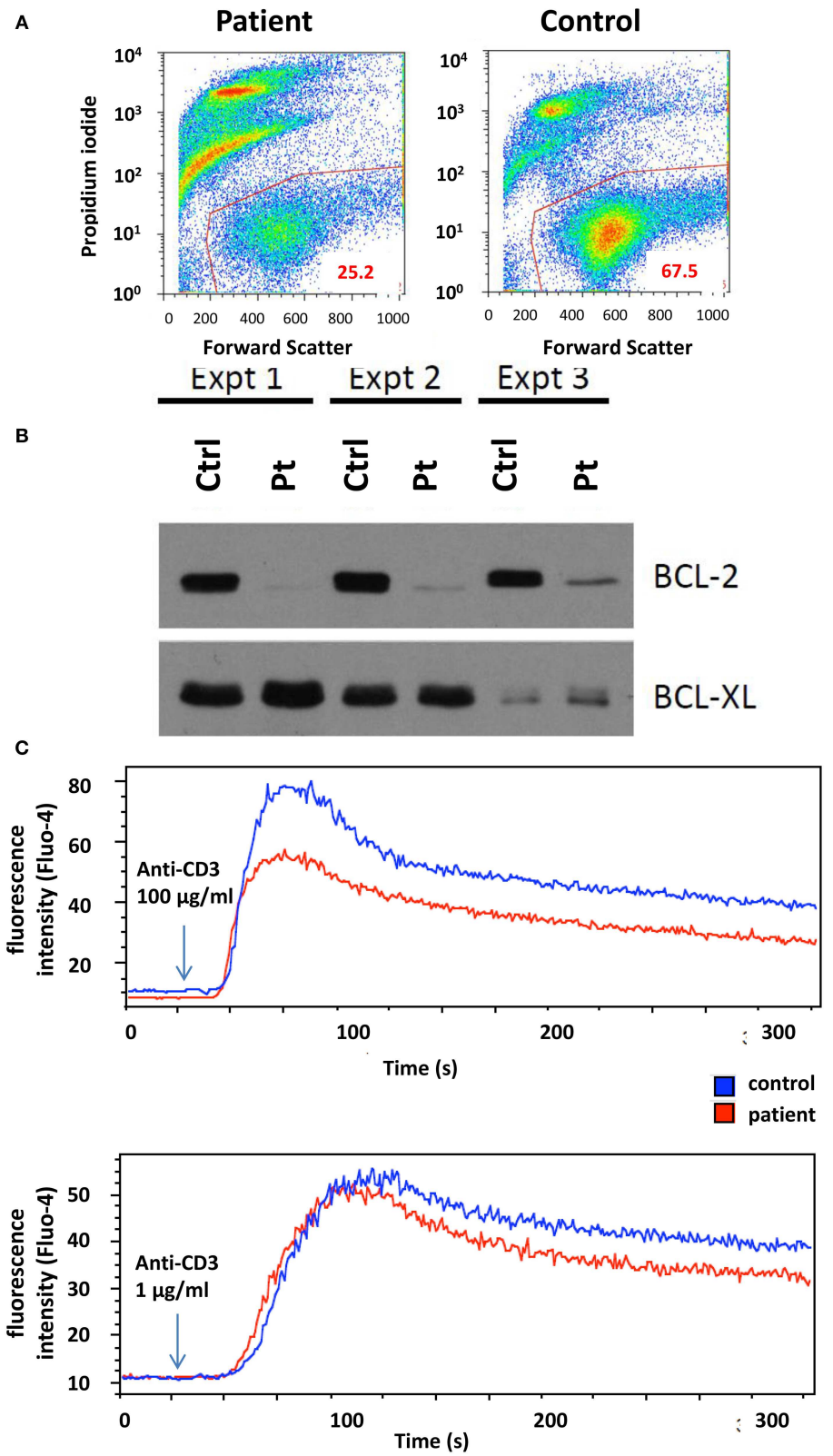

FIGURE 2 | (A) T-cell culture viability determined by flow cytometry. Live cells were gated based on propidium iodide and forward scatter signals. **(B)** Western blot analysis of Bcl-2 and Bcl-xL expression in T cells after 2, 3, and 5 weeks of culture. Ctrl, control, Pt, patient. **(C)** Flow cytometry analysis of T-cell calcium response to activation with 1 and 100 µg/ml anti-CD3ε antibody. The arrow indicates the time point when antibody was added to the sample.

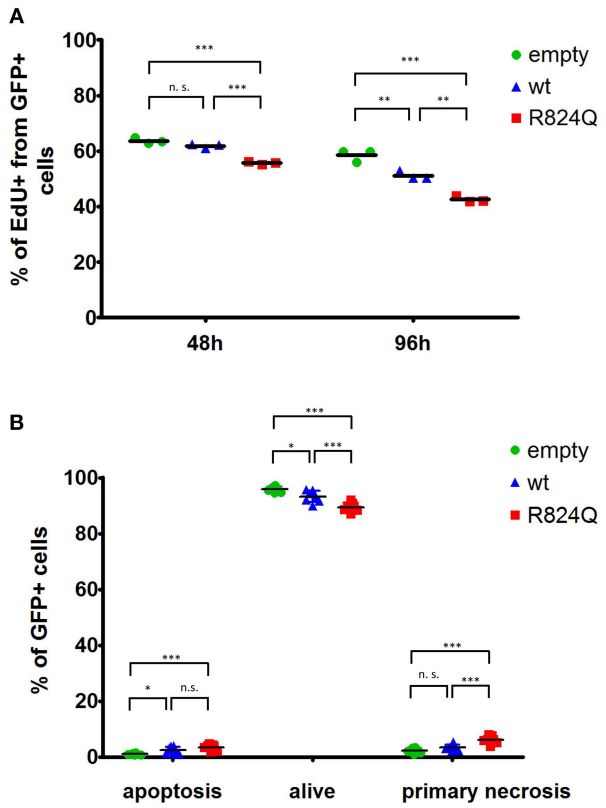

FIGURE 3 | Analysis of proliferation **(A)**, cell death **(B)** of HEK293T cells transfected with wt SAMD9-GFP, mutant SAMD9-GFP or empty GFP-positive control expression vector. Representative data are shown with results depicted as a fraction of GFP+ cells. Statistical significance: (*$P \leq 0.05$; **$P \leq 0.001$; ***$P \leq 0.0001$).

DISCUSSION

In concordance with previously published cases (1, 2), our patient was delivered preterm and seriously ill in the neonatal period and needed intensive care. He showed genital anomalies, and he suffered from recurrent infections and chronic diarrhea. Thus, his phenotype was consistent with MIRAGE syndrome apart from the adrenal insufficiency, the sign that defined the original published cohort. Buonocore et al. reported severe adrenal insufficiency in 6 patients, while mild and no adrenal involvement were reported in the remaining two patients (2). Our patient repeatedly suffered from hyponatremia, but hyperpigmentation of the skin was not observed, and cortisol levels were only found decreased in one of three evaluations.

One of the two dominant clinical features in our patient were the inability to swallow, requiring PEG feeding, and chronic vomiting, symptoms which have not been highlighted as diagnostic signs so far. However, case presentations in the cohort of Narumi et al. reveal that at least four of 11 patients required feeding tubes, and one had a gastrostomy tube due to aspiration pneumonias, esophageal stricture, or achalasia. Also the two patients reported recently by Sarthy et al. had enteral feeding intolerance (9). Thus, SAMD9 mutations should be considered in cases of unexplained disturbances of the upper gastrointestinal tract. His other gastrointestinal symptoms included chronic diarrhea, which is a common symptom in MIRAGE syndrome [reported in 9 of 11 patients in the original cohort (1)].

The second dominant clinical feature was severe neutropenia requiring the administration of G-CSF. One of the three siblings reported by Schwartz et al. manifested with severe neutropenia, but it was associated with macrocytosis, thrombocytopenia and hypocellularity and trilineage dysplasia with 1% blasts in the BM. In our patient, BM aspiration performed at 18 months was without signs of myelodysplasia, only with reduction in the myeloid lineage. Thus, congenital neutropenia was primarily considered at that time. Monosomy 7 was revealed incidentally by SNP array, and retrospective evaluation of BM by FISH revealed monosomy 7 in the 78.5% of nuclei.

The complex immunodeficiency complications in our patient are in good accordance with manifestation of patients described by Narumi et al. where all 7 described patients were prone to complicated or recurrent infections, including episodes of pneumonia; one described patient suffered from severe CMV infection as well. In another patient, recurrent fever with high CRP was reported. Bluteau et al. reported severe recurrent infections in 4/6 patients with SAMD9 mutation (5). Despite clinically manifested immunodeficiency since birth, the laboratory immunological investigation did not show any gross abnormality. Examination of the lymphocyte subsets revealed decreased B lymphocytes, and the lymphocyte proliferation test showed decreased response after PHA stimulation. This finding is consistent with the previous observation by Narumi et al. that showed decreased numbers of B lymphocytes and decreased NK activity in several patients. Bluteau et al. reported immunoglobulin deficiency in 2/6 patients (5). The most prominent sign of immunodeficiency in our patient was non-responsiveness of T lymphocytes to CMV despite severe CMV infection in the early infancy period.

SAMD9 acts as a growth repressor, and SAMD9 mutations are considered gain-of function mutations, thus, further intensifying the growth suppression. The p.R824Q mutation present in our patient was predicted as benign by two prediction tools. However, neither PolyPhen2 (7) nor SIFT (6) tools are adjusted for gain-of-function predictions and, thus, should be used with caution (11). Growth of HEK293 cells transfected with SAMD9 mutants was profoundly restricted in several studies (1, 9, 12). The cells transfected with the p.R824Q mutant showed a significant growth restriction as well. Interestingly, we also observed an increase in cell death of the cultured cells. The involvement of SAMD9 in cell death has already been predicted (13). During the initial evaluation of our patient, we observed a reduced growth, higher rate of apoptosis of cultured T lymphocytes together with the lack of Bcl-2 expression. However, this observation was not confirmed during repeated evaluation after 6 months. We can speculate that the renewal of the proliferation capacity could have been caused by the gradual emergence of cells with compensatory loss of chromosome 7, as observed in other studies (2).

The role of HSCT in the management of patients with SAMD9 mutations is not entirely clear. To our knowledge, 14 transplanted patients with SAMD9 mutation have been reported so far, including our patient. One patient from the cohort of Narumi et al. (1) was transplanted due to MDS, but died due

to Epstein-Barr virus-related post-transplant lymphoproliferative disorder. The only 2 surviving patients from the cohort described by Buonocore et al. (2) were also transplanted due to MDS. However, these patients had the mildest phenotype, with only fewer syndromic features, compared to the rest of the patients. This was also the case of three other reported patients (3, 14) who survived after HSCT. Wilson et al. retrospectively identified a SAMD9 mutation in a patient with MIRAGE phenotype after HSCT due to MDS. The patient survived more than 10 years after transplant but suffered from multiple other medical issues related to syndromic features (12). Bluteau et al. reported four transplanted patients, of whom three survived without major complication, while the only one patient with MIRAGE phenotype died. Interestingly, 11 of 13 patients with SAMD9 or SAMD9L mutations, who were not transplanted immediately, showed spontaneous improvement in blood cell counts, and HSCT was even canceled in 5 of them with no impact on survival (5). Recently, Sarthy et al. reported two patients with SAMD9 mutations and severe MIRAGE phenotype transplanted due to BM failure, who both died after HSCT due to multiorgan complications connected with the syndrome (9). This was also the case of our patient, who tolerated relatively well the transplantation procedure and successfully restored hematopoiesis, but died 14 months after HSCT due to worsening of his other symptoms. Taken together, 5 of 6 reported patients with the MIRAGE phenotype died after SCT, while all 9 reported patients without severe syndromic features survived. These results show that in patients with the MIRAGE phenotype, the transplantation management is rarely successful due to accompanying multiorgan issues. BM disturbances can show spontaneous improvement, including the disappearance of monosomy 7. Thus, a watch and wait strategy should be an option for both syndromic and non-syndromic patients. However, their treatment must be managed by primary immunodeficiency centers with access to intensive care units with multidisciplinary teams.

In conclusion, we report the case of a patient with novel mutation in *SAMD9* with severe gastrointestinal involvement, neutropenia and immunodeficiency, underscoring the role of *SAMD9* in the differential diagnosis of patients with these symptoms. We further question the role of HSCT in the management of the disease.

METHODS

The detailed descriptions of CMV response detection (15), activated T-cell culture (16), cell viability, BCL-2 expression, calcium response (16), TREC/KREC analysis, and of the functional assessment of SAMD9 mutation *in-vitro* are available in the **Supplementary File** (17–19).

ETHICS STATEMENT

This study was carried out in accordance with the recommendations of the 2nd Medical Faculty Ethics Committee Guidelines. The parents of the patient gave written informed consent with the study in accordance with the Declaration of Helsinki. The protocol was approved by the Ethics Committee of the 2nd Medical Faculty, Charles University Prague. Written informed consent was obtained from the parents of the participant for the publication of this case report.

AUTHOR CONTRIBUTIONS

RF, EF, TK, VK, MS, and TB analysis and interpretation of data for the study and drafting the manuscript. MR, KS, VK, MS, TB, EH, and HG functional experiments. PR, MZ, EM, TF, ZZ, EH, JB, PJ, PS, JSo, JSt, MV, JL, JT, IC, FF, PK, and OZ analysis and interpretation of data.

FUNDING

This project was supported by NV18-07-00430 (to EM and JSt), NV19-05-00332 (to EF and VK) projects of the Czech Ministry of Health and by 17-04941Y from the Czech Science Foundation. The research facilities were supported by the project for the conceptual development of research organization 00064203 and LO1604, the infrastructure was supported by CZ.2.16/3.1.00/24505. EF and MS were supported by PRIMUS/17/MED/11. KS and MR were supported by PRIMUS/19/MED/04. ZZ was supported by the project for the conceptual development of research organization RVO-VFN64165.

ACKNOWLEDGMENTS

We would like to thank the family of the patient for their kind cooperation and permission to publish this paper.

SUPPLEMENTARY MATERIAL

The Supplementary Material for this article can be found online at: https://www.frontiersin.org/articles/10.3389/fimmu.2019.02194/full#supplementary-material

REFERENCES

1. Narumi S, Amano N, Ishii T, Katsumata N, Muroya K, Adachi M, et al. SAMD9 mutations cause a novel multisystem disorder, MIRAGE syndrome and are associated with loss of chromosome 7. *Nat Genet.* (2016) 48:792–7. doi: 10.1038/ng.3569
2. Buonocore F, Kühnen P, Suntharalingham JP, Del Valle I, Digweed M, Stachelscheid H, et al. Somatic mutations and progressive monosomy modify SAMD9-related phenotypes in humans. *J Clin Invest.* (2017) 127:1700–13. doi: 10.1172/JCI91913
3. Schwartz JR, Wang S, Ma J, Lamprecht T, Walsh M, Song G, et al. Germline SAMD9 mutation in siblings with monosomy 7 and myelodysplastic syndrome. *Leukemia.* (2017) 31:1827–30. doi: 10.1038/leu.2017.142
4. Chen DH, Below JE, Shimamura A, Keel SB, Matsushita M, Wolff J, et al. Ataxia-pancytopenia syndrome is caused by missense mutations in SAMD9L. *Am J Hum Genet.* (2016) 98:1146–58. doi: 10.1016/j.ajhg.2016.04.009

5. Bluteau O, Sebert M, Leblanc T, Peffault de Latour R, Quentin S, Lainey E, et al. A landscape of germ line mutations in a cohort of inherited bone marrow failure patients. *Blood.* (2018) 131:717–32. doi: 10.1182/blood-2017-09-806489
6. Kumar P, Henikoff S, Ng PC. Predicting the effects of coding non-synonymous variants on protein function using the SIFT algorithm. *Nat Protoc.* (2009) 4:1073–81. doi: 10.1038/nprot.2009.86
7. Adzhubei I, Jordan DM, Sunyaev SR. Predicting functional effect of human missense mutations using PolyPhen-2. *Curr Protoc Hum Genet.* (2013) Chapter 7:Unit7.20. doi: 10.1002/0471142905.hg0720s76
8. Kircher M, Witten DM, Jain P, O'Roak BJ, Cooper GM, Shendure J. A general framework for estimating the relative pathogenicity of human genetic variants. *Nat Genet.* (2014) 46:310–5. doi: 10.1038/ng.2892
9. Sarthy J, Zha J, Babushok D, Shenoy A, Fan JM, Wertheim G, et al. Poor outcome with hematopoietic stem cell transplantation for bone marrow failure and MDS with severe MIRAGE syndrome phenotype. (2018) 2:3–8. doi: 10.1182/bloodadvances.2017012682
10. Lek M, Karczewski KJ, Minikel EV, Samocha KE, Banks E, Fennell T, et al. Analysis of protein-coding genetic variation in 60,706 humans. *Nature.* (2016) 536:285–91. doi: 10.1038/nature19057
11. Flanagan SE, Patch AM, Ellard S. Using SIFT and PolyPhen to predict loss-of-function and gain-of-function mutations. *Genet Test Mol Biomark.* (2010) 14:533–7. doi: 10.1089/gtmb.2010.0036
12. Wilson DB, Bessler M, Ferkol TW, Shenoy S, Amano N, Ishii T, et al. Comment on: acquired monosomy 7 myelodysplastic syndrome in a child with clinical features of dyskeratosis congenita and IMAGe association. *Pediatr. Blood Cancer.* (2018) 65:e26747. doi: 10.1002/pbc.26747
13. Mekhedov SL, Makarova KS, Koonin EV. The complex domain architecture of SAMD9 family proteins, predicted STAND-like NTPases, suggests new links to inflammation and apoptosis. *Biol Direct.* (2017) 12:13. doi: 10.1186/s13062-017-0185-2
14. Wong JC, Bryant V, Lamprecht T, Ma J, Walsh M, Schwartz J, et al. Germline SAMD9 and SAMD9L mutations are associated with extensive genetic evolution and diverse hematologic outcomes. *JCI Insight.* (2018) 3:121086. doi: 10.1172/jci.insight.121086
15. Pelák O, Stuchlý J, Król L, Hubáček P, Keslová P, Sedláček P, et al. Appearance of cytomegalovirus-specific T-cells predicts fast resolution of viremia post hematopoietic stem cell transplantation. *Cytom. Part B Clin. Cytom.* (2017) 92:380–8. doi: 10.1002/cyto.b.21348
16. Horejsí V, Angelisová P, Bazil V, Kristofová H, Stoyanov S, Stefanová I, et al. Monoclonal antibodies against human leucocyte antigens. II. Antibodies against CD45 (T200), CD3 (T3), CD43, CD10 (CALLA), transferrin receptor (T9), a novel broadly expressed 18-kDa antigen (MEM-43) and a novel antigen of restricted expression (MEM-74). *Folia Biol.* (1988) 34:23–34.
17. Knapp W. *Leucocyte Typing IV : White Cell Differentiation Antigens.* New York, NY: Oxford University Press (1989).
18. Fronková E, Klocperk A, Svaton M, Nováková M, Kotrová M, Kayserová J, et al. The TREC/KREC assay for the diagnosis and monitoring of patients with DiGeorge syndrome. *PLoS ONE.* (2014) 9:e114514. doi: 10.1371/journal.pone.0114514
19. Sottini A, Ghidini C, Zanotti C, Chiarini M, Caimi L, Lanfranchi A, et al. Simultaneous quantification of recent thymic T-cell and bone marrow B-cell emigrants in patients with primary immunodeficiency undergone to stem cell transplantation. *Clin Immunol.* (2010) 136:217–27. doi: 10.1016/j.clim.2010.04.005

Conflict of Interest Statement: The authors declare that the research was conducted in the absence of any commercial or financial relationships that could be construed as a potential conflict of interest.

Novel SAMD9 mutation in a patient with immunodeficiency, neutropenia, impaired anti-CMV response and severe gastrointestinal involvement

Supplementary Methods

CMV response

CMV-specific T cell-response was detected by intracellular cytokine staining using flow cytometry after *ex vivo* stimulation with CMV antigen as described in detail previously.[1]

Activated T cell culture

Peripheral blood mononuclear cells (PBMC) prepared after Ficoll-Paque density centrifugation of 1 ml blood were activated by immobilized anti-CD3ε antibody MEM-57[2] in the presence of 50 µ/ml IL-2 (Proleukin, Novartis) in RPMI/FCS. After 2 days, the cells were removed from the antibody and propagated in RPMI/FCS and 50 µ/ml IL-2.

Cell viability analysis

Cells were stained with 0.5 µg/ml propidium iodide (Thermo Fisher Scientific) in PBS and directly analyzed by flow cytometry.

BCL-2 expression

In total, 5×10^6 cells were lysed in 0.2 ml SDS-PAGE sample buffer. The lysates were sonicated for 10 s, and Bcl-2 and Bcl-XL content was analyzed by immunoblotting with respective antibodies (Cell Signaling Technology).

Calcium response

In total, 5×10^6 cells were loaded with 1 µg Fluo-4 calcium sensing dye (Molecular Probes, Thermo Fisher Scientific) in 0.5 ml RPMI/FCS for 30 min at 37°C. Cells were washed, stimulated with varying concentrations of MEM-92 (IgM antibody to CD3ε[3]) and the florescence was continuously measured by flow cytometry for 5 min.

The analysis of T-cell receptor excision circles (TRECs) and kappa-deleting excision circles (KRECs)

PCR-based quantification of TREC and KREC levels from the PB was performed as described previously.[4,5]

Functional assessment of *SAMD9* mutation

The c.2471 G>A mutation was introduced into pCMV6-AC-GFP vector expressing GFP-tagged wild-type *SAMD9* cDNA (RG219076; Origine) by site-directed mutagenesis. Mycoplasma-

negative HEK293T cells (DSMZ) were transfected with wt SAMD9-GFP, mutant SAMD9-GFP or empty GFP-positive control expression vector using polyethylenimine. The GFP+ cells were analyzed by proliferation (after 48 and 96 hours) or apoptosis assay (after 96 hours). Experiments were performed in two biological replicates.

Proliferation assay

Transfected HEK293T cells were cultured for 1.5 hours with 10 µM EdU (Click-iT® Plus EdU Flow Cytometry Kit, Thermo Fisher Scientific), harvested, spun down, and fixed using 10% formaldehyde (Thermo Fisher Scientific) for 10 min at room temperature. Fixed cells were permeabilized using 0.1% Triton X-100 (Thermo Fisher Scientific) for 15 min at 37°C, washed with 1% bovine serum albumin in PBS, spun down and stained with Alexa Fluor 647 picolyl azide for 30 min at room temperature according to manufacturer's protocol. Finally, staining with DNA intercalator 4',6-diamidino-2-phenylindole (DAPI, Thermo Fisher Scientific) was performed for 30 min at 4°C, the cell were washed with PBS and measured on BD LSRII flow cytometer. EdU positivity was determined using FlowJo software (BD Biosciences).

Apoptosis assay

Transfected HEK293T cells were harvested, spun down and resuspended in Annexin V Binding Buffer (Exbio). The cells were stained with Annexin V-Dyomics 647 (Exbio) and DAPI for 30 minutes in the dark on ice. The samples were washed with Annexin V Binding Buffer and measured on BD FACS Celesta flow cytometer. Fractions of Annexin V+ apoptotic cells (Annexin V+ DAPI- (early apoptosis) and Annexin V+ DAPI+ (late apoptosis/secondary necrosis)), and Annexin V- DAPI+ primary necrotic cells were determined using FlowJo software (BD Biosciences).

Statistical analysis

Data from proliferation and apoptosis assays were analyzed using Prism 7 (GraphPad Software, La Jolla, USA). Differences between wt SAMD9, mutant SAMD9 and control cells were compared using 1-way ANOVA with Bonferoni´s multiple comparison posttest.

References

1. Pelák O, Stuchlý J, Król L, et al. Appearance of cytomegalovirus-specific T-cells predicts fast resolution of viremia post hematopoietic stem cell transplantation. *Cytom. Part B Clin. Cytom.* 2017;92(5):380–388.

2. Horejsí V, Angelisová P, Bazil V, et al. Monoclonal antibodies against human leucocyte antigens. II. Antibodies against CD45 (T200), CD3 (T3), CD43, CD10 (CALLA), transferrin

receptor (T9), a novel broadly expressed 18-kDa antigen (MEM-43) and a novel antigen of restricted expression (MEM-74). *Folia Biol. (Praha).* 1988;34(1):23–34.

3. Knapp W. Leucocyte typing IV : white cell differentiation antigens. New York: Oxford University Press; 1989.

4. Sottini A, Ghidini C, Zanotti C, et al. Simultaneous quantification of recent thymic T-cell and bone marrow B-cell emigrants in patients with primary immunodeficiency undergone to stem cell transplantation. *Clin. Immunol.* 2010;136(2):217–27.

5. Froňková E, Klocperk A, Svatoň M, et al. The TREC/KREC assay for the diagnosis and monitoring of patients with DiGeorge syndrome. *PLoS One*. 2014;9(12): e114514

Příloha 6

Parackova Z, Milota T, Vrabcova P, Smetanova J, **Svaton M**, Freiberger T, Kanderova V, Sediva A. Novel XIAP mutation causing enhanced spontaneous apoptosis and disturbed NOD2 signalling in a patient with atypical adult-onset Crohn's disease. *Cell Death Dis.* 2020 Jun 8;11(6):430. doi: 10.1038/s41419-020-2652-4.

Paracková et al. *Cell Death and Disease* (2020)11:430
https://doi.org/10.1038/s41419-020-2652-4

Cell Death & Disease

ARTICLE Open Access

Novel *XIAP* mutation causing enhanced spontaneous apoptosis and disturbed NOD2 signalling in a patient with atypical adult-onset Crohn's disease

Zuzana Paracková[1], Tomas Milota[1], Petra Vrabcova[1], Jitka Smetanova[1], Michael Svaton[2], Tomas Freiberger[3,4], Veronika Kanderova[2] and Anna Sediva[1]

Abstract

X-linked inhibitor of apoptosis (XIAP) is the most potent human inhibitor of apoptosis, and is also involved in NOD2-dependent NFκB and MAPK signalling cascade activation. The absence or defective function of XIAP leads to the development of a rare and severe primary immunodeficiency known as X-linked lymphoproliferative syndrome type 2 (XLP-2), which is characterized by a triad of clinical manifestations, including a high incidence of haemophagocytic lymphohistiocytosis (HLH), lymphoproliferation and inflammatory bowel disease (IBD), usually with very early onset. Here, we present a novel *XIAP* mutation identified in a patient with atypical adult-onset IBD complicated by relapsing HLH, splenomegaly and sarcoid-like disease. The c.266delA mutation in the *XIAP* gene creates a premature stop codon, and causes a severe reduction in XIAP protein expression. The mutation is also associated with impaired spontaneous and staurosporine- and PMA-induced apoptosis accompanied by significantly increased expression of pro-apoptotic genes. We also confirmed the negative impact of this particular *XIAP* mutation on NOD2-dependent NFκB and MAPK activation, while NOD2-independent activation was found to be unaffected. Moreover, we assume that the mutation has an impact on the overproduction of IL-12 and IFNγ, the shift towards the Th1 immune response and increased numbers of central memory and effector memory CD4+ and CD8+ T cells. All these changes contribute to immune dysregulation and the clinical manifestation of XLP-2.

Introduction

X-linked inhibitor of apoptosis (XIAP) or baculoviral IAP repeat-containing protein 4 (BIRC4), localized on the X chromosome, is a part of human IAP family. The protein consists of three different domains: (1) three baculoviral IAP repeat (BIR) domains, which are characteristic of all IAPs, (2) UBA domains that allow binding to ubiquitin and (3) a zinc-binding domain C-terminal RING finger domain, which is associated with E3 ubiquitin ligase activity[1].

One of the major roles of XIAP is the prevention of apoptotic cell death, which is achieved by binding and inhibiting the activity of caspases 3, 7 and 9[2]. In addition to its anti-apoptotic functions, XIAP is also involved in other signalling pathways and cellular responses, mostly because of the ubiquitylation activity through its RING domain[3,4]. XIAP is involved in intracellular pattern-recognition receptor signalling that senses peptidoglycan products, NOD1 and 2[5], leading to NFκB and mitogen-activated protein kinase (MAPK) cascade activation[6–8]. In mouse and human models, the absence of XIAP leads to defective

Correspondence: Zuzana Paracková (zuzana.paracková@fnmotol.cz)
[1]Department of Immunology, 2nd Faculty of Medicine Charles University, University Hospital in Motol, V Uvalu 84, Prague, Czech Republic
[2]CLIP—Childhood Leukaemia Investigation Prague, Department of Paediatric Haematology and Oncology, 2nd Faculty of Medicine, Charles University and University Hospital Motol, Prague, Czech Republic
Full list of author information is available at the end of the article
Edited by H.-U. Simon

SPRINGER NATURE CDDpress

secretion of proinflammatory cytokines after stimulation with NOD ligands[9,10]. Interestingly, NOD2 was the first identified susceptibility gene for Crohn's disease (CD), a typical condition associated with XIAP deficiency[11].

XIAP deficiency is a rare primary immunodeficiency, also known as X-linked lymphoproliferative syndrome type 2 (XLP-2), caused by mutations in the *XIAP (BIRC4)* gene. The estimated incidence is 1–2 cases per million of live-born children. Nevertheless, the real prevalence seems to be higher as the diagnosis of XIAP deficiency may be overlooked or misclassified. Current assessments suggest that up to 4% of early-onset IBD may represent XIAP-deficient patients[12].

Disease onset usually manifests in the first few years of life, and is characterized by a key triad of clinical symptoms consistent with a high incidence of haemophagocytic lymphohistiocytosis (HLH), often triggered by Epstein–Barr (EBV) infections, and characterized by splenomegaly and inflammatory bowel disease (IBD), particularly with features of CD[13]. HLH is a life-threatening condition characterized by hyperinflammation, in which activated T lymphocytes and macrophages accumulate in organs, and produce and induce massive production of proinflammatory cytokines, particularly IFNγ[14], resulting in tissue damage and multiorgan failure that typically affects the liver and bone marrow[15]. IBD in XIAP-deficient patients usually presents with very early onset[16]; however, adult onset has also been described[17], and is characterized by a complicated course, necessity of extensive surgical procedures and unresponsiveness to standard treatment, including biological treatment. These patients have also significantly increased mortality rate, dying within a few years upon manifestation or diagnosis of IBD[18]. In comparison with XLP-1, hypogammaglobulinaemia may accompany XIAP deficiency; however, it is less frequent. Moreover, no lymphoma has been reported, which approximately 30% of XLP-1 patients develop. On the other hand, XLP-1 does not present with higher risk of IBD[19]. Currently, haematopoietic stem cell transplantation is the only causal therapy of XLP-2, although attempts to develop targeted gene therapy seem to be promising[20].

Here, we report a novel XLP-2-causing mutation in the XIAP BIR1 domain, leading to a premature stop codon and a loss of protein expression, which results in impaired lymphocyte apoptosis and NOD2-dependent signalling with clinical manifestations that include a complicated course of IBD, unresponsiveness to standard treatment, including biologics (infliximab and vedolizumab) and relapsing HLH.

Results

Case report

A 32-year-old patient was born to non-consanguineous Caucasian parents. The patient presented without any health complications or abnormalities during the prenatal, perinatal and postnatal periods, and was diagnosed at 17 years of age with CD based on the clinical presentation and histological verification, which revealed nonspecific granulation tissue composed of multinucleated giant cells and lymphocytic infiltration in the submucosa of the colon. Complex examination, including ultrasonography of the abdomen, also revealed splenomegaly. Standard therapy with chimeric monoclonal anti-TNFα antibody (infliximab) at a standard dose of 5 mg/kg was initiated. However, the course of the CD was complicated by the development of an intra-abdominal abscess compressing the bladder, which required surgical intervention. Then, the biological therapy was switched to fully human monoclonal anti-TNFα (adalimumab), which successfully led to CD remission. Three years later (at the age of 20), the patient was admitted to the hospital for fever, elevation of inflammatory markers (including C-reactive protein), progressive splenomegaly, anaemia, leukocytopenia and decreased platelet count. Further testing revealed hypertriglyceridaemia, elevated transaminases and increased serum concentrations of ferritin. The results from extensive infectious diagnostic work identified the EBV as a possible trigger. The evaluation of bone marrow biopsy samples confirmed the suspicion of HLH. Thus, according to the Histocyte Society standards, the HLH diagnostic criteria were fulfilled, and adequate therapy started with a high-dose corticosteroid regimen (1000 mg of Solu-Medrol per day) for 3 consecutive days and intravenously administered cyclosporine at a dosage of 2 mg/kg/day, which led to normalization of the blood count values and inflammatory marker, liver transaminase, triglyceride and ferritin levels (Supplementary Table 1 and Table 1). Later, the therapy was switched to peroral corticosteroids and cyclosporin as long-term maintenance therapy. Despite this effort, HLH relapse occurred 4 years later (at the age of 24), and no infection or any other trigger was identified. Moreover, the patient developed mediastinal lymphadenopathy, histologically verified as epithelioid granuloma with images indicative of a sarcoid-like disease. Clinical manifestations and therapy are illustrated in Supplementary Fig. 1A. Suspicions about the primary aetiology arose despite the patient's age, and genetic testing was indicated. WES was performed because of the broad differential diagnosis of HLH and monogenic causes of CD, and the results revealed a novel c.266delA mutation in the *XIAP* (*BIRC4*) gene. This finding was subsequently confirmed by Sanger sequencing (Fig. 1a). Further genetic counselling with the patient's family members revealed that the patient's mother as a healthy carrier and two healthy siblings were without the mutation (Fig. 1b). When we searched the patient's pedigree, we also identified the mother's brother as a potentially affected family member who died of severe

Table 1 Laboratory values of the patient samples.

Immunology	Patient's values	Referential value
IgG (g/l)	13.00	7.65–13.60
IgG1 (g/l)	7.13	4.9–11.4
IgG2 (g/l)	4.13	1.50–6.40
IgG3 (g/l)	0.316	0.2–1.1
IgG4 (g/l)	0.342	0.08–1.4
IgA (g/l)	2.03	0.91–2.9
IgM (g/l)	↓ 0.38	0.47–1.95
IgE (IU/ml)	↑2.161	0–150
C3 (g/l)	0.98	0.83–2.25
C4 (g/l)	0.22	0.14–0.35
Tetanus (IU/ml)	1.01	0.1
Haemphilus (IU/ml)	9.00	6.00
ANA	neg	–
ANCA	pos (p-ANCA)	–
RF IgG (IU/ml)	4.4	0–22
RF IgA (IU/ml)	2.3	0–22
RF IgM (IU/ml)	2.7	0–22
aTRG (IU/ml)	2.48	0–10
ASCA IgG (IU/ml)	↑ 43.713	0–10
ASCA IgA (IU/ml)	↑ 12.36	0–10

infection-induced sepsis accompanied by splenomegaly and lymphadenopathy (major symptoms of HLH); however, biological material was not available for genetic testing to confirm the diagnosis or the cause of death.

Novel c.266delA mutation leads to a premature stop codon and loss of function of the XIAP molecule

A novel c.266delA frameshift mutation in the *XIAP* gene of the patient, leading to a premature stop codon after the translation of 41 amino acids (p. Asn89fs*41), was detected by whole-exome sequencing (WES) and confirmed by Sanger sequencing (Fig. 1a). The mother of the patient was confirmed to be a healthy heterozygous carrier (Fig. 1b). The mutation is in the first BIR domain of the protein, as shown in the scheme of the XIAP protein in Fig. 1c. The results from a Western blot analysis showed no XIAP expression in the patient PBMCs and reduced expression of XIAP in the mother's samples compared with healthy donors (Fig. 1d). We also observed reduced expression of the housekeeping protein β-actin, a finding in agreement with a previously reported role of XIAP in cytoskeleton regulation with reduced β-actin expression[21]. Expression of HSP90 and tubulin, additional housekeeping proteins, was comparable to controls (Supplementary Fig. 1E).

XIAP LOF mutation results in augmented apoptosis

As XIAP is an important molecule in apoptosis regulation, we decided to verify the XIAP LOF by analyzing spontaneous as well as induced apoptosis by staurosporine and PMA. We measured the activation of caspase-3 and -7 with a FAM-FLICA caspase-3,7 assay kit, and noticed elevated numbers of CD3 lymphocytes that were positive for activated caspase-3 and -7 in patient samples. Not only was staurosporine and PMA-induced apoptosis, but also spontaneous apoptosis was markedly enhanced in the patient's T lymphocytes (Fig. 2a, b). The augmented spontaneous apoptosis was confirmed by Annexin V and DAPI staining, verifying the results of the FLICA experiments (Fig. 2c, d).

In addition, we analyzed the expression of pro-apoptotic (*BAX* and *BAK*) and anti-apoptotic (*Bcl2*) genes. The ratio of *BAK/Bcl2* and *BAX/Bcl2* was highly increased in both induced and spontaneous apoptotic patient cells (Fig. 3a). Interestingly, the genes involved in caspase-independent apoptosis, *ENDOG* and *AIMF1*, were reduced in the samples (Fig. 3b). When a caspase inhibitor Z-VAD-FMK was applied, both patient and control samples displayed reduced apoptosis (Supplementary Fig. 2A, B). These observations suggest an enhanced caspase-dependent apoptosis. To test whether there was a compensatory mechanism critical for defective *XIAP* expression, we analyzed the presence of the *BIRC2* (*cIAP*) gene in patient cells. However, we did not observe enhanced compensatory *cIAP* expression in patient cells compared with healthy controls (Fig. 3c).

XIAP LOF abrogates NOD2 signalling

Moreover, XIAP is involved in NOD2 signalling; hence, we investigated whether the pathway was affected. Stimulation of NOD2 with muramyl dipeptide (MDP) leads to activation of NFκB and MAPK. We focused on the phosphorylation of the MAP kinases p38 and Erk (Fig. 4a), and observed diminished levels of kinase phosphorylation in response to MDP in patient monocytes detected by flow cytometry. Western blot analysis of MAPK activation confirmed this assessment (Fig. 4b). Furthermore, we examined the NFκB pathway activation after MDP stimulation, expressed as IκB (inhibitor of κB) degradation, and NFκB phosphorylation by flow cytometry and Western blot. Degradation of IκB leads to NFκB activation and its translocation to the nucleus. As anticipated, we detected neither inhibited IκB degradation in the patient's samples (Fig. 4c, d) nor NFκB phosphorylation in response to MDP stimulation. However, the patient's cells were able to phosphorylate MAPKs, as well as activate the NFκB pathway in response to PMA or TNFα stimulation

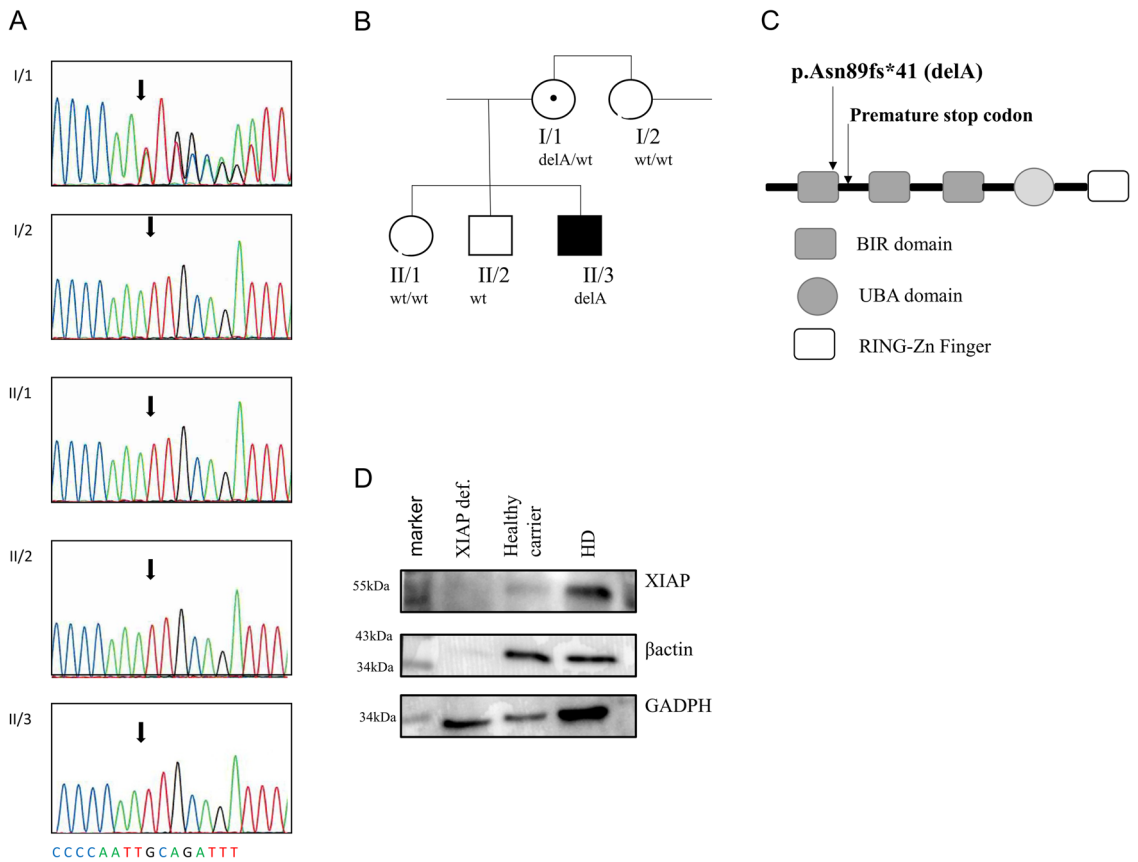

Fig. 1 c.266delA mutation. a DNA-sequencing chromatogram of the relevant *XIAP* gene regions in the patient (II/3) and his first-degree relatives. The same mutation was detected in a heterozygous form in his mother (I/1), while other relatives carry wild-type (WT) alleles. Arrows show the mutation position. **b** Pedigree of the family showing segregation of the *XIAP* mutation. **c** Protein structure with highlighted position of the mutation. **d** Western blot analysis of XIAP presence in the PBMCs of the patient, his mother and the controls.

(Supplementary Fig. 3A), suggesting that only the NOD2 pathway was affected. Next, we assessed cytokine production (IL-1β, IL-6 and TNFα) after stimulation of patient PBMCs with MDP and lipopolysaccharide (LPS) (Fig. 4e) using the Luminex method. The patient's cells produced decreased levels of cytokines after MDP stimulation compared with the healthy controls; however, in response to LPS stimulation, the patient's PBMCs produced comparable levels of cytokines, confirming defective NOD2 signalling in the patient's cells.

XIAP deficiency affects T-cell homoeostasis

To test whether XIAP deficiency and impaired apoptosis influenced the distribution of the patient's B- and T-cell subpopulations, we analyzed these subsets. The gating strategies used to distinguish between naive, central memory (CM), effector memory (EM), terminal effector T cells re-expressing CD45RA (TEMRA), recent thymic emigrants (RTEs) and B-cell subsets, are illustrated in Supplementary Fig. 4. The analysis showed a shift towards mature stages of CD4+ and CD8+ T cells in the patient samples (Fig. 5a, b). We found a noteworthy increase in the count of CM and EM, and a reduction in naive forms of the T cells; however, the percentage of RTEs was unaffected. Consequently, we analyzed the patient's T-lymphocyte ability to produce IFNγ by flow cytometry. The patient's T cells produced higher levels of IFNγ even in the unstimulated state, which was significantly elevated upon PMA stimulation. The percentage of IFNγ-producing CD4+ T cells (20.1%) was considerably higher than that of the healthy donors (5.3%) (Fig. 5d, e). In addition, analysis of activation marker expression on T cells, HLA-DR as a marker of chronic activation, and CD69 as the earliest activation marker, revealed a shift towards late stages of activation. HLA-DR expression was threefold higher on the CD8+ T cells and twofold higher on CD4+ T cells than it was in the healthy controls (Fig. 5a, b). CD69 expression was unaffected (Supplementary Fig. 3C). T-cell proliferation was negligibly decreased (55.2% patients; controls 74.7% after PMA and ionomycin stimulation) (Supplementary Fig. 3D). Moreover, we also observed higher production of IL-12 in response to LPS in

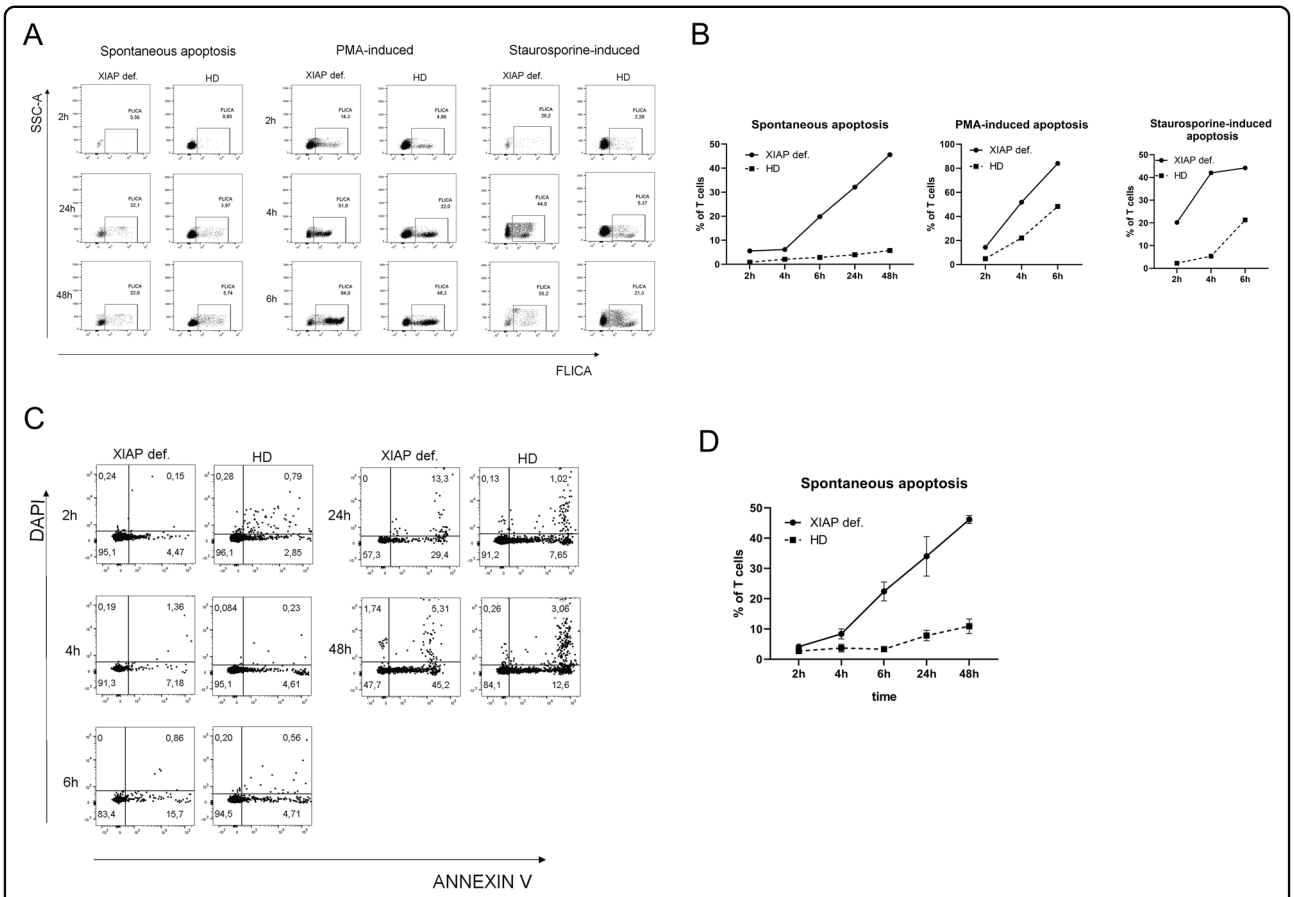

Fig. 2 Apoptosis. Patient PBMCs were treated with staurosporine (1 mmol) and 50 ng/ml PMA for 2, 4 and 6 h, or left untreated for an additional 24 and 48 h. The level of spontaneous and induced apoptosis was detected by **a** and **b** FLICA, in which the fluorescein-labelled inhibitor Z-YVAD-fmk is bound to activated caspase-3 and -7 signals as detected by flow cytometry. **c**, **d** The level of spontaneous apoptosis detected by flow cytometry of cells stained with Annexin V and DAPI. Annexin + DAPI cells were considered to be undergoing early apoptosis.

patient PBMCs, supporting a Th1-polarizing environment (Fig. 5f). No significant differences were found in the B-cell department (Fig. 5c).

Discussion

Here, we report the case of a patient who developed adult-onset IBD refractory to treatment and complicated by several episodes of HLH, and for whom WES revealed a novel previously unpublished c.266delA mutation in the *XIAP* (*BIRC4*) gene that led to its loss of function. HLH and IBD are the most common first manifestations of XIAP deficiency, which usually occurs in the first few years of life, and for which the potentially lethal outcome requires HSCT[13]. Adult-onset HLH and IBD associated with XIAP deficiency, although rare, have also been described[17,22]. In a large cohort of 54 XIAP-deficient patients, IBD manifestation was the main clinical feature in 17 of them. The remaining patients usually manifested with HLH as a major disease complication. The average age at the time of diagnosis of IBD was 11 years (range 3 months–41 years) compared with patients manifested with HLH (average age 6.5 years and range 0.1–23 years). In our patient, IBD manifested at the age of 17 and HLH at the age of 20. The majority of the first HLH attacks was associated with EBV infection; however, HHV6 and HSV1 were identified as potential triggers as well. IBD-related complications were the main cause of death in three of them at the average age 24 years (range 4–42 years) and after 4 years of disease duration (range 0–7 years). Interestingly, only four patients presented in a form of the adult-onset IBD[22,23].

Most of the *XIAP* mutations identified in XLP-2 patients are nonsense mutations, frameshift mutations or deletions that cause severe aberrations in the encoded protein or loss of its expression. They are distributed along all coding exons[10,13,24–26]. Neither type nor position of the mutation, as well as residual protein expression, do not correlate with the clinical manifestation and severity of the disease[23].

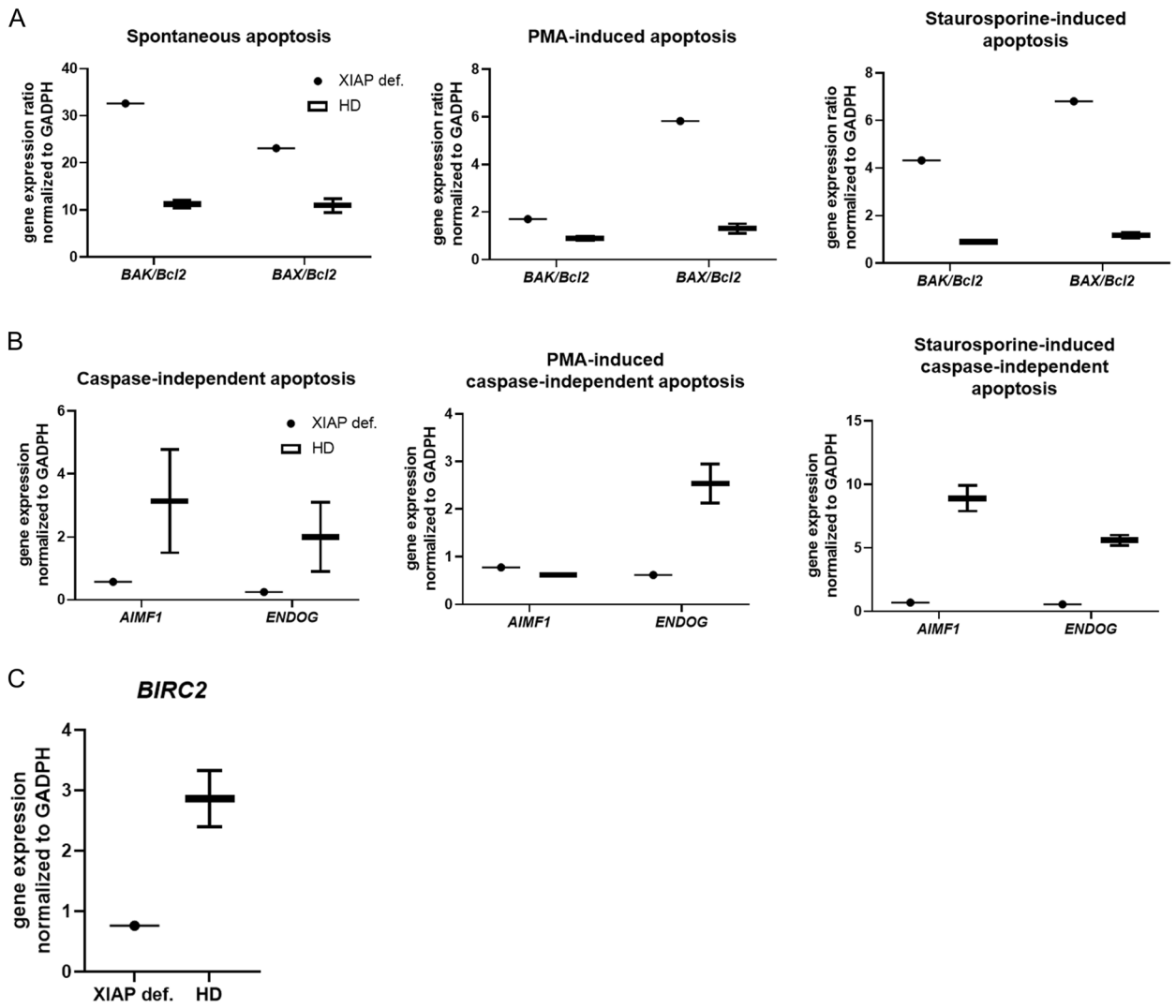

Fig. 3 Apoptotic genes' expression. a Ratio of pro- and anti-apoptotic genes *BAK*, *BAX* and *Bcl2* in the patient and control ($n = 2$) PBMCs after 6 h of stimulation with staurosporine (1 mmol) or PMA (50 ng/ml) as detected by RT-PCR. **b** Expression of caspase-independent genes involved in apoptosis, *AIMF1* and *ENDOG*, in the patient and control ($n = 2$) PBMCs after 6 h of stimulation with staurosporine (1 mmol) or PMA (50 ng/ml) as detected by RT-PCR. **c** Expression of the *BIRC2* gene in control ($n = 2$) PBMCs as detected by RT-PCR. Gene expression was normalized to that of *GAPDH*.

We report a novel deletion mutation c.266delA, resulting in a premature stop codon (p. Asn89fs*41), loss of protein expression and, as a consequence, a patient suffering from XLP-2 and lower expression in his mother, who is a healthy carrier of the mutation.

XIAP-deficient T cells are characterized by a high susceptibility to apoptosis ex vivo in response to apoptotic stimulus or upon activation[17,23,27]. Indeed, we observed an enhanced level of apoptosis in response to staurosporine, an inducer of apoptosis, as well as upon activation by PMA. Interestingly, we also observed increased spontaneous apoptosis in patient lymphocytes, which was reduced when a caspase inhibitor was applied. However, the sensitivity to apoptosis of T cells was found to have no influence on circulating blood lymphocyte numbers in patients[27]. Accordingly, circulating T-cell numbers were in the normal range in the patient, although we observed a shift to their more mature stages. Considering T-lymphocyte function, the expansion and proliferation of virus-specific T lymphocytes might be compromised in XIAP deficiency. XIAP-deficient patients suffer from an increased risk of EBV infections, and in a mouse model[28], XIAP and cIAP1 were required for the survival and expansion of virus-specific T cells. In addition, defective NOD2 signalling might also contribute to a higher risk of EBV infection[29,30]. Apoptosis may be further ameliorated

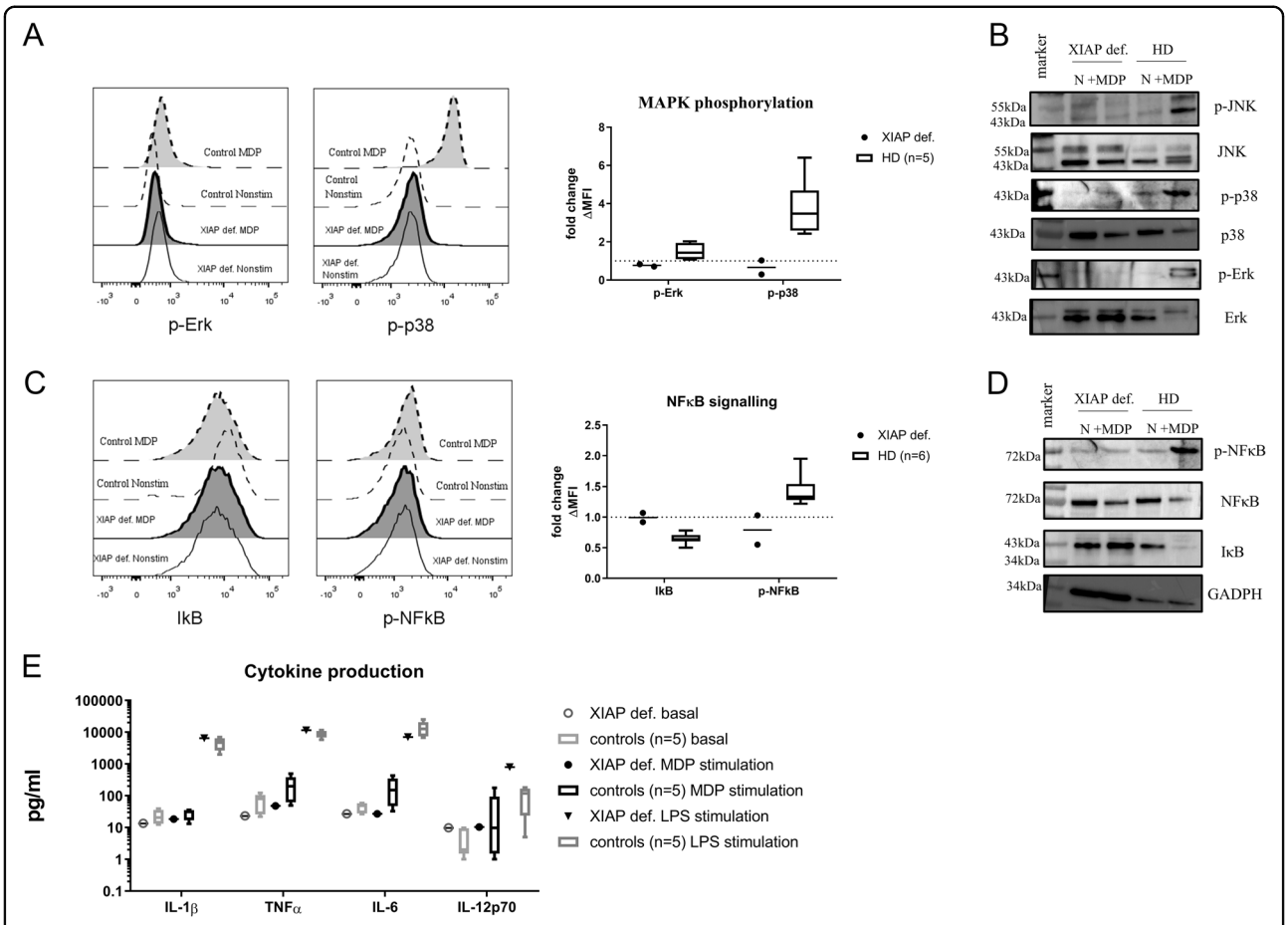

Fig. 4 NOD2 signalling. Patient and control ($n = 5$) peripheral blood was stimulated with MDP (10 µg/ml) for 20 min, and phosphorylation of **a** MAP kinases were detected by phospho-flow cytometry **b** and by Western blot. NFκB signalling, expressed as IκB degradation and NFκB phosphorylation, was detected by **c** flow cytometry and **d** by Western blot after MDP (10 µg/ml) stimulation of patient and control ($n = 5$) peripheral blood cells. **e** Production of IL-1β, TNFα, IL-6 and IL-12p70 after MDP (10 µg/ml) or LPS (1 µg/ml) stimulation of patient and control ($n = 5$) PBMCs was detected by Luminex.

by increased production of IFNγ, which further enhances the expression of pro-apoptotic genes (such as *BAX*, *BAK1* and/or *XAF1*)[31].

The aforementioned shift in the spectrum of T lymphocytes to their more mature stages seems to be related to the alteration of the apoptosis process. It has been previously reported that T lymphocytes at different stages of development have different sensitivities to apoptosis, possibly resulting from different expression of pro- and anti-apoptotic proteins[32,33]. These differences may lead to a significant reduction in naive and the subsequent survival of the mature memory forms of T cells, including CM and EM T cells, as observed in the patient.

HLH is the most severe and life-threatening manifestation in patients with XIAP deficiency, but the exact mechanism by which mutated *XIAP* results in HLH manifestations is not entirely clear. The mechanism differs from other genetic disorders associated with HLH, such as XLP-1, in which the impaired cytotoxic responses by CD8+ lymphocytes and NK cells result in exaggerated amounts of IFNγ and the activation of macrophages, thus explaining the positive effect of the IFNγ blockade on the outcome of HLH[15]. The patient's T lymphocytes produced markedly higher levels of IFNγ in comparison with the healthy donors, even though XIAP deficiency was not connected with defects in the cytotoxic responses by CD8+ lymphocytes or NK cells, as is typical in XLP-1[27]. The shift towards the Th1 immune response and increased production of IFNγ was further supported by the overproduction of IL-12, a crucial cytokine for Th1 polarization[34]. Observations in a mouse model propose, as a possible explanation, that HLH is due to NLRP3 inflammasome dysregulation and increased proinflammatory cytokine production[35,36]. Although it is still unclear whether XIAP in humans also acts as an NLRP3 inhibitor, impairment to this control might represent a key pathological mechanism. XIAP-deficient mice also develop splenomegaly when treated with an activator of

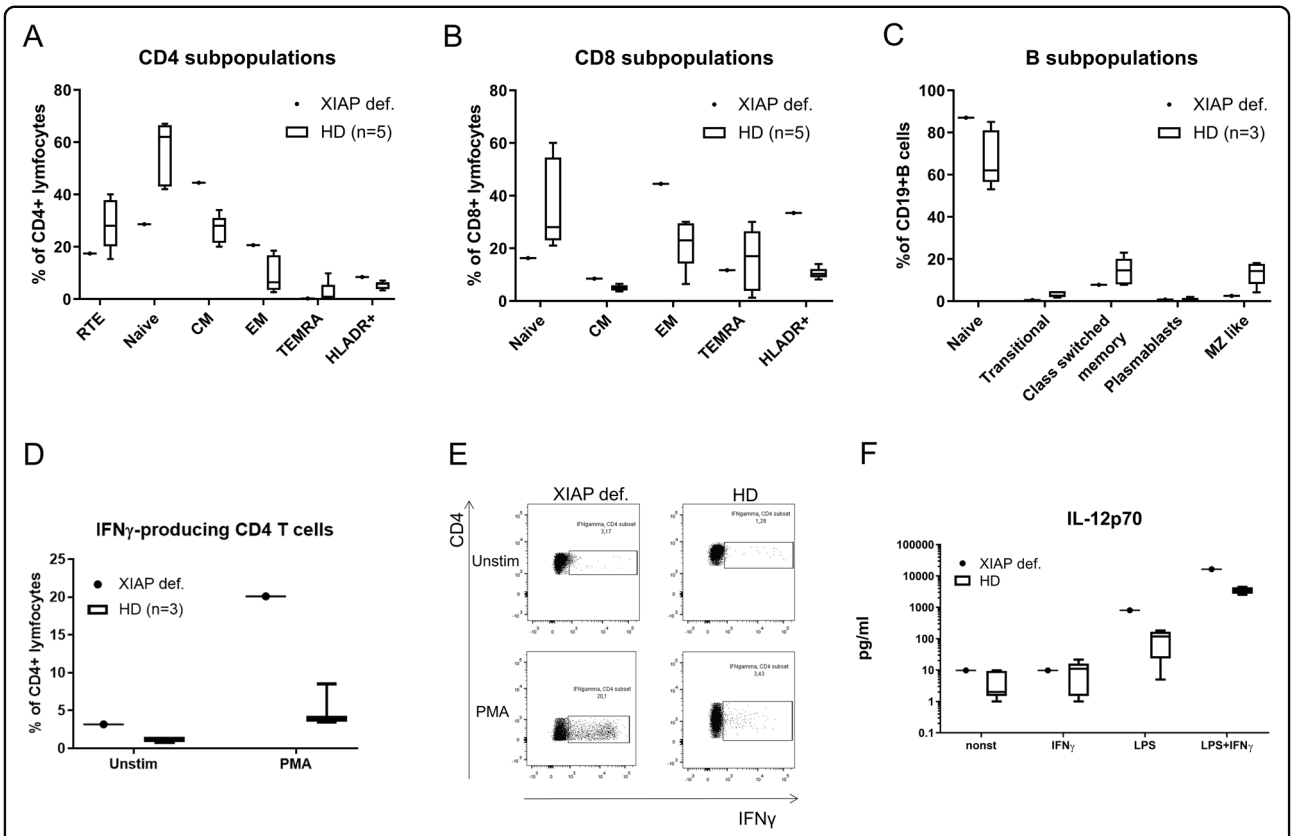

Fig. 5 T cells. Proportion of **a** CD4+, **b** CD8+ T cells and **c** B-cell subpopulations of the patient and control ($n = 3$) samples detected by flow cytometry. **d**, **e** Percentage of IFNγ-producing T cells upon PMA (20 ng/ml) stimulation for 6 h. **e** IL-12p70 production upon stimulation with LPS (1 μg/ml), IFNγ (1 μg/ml) or their combination of patient and control ($n = 5$). PBMCs were detected by Luminex.

the NLRP3 inflammasome[36]; therefore, this mechanism may explain two of three typical pathologies associated with XIAP deficiency. Interestingly, mutations in the human NLRC4 inflammasome were identified in patients suffering from recurrent HLH and autoinflammation, supporting a role of the inflammasome in HLH[37,38]. However, we observed only slightly higher IL-1β and TNFα production in the patient in response to LPS stimulation.

In line with previous reports, the patient displayed diminished proinflammatory cytokine production after NOD2 ligand stimulation[12,39,40], thus connecting the potential role for altered NOD2 signalling with IBD in XIAP patients. NOD2 mutations represent a strong genetic risk factor for CD[11], as NOD2-impaired secretion of cytokines and an altered gut microbiome may disturb intestinal homoeostasis. Like HLH, IFNγ is one of the most important cytokines in CD pathophysiology. Indeed, as shown here for the XIAP-deficient patient, altered NOD2-mediated signalling and high IFNγ production by T cells might explain, in an analogy to CD, the gastrointestinal IBD-like presentation as a feature of XIAP deficiency.

Taken together, our data reveal a novel mutation in a patient suffering from recurrent HLH, IBD and splenomegaly, typical conditions associated with XIAP deficiency. The deletion mutation leads to loss of XIAP expression, and it functions as a negative regulator of apoptosis. The absence of XIAP clearly leads to enhanced cell death, which may amplify inflammation. XIAP deficiency negatively influences MDP-induced NOD2 signalling, with implications for IBD. Changes in innate immunity, highlighted together with the role of IFNγ, contribute to XLP-2 pathogenesis and complex clinical presentation. Whereas HSCT in patients with the early onset of the disease represents a method of choice, in adult patients, such as in the index patient in our study, the therapeutic options are more limited. Emapalumab, a monoclonal antibody that targets IFNγ, was approved for the treatment of relapsed/refractory HLH[14] with a possible influence on the symptoms of CD, and anti-IL-12/23 (ustekinumab) therapy[41] is also available. The overlap in pathogenetic mechanisms gives hope for the use of this strategy to treat XIAP deficiency.

Patient and methods

Informed written consent was obtained from all subjects involved in the study and all controls in accordance with the Declaration of Helsinki, and according to the procedures established by the Ethical Committee of our institution.

Whole-exome sequencing

WES was performed on a NextSeq 500 instrument (Illumina, San Diego, CA), and sequencing libraries were prepared using the SureSelectXT Human All Exon V6 + UTR kit (Agilent Technologies, Santa Clara, CA). Sequencing reads were aligned against the human reference genome hg19 by BWA[42], and variant calling was performed using SAMtools[43] and VarScan 2[44] and their annotation using SnpEff[45].

Apoptosis

Peripheral blood was collected from the patient and healthy volunteers into EDTA-coated tubes. Peripheral blood mononuclear cells (PBMCs) were isolated using Ficoll-Paque (GE Healthcare Biosciences, Uppsala, Sweden). The obtained cells were resuspended in RPMI 1640 medium with a sodium bicarbonate buffer system supplemented with 2% autologous serum, 1% penicillin and streptomycin and 1% GlutaMAX (Thermo Fisher Scientific, Waltham, CA, USA). PBMCs (10^6/ml) stimulated with staurosporine (1 mmol) (Abcam, Cambridge, UK) for 4 and 6 h, PMA (50 ng/ml) (Sigma-Aldrich, Darmstadt, Germany) for 4 h or left untreated for 4, 6, 24 and 48 h. When indicated, 20 μM Z-VAD-FMK was added in the culture 30 min before apoptosis induction. Then, the cells were washed in Annexin V binding buffer and stained with Annexin V–Dyomics 647 (EXBIO) and DAPI (Thermo Fisher Scientific).

FLICA staining

Active caspase-3 and -7 were detected using a FLICA caspase-3 and 7 assay kit (Thermo Fisher Scientific). PBMCs were stimulated as described above prior to treatment with the fluorescein-labelled inhibitor Z-YVAD-fmk (10 μM) for 1 h at 37 °C and CD3-A700 (clone MEM-57) (EXBIO, Prague, Czech Republic). The cells were washed three times and analyzed by flow cytometry with a FACS Fortessa flow cytometer (BD Biosciences, San Diego, CA, USA).

Phospho-flow cytometry

Detection of MAPK and NFκB activation was performed according to a previously published protocol[46]. Briefly, peripheral blood was stimulated with 10 μg/ml MDP (InvivoGen, San Diego, CA, USA) for 20 min at 37 °C or left unstimulated. Subsequently, the cells were fixed using 4% formaldehyde for 10 min at 25 °C, erythrocytes were lysed using 0.1% Triton X-100 (Sigma-Aldrich) for 15 min at 37 °C and the leukocytes were permeabilized using 80% ice-cold methanol for 30 min.

The following antibodies were used: CD3—A700 (clone MEM-57), CD14—PEDy594 (EXBIO) and CD19—PC7 (clone J3-119) (Beckman Coulter, USA, Brea, USA), phospho38 (Thr180)—A647 (#4552 S), phosphoErk1/2 (Thr202/Tyr204)—A488 (#4374 S), phosphoSAPJ/JNK (Thr183/185)—PE (#5755 S) (Cell Signaling, Denvers, MA, USA), phosphoNFκB—A647 (#4887) and anti-IκB—A488 (#5743) (both from Cell Signaling).

Cytokine production

Cytokines were detected using a multiplex Luminex cytokine-fluorescent bead-based immunoassay (Merck Millipore, Beerlengton, MA, USA) with cell-free supernatants. A total of 2×10^5 PBMCs were stimulated with MDP (10 μg/ml) (InvivoGen), *E. coli* LPS (1 μg/ml) (Sigma-Aldrich) or left untreated for 24 h.

T- and B-cell analysis

Immunophenotyping of T and B cells was performed according to a previously published protocol[47], and the gating strategy is shown in Supplementary Fig. 2B.

For IFNγ-producing cell detection, we applied an already-published protocol[46].

T-cell proliferation

The proliferation of CD3+ T lymphocytes was determined according to a previously published protocol[48].

RT-PCR

PBMCs were stimulated as stated in the 'Apoptosis' section. RNA isolation, reverse transcription and RT-PCR were performed according to a previously published protocol[49]. TaqMan primer/probe sets (Thermo Fisher Scientific) were used. The sample data were matched to a standard curve generated by amplifying serially diluted products using the same PCR, and normalized to *GAPDH* (TIB Molbiol, Berlin, Germany) to obtain the relative expression value. Real-time assays were run on an FX96 cycler (Bio-Rad). The primer/probe sets are available from the authors upon request.

Western blotting

Detection of proteins was performed according to a previously published protocol[46]. The membranes were incubated with the following primary antibodies: anti-XIAP (clone D2Z8W), anti-β-actin (clone D6A8), anti-GAPDH (clone D16H11), IκB anti (clone L35A5), anti-NFκB (clone D14E12) (all from Cell Signaling), anti-tubulin (clone TU-07), anti-HSP-90 (clone MBH90AB) (both from Exbio), anti-Erk1/2 (ab17942), anti-p-Erk1/2 (ab76299), anti-p-p38 (ab4822), anti-p38 (ab170099),

anti-p-JNK1/2/3 (ab124956), anti-JNK1/2/3 (ab208035) and anti-p-NFκB (ab76302) (all from Abcam) overnight, followed by incubation with peroxidase-conjugated anti-rabbit or anti-mouse secondary antibodies for 2 h. The membranes were developed using SuperSignal West Femto (Thermo Fisher Scientific).

Acknowledgements
The study was supported by the Czech Ministry of Health AZV NV18-05-00162, GAUK 460218 issued by Charles University in Prague, Czech Republic and by the NV19-05-00332 project of the Czech Ministry of Health. The infrastructure was supported by CZ.2.16/3.1.00/24505. We thank the patient and the healthy volunteers for the blood samples used in this study. We confirm that this paper has not been published elsewhere and is not under consideration by another journal.

Author details
[1]Department of Immunology, 2nd Faculty of Medicine Charles University, University Hospital in Motol, V Uvalu 84, Prague, Czech Republic. [2]CLIP—Childhood Leukaemia Investigation Prague, Department of Paediatric Haematology and Oncology, 2nd Faculty of Medicine, Charles University and University Hospital Motol, Prague, Czech Republic. [3]Molecular Genetics Laboratory, Center of Cardiovascular Surgery and Transplantation, Brno, Czech Republic. [4]Faculty of Medicine, Masaryk University, Brno, Czech Republic

Author contributions
Z.P. designed the study and experiments, performed the experiments, analyzed the data, interpreted the results and wrote the paper. T.M. designed the experiments, interpreted the results, and provided patient information. P.V. performed the RT-PCR. J.S. acquired the data regarding apoptosis and T-cell proliferation. M.S. provided the NGS results. T.F. provided the Sanger sequencing data. V.K. performed the T- and B-cell analysis. A.S. reviewed and edited the paper.

Conflict of interest
The authors declare that they have no conflict of interest.

Supplementary Information accompanies this paper at (https://doi.org/10.1038/s41419-020-2652-4).

Received: 23 January 2020 Revised: 7 May 2020 Accepted: 11 May 2020
Published online: 08 June 2020

References

1. Wilkinson, J. C., Cepero, E., Boise, L. H. & Duckett, C. S. Upstream regulatory role for XIAP in receptor-mediated apoptosis. *Mol. Cell. Biol.* **24**, 7003–7014 (2004).
2. Deveraux, Q. L., Takahashi, R., Salvesen, G. S. & Reed, J. C. X-linked IAP is a direct inhibitor of cell-death proteases. *Nature* **388**, 300–304 (1997).
3. Kenneth, N. S. & Duckett, C. S. IAP proteins: regulators of cell migration and development. *Curr. Opin. Cell Biol.* **24**, 871–875 (2012).
4. Galbán, S. & Duckett, C. S. XIAP as a ubiquitin ligase in cellular signaling. *Cell Death Differ.* **17**, 54–60 (2010).
5. Bertrand, M. J. M. et al. Cellular inhibitors of apoptosis cIAP1 and cIAP2 are required for innate immunity signaling by the pattern recognition receptors NOD1 and NOD2. *Immunity* **30**, 789–801 (2009).
6. Wang, C. et al. TAK1 is a ubiquitin-dependent kinase of MKK and IKK. *Nature* **412**, 346–351 (2001).
7. Hasegawa, M. et al. A critical role of RICK/RIP2 polyubiquitination in Nod-induced NF-κB activation. *EMBO J.* **27**, 373–383 (2008).
8. Krieg, A. et al. XIAP mediates NOD signaling via interaction with RIP2. *Proc. Natl Acad. Sci. USA* **106**, 14524–14529 (2009).
9. Damgaard, R. B. et al. The ubiquitin ligase XIAP Recruits LUBAC for NOD2 Signaling in Inflammation and Innate Immunity. *Mol. Cell* **46**, 746–758 (2012).
10. Damgaard, R. B. et al. Disease-causing mutations in the XIAP BIR 2 domain impair NOD 2-dependent immune signalling. *EMBO Mol. Med.* **5**, 1278–1295 (2013).
11. Van Limbergen, J., Wilson, D. C. & Satsangi, J. The genetics of Crohn's disease. *Annu. Rev. Genomics Hum. Genet.* **10**, 89–116 (2009).
12. Zeissig, Y. et al. XIAP variants in male Crohn's disease. *Gut* **64**, 66–76 (2015).
13. Latour, S. & Aguilar, C. XIAP deficiency syndrome in humans. *Semin. Cell Dev. Biol.* **39**, 115–123 (2015).
14. Vallurupalli, M. & Berliner, N. Emapalumab for the treatment of relapsed/refractory hemophagocytic lymphohistiocytosis. *Blood* https://doi.org/10.1182/blood.2019002289 (2019).
15. Usmani, G. N., Woda, B. A. & Newburger, P. E. Advances in understanding the pathogenesis of HLH. *Br. J. Haematol.* **161**, 609–622 (2013).
16. Shim, J. O. Recent advance in very early onset inflammatory bowel disease. *Pediatr. Gastroenterol. Hepatol. Nutr.* **22**, 41 (2019).
17. Speckmann, C. et al. X-linked inhibitor of apoptosis (XIAP) deficiency: the spectrum of presenting manifestations beyond hemophagocytic lymphohistiocytosis. *Clin. Immunol.* **149**, 133–141 (2013).
18. Nielsen, O. H. & LaCasse, E. C. How genetic testing can lead to targeted management of XIAP deficiency–related inflammatory bowel disease. *Genet. Med.* **19**, 133–143 (2017).
19. Xu, T. et al. X-linked lymphoproliferative syndrome in mainland China: review of clinical, genetic, and immunological characteristic. *Eur. J. Pediatr.* **179**, 327–338 (2020).
20. Y., T. et al. Gene therapy for X-linked inhibitor of apoptosis protein (XIAP) deficiency. *Hum. Gene Ther.* **28**, A31–A32 (2017).
21. Liu, J. et al. X-linked inhibitor of apoptosis protein (XIAP) mediates cancer cell motility via rho GDP dissociation inhibitor (RhoGDI)-dependent regulation of the cytoskeleton. *J. Biol. Chem.* **286**, 15630–15640 (2011).
22. Quaranta, M. et al. Consequences of identifying XIAP deficiency in an adult patient with inflammatory bowel disease. *Gastroenterology* **155**, 231–234 (2018).
23. Schmid, J. P. et al. Clinical similarities and differences of patients with X-linked lymphoproliferative syndrome type 1 (XLP-1/SAP deficiency) versus type 2 (XLP-2/XIAP deficiency). *Blood* **117**, 1522–1529 (2011).
24. Yang, X. et al. Clinical and genetic characteristics of XIAP deficiency in Japan. *J. Clin. Immunol.* **32**, 411–420 (2012).
25. Marsh, R. A. et al. XIAP deficiency: a unique primary immunodeficiency best classified as X-linked familial hemophagocytic lymphohistiocytosis and not as X-linked lymphoproliferative disease. *Blood* **116**, 1079–1082 (2010).
26. Filipovich, A. H., Zhang, K., Snow, A. L. & Marsh, R. A. X-linked lymphoproliferative syndromes: brothers or distant cousins? *Blood* **116**, 3398–3408 (2010).
27. Rigaud, S. et al. XIAP deficiency in humans causes an X-linked lymphoproliferative syndrome. *Nature* **444**, 110–114 (2006).
28. Gentle, I. E. et al. Inhibitors of apoptosis proteins (IAPs) are required for effective T-cell expansion/survival during antiviral immunity in mice. *Blood* **123**, 659–668 (2014).
29. Sabbah, A. et al. Activation of innate immune antiviral responses by Nod2. *Nat. Immunol.* **10**, 1073–1080 (2009).
30. Kapoor, A., Forman, M. & Arav-Boger, R. Activation of nucleotide oligomerization domain 2 (NOD2) by human cytomegalovirus initiates innate immune responses and restricts virus replication. *PLoS ONE* **9**, e92704 (2014).
31. Ellison, M. A., Gearheart, C. M., Porter, C. C. & Ambruso, D. R. IFN-γ alters the expression of diverse immunity related genes in a cell culture model designed to represent maturing neutrophils. *PLoS ONE* **12**, e0185956 (2017).
32. Zhan, Y., Carrington, E. M., Zhang, Y., Heinzel, S. & Lew, A. M. Life and death of activated T cells: how are they different from naïve T cells? *Front. Immunol.* **8**, 1809 (2017).
33. Hildeman, D., Jorgensen, T., Kappler, J. & Marrack, P. Apoptosis and the homeostatic control of immune responses. *Curr. Opin. Immunol.* **19**, 516–521 (2007).
34. Mikhalkevich, N. et al. Responsiveness of naive CD4 T cells to polarizing cytokine determines the ratio of Th1 and Th2 cell differentiation. *J. Immunol.* **176**, 1553–1560 (2006).
35. Vince, J. E. et al. Inhibitor of apoptosis proteins limit RIP3 kinase-dependent interleukin-1 activation. *Immunity* **36**, 215–227 (2012).
36. Yabal, M. et al. XIAP restricts TNF- and RIP3-dependent cell death and inflammasome activation. *Cell Rep.* **7**, 1796–1808 (2014).

37. Canna, S. W. et al. An activating NLRC4 inflammasome mutation causes autoinflammation with recurrent macrophage activation syndrome. *Nat. Genet.* **46**, 1140–1146 (2014).
38. Romberg, N. et al. Mutation of NLRC4 causes a syndrome of enterocolitis and autoinflammation. *Nat. Genet.* **46**, 1135–1139 (2014).
39. Aguilar, C. et al. Characterization of Crohn disease in X-linked inhibitor of apoptosis–deficient male patients and female symptomatic carriers. *J. Allergy Clin. Immunol.* **134**, 1131–1141.e9 (2014).
40. Ammann, S. et al. A new functional assay for the diagnosis of X-linked inhibitor of apoptosis (XIAP) deficiency. *Clin. Exp. Immunol.* **176**, 394–400 (2014).
41. Engel, T. et al. Effectiveness and safety of Ustekinumab for Crohn's disease; systematic review and pooled analysis of real-world evidence. *Dig. Liver Dis.* **51**, 1232–1240 (2019).
42. Li, H. & Durbin, R. Fast and accurate short read alignment with Burrows-Wheeler transform. *Bioinformatics* **25**, 1754–1760 (2009).
43. Li, H. et al. The Sequence Alignment/Map format and SAMtools. *Bioinformatics* **25**, 2078–2079 (2009).
44. Koboldt, D. C. et al. VarScan 2: somatic mutation and copy number alteration discovery in cancer by exome sequencing. *Genome Res.* **22**, 568–576 (2012).
45. Cingolani, P. et al. Using *Drosophila melanogaster* as a model for genotoxic chemical mutational studies with a new program, SnpSift. *Front. Genet.* **3**, 35 (2012).
46. Parackova, Z. et al. Mutual alteration of NOD2-associated Blau syndrome and IFNγR1 deficiency. *J. Clin. Immunol.* https://doi.org/10.1007/s10875-019-00720-6 (2019).
47. Kanderova, V. et al. Lymphoproliferation, immunodeficiency and early-onset inflammatory bowel disease associated with a novel mutation in Caspase 8. *Haematologica* https://doi.org/10.3324/haematol.2018.201673 (2018).
48. Lašťovička, J., Rataj, M. & Bartůňková, J. Assessment of lymphocyte proliferation for diagnostic purpose: comparison of CFSE staining, Ki-67 expression and 3H-thymidine incorporation. *Hum. Immunol.* **77**, 1215–1222 (2016).
49. Zentsova, I. et al. Monocytes contribute to DNA sensing through the TBK1 signaling pathway in type 1 diabetes patients. *J. Autoimmun.* https://doi.org/10.1016/j.jaut.2019.06.005 (2019).

NOVEL *XIAP* MUTATION CAUSING ENHANCED SPONTANEOUS APOPTOSIS AND DISTURBED NOD2 SIGNALLING IN A PATIENT WITH ATYPICAL ADULT ONSET CROHN'S DISEASE

Short running title: A novel XIAP mutation

Zuzana Parackova[1], Tomas Milota[1], Petra Vrabcova[1], Jitka Smetanová[1], Michael Svaton[2], Tomas Freiberger[3, 4], Veronika Kanderova[2], Anna Sediva[1]

[1] Department of Immunology, 2nd Faculty of Medicine Charles University, University Hospital in Motol, V Uvalu 84, Prague, Czech Republic
[2] CLIP - Childhood Leukaemia Investigation Prague, Department of Paediatric Haematology and Oncology, 2nd Faculty of Medicine, Charles University and University Hospital Motol, Prague, Czech Republic
[3] Molecular Genetics Laboratory, Center of Cardiovascular Surgery and Transplantation, Brno, Czech Republic
[4] Faculty of Medicine, Masaryk University, Brno, Czech Republic

Correspondence:

Zuzana Paračková, Department of Immunology, 2nd Faculty of Medicine Charles University, Faculty Hospital in Motol, V Uvalu 84, Prague 5, 15006, +420224435971, zuzana.parackova@fnmotol.cz

Keywords: XIAP, BIRC4, XLP, NOD2, apoptosis, HLH, IFNγ, Crohn's disease

Supplementary Table 1: Laboratory values during HLH episode and remission, including complete blood count and differential lymphocyte subpopulations (NK – natural killer), biochemistry (ALT – alanine aminotransferase, AST – aspartate aminotransferase, GGT-gamma-glutamyl transferase, ALP – alkaline phosphatase, bili – bilirubin, TAG – triacylglycerol, and Chol – cholesterol) and inflammatory markers (C reactive protein), ↑↓ - value above and below the reference range, respectively.

Hematology	**HLH**	**Remission**	**Reference value**
Leukocytes (E9/l))	↓ **2.8**	5.3	4-10
Neutrophils (%)	↑ **77.5**	58.8	45-70
Monocytes (%)	↓ **15.5**	↓ **9.9**	20-45
Bazophiles (%)	↑ **5.6**	0.2	0-2
Eozinophiles(%)	0	1.1	0-5
HGB (g/l)	↓ **0**	147	135-175
PLT (E9/l)	↓ **75**	208	150-400
Lymphocytes (%)	↑ **67**	29.8	20-45
CD3 (%)	83	86	57-94
CD4 (%)	40	47	20-70
CD8 (%)	37	33	10-48
CD19 (%)	12	9	4-23
NK (%)	↓ **3**	↓ **4**	6-33
CD3 HLADR (%)	↑**17**	15	0-15
Biochemistry	**HLH**	**Remission**	**Reference value**
ALT (ukat/l)	0.4	0.45	0.17-0.78
AST (ukat/l)	0.18	0.32	0.16-0.72
GGT (ukat/l)	↑ **9.01**	0.66	0.14-0.84
ALP (ukat/l)	↓ **0.4**	1.38	0.66-2.20
Bili (umol/l)	↑ **24**	13.5	5-21
TAG (mmol/l)	↑ **4.65**	↑ **2**	0.7-1.7
Chol (mmol/l)	4.4	↑ **5.5**	3.4-5.0
Fe (umol/l)	↓ **1.9**	11.1	7.2-29
Ferritin (ug/l)	↑ **16,500**	62	22-322
CRP (mg/l)	↑ **14**	↑ **55.3**	0-5

Supplementary Figure 1: A. Patient's clinical manifestations and therapy. Uncropped membranes from the Western blot analyses of **B.** XIAP, **C.** β actin **D.** and GAPDH. Expression of housekeeping proteins **E.** tubulin and HSP90 in patient and control PBMCs.

A

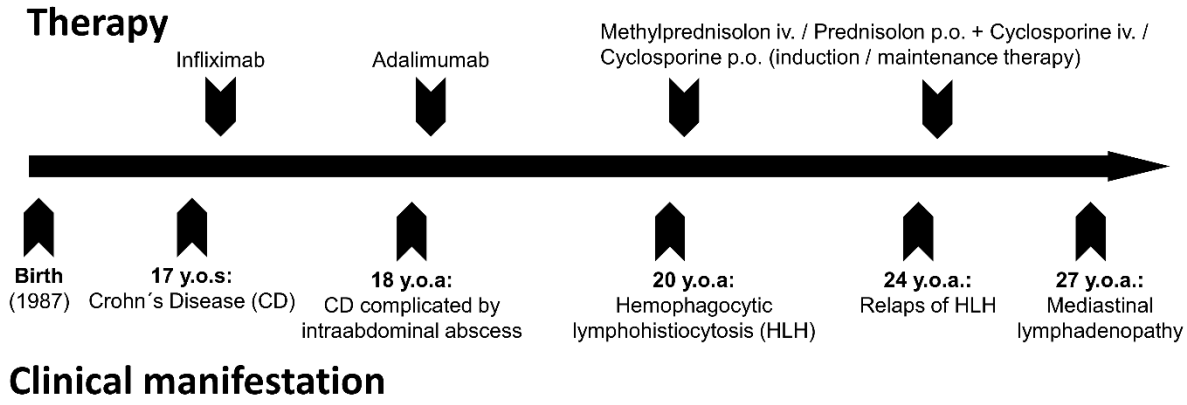

B

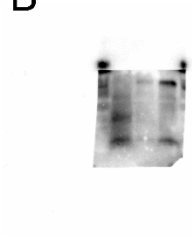

C

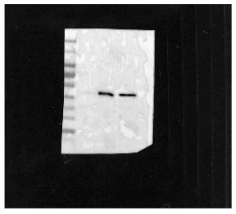

D

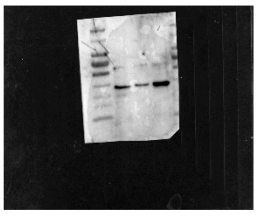

E

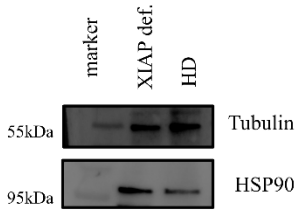

Supplementary Figure 2: Apoptosis. Patient PBMCs were treated with staurosporine (1 mmol) and 50 ng/ml PMA for 2, 4 and 6 hours or left untreated for an additional 24 and 48 hours. When indicated the cells were pre-treated with 20μM Z-VAD-fmk for 30 minutes. The level of spontaneous and induced apoptosis was detected by **A**. FLICA, in which the fluorescein-labelled inhibitor Z-YVAD-fmk is bound to activated caspase -3 and 7, signal as detected by flow cytometry. **B.** The level of spontaneous apoptosis detected by flow cytometry of cells stained with Annexin V and DAPI. Annexin+ DAPI cells were considered to be undergoing early apoptosis.

A

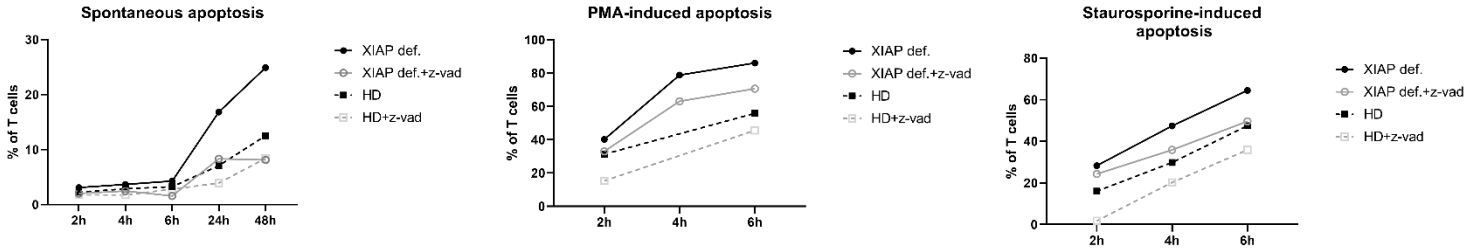

B

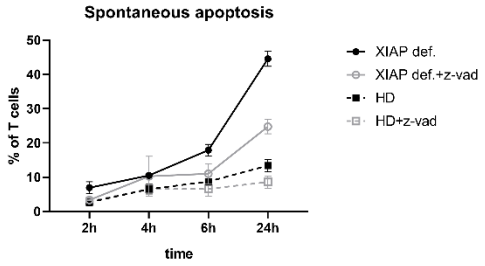

Supplementary Figure 3: A. MAPK and NFκB signalling pathways activation upon PMA or TNFα stimulation for 20 minutes of patient and control peripheral blood. **B.** Uncropped membranes from the Western blot analyses for MAPK and NFκB signalling pathways activation. **C.** CD69 expression on T cells expressed as MFI. **D.** T cell proliferation. Proliferating cells are expressed as Ki67+CD4+ T cells.

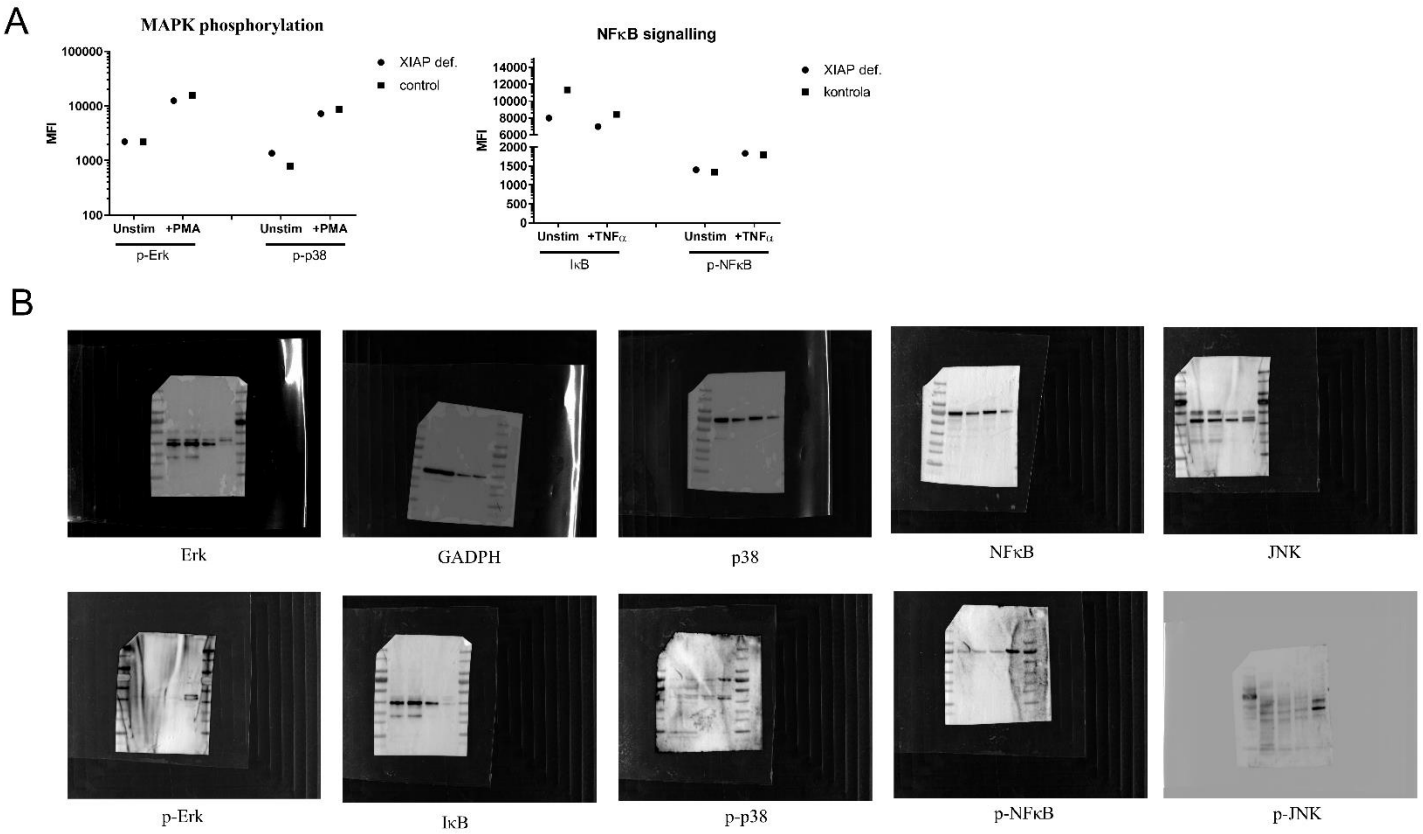

Supplementary Figure 4: Gating strategies for determining the populations of T and B cells in the patient.

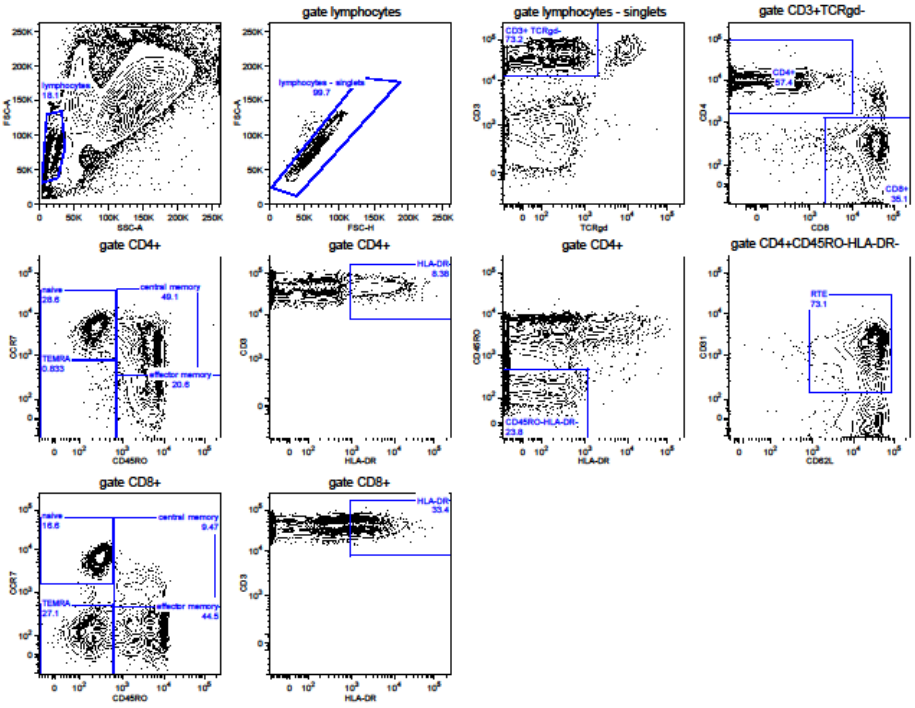

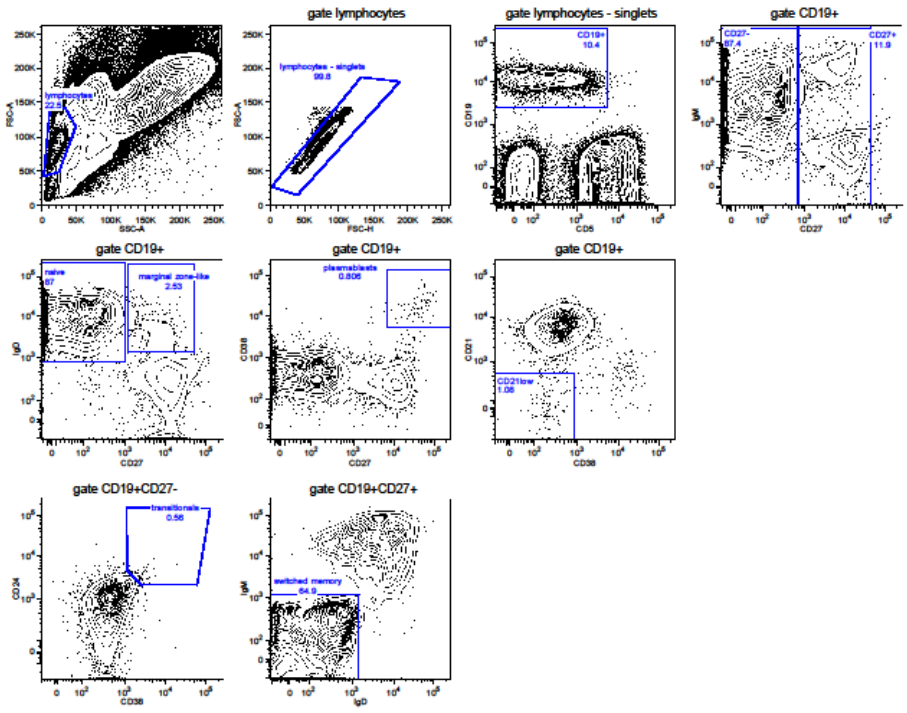

Příloha 7

Parackova Z, Bloomfield M, Vrabcova P, Zentsova I, Klocperk A, Milota T, **Svaton M**, Casanova JL, Bustamante J, Fronkova E, Sediva A. Mutual alteration of NOD2-associated Blau syndrome and IFNγR1 deficiency. J Clin Immunol. 2020 Jan;40(1):165-178. doi: 10.1007/s10875-019-00720-6.

Journal of Clinical Immunology
https://doi.org/10.1007/s10875-019-00720-6

ORIGINAL ARTICLE

Mutual alteration of NOD2-associated Blau syndrome and IFNγR1 deficiency

Zuzana Parackova[1] · Marketa Bloomfield[1,2] · Petra Vrabcova[1] · Irena Zentsova[1] · Adam Klocperk[1] · Tomas Milota[1] · Michael Svaton[3] · Jean-Laurent Casanova[4,5,6,7,8] · Jacinta Bustamante[4,5,6,9] · Eva Fronkova[3] · Anna Sediva[1]

Received: 11 July 2019 / Accepted: 25 September 2019

Abstract

Blau syndrome (BS) is an auto-inflammatory granulomatous disease that possibly involves abnormal response to interferon gamma (IFNγ) due to exaggerated nucleotide-binding oligomerization domain containing 2 (NOD2) activity. Mendelian susceptibility to mycobacterial diseases (MSMD) is an infectious granulomatous disease that is caused by impaired production of or response to IFNγ. We report a mother and daughter who are both heterozygous for *NOD2*$^{c.2264C>T}$ variant and dominant-negative *IFNGR1*^{818del4} mutation. The 17-year-old patient displayed an altered form of BS and milder form of MSMD, whereas the 44-year-old mother was completely asymptomatic. This experiment of nature supports the notion that IFNγ is an important driver of at least some BS manifestations and that elucidation of its involvement in the disease immunopathogenesis may identify novel therapeutic targets.

Keywords NOD2 · IFNγR1 · IFNγ · WES · MSMD · Blau syndrome · methotrexate

Introduction

Blau syndrome (BS) (OMIM, #186580) is a rare, autosomal-dominant (AD) childhood-onset systemic auto-inflammatory disorder classically characterized by a triad of arthritis, dermatitis, and uveitis, and the presence of non-caseating sterile granulomas [1–3]. It is caused by mutations in nucleotide-binding oligomerization domain containing 2 (*NOD2*), also

Zuzana Parackova and Marketa Bloomfield contributed equally to this work.

Summary A kindred harboring *NOD2*$^{c.2264C>T}$ and *IFNGR1*^{818del4} mutations is reported, manifesting as combined phenotype of altered Blau syndrome and mitigated partial IFNγR1 deficiency.

Electronic supplementary material The online version of this article (https://doi.org/10.1007/s10875-019-00720-6) contains supplementary material, which is available to authorized users.

✉ Zuzana Parackova
zuzana.parackova@fnmotol.cz

[1] Department of Immunology, 2nd Faculty of Medicine, Charles University and Motol University Hospital, V Uvalu 84, 15006 Prague 5, Czech Republic

[2] Department of Pediatrics, 1st Faculty of Medicine Charles University and Thomayer's Hospital, Prague, Czech Republic

[3] CLIP - Childhood Leukaemia Investigation Prague, Department of Paediatric Haematology and Oncology, 2nd Faculty of Medicine, Charles University and Motol University Hospital, Prague, Czech Republic

[4] Laboratory of Human Genetics of Infectious Diseases, Necker Branch, INSERM U1163, Necker Hospital for Sick Children, Paris, France

[5] Imagine Institute, Paris Descartes University, Paris, France

[6] St. Giles Laboratory of Human Genetics of Infectious Diseases, Rockefeller Branch, The Rockefeller University, New York, NY, USA

[7] Howard Hughes Medical Institute, New York, NY, USA

[8] Pediatric Hematology-Immunology Unit, Necker Hospital for Sick Children, AP-HP, Paris, France

[9] Study Center for Primary Immunodeficiencies, AP-HP, Necker Children Hospital, Paris, France

Published online: 23 November 2019

known as *CARD 15* (caspase activation and recruitment domain 15) [1, 2]. NOD2 is an innate immune system pattern-recognition receptor expressed mostly by not only monocytes, macrophages, and dendritic cells but also hepatocytes, preadipocytes, and pulmonary and intestinal epithelial cells [4, 5]. The three-domain protein recognizes and binds peptidoglycans contained in bacterial cell walls, chiefly muramyl dipeptide (MDP), and various other bacterial and viral products [6]. After ligand recognition, NOD2 activates the transcription factor NFκB and MAPKs (mitogen-activated protein kinases), thereby promoting inflammatory responses against pathogens [1, 2]. In particular, NOD2-mediated signaling can be triggered by mycobacteria [7, 8], including the attenuated vaccinal substrains *Bacillus Calmette-Guérin* (BCG) [9].

The importance of NOD2 in human health has been intensively studied. Heterozygous mutations in *NOD2* gene were first identified in Blau syndrome patients in 2001 [10]. Since then, twenty-seven variants have been found in patients with Blau syndrome (Infevers https://infevers.umai-montpellier.fr/web/). Most mutations occur at or near the NACHT domain of the protein, which is important for ATP-dependent self-oligomerization [11], while several other mutations are located within the leucine-rich repeat (LRR) motif or between the two domains. However, pathophysiologic mechanisms and genotype-phenotype correlation have yet not been ascertained. Even an argument of the gain-of-function (GOF) vs. loss-of-function (LOF) effect of the mutations remains unresolved.

Due to the granulomatous character of BS, the GOF phenotype was originally proposed and this was supported by studies using in vitro transient transfection assays with overexpressed NOD2 which demonstrated an elevated basal NFκB activation [3, 12]. However, this hypothesis was not confirmed by consecutive ex vivo experiments, as other studies fail to demonstrate the supposed exaggerated cytokine release by patients' peripheral blood mononuclear cells (PBMCs) after MDP stimulation [13, 14]. In parallel, the murine Blau syndrome model also showed reduced cytokine production and NFκB signaling and overall reduced response to MDP [15]. Nevertheless, the most recent evidence suggests that the proinflammatory state in BS may, indeed, be due to an increased NOD2 response and that interferon gamma (IFNγ) might play a crucial role in the disease pathophysiology. In healthy cells, IFNγ acts as a priming signal to upregulate NOD2 expression in order to mount an efficient inflammatory response against pathogens containing peptidoglycans [16]. In BS, such priming with IFNγ was shown to result in an abnormal spontaneous NOD2 activation even in the absence of infectious ligand [17].

AD (autosomal dominant) partial IFNγR1 deficiency is one of the genetic etiologies of Mendelian susceptibility to mycobacterial disease (MSMD; OMIM, #209950) [18–20]. The majority of MSMD genetic etiologies impair IFNγ immunity, either by impairing its production or by diminishing cellular responses to it [18–30]. MSMD patients suffer from increased susceptibility to intra-macrophagic pathogens, especially weakly virulent mycobacteria, such as environmental mycobacteria (EM) and attenuated BCG vaccinal substrains. Infections with *Salmonella* spp. are also commonly seen, whereas infections by *Nocardia* spp., *Histoplasma capsulatum*, and other microorganisms are rarer [21].

Twenty-nine genetic etiologies of MSMD have been discovered, with 12 "isolated MSMD"–causing loci (*IFNGR1*, *IFNGR2*, *STAT1*, *IL12RB1*, *IL-12B2*, *IL-12p40*, *IL-23R*, *TYK2*, *IRF8*, *SPPL2A*, *CYBB*, and *NEMO*) and with three "syndromic-MSMD" loci (*RORC*, *JAK1*, and *ISG15*) [22–28]. AD partial IFNγR1 deficiency is one of the most common causes of MSMD, in part because it is due to a mutation that is recurrent by hotspot [29]. As many as 45 unrelated kindreds have already been reported since 1999 and many more have been diagnosed [20–22, 27–30]. It is due to heterozygous mutations that truncate the cytoplasmic domain of the protein. The mutated receptor accumulates on the cellular surface due to a lack of recycling motif and exerts a dominant-negative effect over the wild-type receptors. This results in weakened, but not abolished, downstream signaling [29, 30]. This form of AD partial IFNγR1 deficiency causes a clinical susceptibility to environmental mycobacteria (EM) and non-typhoid *Salmonellae*. In over 70% of cases, the infections affect the bones [21]. Overall, the presentation is less severe than patients with complete IFNγR1 deficiency, which is a fatal condition with an early onset and a poor prognosis. Patients with AD partial IFNγR1 are treated with prolonged courses of antimycobacterial drugs and IFNγ [27, 30].

We were intrigued by a 17-year-old patient whose clinical features were reminiscent of both BS and MSMD who was found to harbor *NOD2*$^{c.2264C>T}$ and *IFNγR1*^{818del4} mutation. The patient's mother is completely asymptomatic despite carrying both mutations. Here, we describe the clinical and immunological phenotype of the kindred, as well as their *NOD2* and *IFNGR1* genotypes.

Materials and methods

Informed consent was obtained from all subjects involved in the study and all controls in accordance with the Declaration of Helsinki and according to the procedures established by the Ethical Committee of our institution.

Whole exome sequencing

DNA was isolated with QIAamp DNA Mini Kit (Qiagen, Hilden, Germany) and sequencing libraries were prepared using SureSelectXT Human All Exon + UTRs V6 kit (Agilent Technologies, Santa Clara, CA) and sequenced on

the NextSeq 500 instrument with the High Output V2 kit (Illumina, San Diego, CA). The reads in resulting FASTQ files were aligned against the human reference genome hg19 with BWA [31]. Genomic variants were called with samtools [32] and VarScan [33]. Variant annotation was performed using SnpEff [34]. Identification of causal variants was performed with Ingenuity® Variant Analysis™ software (https://www.qiagen-bioinformatics.com/products/ingenuity-variant-analysis, Qiagen).

IFNγR1 expression

Peripheral blood drawn into EDTA-coated tubes was labeled with antibodies against lineage-specific markers (CD3 clone MEM-57, CD19 clone LT19, CD20 clone LT20, CD16 clone LNK16, CD56 clone MEM-188) - FITC, CD14 - PEDy594 (clone MEM-15), CD11c - APC (clone BU15) (Exbio, Prague, Czech Republic), CD123 - PC7 (clone 6H6), HLA-DR - A700 (clone L243), IFNγR1 - PE (clone GIR-2018) (BioLegend, San Diego, CA, USA) for 20 min at room temperature and then lysed with hypotonic solution. Samples were acquired on AriaII (BD Biosciences, San Jose, CA, USA), analyzed using FlowJo (TreeStar, Ashland, OR, USA) and IFNγR1 was shown as MFI (mean fluorescence intensity).

Intracellular signaling and phospho flow

For IFNγR1 signaling, peripheral blood was stimulated with 1 μg/ml IFNγ (R&D, Minneapolis, MN, USA) (or with 100 ng/ml and 10 μg/ml when indicated) or 1 μg/ml IFNα (Abcam, Cambridge, UK) for 5 min (or for 30 or 60 min when indicated) at 37 °C. For MAPK phosphorylation, peripheral blood was left unstimulated. Subsequently, the cells were fixed using 4% formaldehyde for 10 min at 25 °C; erythrocytes were lysed using 0.1% Triton X-100 (Sigma-Aldrich, Darmstadt, Germany) for 15 min at 37 °C and the leukocytes were permeabilized using 80% ice-cold methanol for 30 min.

Samples for IFNγR1 signaling were labeled with antibodies against lineage-specific markers (CD3, CD19, CD20, CD16, CD56) - FITC, CD14 - PEDy594, CD11c - APC (Exbio), CD123 - PC7, HLA-DR - A700 (BioLegend) and intracellular signaling was detected using anti-phospho-STAT1 (Tyr701) - BV421 (clone 4a) antibody (BD Bioscience).

Samples for MAPK phosphorylation were labeled with antibodies against CD3 - A700 (clone MEM-57), CD14 - PEDy594 (Exbio), and CD19 - PC7 (clone J3-119) (Immunotech) and intracellular signaling was detected using anti-phospho-p38 (Thr180) - A647 (#4552S), anti-phosphoErk1/2 (Thr202/Tyr204) - A488 (#4374S), and anti phospho-SAPJ/JNK (Thr183/185) - PE (#5755S) antibody (Cell Signaling, Denvers, MA, USA).

Data were collected using BD FACSAria II, and BD FACSDiva (BD Biosciences) software was used for signal acquisition and then they were analyzed using FlowJo (Treestar) analysis platform.

Cytokine production

2×10^5 peripheral blood mononuclear cells (PBMCs) were re-suspended in 200 μl of complete media and were stimulated with muramyl dipeptide (MDP) (10 μg/ml) (Invivogen, San Diego, CA) and *E. coli* lipopolysaccharide (LPS) (1 μg/ml) (Sigma-Aldrich) or left untreated. When indicated, prestimulation with IFNγ (R&D) was used. After 24-h incubation at 37 °C, the supernatants were harvested and the cytokines were determined using multiplex Luminex cytokine fluorescent bead-based immunoassay (Merck Millipore, Beerlengton, MA). Data were collected using Luminex-100 system (Luminex, Austin, TX). A five-parameter regression formula was used to calculate the sample concentrations from standard curves.

CD4+ subset analysis

PBMCs were stimulated with phorbol 12-myristate 13-acetate (PMA) (50 ng/ml) and ionomycin (750 ng/ml) (both from Sigma-Aldrich, Darmstadt, Germany); 1 h later, brefeldin A (10 mg/ml) (BioLegend) was added for additional 3 h. Cells were harvested and stained with CD3 - A700, CD8 - PEDy594 (clone MEM-31) (Exbio), CD4 - PC7 (clone RPA-T4) (eBioscience, San Diego, CA), before being fixed and permeabilized using eBioscience fixation/permeabilization solutions. The following Abs were added: IFNγ - FITC (clone 4S.B3) (BD Biosciences) and IL-17A - A647 (clone BL168) (Biolegend). Samples were acquired on AriaII and analyzed using FlowJo software.

RT-PCR gene expression analysis

PBMCs were stimulated with IFNγ (1 μg/ml) (R&D) for 5 h for *IRF1* (Hs00971965_m1) and *CXCL10* (Hs00171042_m1) detection, or left untreated for *c-Fos* (Hs04194186_s1) and *c-Jun* (Hs99999141_s1) detection. Total RNA was isolated using RNeasy Mini Kit following manufacturer's instructions (Qiagen, MD, USA) and complementary DNA (cDNA) was synthetized using M-MLV reverse transcriptase (Thermo Fisher Scientific, Waltham, MA). RT-PCR was performed in duplicates using the cDNA and platinum Taq polymerase (Thermo Fisher Scientific), 200 nM dNTP (Promega, Southampton, UK), 50 mM $MgCl_2$ (Thermo Fisher Scientific), and TaqMan primer/probe sets (Thermo Fisher Scientific). Samples were matched to a standard curve generated by amplifying serially diluted products using the same PCR reaction and normalized to *GAPDH* (forward primers GAAGGTGAAGGTCGGAGTC; reverse primers GAAGATGGTGATGGGATTTC; FAM/TAMRA CAAGCTTCCCGTTCTCAGCC) (TIB MOLBIOL, Berlin, Germany) to obtain the relative expression value. Real-time assays were run on iQ5 Cycler (Bio-Rad, CA, USA).

NFκB translocation and Image Stream analysis

PBMCs were stimulated with MDP (10 μg/ml) (Invivogen) for 30 min or left untreated, then fixed and permeabilized following manufacturer's instructions described in protocol III of the BD phosphoflow protocols (BD Bioscience). The cells were then stained with anti CD14 - PEDy594 (Exbio), NFκB - A488 (#532301) (R&D system), Draq5 fluorescent probe solution (Thermo Fisher Scientific) and then washed. The data were acquired using ImageStream (Merck Millipore) and analyzed using IDEAS software's guided analysis for nuclear translocation (Merck Millipore). The data are expressed as similarity score and value of co-expressed NFκB and Draq5.

Western blot analysis of NFκB signaling

PBMCs were stimulated for 20 min with MDP (10 μg/ml) or left untreated. The cells were then washed and lysed in RIPA lysis buffer and PMSF (Cell Signaling), placed on ice, sonificated, and then centrifuged at 14000*g* to remove cell debris. For western blot analysis, samples were resuspended on Laemli buffer (Sigma-Aldrich) at 1:1 ratio and boiled for 5 min. Proteins were separated by SDS-PAGE and transferred to PVDF membrane. After blocking with 5% BSA in TBST (TBS and 0.1%Tween, both from Bio-Rad), membranes were incubated with the primary antibodies anti-IκB (#4814S), IKK (#2682S and #2370), phospho IKK (S176/S177) (#2078S), and β-actin (#8457S) (all from Cell Signaling) overnight, followed by incubation with peroxidase-conjugated anti-rabbit or anti-mouse secondary antibodies for 2 h. Membranes were developed using SuperSignal West Femto (Thermo Fisher Scientific). Densitometry was performed with ImageJ software (National Institutes of Health, USA). Band area values were used for semi-quantification. Graphs are expressed as ratio of stimulated/unstimulated cells of band area value calculated from band area of phosphorylated forms/band area of unphosphorylated forms.

Results

Case report

The proband (P1) is a 17-year-old female born to non-consanguineous Czech parents. Her father has rheumatoid arthritis and her maternal grandmother had reportedly suffered from frequent skin ulcerations, while her mother (P2) and sister are healthy. At the age of 6 weeks, the proband developed a post-vaccination BCGitis that was treated with isoniazid and rifampicin. The originally increased inflammatory markers decreased slightly but after 2 months of treatment, only partial improvement of the BCGitis was achieved. A new increase of inflammatory parameters (CRP 55 mg/l, erythrocyte sedimentation rate - ESR 120 mm/h, leukocytes 23,500/mm^3) prompted further investigation, which revealed anterior uveitis and severe osteomyelitis of mandible. Oral prednisone 1 mg/kg and clindamycin were added to the treatment. The symptoms regressed completely after 6 months of therapy and she appeared healthy until the age of 6 years. She then started experiencing recurrent flares of high-grade fever, accompanied with aseptic arthritis of sternoclavicular joints, knees, and elbows, developed maculopapular rash, often progressing into pustulosis of face and palms, and vasculitis-like rash on lower extremities. She also suffered from recurrent erythema nodosum and cervical lymphadenitis. Multiple biopsies from the lymph nodes showed well-formed granulomas with epithelioid and multinucleated giant cells; some of the granulomas also contained areas of non-caseating necrosis. Microbiologic investigations, including mycobacterial detection (acid-fast staining, PCR for tuberculous and non-tuberculous mycobacteria and cultures), were negative on all occasions. Her laboratory evaluation revealed signs of chronic inflammation (mildly increased ESR, increased serum amyloid A, microcytic anemia), along with elevated serum IgG, contrasting with gradually decreasing CD19$^+$ B lymphocyte count. A marked increase of activated CD3$^+$ HLA-DR$^+$ cells was noted (Table 1). A tentative diagnosis of Saphó or Blau syndrome was considered based on the cutaneous and joint features and the history of infantile uveitis. She was initially managed with oral steroids in flares and occasional courses of antibiotics (sulfamethoxazole/trimethoprim – STX/TMP, azithromycin, clindamycin); later she received STX/TMP prophylaxis alone. At 15 years of age, multifocal granulomatous osteomyelitis of hipbone (containing necrosis within some granulomas), multiple vertebrae and ribs, multiple splenic, hepatic lesions, and lymphadenopathy were detected (Fig. 1a, b). No mycobacteria were found in the bone lesions. The inflammatory markers were only mildly elevated, and she reported no pain. At that point, a heterozygous mutation in *IFNGR1* and a variant in *NOD2* (Fig. 2a, b) was discovered. The patient was thus diagnosed with MSMD and BS with extended phenotype. The STX/TMP was discontinued and she was started on methotrexate (MTX) 20 mg weekly which resolved her clinical symptoms within 6 months. A 2-week unplanned withdrawal of methotrexate resulted in a formation of deep ulceration on the foot which healed promptly after the drug reintroduction (Fig. 1c). Twelve months on the treatment, she experienced no further infectious or non-infections complications, including mycobacteriosis, despite the imune suppression.

The patient's mother carries both mutations but has never experienced any BS-related symptoms, nor has she contracted any apparent mycobacteriosis to date, despite being vaccinated with BCG as an infant. Her basic immune phenotype (lymphocytes subpopulations, immunoglobulin levels, etc.) was normal.

The clinical features of our *IFNGR1*^{818del4} and *NOD2*$^{c.2264C>T}$ proband, as well as comparison with another

Table 1 Laboratory values of proband1 (*NOD2c.2264C>T + IFNGR1818del4*)

	Pre-treatment	3 month on MTX treatment	12 months on MTX treatment	Age-matched reference values
Haemoglobin (g/l)/ MCV (fl)/ MCH (pg)	109↓/69.8↓/21.6↓	114↓/74.3↓/23.4↓	100↓/75.1↓/24.2↓	120–160/82.0–98.0/28.0–34.0
Leukocytes (cells/μl)	9900	9600	7600	4 000–10 000
Lymphocytes (cells/μl)	3440	3350	1820	800–4 000
Neutrophils (cells/μl)	4550	4790	4730	2 000–7 000
Monocytes (cells/μl)	430	500	550	80–1200
Eosinophils (cells/μl)	1410↑	760↑	460	0–500
$CD3^+$ (%[a], cells/μl)	87↑/ 2990	89↑ 2150	86↑/1570	60–85/1000–3900
$CD3^+$ $CD4^+$ (%[a], cells/μl)	59↑/2030	59↑/ 1430	58↑/1060	27–57/560–2700
$CD3^+$ $CD8^+$ (%[a], cells/μl)	24/830	26/630	25/460	18–40/300–1400
$CD3^+$ HLA-DR^+ (%[a])	37↑	29↑	22↑	0–10
$CD19^+$ (%[a], cells/μl)	4↓/140↓	4↓/100↓	5↓/90↓	7–30/200–1500
$CD16^+/CD56^+$ (%[a], cells/μL)	9/310	5/120	7/130	6–28/50–1000
$CD4^+$ $IL17^+$ (%[b])	0.61	0.33ê	0.37ê	0.5–5.97
Regulatory T cells (%[b]) $CD4^+CD25^+FOXP3^+$	5.9	3.9	6.13	3.0–10.0
Immunoglobulins IgG (g/l)	27.40↑	17.70↑	17.2↑	7.65–13.60
IgA (g/l)	2.44	1.86	2.25	0.91–2.90
IgM (g/l)	1.43	1.29	1.26	0.47–1.95
IgD (g/l)	53.5	27.0	-	0.0–100.0
IgE (IU/ml)	102	26	49.2	0.0–150
Circulating immune complexes	149↑	126↑	166↑	10–46 arb.units
Serum amyloid A (mg/l)	52↑	20↑	14.6↑	0.0–10.0
Autoantibodies (ANA , ENA, ANCA, ASCA, a-dsDNA, a-TPO, a-TG)	Negative	ND	Negative	NA

[a] % of total peripheral lymphocytes, [b] % of $CD4^+$, [c] % of $CD8^+$. *ND*, not done; *NA*, not applicable; *ANA*, antinuclear antibodies; *ENA*, extractable nuclear antigen antibodies; *ANCA*, anti-neutrophil cytoplasm antibodies; *ASCA*, anti-saccharomyces cerevisiae antibodies; *a-dsDNA*, anti-double-stranded DNA antibodies; *a-TPO*, anti-thyreoperoxidase antibodies; *a-TG*, anti-thyroglobulin antibodies; *MTX*, methotrexate. ↑↓ value above and below the reference range, respectively

patient with AD $IFNGR1^{818del4}$ mutation and a BS patient reported previously by Rosé et al [2] to carry the identical $NOD2^{c.2264C>T}$ [2] mutation, are summarized in Table 2.

Whole exome sequencing

In the proband, whole exome sequencing performed on PBMCs revealed simultaneously two mutations. A heterozygous mutation c.819_822delTAAT in *IFNGR1* (NM_000416.2, dbSNP rs587776856) leads to a 4-bp deletion and premature stop codon p.N274fs*2. The mutation, arbitrarily designed as c.818del4, was previously reported in patients with AD partial IFNγR1 deficiency and exerts a dominant-negative effect (DN) [29]. The second variant was found in *NOD2* gene c.2264C>T (NM_022162.2, rs61747625) at heterozygous state. It leads to amino acid substitution p.A755V in the LRR domain of the protein (Fig. 2C) and was previously reported in a patient with Blau syndrome [2].

Both mutations were found in heterozygous state in the patient's asymptomatic mother at the age of 44 years (Fig. 2a, b). The father and the proband's sister are wild-type for both mutations (Fig. 2b). DNA of the maternal grandmother was not available.

The $IFNGR1^{818del4}$ mutation is dominant-negative and underlies MSMD

In accordance with other AD partial IFNγR1-deficient patients, the proband showed significantly increased expression of IFNγR1 on monocytes and dendritic cells compared with 7 healthy controls (Fig. 3a). To analyze the AD $IFNγR1^{818del4}$ downstream signaling, we quantified the STAT1 phosphorylation (pSTAT1) after IFNγ stimulation. IFNα was used as a control STAT1-activating agent. Using phosphoflow, proband's monocytes displayed an impaired responsiveness to IFNγ stimulation compared with healthy donors; conversely, the level of STAT1 phosphorylation after IFNα administration was comparable to that in healthy donors (Fig. 3b), which indicated that the defect was not in STAT1 protein but, indeed, in the IFNγ receptor.

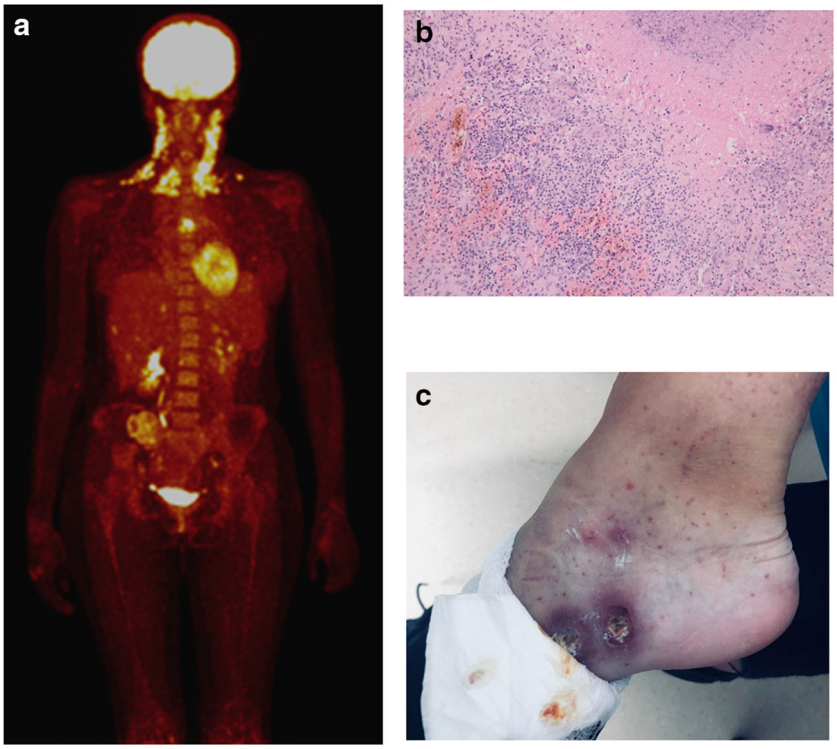

Fig. 1 PET MRI and histology images. **a** Whole-body PET MRI scan of the *NOD2*$^{p.A755V}$ and *IFNGR1*^{818del4} proband at the age 17 years showing increased metabolic activity in cervical lymph nodes, hipbone, multiple vertebrae and ribs, and splenic and hepatic lesions. **b** Microscopic image depicting granulomas with non-caseating necrosis in a biopsy sample from hipbone of the proband. **c** The deep ulceration on the foot after 2 weeks of unplanned withdrawal of methotrexate

Furthermore, to evaluate the severity of IFNγ signaling defect, we analyzed the expression of IFNγ-inducible genes, *CXCL10* and *IRF1* using RT-PCR. We noticed reduced, but not completely lost, expression of the genes (Fig. 3c) in the proband's PBMCs. In line with previous results, the defective IFNγR1^{818del4} signaling also manifested as decreased IL-12p70 production after simultaneous LPS and IFNγ stimulation (Fig. 3d). Proband's PBMCs were able to produce normal levels of cytokines in response to LPS; however, when simultaneously stimulated with LPS and IFNγ, the cytokine production increased to a much lesser degree than in healthy controls. This was particularly prominent in IL-12p70 production. Next, we analyzed the ability of the CD4^{+} and CD8^{+} T cells to produce IFNγ after nonspecific stimulation with PMA (Fig. 3e) and noticed that the proband's lymphocytes produced unexpectedly high amounts of IFNγ compared with seven age-matched healthy controls.

We were also able to perform a series of experiments on the proband's mother (P2) who is healthy, yet carries both mutations. We observed similar results, i.e., increased IFNγR1

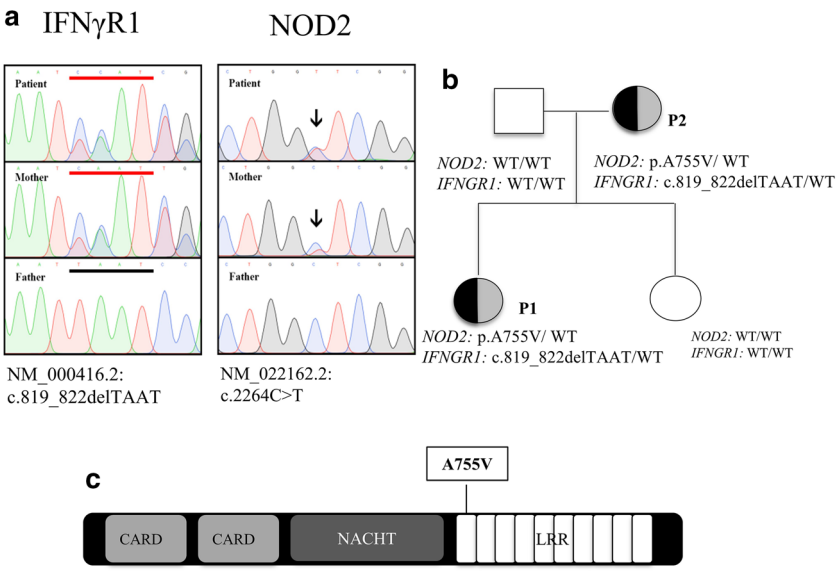

Fig. 2 Genetic analysis of the kindred. **a** DNA sequencing chromatograms of the relevant *NOD2* and *IFNGR1* gene regions of the proband (P1), her mother (P2), and father. **b** Pedigree of the kindred showing the familial segregation of the *NOD2*$^{p.A755V}$ and *IFNGR1*^{818del4} mutations. **c** NOD2 protein structure highlighting the position of alanine-for-valine substitution in the proband

Table 2 Characteristic symptoms of Blau syndrome and partial IFNγR1 deficiency. Specific symptoms in Blau syndrome associated with *NOD2c.2264C>T* mutation, patient with partial IFNγR1818del14 deficiency, patient with Blau syndrome caused by NOD2p.I37T mutation and AR IFNγR1P268S deficiency and the proband

Characteristics		Blau syndrome	Blau syndrome $NOD2^{c.2264^{C>T}}$	Partial AD *IFNGR1* deficiency	Partial $IFNGR1^{818del4}$ deficiency	Blau syndrome $NOD2^{c.2264\ C>T}$+ $IFNGR1^{818del4}$ P1	Blau syndrome $NOD^{c.802^{C>T}}$+ $IFNGR1^{c.110T>C}$ P*
Sex		F > M	Not reported	F = M	Female	Female	Male
Age of onset		< 4 years	Not reported	Mean 13 years	2 months	2 months	11 months
Clinical features	Uveitis	++	–	–	–	+	-
	Arthritis / arthralgia	++	–	–	+	+	+
	Skin rash / dermatitis	++	+	–	–	+	+
	Recurrent fever	++	+	–	–	+	+
	Periodic occurrence	++	+	–	–	+	+
	Infectious susceptibility	–	–	*BCG, NTM, Salmonella, Coccidioides, Histoplasma capsule, VZV*	*BCG, M. avium, M. abscessus–-immunogenum*	BCG	BCG
	BCGitis/BCGosis	+	–	++	+	+	+
	Multiple osteomyelitis	–	–	++	+	Iliac crest, costae, vertebrae	Iliac crest, costae, humerus
	Lymphadenopathy	+	–	++	+	+	+
	Erythema nodosum	+	+	–	–	+	–
	Hypertension	+	+	–	–	–	–
	Lung involvement	+	Interstitial lung disease	+	–	–	Interstitial lung disease
	Renal disease	+	Interstitial nephritis	–	–	–	Kidney stones
	Hepatosplenomegaly	+	–	+	–	+ Hepatic and splenic lesions	+ Hepatic lesions
	Neurological symptoms	+	–	–	–	–	Facial palsy
	Vasculitis	+	–	–	–	Likely, unconfirmed	–
Histologic appearance of lesions		Non-caseating granulomas, some fibrinoid necrosis	Not reported	Caseating/non-caseating/granulomas	Caseating/non-caseating granulomas	Non-caseating granulomas, some with non-caseating necrosis	Granulomatous inflammation

++ common, + reported, – uncharacteristic

BCG, *Bacillus Calmette-Guérin*; *NTM*, non-tuberculous mycobacteria; *VZV*, *varicella zoster virus, AD*, autosomal dominant; *AR*, autosomal recessive

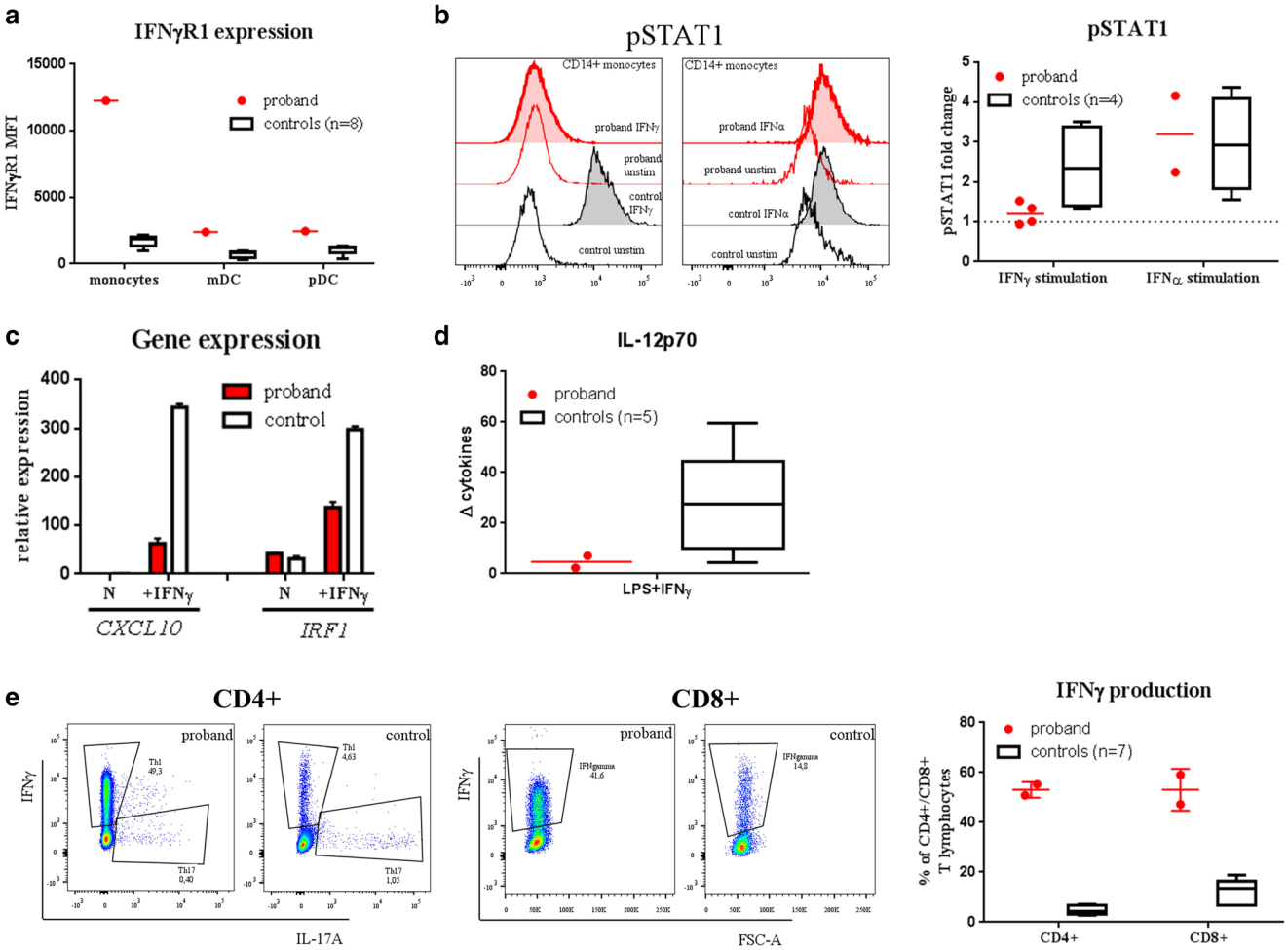

Fig. 3 Functional verification of *IFNGR1*^{818del4} mutation in the proband (P1). **a** Increased IFNγR1 expression on cell surface of proband's monocytes (Lin-, HLA-DR+, CD14+), myeloid (Lin-, HLA-DR+, CD14-, CD11c+), and plasmacytoid (Lin-, HLA-DR+, CD14-, CD123+) dendritic cells compared with healthy controls (n = 8). Data are expressed as MFI (mean fluorescence intensity). **b** Reduced STAT1 phosphorylation (Tyr701) after IFNγ (1 μg/ml) stimulation and preserved STAT1 phosphorylation after IFNα (1 μg/ml) stimulation in proband's monocytes compared with healthy controls (n = 4). **c** Diminished *CXCL10* and *IRF1* relative expression normalized to *GAPDH* in proband's PBMCs after IFNγ (1 μg/ml) stimulation compared with healthy controls (n = 3). **d** Decreased IL-12p70 production in proband's PBMCs in response to LPS (1 μg/ml) or LPS and IFNγ (1 μg/ml) combined compared with healthy controls (n = 5). The results are expressed as IFNγ response index (LPS + IFNγ–stimulated/LPS-stimulated PBMCs). **e** Elevated IFNγ production by proband's CD4+ and CD8+ T after PMA (50 ng/ml) and ionomycin (750 ng/ml) stimulation compared with healthy controls (n = 7)

expression, diminished STAT1 phosphorylation, reduced IL-12p70 production after LPS and IFNγ stimulation, and increased IFNγ production by T cells (Fig. 5a–d). The only difference between the mother and the proband was detected in IFNγ-induced expression of *CXCL10*; this was comparable to healthy donors in the mother but decreased significantly in the proband (Fig. 5e).

We also had the opportunity to examine samples from another carrier of the same AD *IFNGR1*^{818del4} mutation and compared the results with the proband. The patient presented with BCGitis and EM osteomyelitis and her laboratory findings were similar to our proband (Suppl. Fig. 1A-D) except of the IFNγ production by T cells, which was only slightly increased, compared to our proband.

The *NOD2*$^{c.2264C>T}$ variant is hyperactivating and causes augmented NFκB and MAPK signaling

NOD2 stimulation with muramyl dipeptide (MDP) leads to the activation of the NFκB and MAPK signaling pathways. We analyzed cellular responses to MDP stimulation using different approaches. Firstly, we used image cytometry to determine NFκB nuclear translocation after MDP stimulation. We observed increased level of translocation in proband's (P1) cells compared with controls (Fig. 4a). Interestingly, we also noticed higher level of translocation in proband's unstimulated cells, suggesting a ligand-independent activation.

Secondly, using Western blot analysis, we examined the NFκB activation pathway after MDP stimulation, expressed as IκB (inhibitor of κB) degradation and IKK (IκB kinase)

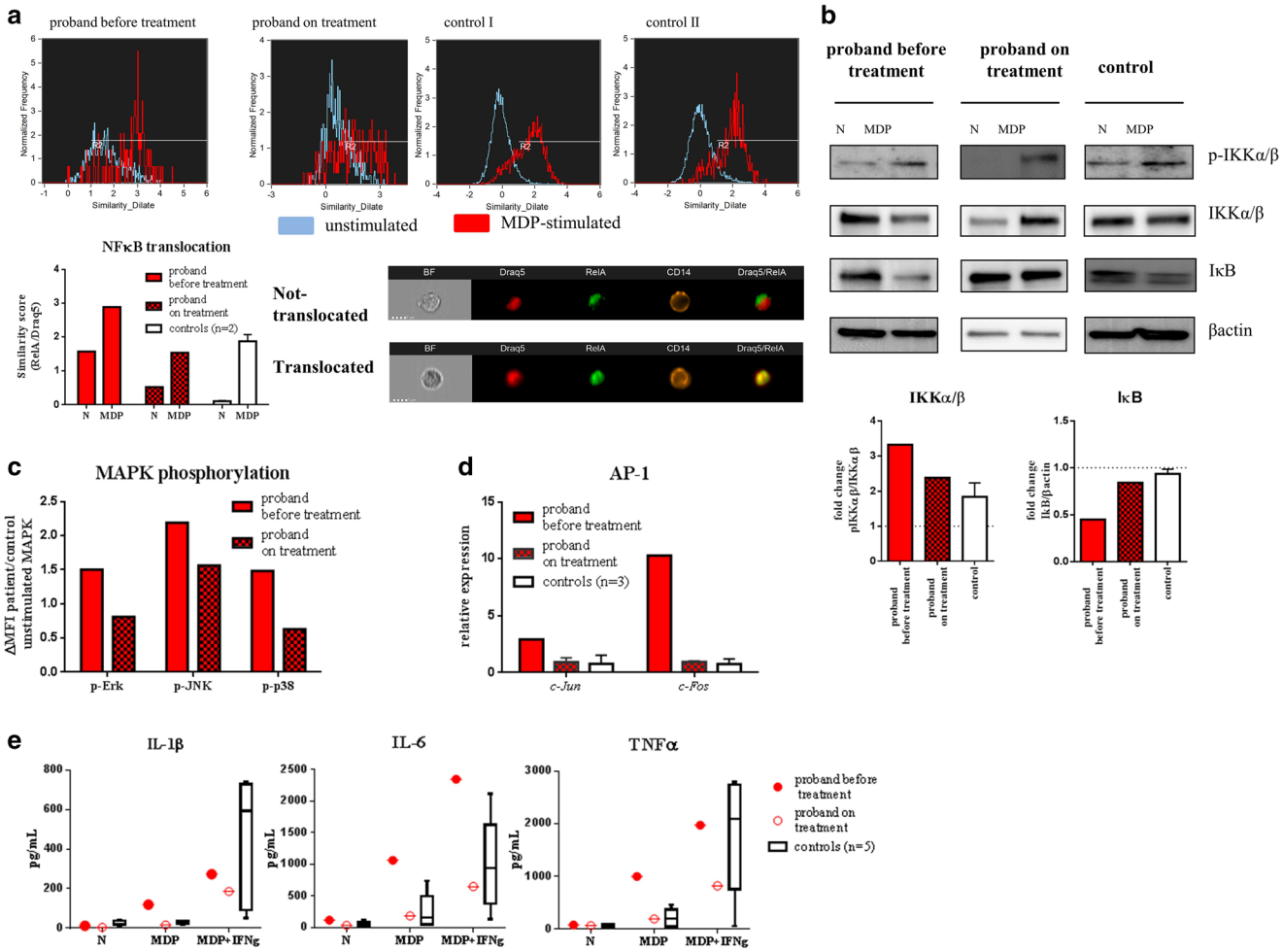

Fig. 4 Functional verification of *NOD2*$^{p.A755V}$ mutation in the proband (P1) and the effect of methotrexate treatment. **a** Elevated NFκB translocation after MDP (10 μg/ml) stimulation detected by image cytometry in the proband's CD14+ monocytes compared with healthy donors (n = 2). Data are expressed as similarity score, i.e., the level of co-expression of NFκB and Draq5-labeled nuclei. **b** Increased NFκB pathway activation after MDP (10 μg/ml) stimulation in proband's PBMCs compared with healthy controls (n = 2). The pathway was analyzed through degradation of IκB (inhibitor of κB) and phosphorylation of IKK (IκB kinase α and β) using Western blot. Band area values were used for semi-quantification. Graphs are expressed as a ratio of stimulated/unstimulated cells of band area value calculated from band area of pIKK/IKK or IκB/β-actin ratio, respectively. **c** Elevated ligand-independent Erk, JNK, and p38 MAPK phosphorylation (expressed as MFI-unstimulated proband's MAPK/MFI unstimulated control's MAPK) detected in CD14+ monocytes using phosphoflow cytometry. **d** Increased ligand-independent relative expression of *c-Fos* and *c-Jun* in proband's PBMCs compared with controls (n = 3). **e** Cytokine production by proband's and control's (n = 5) PBMCs after MDP (10 μg/ml) stimulation or combination of MDP (10 μg/ml) and IFNγ (1 μg/ml) stimulation. All experiments were performed before and after 3 months on treatment with methotrexate

phosphorylation. The activation of IKK leads to phosphorylation of IκB which provides a signal to the inhibitor degradation. Once the inhibitor is degraded, NFκB is activated and translocated to the nucleus. We detect higher intensity of phosphorylated IKK and more intense IκB degradation in proband (Fig. 4b), which was in line with previous observations of higher NFκB activity in the proband's monocytes.

Finally, we focused on phosphorylation of MAP kinases—p38, JNK, and Erk (Fig. 4c). We observed normal levels of phosphorylation of all kinases in response to MDP in proband's monocytes (data not shown), but higher phosphorylation in their unstimulated state, once again suggesting ligand-independent activation. To confirm the observation, we evaluated basal expression of MAPK-inducible genes *c-Fos* and *c-Jun*, which form AP-1 complex and noticed slightly increased ligand-independent expression of these genes compared with controls (Fig. 4d). We observed similar trends in MAPK basal phosphorylation in the proband's mother (Fig. 5F).

Next, we assessed the cytokine production (IL-1β, IL-6, and TNFα) after stimulation of proband PBMCs with MDP, IFNγ, or their combination using Luminex method (Fig. 4e). The proband's cells produced higher levels of cytokines after MDP stimulation compared with healthy controls. IFNγ alone did not induce cytokine release in proband or in healthy donors (data not shown). However, the combination of IFNγ and MDP led to increased cytokine production in both controls

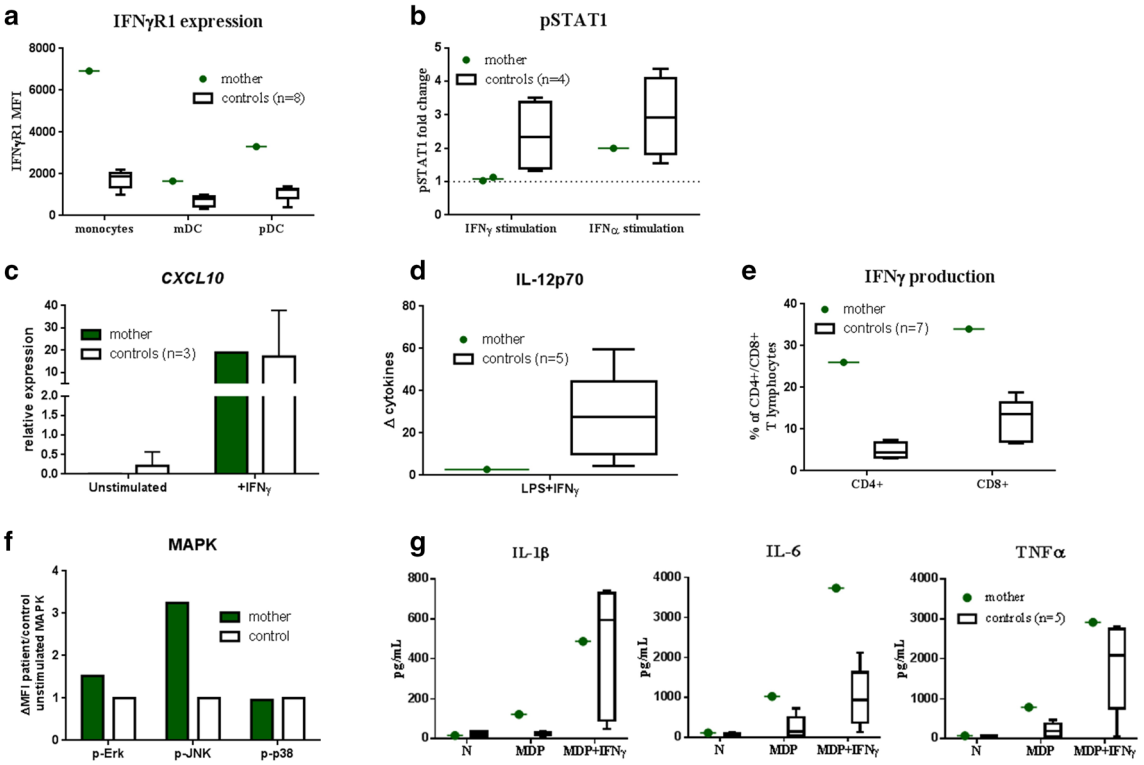

Fig. 5 Functional assays in the proband's mother (P2): **a** Increased IFNγR1 expression on cell surface of P2's monocytes (Lin-, HLA-DR+, CD14+), myeloid (Lin-, HLA-DR+, CD14-, CD11c+), and plasmacytoid (Lin-, HLA-DR+, CD14-, CD123+) dendritic cells compared with healthy controls (n = 8). Data are expressed as MFI (mean fluorescence intensity). **b** Reduced STAT1 phosphorylation (Tyr701) after IFNγ (1 μg/ml) stimulation and preserved STAT1 phosphorylation after IFNα (1 μg/ml) stimulation in P2's CD14+ monocytes compared with healthy controls (n = 4). **c** Preserved *CXCL10* relative expression normalized to *GAPDH* in P2 PBMCs after IFNγ (1 μg/ml) stimulation compared to healthy controls (n = 3). **d** Decreased IL-12p70 production in P2's PBMCs in response to LPS (1 μg/ml) or LPS and IFNγ (1 μg/ml) combined compared with healthy controls (n = 5). The results are expressed as IFNγ response index (LPS + IFNγ–stimulated/LPS-stimulated PBMCs). **e** Elevated IFNγ production by P2's CD4+ and CD8+ T lymphocytes after PMA (50 ng/ml) and ionomycin (750 ng/ml) stimulation compared with healthy controls (n = 7). **f** Elevated ligand-independent Erk, JNK, and p38 MAPK phosphorylation (expressed as MFI-unstimulated P2's MAPK/MFI-unstimulated control's MAPK) detected in CD14+ monocytes using phosphoflow cytometry

and also in the proband. Given the AD partial IFNγR1 defect, it was surprising to find that the level of proinflammatory cytokines produced by the proband's cells was even slightly higher than in healthy controls. We observed similar results in cells from the proband's mother (Fig. 5g).

Finally, another carrier of the same *IFNGR1*^{818del4} mutation was shown to have a normal basal MAPK phosphorylation as well as c-Fos and c-Jun expression (Suppl. Fig. 1E and F), suggesting that the observed increased MAPK signaling in proband and the mother may not be attributed to the *IFNGR1* mutation and is therefore likely due to hyperactivation of NOD2.

A designated set of experiments was repeated 3 and 7 months on MTX treatment in the proband. While no changes in IFNγR1^{818del4} signaling (data not shown) were noted a sustained significant decrease of NFκB and MAPK signaling, and the overall cytokine production was detected (Fig. 4a–e) as the proband's symptoms regressed.

Overall, the results suggest that the *NOD2*$^{c.2264C>T}$ variant exerts a gain-of-function effect and likely underlies at least some auto-inflammatory features of the proband.

Discussion

In this study, we report a child and her mother harboring two heterozygous mutations in the innate mechanisms of antimicrobial defense, the *IFNGR1*^{818del4} and *NOD2*$^{c.2264C>T}$, presenting as combined phenotype of altered BS and milder MSMD in the 17-year-old proband, while the proband's mother is asymptomatic.

The *IFNGR1*^{818del4} is the most frequent mutation in the "818del4" hotspot, reported in over 80% of patients with AD IFNγR1 deficiency. Both the proband and her mother displayed the corresponding cellular phenotype. The proband's BCGitis represents a classic feature of AD IFNγR1 deficiency, but no infectious pathogens were ever detected in any of her later sites of inflammation. Particularly, thorough investigation was performed to elucidate the etiology of the osteomyelitis, a common feature of AD IFNγR1. Despite the fact that some of the granulomas showed prominent necrotic features, which is characteristic for AD IFNγR1 deficiency and less typical for BS [35], no mycobacteria were detected.

However, it should be stressed out that these pathogens are notoriously difficult to detect in bones. On the other hand, the effect of MTX advocates strongly for non-infectious etiology.

Curiously, the proband's mother received BCG vaccine without any complications (her skin tuberculin test was indicative of having received the BCG vaccine) and remained altogether healthy. This may be due to a phenomenon of incomplete penetrance, which has been reported to some degree in many immune deficiencies [36–40], including AD IFNγR1 [31, 41]. The penetrance of vaccine-associated BCG disease in AD IFNγR1 deficiency appears to be high (uncalculated), but several mutation carriers have been reported to suffer no adverse reactions to BCG. The penetrance of environmental mycobacterial disease was calculated in 2004 to be 21% by 5 years of age and 45% by 10 years of age [30]. The underlying mechanisms of incomplete penetrance are unknown.

The *NOD2*$^{c.2264C>T}$ allele frequency in general population is 0.2%, according to ExAC database and as such, it is classed as "variant of unknown significance." One other BS patient was previously reported to harbor this mutation, presenting with non-classic phenotype (Table 2). Our experiments demonstrate a hyperactivation of downstream NOD2 signaling via augmented NFκB and MAPK, which corresponds with the findings of some previously published data on the cellular disturbances in BS [3, 17] but is in conflict with others [13]. This hyperactivation may not be attributed to the AD IFNGR1 deficiency. Whereas most of the BS-associated mutations are found in NACHT domain, the *NOD2*$^{c.2264C>T}$ mutation is located in LRR domain. Taken together, it is therefore possible that this is an atypical BS mutation that does not reflect mechanisms operative in the majority of patients.

In the proband, the hallmark features of BS, e.g., dermatitis and arthritis, were fully expressed. Uveitis, the remaining symptom of the classic BS triad, occurred during the treatment of BCGitis. The fact that it resolved after addition of steroids suggests a non-infection background and we therefore consider it a probable attribute of BS. An additional feature in the proband was multifocal granulomatous osteomyelitis, which responded well to MTX. Again, the mother also carries the heterozygous *NOD2*$^{c.2264C>T}$ yet suffers no related symptoms. The penetrance of BS-associated *NOD2* mutations is not known but appears to be high. Nevertheless, at least 5 asymptomatic mutation carriers have been reported, two of them healthy and well into their adulthood [42–44].

A puzzling excess of IFNγ production by T cells was detected in our kindred. Such overt IFNγ production has not been described in BS [45], nor is the excess of IFNγ found in the sera of patients with partial IFNγR1 deficiency [30, 46]. To confirm this, we evaluated the IFNγ production in another AD IFNγR1 MSMD patient and another NOD2-associated BS patient and found it to be normal in both cases. The overproduction of IFNγ in our patient therefore appears to be the result of a combined effect of both mutations but the underlying mechanism is unclear. As the patient improved on treatment, the NFKB, MAPK signaling, and the cytokine production decreased but the IFNγR1 signaling and the IFNγ production by T cells remained unaltered. This finding supports the notion that the major culprit in the patient's BS symptoms is the NOD2$^{c.2264C>T}$ downstream hyperresponsiveness and not merely the increased IFNγ.

Several examples of overlapping aspects of BS and AD IFNγR1 MSMD led us to hypothesize that the co-existence of both mutations would exhibit certain functional alterations and that IFNγ is the common denominator. Both diseases present histologically with the formation of granulomas. In BS patients, IFNγ was shown to be overexpressed in cells within the granulomas [35]. Conversely, the inflammatory lesions of patients with complete IFNγR1 signaling arrest, such as the autosomal recessive *IFNGR1* mutation, show poorly established granulomas with very few giant cells [47]. The recently published research implies a novel activation pathway in BS, in which IFNγ primes the NOD2-mutated induced pluripotent stem cell-derived macrophages to a pre-activated state, independently of IFNγR/STAT1-mediated signaling [17]. The excessive IFNγ production by T cells found in our proband may therefore account for her altered BS phenotype, even in the setting of impaired IFNγR signaling.

Moreover, both receptors are involved in antimycobacterial immune response [35, 48, 49]. In fact, the BCG was reported as a suspected culprit in triggering or worsening BS in some patients [50–52]. The post-vaccination increase of IFNγ expression [53] suggests a possible mechanism via which the BCG may accentuate the NOD2-driven inflammatory response. In our proband, the BS-associated uveitis, arising after BCG vaccination, resonates with the notion.

On the other hand, given the well-known therapeutic effect of exogenous IFNγ on mycobacterial infections in AD IFNγR1 deficient patients, we suggest that the exaggerated IFNγ production provides a certain protection against mycobacterial infections for the proband and may perhaps compensate for the mother's AD IFNγR1 deficiency. Illustratively, another AD IFNγR1^{818del4} patient, who we examined, suffered three different EM by the age of 9 years, at least one of them shortly after withdrawal of IFNγ treatment (Table 2). This patient showed identically disturbed IFNγR1 signaling but a near-normal IFNγ production.

Interestingly, in 2016, a Turkish patient was briefly reported to harbor heterozygous missense *NOD2* mutation (*c.802C>T*, p.P268S, classed as variant of unknown significance) and homozygous mutation in *IFNGR1* gene (*c.110T>C*, I37T) presenting as BS and AR partial IFNγR1 deficiency [54]. The clinical similarity to our proband is striking (Table 2), including the presence of multifocal osteomyelitis and the response to MTX. Curiously, this patient also developed acute macrophage-activation syndrome (MAS). MAS is thought to result from uncontrolled macrophage

activation due to hypercytokinemia, particularly under the overproduction of IFNγ by T cells [55]. In our proband, such excessive production of IFNγ was a hallmark of her T cell phenotype, although she did not experience MAS.

The presented patient represents a model of BS with impaired IFNγ signaling via IFNγR1. Given the possible role of IFNγ in the pathogenesis of BS, the clinical presentation described here may be of interest to those exploring targeting of its signaling as a therapeutic strategy for BS. However, our study has several limitations; therefore, the findings must be interpreted with care. Because of the dilemmas emphasized above, such as the location and pathogenicity of $NOD2^{c.2264C>T}$ mutation, the nature of the osteomyelitis, or the genotype-phenotype discordance between two carriers, the exact immunopathogenesis of the patient's symptom complex may only be assumed but remains unverified.

In conclusion, we identified a patient with $IFNGR1^{818del4}$ and $NOD2^{c.2264C>T}$ mutations presenting with a unique phenotype and suggest that the functional cross-talk between IFNγ and NOD2 pathways in BS warrants further exploration in future studies.

Author contribution ZP designed the study, performed the experiments, analyzed and interpreted the results, co-wrote the manuscript, and supervised all work. MB treated the patient, interpreted the results, and co-wrote the manuscript. PV, IZ, MR, and AK performed the experiments and analyzed the data. TM provided clinical information. EF and MS performed genetic analysis. JB and JLC revised the manuscript and contributed to the discussion. AS treated the patient and supervised the manuscript preparation. All authors contributed to manuscript revision, read and approved the submitted version.

Funding information This work was supported by grants GAUK 460218 and 954218 issued by the Charles University in Prague, Czech Republic, and AZV NV18-05-00162 from the Ministry of Health of the Czech Republic.

Compliance with ethical standards

Conflict of interest The authors declare that they have no conflicts of interest.

Ethics statement This study was carried out in accordance with the recommendation of the Ethical Committee of the 2nd Faculty of Medicine, Charles University, in Prague and University Hospital in Motol, Czech Republic. The protocol was approved by the Ethical Committee and all subjects gave informed consent in accordance with the Declaration of Helsinki.

References

1. Wouters CH, Maes A, Foley KP, Bertin J, Rose CD. Blau syndrome, the prototypic auto-inflammatory granulomatous disease. Pediatr Rheumatol Online J. 2014;12:33. https://doi.org/10.1186/1546-0096-12-33.
2. Rose CD, Pans S, Casteels I, Anton J, Bader-Meunier B, Brissaud P, et al. Blau syndrome: cross-sectional data from a multicentre study of clinical, radiological and functional outcomes. Rheumatology. 2015;54:1008–16. https://doi.org/10.1093/rheumatology/keu437.
3. Kanazawa N, Okafuji I, Kambe N, Nishikomori R, Nakata-Hizume M, Nagai S, et al. Early-onset sarcoidosis and CARD15 mutations with constitutive nuclear factor-kappaB activation: common genetic etiology with Blau syndrome. Blood. 2005;105:1195–7. https://doi.org/10.1182/blood-2004-07-2972.
4. Philpott DJ, Sorbara MT, Robertson SJ, Croitoru K, Girardin SE. NOD proteins: regulators of inflammation in health and disease. Nat Rev Immunol. 2014;14:9–23. https://doi.org/10.1038/nri3565.
5. Negroni A, Pierdomenico M, Cucchiara S, Stronati L. NOD2 and inflammation: current insights. J Inflamm Res. 2018;11:49–60. https://doi.org/10.2147/JIR.S137606.
6. Girardin SE, Boneca IG, Viala J, Chamaillard M, Labigne A, Thomas G, et al. Nod2 is a general sensor of peptidoglycan through muramyl dipeptide (MDP) detection. J Biol Chem. 2003;278:8869–72. https://doi.org/10.1074/jbc.C200651200.
7. Landes MB, Rajaram MVS, Nguyen H, Schlesinger LS. Role for NOD2 in Mycobacterium tuberculosis -induced iNOS expression and NO production in human macrophages. J Leukoc Biol. 2015;97:1111–9. https://doi.org/10.1189/jlb.3A1114-557R.
8. Brooks MN, Rajaram MVS, Azad AK, Amer AO, Valdivia-Arenas MA, Park J-H, et al. NOD2 controls the nature of the inflammatory response and subsequent fate of Mycobacterium tuberculosis and M. bovis BCG in human macrophages. Cell Microbiol. 2011;13:402–18. https://doi.org/10.1111/j.1462-5822.2010.01544.x.
9. Kleinnijenhuis J, Quintin J, Preijers F, Joosten LAB, Ifrim DC, Saeed S, et al. Bacille Calmette-Guerin induces NOD2-dependent nonspecific protection from reinfection via epigenetic reprogramming of monocytes. Proc Natl Acad Sci. 2012;109:17537–42. https://doi.org/10.1073/pnas.1202870109.
10. Miceli-Richard C, Lesage S, Rybojad M, Prieur A-M, Manouvrier-Hanu S, Häfner R, et al. CARD15 mutations in Blau syndrome. Nat Genet. 2001;29:19–20. https://doi.org/10.1038/ng720.
11. Rose CD, Martin TM, Wouters CH. Blau syndrome revisited. Curr Opin Rheumatol. 2011;23:411–8. https://doi.org/10.1097/BOR.0b013e328349c430.
12. Ebrahimiadib N, Samra KA, Domina AM, Stiles ER, Ewer R, Bocian CP, et al. A novel NOD2-associated mutation and variant Blau syndrome: phenotype and molecular analysis. Ocul Immunol Inflamm. 2018;26:57–64. https://doi.org/10.1080/09273948.2016.1185529.
13. Martin TM, Zhang Z, Kurz P, Rosé CD, Chen H, Lu H, et al. The NOD2 defect in Blau syndrome does not result in excess interleukin-1 activity. Arthritis Rheum. 2009;60:611–8. https://doi.org/10.1002/art.24222.
14. Son S, Lee J, Woo C-W, Kim I, Kye Y, Lee K, et al. Altered cytokine profiles of mononuclear cells after stimulation in a patient with Blau syndrome. Rheumatol Int. 2010;30:1121–4. https://doi.org/10.1007/s00296-009-1342-4.
15. Dugan J, Griffiths E, Snow P, Rosenzweig H, Lee E, Brown B, et al. Blau syndrome–associated Nod2 mutation alters expression of full-length NOD2 and limits responses to muramyl dipeptide in knock-in mice. J Immunol. 2015;194:349–57. https://doi.org/10.4049/jimmunol.1402330.
16. Rosenstiel P, Fantini M, Bräutigam K, Kühbacher T, Waetzig GH, Seegert D, et al. TNF-α and IFN-γ regulate the expression of the NOD2 (CARD15) gene in human intestinal epithelial cells. Gastroenterology. 2003;124:1001–9. https://doi.org/10.1053/gast.2003.50157.
17. Takada S, Kambe N, Kawasaki Y, Niwa A, Honda-Ozaki F, Kobayashi K, et al. Pluripotent stem cell models of Blau syndrome reveal an IFN-γ–dependent inflammatory response in macrophages. J Allergy Clin Immunol. 2018;141:339–349.e11. https://doi.org/10.1016/j.jaci.2017.04.013.

18. Newport MJ, Huxley CM, Huston S, Hawrylowicz CM, Oostra BA, Williamson R, et al. A mutation in the interferon-γ –receptor gene and susceptibility to mycobacterial infection. N Engl J Med. 1996;335: 1941–9. https://doi.org/10.1056/NEJM199612263352602.
19. Casanova JL, Ochs H. Interferon-gamma receptor deficiency: an expanding clinical phenotype? J Pediatr. 1999;135:543–5. https://doi.org/10.1016/S0022-3476(99)70050-8.
20. Jouanguy E, Lamhamedi-Cherradi S, Altare F, Fondanèche MC, Tuerlinckx D, Blanche S, et al. Partial interferon-gamma receptor 1 deficiency in a child with tuberculoid bacillus Calmette-Guérin infection and a sibling with clinical tuberculosis. J Clin Invest. 1997;100:2658–64. https://doi.org/10.1172/JCI119810.
21. Bustamante J, Boisson-Dupuis S, Abel L, Casanova J-L. Mendelian susceptibility to mycobacterial disease: genetic, immunological, and clinical features of inborn errors of IFN-γ immunity. Semin Immunol. 2014;26:454–70. https://doi.org/10.1016/j.smim.2014.09.008.
22. Rosain J, Kong X-F, Martinez-Barricarte R, Oleaga-Quintas C, Ramirez-Alejo N, Markle J, et al. Mendelian susceptibility to mycobacterial disease: 2014-2018 update. Immunol Cell Biol. 2018. https://doi.org/10.1111/imcb.12210.
23. Oleaga-Quintas C, Deswarte C, Moncada-Vélez M, Metin A, Krishna Rao I, Kanık-Yüksek S, et al. A purely quantitative form of partial recessive IFN-γR2 deficiency caused by mutations of the initiation or second codon. Hum Mol Genet. 2018;27:3919–35. https://doi.org/10.1093/hmg/ddy275.
24. Boisson-Dupuis S, Ramirez-Alejo N, Li Z, Patin E, Rao G, Kerner G, et al. Tuberculosis and impaired IL-23–dependent IFN-γ immunity in humans homozygous for a common TYK2 missense variant. Sci Immunol. 2018;3:eaau8714. https://doi.org/10.1126/sciimmunol.aau8714.
25. Martínez-Barricarte R, Markle JG, Ma CS, Deenick EK, Ramírez-Alejo N, Mele F, et al. Human IFN-γ immunity to mycobacteria is governed by both IL-12 and IL-23. Sci Immunol. 2018;3:eaau6759. https://doi.org/10.1126/sciimmunol.aau6759.
26. Kong X-F, Martinez-Barricarte R, Kennedy J, Mele F, Lazarov T, Deenick EK, et al. Disruption of an antimycobacterial circuit between dendritic and helper T cells in human SPPL2a deficiency. Nat Immunol. 2018;19:973–85. https://doi.org/10.1038/s41590-018-0178-z.
27. Filipe-Santos O, Bustamante J, Chapgier A, Vogt G, de Beaucoudrey L, Feinberg J, et al. Inborn errors of IL-12/23- and IFN-γ-mediated immunity: molecular, cellular, and clinical features. Semin Immunol. 2006;18:347–61. https://doi.org/10.1016/j.smim.2006.07.010.
28. Rosenzweig SD, Holland SM. Defects in the interferon-gamma and interleukin-12 pathways. Immunol Rev. 2005;203:38–47. https://doi.org/10.1111/j.0105-2896.2005.00227.x.
29. Casanova J-L, Jouanguy E, Lamhamedi-Cherradi S, Lammas D, Dorman SE, Fondanèche M-C, et al. A human IFNGR1 small deletion hotspot associated with dominant susceptibility to mycobacterial infection. Nat Genet. 1999;21:370–8. https://doi.org/10.1038/7701.
30. Dorman SE, Picard C, Lammas D, Heyne K, van Dissel JT, Baretto R, et al. Clinical features of dominant and recessive interferon γ receptor 1 deficiencies. Lancet. 2004;364:2113–21. https://doi.org/10.1016/S0140-6736(04)17552-1.
31. Li H, Durbin R. Fast and accurate short read alignment with Burrows-Wheeler transform. Bioinformatics. 2009;25:1754–60. https://doi.org/10.1093/bioinformatics/btp324.
32. Li H, Handsaker B, Wysoker A, Fennell T, Ruan J, Homer N, et al. 1000 genome project data processing subgroup. The Sequence Alignment/Map format and SAMtools. Bioinformatics. 2009;25: 2078–9. https://doi.org/10.1093/bioinformatics/btp352.
33. Koboldt DC, Zhang Q, Larson DE, Shen D, McLellan MD, Lin L, et al. VarScan 2: Somatic mutation and copy number alteration discovery in cancer by exome sequencing. Genome Res. 2012;22: 568–76. https://doi.org/10.1101/gr.129684.111.
34. Cingolani P, Patel VM, Coon M, Nguyen T, Land SJ, Ruden DM, et al. Using drosophila melanogaster as a model for genotoxic chemical mutational studies with a new program. SnpSift Front Genet. 2012;3:35. https://doi.org/10.3389/fgene.2012.00035.
35. Janssen CEI, Rose CD, De Hertogh G, Martin TM, Bader Meunier B, Cimaz R, et al. Morphologic and immunohistochemical characterization of granulomas in the nucleotide oligomerization domain 2–related disorders Blau syndrome and Crohn disease. J Allergy Clin Immunol. 2012;129:1076–84. https://doi.org/10.1016/j.jaci.2012.02.004.
36. Mitsuiki N, Schwab C, Grimbacher B. What did we learn from CTLA-4 insufficiency on the human immune system? Immunol Rev. 2019;287:33–49. https://doi.org/10.1111/imr.12721.
37. Schwab C, Gabrysch A, Olbrich P, Patiño V, Warnatz K, Wolff D, et al. Phenotype, penetrance, and treatment of 133 cytotoxic T-lymphocyte antigen 4–insufficient subjects. J Allergy Clin Immunol. 2018;142: 1932–46. https://doi.org/10.1016/j.jaci.2018.02.055.
38. La Cava A. Common variable immunodeficiency: two mutations are better than one. J Clin Invest. 2013;123:4142–3. https://doi.org/10.1172/JCI72476.
39. Zhang S-Y, Jouanguy E, Ugolini S, Smahi A, Elain G, Romero P, et al. TLR3 deficiency in patients with herpes simplex encephalitis. Science (80-). 2007, 317:1522–7. https://doi.org/10.1126/science.1139522.
40. Chapgier A, Boisson-Dupuis S, Jouanguy E, Vogt G, Feinberg J, Prochnicka-Chalufour A, et al. Novel STAT1 Alleles in otherwise healthy patients with mycobacterial disease. PLoS Genet. 2006;2: e131. https://doi.org/10.1371/journal.pgen.0020131.
41. Takeda K, Kawai T, Nakazawa Y, Komuro H, Shoji K, Morita K, et al. Augmentation of antitubercular therapy with IFNγ in a patient with dominant partial IFNγ receptor 1 deficiency. Clin Immunol. 2014;151:25–8. https://doi.org/10.1016/j.clim.2014.01.004.
42. Saulsbury FT, Wouters CH, Martin TM, Austin CR, Doyle TM, Goodwin KA, et al. Incomplete penetrance of the NOD2 E383K substitution among members of a pediatric granulomatous arthritis pedigree. Arthritis Rheum. 2009;60:1804–6. https://doi.org/10.1002/art.24532.
43. Rosé CD, Aróstegui JI, Martin TM, Espada G, Scalzi L, Yagüe J, et al. NOD2-associated pediatric granulomatous arthritis, an expanding phenotype: study of an international registry and a national cohort in Spain. Arthritis Rheum. 2009;60:1797–803. https://doi.org/10.1002/art.24533.
44. Harada J, Nakajima T, Kanazawa N. A case of Blau syndrome with NOD2 E383K mutation. Pediatr Dermatol. 2016;33:e385–7. https://doi.org/10.1111/pde.12908.
45. Galozzi P, Negm O, Greco E, Alkhattabi N, Gava A, Sfriso P, et al. Ex vivo and in vitro production of pro-inflammatory cytokines in Blau syndrome. Reumatismo. 2015;66:277–84. https://doi.org/10.4081/reumatismo.2014.772.
46. Fieschi C, Dupuis S, Picard C, Smith CI, Holland SM, Casanova JL. High levels of interferon gamma in the plasma of children with complete interferon gamma receptor deficiency. Pediatrics. 2001;107:E48. https://doi.org/10.1542/PEDS.107.4.E48.
47. J-Fran EMILE, PATEY N, Fr ALTARE, LAMHAMEDI S, JOUANGUY E, Fran BOMAN, et al. MOUSNIER J-Fran, et al. Correlation of granuloma structure with clinical outcome defines two types of idiopathic disseminated BCG infection. J Pathol. 1997;181:25–30. https://doi.org/10.1002/(SICI)1096-9896(199701)181:1<25::AID-PATH747>3.0.CO;2-Z.
48. Xie J, Deng W. NOD2 signaling and role in pathogenic mycobacterium recognition, infection and immunity. Cell Physiol Biochem. 2012;30:953–63. https://doi.org/10.1159/000341472.
49. Ferwerda G, Girardin SE, Kullberg B-J, Le Bourhis L, de Jong DJ, Langenberg DML, et al. NOD2 and toll-like receptors are nonredundant recognition systems of mycobacterium tuberculosis. PLoS Pathog. 2005;1:e34. https://doi.org/10.1371/journal.ppat.0010034.

50. Osborne GEN, Mallon E, Mayou SC. Juvenile sarcoidosis after BCG vaccination. J Am Acad Dermatol. 2003;48:S99–S102. https://doi.org/10.1067/mjd.2003.158.
51. Okafuji I, Nishikomori R, Kanazawa N, Kambe N, Fujisawa A, Yamazaki S, et al. Role of the NOD2 genotype in the clinical phenotype of Blau syndrome and early-onset sarcoidosis. Arthritis Rheum. 2009;60:242–50. https://doi.org/10.1002/art.24134.
52. Sakai H, Ito S, Nishikomori R, Takaoka Y, Kawai T, Saito M, et al. A case of early-onset sarcoidosis with a six-base deletion in the NOD2 gene. Rheumatology. 2010;49:194–6. https://doi.org/10.1093/rheumatology/kep315.
53. Black GF, Weir RE, Floyd S, Bliss L, Warndorff DK, Crampin AC, et al. BCG-induced increase in interferon-gamma response to mycobacterial antigens and efficacy of BCG vaccination in Malawi and the UK: two randomised controlled studies. Lancet. 2002;359:1393–401. https://doi.org/10.1016/S0140-6736(02)08353-8.
54. Çakan M, Keskindemirci G, Aydoğmuş Ç, Akı H, Hatipoğlu N, Kıyak A, et al. Coexistence of early onset sarcoidosis and partial interferon-γ receptor 1 deficiency. Turk J Pediatr. 2016;58:545–9. https://doi.org/10.24953/turkjped.2016.05.015.
55. Henter JI, Elinder G, Söder O, Hansson M, Andersson B, Andersson U. Hypercytokinemia in familial hemophagocytic lymphohistiocytosis. Blood. 1991;78:2918–22 Available at: http://www.ncbi.nlm.nih.gov/pubmed/1954380 [Accessed February 19, 2019].

Supplementary Material

Mutual alteration of NOD2-associated Blau syndrome and IFNγR1 deficiency